EVALUATION OF DESIGN METHODOLOGIES FOR SOIL-NAILED WALLS, VOLUME 1

WA-RD 371.1

Final Report
July 1998

Washington State Department of Transportation

Washington State Transportation Commission
Planning and Programming Service Center
in cooperation with the U.S. Department of Transportation
Federal Highway Administration

TECHNICAL REPORT STANDARD TITLE PAGE

1. REPORT NO.	2. GOVERNMENT ACCESSION NO.	3. RECIPIENT'S CATALOG NO.
WA-RD 371.1		

4. TITLE AND SUBTITLE	5. REPORT DATE
EVALUATION OF DESIGN METHODOLOGIES FOR SOIL-NAILED WALLS, VOLUME 1	July 1998
	6. PERFORMING ORGANIZATION CODE

7. AUTHOR(S)	8. PERFORMING ORGANIZATION REPORT NO.
Sunirmal Banerjee, Andrew Finney, Todd Wentworth, Mahalingam Bahiradhan	

9. PERFORMING ORGANIZATION NAME AND ADDRESS	10. WORK UNIT NO.
Washington State Transportation Center (TRAC) University of Washington, JD-10 University District Building; 1107 NE 45th Street, Suite 535 Seattle, Washington 98105-4631	11. CONTRACT OR GRANT NO. Agreement T9233, Task 39

12. SPONSORING AGENCY NAME AND ADDRESS	13. TYPE OF REPORT AND PERIOD COVERED
Washington State Department of Transportation Transportation Building, MS 7370 Olympia, Washington 98504-7370	Research report
	14. SPONSORING AGENCY CODE

15. SUPPLEMENTARY NOTES

This study was conducted in cooperation with the U.S. Department of Transportation, Federal Highway Administration.

16. ABSTRACT

Comparative evaluations of seven soil nail wall design computer programs are described and analyzed. The performance evaluations of the available programs (**SNAIL**, **NAIL-SOLVER**, **STARS**, **NAILM**, **GOLDNAIL**, **TALREN**, and **COLDUIM**) was accomplished by conducting a number of example analyses. Ten hypothetical cases and five case studies used in the analyses represented common design scenarios. Also examined were the magnitude and distribution of loads on the nails under normal working conditions. This was accomplished by observing the response of soil nails for a number of walls instrumented with strain gages. From this a general approach for estimating nail loads from strain history data was developed.

17. KEY WORDS	18. DISTRIBUTION STATEMENT
Soil nailing, walls, computer program, design, working loads	No restrictions. This document is available to the public through the National Technical Information Service, Springfield, VA 22616

19. SECURITY CLASSIF. (of this report)	20. SECURITY CLASSIF. (of this page)	21. NO. OF PAGES	22. PRICE
None	None	194	

Research Report
Research Project T9233, Task 39
Evaluation of Design Methodologies for Soil Nailed Walls

EVALUATION OF DESIGN METHODOLOGIES FOR SOIL-NAILED WALLS

VOLUME 1

by

Professor Sunirmal Banerjee
Department of Civil Engineering
University of Washington

Mahalingam Behiradhan
Civil Engineering
University of Washington

Andrew Finney
Civil Engineering
University of Washington

Todd D. Wentworth
Civil Engineering
University of Washington

Washington State Transportation Center (TRAC)
University of Washington, Box 354802
University District Building
1107 NE 45th Street, Suite 535
Seattle, Washington 98105-4631

Washington State Department of Transportation
Technical Monitor
Tony Allen
Geotechnical Engineer

Prepared for

Washington State Transportation Commission
Department of Transportation
and in cooperation with
U.S. Department of Transportation
Federal Highway Administration

July 1998

ACKNOWLEDGMENTS

The writers are grateful for the effort and support of many persons and organizations. The project report combines the results of the studies of several graduate students at the University of Washington. These students are Andrew Finney, Todd Wentworth, M. Bahiradhan, and K. Sribalaskandarajah. Andrew Finney conducted the comparative evaluation of the existing design packages. Todd Wentworth analyzed the field performance data to estimate the loads carried by the soil nails, and M. Bahiradhan worked on the development of the database for the soil-nailed walls. Theoretical analyses of the relevant stress-deformation problems were carried out by Bahiradhan and Sribalaskandarajah.

The project was funded jointly by the WSDOT and the Federal Highway Administration. Mr. Al Kilian and Mr. Tony Allen of the WSDOT Materials Laboratory, Geotechnical Division, and Mr. Ron Chassie of the Region 10 Office of FHWA in Portland served as technical contacts. Their advice and encouragement is appreciated.

Andrew Finney was supported by the Valle Foundation scholarship at the University of Washington. M. Bahiradhan and K. Sribalaskandarajah were partially supported by grants from the National Science Foundation and the Air Force Office of Scientific Research. The support of these graduate students is also acknowledged.

This report was prepared with the editorial assistance of TRAC staff members Amy O'Brien, Ron Porter and Duane Wright.

Finally, during the execution of this project, numerous colleagues throughout the world were contacted. Although their names are not individually mentioned here for the sake of brevity, the cooperation received from these colleagues is highly appreciated.

TABLE OF CONTENTS

Chapter		Page
Foreword		**viii**
Executive Summary		**ix**
1. Introduction		**1**
1.1	Context	1
1.2	Research Objectives	4
1.3	Overview of the Present Study	5
2. Literature Review		**6**
2.1	Historical Context	6
2.2	Design Analysis Methods	7
2.3	Nail Loads	16
3. Interpretation of Strain Gauge Data		**24**
3.1	Development and Distribution of Nail Forces	26
3.2	Estimating Axial Nail Forces	27
3.3	Comparison With Other Methods of Estimating Nail Loads	41
4. Nail Load Estimates for In-Service Walls		**43**
4.1	Examples of Strain Data Interpretations	43
4.2	Results of Instrumented Soil-Nailed Walls	45
5. Design Analysis Packages		**71**
5.1	SNAIL	71
5.2	NAIL-SOLVER	75
5.3	STARS	78
5.4	NAILM	82
5.5	GOLDNAIL	84
5.6	TALREN	88
5.7	CLOUDIM	95
6. Evaluation of Design Methods		**97**
6.1	Method of Comparison	97
6.2	Additional Observations	114
7. Conclusions		**146**
7.1	Analysis Package	146
7.2	Nail Loads	146

TABLE OF CONTENTS (Continued)

	Page
References	149
Appendix A: Procedure for Estimation of Soil Nail Loads	A-1
Appendix B: Input Parameters for Example Problems	B-1
Appendix C: CLOUDIM Plots	C-1

LIST OF FIGURES

Figure		Page
1.1	Typical soil nail cross-section	2
1.2	Construction sequence for soil nail walls	3
2.1	Empirical earth pressure diagram	19
3.1	Typical soil nail cross-section	24
3.2	Idealized soil nail reinforcement	26
3.3a	A hypothetical laboratory load-deformation plot of a composite soil nail in axial tension	28
3.3b	Concrete tensile strength with curing age	28
3.4	Determination of average grout age	29
3.5	Long-term strain increases that resemble creep	31
3.6	Response of soil nail, grout, and steel to grout creep and stress relaxation	32
3.7	Typical stress-strain plot noting required time factors for estimating concrete grout creep	34
3.8	Idealized concrete grout stress-strain plot displaying effective modulus method	35
3.9	Steel, concrete, and bond stress in a cracked prism	37
3.10	Typical stiffness relationship with limit strain and limit strain and limit composite nail load noted	38
3.11	Estimated nail load, lower, and upper bounds for a typical nail	40
4.1	Examples of interpreted nail forces	44
4.2	Swift-Delta Soil Nail Wall Station 1 axial nail force results	49
4.3	Swift-Delta Soil Nail Wall Station 2 axial nail force results	52
4.4	Polyclinic Soil Nail Wall axial nail force results	53
4.5	Peasmarsh Soil Nail Wall axial nail force results	56
4.6	Guernsey Soil Nail Wall axial nail force results	57
4.7	IH-30 Rockwall, Texas Soil Nail Wall A axial nail force results	60
4.8	IH-30 Rockwall, Texas Soil Nail Wall B axial nail force results	61
4.9	San Bernadino, Left Station axial nail force results	62
4.10	San Bernadino, Right Station axial nail force results	63
4.11	Cumberland Gap, 1988 Soil Nail Wall axial nail force results	66
4.12	I-78 Allentown Grid 24 axial nail force results	68
4.13	I-78 Allentown Grid 33 axial nail force results	69
5.1	Search Grid Pattern for SNAIL	74
5.2	Output for SNAIL	74
5.3	Output for NAILSOLVER	78
5.4	Assumed tension and cohesion on log spiral surface for STARS	80
5.5	Output for STARS	81
5.6	Assumed failure surface for NAILM9	83
5.7	Assumed nail tension distribution for GOLDNAIL	86
5.8:	Output for GOLDNAIL	88
5.9	Composite failure surface for TALREN	90
5.10	Multicriteria envelope used for TALREN	92
5.11	Output for TALREN	94
6.1	Comparison of computed results — Example 1	98
6.2	Comparison of computed results — Example 2	99
6.3	Comparison of computed results — Example 3	100
6.4	Comparison of computed results — Example 4	101

LIST OF FIGURES (Continued)

Figure		Page
6.5	Comparison of computed results — Example 5	102
6.6	Comparison of computed results — Example 6	103
6.7	Comparison of computed results — Example 7	104
6.8	Comparison of computed results — Example 8	105
6.9	Comparison of computed results — Example 9	106
6.10	Comparison of computed results — Example 10	107
6.11	Comparison of computed results — San Bernadino Wall	108
6.12	Comparison of computed results — Swift Delta 1 Wall	109
6.13	Comparison of computed results — Polyclinic Wall	110
6.14	Comparison of computed results — Eparris Wall	111
6.15	Comparison Of Computed Results — Bodenvernag. B Wall	112
6.16	Effect of face pressure on *SNAIL* Results — Example 1	115
6.17	Effect of face pressure on *SNAIL* Results — Example 2	116
6.18	Effect of face pressure on *SNAIL* Results — Example 3	117
6.19	Effect of face pressure on *SNAIL* Results — Example 4	118
6.20	Effect of face pressure on *SNAIL* Results — Example 5	119
6.21	Effect of face pressure on *SNAIL* Results — Example 6	120
6.22	Effect of face pressure on *SNAIL* Results — Example 7	121
6.23	Effect of face pressure on *SNAIL* Results — Example 8	122
6.24	Effect of face pressure on *SNAIL* Results — Example 9	123
6.25	Effect of face pressure on *SNAIL* Results — Example 10	124
6.26	Effect of face pressure on *SNAIL* Results — San Bernadino Wall	125
6.27	Effect of face pressure on *SNAIL* Results — Swift Delta 1 Wall	126
6.28	Effect of face pressure on *SNAIL* Results — Polyclinic Wall	127
6.29	Effect of face pressure on *GOLDNAIL* Results — Example 1	128
6.30	Effect of face pressure on *GOLDNAIL* Results — Example 2	129
6.31	Effect of face pressure on *GOLDNAIL* Results — Example 3	130
6.32	Effect of face pressure on *GOLDNAIL* Results — Example 4	131
6.33	Effect of face pressure on *GOLDNAIL* Results — Example 5	132
6.34	Effect of face pressure on *GOLDNAIL* Results — Example 6	133
6.35	Effect of face pressure on *GOLDNAIL* Results — Example 7	134
6.36	Effect of face pressure on *GOLDNAIL* Results — Example 8	135
6.37	Effect of face pressure on *GOLDNAIL* Results — Example 9	136
6.38	Effect of face pressure on *GOLDNAIL* Results — Example 10	137
6.39	Effect of face pressure on *GOLDNAIL* Results — San Bernadino Wall	138
6.40	Effect of face pressure on *GOLDNAIL* Results — Swift Delta 1 Wall	139
6.41	Effect of face pressure on *GOLDNAIL* Results — Polyclinic Wall	140
A2.1	Swift — Delta Station 1 axial force vs. nail length plots	A-3
A2.2	Swift — Delta Station 2 axial force vs. nail length plots	A-4
A2.3	Polyclinic axial force vs. nail length plots	A-5
A2.4	Peasmarsh axial force vs. nail length plots	A-6
A2.5	Guernsey axial force vs. nail length plots	A-7
A2.6	IH-30 Rockwall, Texas Range A axial force vs. nail length plots	A-8
A2.7	IH-30 Rockwall, Texas Range B axial force vs. nail length plots	A-9
A2.8	San Bernadino Left Station axial force vs. nail length plots	A-10
A2.9	San Bernadino Right Station axial force vs. nail length plots	A-11
A2.10	Cumberland Gap, 1988 axial force vs. nail length plots	A-12
A2.11	I-78 Allentown Grid 24 axial force vs. nail length plots	A-13
A2.12	I-78 Allentown Grid 33 axial force vs. nail length plots	A-14

List of Tables

Table		Page
4.1	Geometry and structure characteristics of analyzed soil nail walls	47
5.1	TALREN Nail Modeling.....	92
5.2	Summary of program features.....	96
6.1	Summary of example problems.....	113

FOREWORD

Dr. Sunirmal Banerjee died shortly after producing the draft report for this document. Our sympathies go to his family and friends. The three-volume set that make up this report attempt to document the work that was accomplished under Dr. Banerjee's able direction. Volume 1 is the draft final report mentioned previously. Volume 2 is the master's thesis produced by Mr. Todd D. Wentworth, and Volume 3 is the master's thesis produced by Mr. Andrew Finney, both students working on the project at the time.

EXECUTIVE SUMMARY

Soil nailing is emerging as a primary support system for construction excavations, walls, and slopes. In spite of its successes, engineers are realizing that the current design approaches for soil nailing systems are not sufficiently evolved to predict the performance of the systems under working stress conditions. The current design concepts for such walls are largely based on the limit equilibrium approach, which does not provide any insight about the actual load transfer and deformation mechanisms.

This research project was undertaken to systematically evaluate existing design methodologies for soil-nailed walls. The major tasks of the project included a) comparative assessment of the existing design analysis packages, b) interpretation of the performance data of in-service walls to estimate the loads carried by the soil nails, and c) development of a database for the soil-nailed walls.

The evaluation of the performance of the available programs (*SNAIL, NAILSOLVER, STARS, NAILM, GOLDNAIL, TALREN,* and *CLOUDIM*) was accomplished by conducting a number of example analyses. The ten hypothetical cases and five case studies chosen in this comparison were meant only to represent common design scenarios and not to reveal any discrepancies among program output. Some of the examples were adapted from a previous FHWA study. The following trends, revealed by the analyses of the example cases, were particularly noteworthy :

- The global safety factor predicted by one of the programs was somewhat lower than those predicted by the other five programs.
- The safety factors predicted by *SNAIL* and *GOLDNAIL* were bounded by those of the three other programs in 10 of the 15 cases.
- The largest difference between predicted safety factors was 0.7, which occurred for the San Bernadino wall. For the other cases, an average spread

among the remaining programs was about 0.1, with the smallest difference being 0.04.

- The predicted locations of the failure surfaces were almost identical for all of the 15 examples and case studies, with one notable exception, the Eparris wall, for which the predicted slip surfaces were shallower than the actual failure surface.
- Face pressure is an important design parameter and a desirable feature to be included in a soil-nailing analysis package. Most of the programs used to analyze a wall do not consider the wall's structural contribution to stability.

A better understanding of the magnitude and distribution of the loads experienced by the nails under normal working conditions was also sought as a part of this study. For that purpose, the researchers reviewed the observed response of soil nails for a number of walls instrumented with strain gages and developed a general approach for estimating nail loads from strain history data.

The proposed approach accounts for the contribution of the concrete grout to the total axial stiffness of the soil nail. Furthermore, the effects of curing, creep, and the concrete grout cracking on the development of the composite nail loads are incorporated in the proposed approach for estimating the nail load from measured strains at the steel-grout interface.

These procedures were applied to the strain data obtained from ten instrumented walls. The estimated distributions of the nail loads along the length of the nails and the maximum loads versus depth were investigated for each case history. The estimated maximum loads were compared with the empirical apparent pressure diagram proposed by Juran and Elias.

Finally, a survey of national and international sources of case histories and instrumentation data for full-scale soil-nailed walls was carried out by the entire project team, with the help of Washington State Department of Transportation and Federal

Highway Administration personnel. Researchers in other countries (e.g., France, Germany, Japan, and England) and U. S. specialty contractors were contacted. These efforts have resulted in the development of a database worldwide of instrumentation results from previous full-scale studies.

CHAPTER 1

INTRODUCTION

1.1 CONTEXT

Soil nailing offers a practical and cost-effective technique of stabilizing vertical excavations and steep slopes of a natural soil mass by using passive structural inclusions. Shortly after an excavation step has been completed, the nails, which are typically steel reinforcing rods, are inserted in horizontal or inclined drilled holes and grouted along their full length. The inclusions enable the reinforced soil zone to safely withstand tensile forces and to resist soil movements by bond stress at the soil-inclusion interface. In principle, the nails work to resist tension and shear stresses in the ground as it deforms because of further excavation. As a result, the composite soil mass becomes relatively more stable and experiences limited deformations. The approach is to form a reinforced soil zone that acts much like a gravity wall supporting the in situ soil behind it (Figure 1.1). The face of the excavation is usually protected from erosion and surface ravelling by shotcrete and geogrid facing. The nails are connected to the facing with a small steel plate (with the threaded end of the rebar extending through it), and a nut is hand tightened on the bar against the plate. The next row of nails is constructed by excavating below the completed portion of the wall and repeating the above procedure (Figure 1.2).

In many design situations, soil nailing can be more attractive than other retaining systems. Soil nail walls

- can be constructed more rapidly
- do not require over-excavation or fill
- involve less expensive materials and equipment (no sheet piles, soldier piles, or tensioning equipment)
- can easily accommodate design changes during construction.

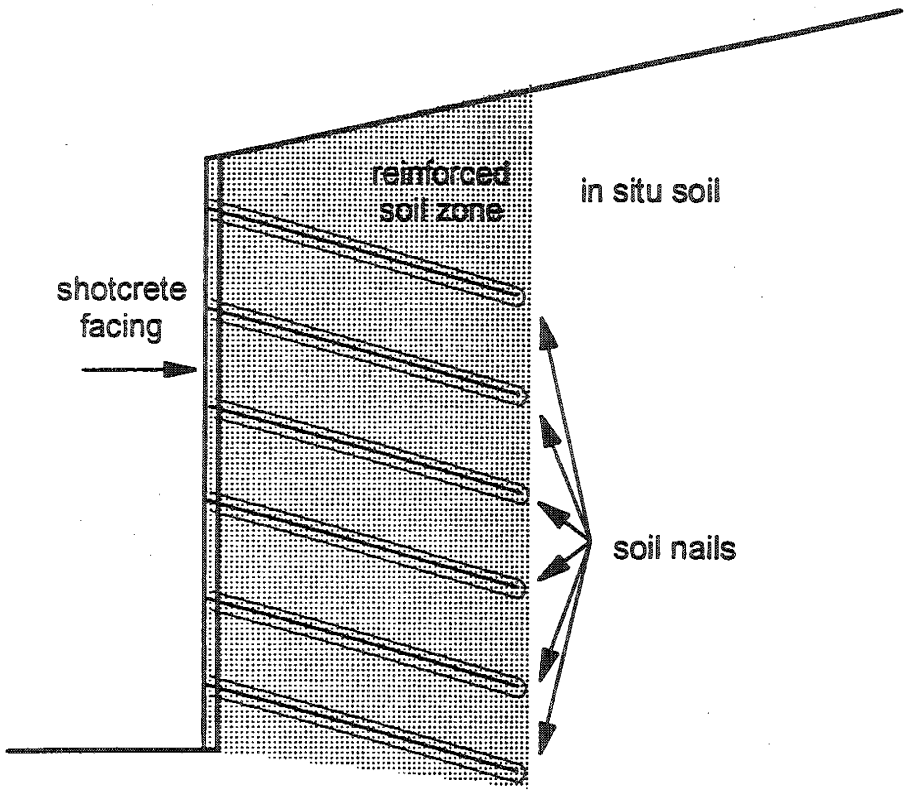

Figure 1.1. Typical soil nail cross-section

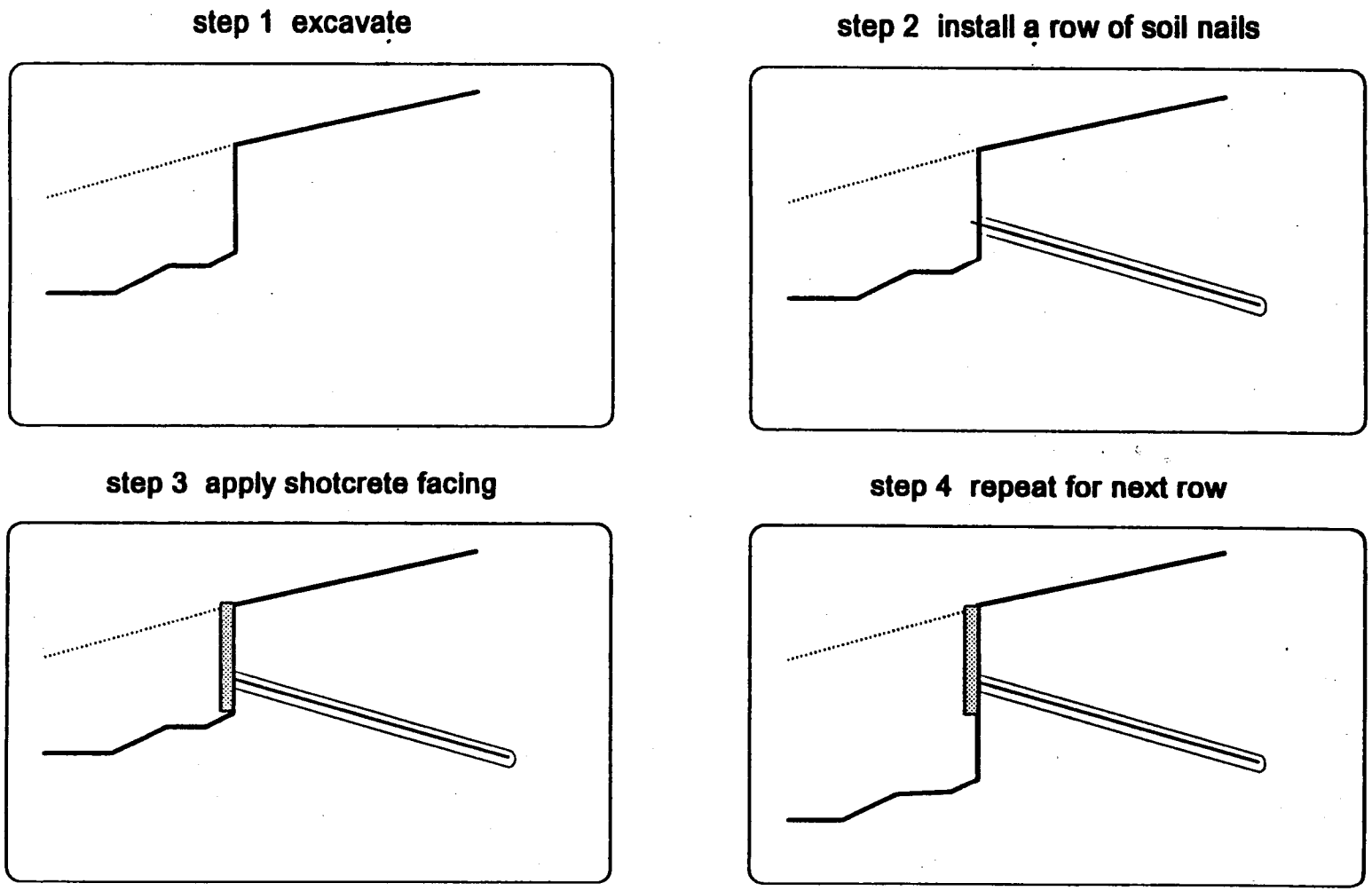

Figure 1.2. Construction sequence for soil nail walls

For these reasons, soil nailing has been utilized to support excavated slopes for highways and railroads and construction excavations for underground facilities. The technique has also been used to stabilize landslides and repair existing retaining structures.

Detailed descriptions of soil nailing technique have been presented by Chassie (1992), Juran and Elias (1991), Gassler (1990a), and Jewell (1990).

1.2 RESEARCH OBJECTIVES

To date, soil nailing has been advanced primarily by specialty contractors, on the basis of their experience with the technique from site to site, and the design procedure is governed primarily by overall stability concerns. However, designers' real concern is to estimate the loads that will be carried by the individual nails and to predict the magnitude of the displacement along the face of the cut. In the final analysis, designers must address these concerns even after they meet the overall stability concerns. Designers must also make important decisions regarding the appropriate size and spacing of the manufactured components and the design pressures for the facing elements, given the anticipated performance of the nailed soil mass.

The current design concepts for such walls are largely based on the limit equilibrium approach, which does not provide any insight about actual load transfer and deformation mechanisms. Again, because nailed walls are relatively novel structures, the available experience bases are also relatively limited. Consequently, no standardized design methodology has evolved for these structures, and engineers lack a high level of confidence in the accuracy of any of the current design approaches.

The objectives of the proposed research were to validate, if possible, some of the available limit-equilibrium methods and to develop an improved and well-substantiated design procedure for soil-nailed walls using instrumentation data from available case histories.

1.3 OVERVIEW OF THE PRESENT STUDY

The purposes of this study were to

- obtain an improved understanding of the stress-deformation mechanisms in soil-nailed walls
- assess current design procedures for these walls
- create a worldwide field instrumentation database
- realize substantial savings in the design and construction of soil-nailed walls.

However, the finite element study of the stress-deformation mechanisms in soil-nailed walls is not included as a part of this report. A graduate thesis being prepared on the topic will be published separately. This exclusion from the original action plan was supported by the project's sponsors. The database of worldwide actual and processed instrumentation results from previous full-scale studies can also be found in a supplemental report.

Chapter 2 of this report summarizes the historical context of soil-nailed walls, existing design analysis methods, and the nail load distributions and magnitudes published in the literature. Chapter 3 describes the method developed in this study to estimate working nail loads on the basis of the their performance record . The basis of the adopted procedure is explained in detail. In Chapter 4, the proposed method is applied to ten instrumented soil-nailed walls. A short description of the case histories and the corresponding nail forces are presented. Chapter 5 describes the design analysis packages, and Chapter 6 presents the evaluation of the performance of these programs. This chapter includes the details of the example analyses. Chapter 7 contains a discussion of the results and conclusions of the study. The algorithm for estimating nail loads is provided in a concise step-by-step format in Appendix A. Appendix B presents the complete sets of input variables required for the analyses.

CHAPTER 2

LITERATURE REVIEW

2.1 HISTORICAL CONTEXT

Soil nailing was introduced in Europe, specifically with the New Austrian Tunneling Method (NATM). This method, utilizing bonded steel bars and shotcrete facing, was initially employed as a hard rock tunneling technique in Germany in the early 1960s. The same technique was applied to less competent formations, such as graphitic shales and Keuper Marl (Bruce et al., 1986). Trials were also conducted in silts, gravels, and sands, with early applications in Frankfurt in 1970 to metro tunnels. The method gained respect in the early 1970s, especially in Germany. A French construction company, Bouygues, had experience in France with the NATM, and in 1972, in a joint venture with Soletanche, started construction on a 70-degree cut slope for a railroad near Versailles. Over 25,000 steel bars were used in this first recorded application of soil nailing (Bruce et al., 1986).

In the U.S., the first recorded use of soil nailing was in 1976, with the construction of an addition to the Good Samaritan Hospital in Portland, Oregon. A research team from the University of California at Davis was involved in the construction monitoring program, and, as a result of interest generated by the project, conducted a research program that also included full-scale testing of an experimental wall (Shen et al., 1981a, 1981b).

In West Germany, specialty contractor Karl Bauer AG led developments in soil nailing in association with the Institut fur Bodenmechanik und Karlsruhe with support from the West German federal government (Bruce et al., 1986). Starting in 1975, four large-scale tests were conducted, the results of which were published by Stocker et al. (1979).

In France, the success of the Versailles project led Bouygues to construct a number of other soil-nailed walls, both temporary and permanent, one of which was the Les Invalides Metro station in Paris in 1974. In this case the nails were driven, rather than grouted, and this marked

the development of the Hurpinoise system of soil nailing, named for its inventor. A number of specialty contractors, such as Bachy, Intrafor Cofor, SEFI, and Soletanche, began to develop their own methods for nailing based on the drilled and grouted nail. In the mid 1980s a large testing program was organized under a French national project called "Programme Clouterre," the results of which were published in English in 1992 (Schlosser et al., 1992).

2.2 DESIGN ANALYSIS METHODS

While specialty contractors in Europe and the U.S. were gaining practical experience with soil nailing, no consensus could be reached on the best way to model and design the walls. Not until 1979 at the Paris conference on the reinforcement of soils was soil nailing design provided any forum. At this conference, both the French and German design methods, on which many of today's designs are based, were presented. The major methods analyzing soil nailing design are reviewed below.

German Gravity Wall Analysis

Stocker et al. (1979) presented a design method based on a force equilibrium approach with a bilinear slip surface. The authors believed that soil-nailed walls should be designed as gravity retaining walls. The reinforced zone with soil nails is modeled as a single composite mass acting to retain the soil behind it. It is modeled with a bilinear wedge, and the location of the intersection of the two angled failure surfaces must be behind the nailed zone.

The work presented by the Germans at this conference has evolved into the concept of the soil-nailed gravity wall. Subsequently, several improvements have been proposed to refine the original method. Experimental work by Gässler and Gudehus (1981) showed that a two-plane translational failure mode is the only mode that warrants consideration. Their research showed that all other modes of failure (deep slip surfaces, steep circular surfaces, and combined tilting failures) produce higher factors of overall safety. The definition of overall safety was given as the ratio of dissipative forces along the slip surface combined with the nail effects, divided by the external forces applied to the system. The procedure is to vary the first planar

angle at the toe, measured from the horizontal, while keeping the second planar angle, also measured from the horizontal (starting from the back of the nailed zone), at $45° + \phi/2$, where ϕ is the friction angle of the soil. A further refinement came in 1983 with the adoption of a statistical design method to meet the new Eurocode 7 requirements (Gässler and Gudehus, 1983).

Gässler (1988) conducted another comparison and analysis and examined the four commonly assumed failure modes employed in soil nailing design: translation of a single rigid body, translation of two rigid bodies, rotation of one rigid body, and rotation of two rigid bodies. The results are summarized below for different ranges of soil cohesion, C:

C = 0 soils	The bilinear wedge is the most critical case if the walls are near vertical. The slip circle is critical if the walls are angled at less than 80° from the horizontal, or if longer nails are used in the upper rows.
Medium Cohesion soils	The slip circle and bilinear wedge are equivalent.
High Cohesion soils	The slip circle is critical

Gässler (1988) also concluded that the simple wedge, bilinear wedge, and slip circle are the only relevant failure mechanisms. Further conclusions of the paper were that only axial forces need be considered in near vertical walls and that the internal nail force is based on the mean shear per length of nail, T_m, which is constant with depth. The earlier gravity wall design method was refined by using a velocity hodogragh (velocity vector diagram) to obtain kinematical compatibility. As a final note, the author recommended that various partial material safety factors be used in a two-step process for design. In the preliminary design one examines various failure modes and varied surfaces to determine the most critical case. In the final design the most critical surface is used to assess the suitability of the design reinforcement.

The gravity wall design concept was furthered by Riedinger and Stocker (1990) with the consideration of internal stability, that is, the pulling away of a failure wedge of soil, leaving only the nails in place. The authors concluded that external stability should be checked using a two-part rigid body translation, with the second wedge angled at 45° + $\phi/2$ to exert an active pressure on the back of the nailed zone. Internal stability should be checked using wedges angled at any inclination from the toe, with reinforcement contributions coming from that portion of the nail located between the failure plane and the wall face.

French Multicriteria Analysis

The French developed a somewhat different method of analysis, which considered the contribution of nail bending resistance, as well as tensile strength, to the overall wall stability. Early work by Schlosser and Juran (1979) identified the need to differentiate between excavation support and slope stability. According to their work, it is important to distinguish between the two applications. The excavations must be designed with consideration for nail tension, as is done in Reinforced Earth (RE), and the slope stability cases require nail designs modeled after laterally loaded piles. The other conclusions of this paper were that the slip surface should follow the line of maximum tensile forces from RE, and that failure of the wall is rotational.

Further work by Schlosser et al. (1983) resulted in a soil/grout interaction model based on the overburden stress, with a coefficient that attempted to correct for dilation of the soil during shearing. They presented the following equation:

$$\tau = C_0' + \sigma' \tan\phi' + \Delta\tau \qquad (2.1)$$

where τ = shearing resistance of the nailed soil,

C_0' = apparent cohesion due to the mobilized shear force in the bars

σ' = effective normal stress acting on the bar

$\Delta\tau$ = variation of the shear stresses in the soil due to the effect of the reinforcing bars

The conclusion of the paper was that tensile forces in the nail are affected by small, relative soil/grout deformations, but the shear and moments in the nail are affected by large soil deformations. Schlosser (1985) presented the Multicriteria theory for soil nailing. The

delineation between excavation and slope stability applications is no longer necessary with the presentation of a limit envelope in normal and shear space that considered the tensile strength of the nails, the shear strength of the soil, the soil/nail friction, and the limiting lateral earth pressure acting on the nail. The method uses a circular slip surface with a method of slices; however, it also considers the mobilization of the lateral earth pressure on the inclusions, as **it controls** the maximum shear force developed in the nails. The basis for the limit criteria came from work by Baguelin and Jezequel (no reference given), which modeled the nail as a laterally loaded, long elastic pile with a constant K_S of the soil, where K_S is the modulus of subgrade reaction of the soil.

Schlosser and DeBuhan (1990) presented a paper on the composite behavior of nailed soil. They concluded that the design of soil-nailed walls has been oversimplified by not considering the soil/nail interaction on the stress/strain patterns of the soil. They suggested that failure planes in the reinforced soil are very different from the Mohr-Coulomb failure planes of the unreinforced soil. Furthermore, they concluded that tensile forces in the nail are rapidly mobilized and that nail shearing resistance is not efficiently mobilized until there have been significant displacements. Various assumed failure planes were rated in order of decreasing accuracy: log spiral, circular with slices, and bilinear wedge. The final recommendation was that a method like Juran's Kinematical method, described in the following section, be used.

Kinematical Limit Analysis

Juran and Elias (1988) proposed a "Kinematical Limit Analysis Approach." They departed from methods developed by Schlosser and DeBuhan (1990) and Stocker et al. (1979), claiming that these could not be used to adequately assess the global safety with respect to shear strength characteristics of the soil and the friction at the soil/inclusion interface. According to the authors, these methods do not allow of the local stability of the reinforced soil mass to be evaluated, or the forces in the nails, which they claimed were often critical, to be determined. A log spiral slip surface is used with a method of horizontal slices. The horizontal components of the interslice forces are assumed to be equal. The yield criterion for the nails is based on

Schlosser's earlier Multicriteria envelope (Schlosser, 1985). Juran's method uses Kotter's equation (no reference given) to determine the distribution of normal forces on the slip surface. Nails are modeled as rigid, laterally loaded piles on the basis of work by Hansen and Lundgren (no reference given). Furthermore, nail forces are determined by considering the equilibrium of a given horizontal wedge of soil surrounding a nail.

Juran and Elias (1990) further developed the kinematical limit analysis with additional discussion of the failure envelope and the added suggestion that the value of K_S could be found from the Soletanche charts developed by Pfister et al. (1982). The benefit of this method, according to authors, is that by analyzing every nail level and by avoiding a global safety factor, the procedure guards against progressive failure.

The final version of the method involves four specific design steps (Juran and Elias, 1990). First, estimate the location and magnitude of the maximum working stresses. Second, analyze local stability at each nail level. Third, look at overall or global stability. Finally, consider the adequacy of the facing. The major point to this approach is that local nail stability can be far more critical than global stability in the consideration of progressive failure. Juran and Elias recommended that the local stability be analyzed using their kinematical method, and global stability be analyzed with a method like that developed at Davis by Shen et al. (1978) and extended by Bang and Erickson (1989), or like Schlosser's Multicriteria method (Schlosser, 1985). The Davis method was favored because of its simplicity and consideration of nail tensile forces alone, which the authors claimed to be the most accurate representation of the wall's behavior. The paper also discussed the observation that the behavior of a nailed wall is similar to that of a braced cut, and therefore, it may be possible to use semi-empirical earth pressure diagrams in future developments.

U.C. Davis Method

This method, developed at the University of California, Davis, was originally presented at a symposium on earth reinforcement (Shen et al., 1978). Soil nailing was described as the use

of passive or non-pretensioned inclusions to be used for temporary excavation support. The maximum bond stresses are the following:

$$\tau_{max} = C + \sigma_v \tan\phi \tag{2.2}$$

where τ_{max} = maximum shear stress between the soil and nail

C = cohesion of soil

σ_v = vertical overburden stress acting on the nail.

No yielding of the reinforcement is mentioned. The entire system is considered a composite material, and the solution to the overall stability is found by minimizing the incremental potential energy. The failure surface is given as a parabolic surface on the basis of the results of the finite element study conducted on in-situ reinforced soil at Davis and on a full-scale test wall (Shen et al., 1981a, 1981b).

Bang et al. (1980) expanded on the Davis method by describing the assumed soil failure parabola as being divided into two sections, one with reinforcement, one without. The design method is limited to vertical walls, horizontal back slopes, and homogeneous soil profiles. Bang and Erickson (1989) modified the method to handle irregular ground surfaces, wall inclinations, and up to two layers of soil.

The method is based on a force equilibrium with a parabolic slip surface. The resisting force, F_R is defined as follows:

$$F_R = C'L + T_f \tan\phi' + T_t \tag{2.3}$$

where C' = developed cohesion (C/material safety factor)

L = length of potential failure surface

$T_f = F_n + T_n$

F_n= normal force acting on the base of a given vertical slice

T_n= normal component of the resultant of the axial forces in nails

T_t= tangential component of the resultant of the axial forces in nails

Pullout capacity is based on the overburden stress and is limited by the yield strength of the nails.

Developments in England

Bridle (1989) presented a method of analysis with log spiral failure surface and moment equilibrium. Both tension and shear contributions from the nail were considered, with a composite failure envelope based on the nail's capabilities and the bearing pressure under each nail. Equations were presented to define the log spiral's exit angle and its angle with the horizontal at the wall toe. According to the author, the exit angle, α, is about 3 degrees. β, the angle of the slip surface at the wall toe, is given by

$$\beta = 0.5\phi + 0.201\alpha\phi + 0.265\alpha + 0.087 \tag{2.4}$$

The purpose of the reinforcement in this method is to take up the Out of Balance Moment, or OBM. The OBM is defined as the difference between the driving and resisting moments. The method utilizes two existing relationships. The first is borrowed from Juran (1990) and relates the normal force, σ, and shear force, τ, in the nail:

$$\sigma = \tau \tan 2\rho \tag{2.5}$$

where ρ = angle of inclination of the nail with the normal to the slip surface.

The other formula is based on the previous work on laterally loaded piles by Matlock and Reese (1962). This formula allows the calculation of the nail deflections on either side of the slip surface. The bearing pressure under the nail is given by Terzaghi's general bearing capacity formula (Terzaghi, 1943).

The aforementioned analysis (Bridle, 1989) touched off a debate centered around the contribution of nail shearing resistance to overall wall stability. Pedley and Jewell (1990) addressed the issue of shearing by carefully showing its contribution to be negligible. Their analysis started with the Tresca criterion of failure for combined shear and tension. The combined moment and tension is limited by the following :

$$(M/M_p) + (P/P_p)^2 = 1.0 \tag{2.6}$$

where M = nail bending moment

M_p = maximum plastic moment

P = axial nail force

P_p= maximum plastic axial nail force

This equation is conservative for bars of circular cross-section, but it offers more benefit from shear than the current British structural steel codes, such as BS5950 (1985). An upper bound for the determination of the effect of shear is given by Schlosser's elastic analysis (Schlosser, 1985):

$$P_S = 4.9\, M_{max}/L_S \tag{2.7}$$

where P_S = maximum nail shear force

L_S = distance between either side of the nail centerline

A simple limit-plasticity model developed by the authors acts as the lower bound:

$$P_S = 2M_{max}/L_S \tag{2.8}$$

With further manipulation, the conclusion was drawn that the shear width, L_S, must be minimized to maximize the mobilized shear. Using the range of analysis methods presented in preceding sections, the authors showed that the practical range of shear widths is very limited. Using nails perpendicular to the slip surface for maximum benefit from shear, and both plastic and elastic analyses, the authors found that a relatively small nail shear force is mobilized in comparison to the nail tensile force. The major conclusion was that the benefit to overall stability from nail shear is minimal, and more importantly, that Schlosser's Multicriteria analysis method was based on an incorrect relationship:

$$(P/P_p)^2 + (2P_S/P_p)^2 = 1.0 \tag{2.9}$$

The authors claimed that the above relationship is valid only for combined axial force and torsion. They also claimed that the analysis includes an assumption that $M_{max} = M_{plastic}$, regardless of the applied axial force.

Glasgow Conference

The Glasgow Conference (1990) was an opportunity for all the members of the debate to voice their opinions in a single forum. Two papers were particularly noteworthy. Bastick (1990) recommended that one should avoid Schlosser's (1985) equation for unit soil/grout shear stress,

which includes an apparent coefficient of friction term for soil dilation. His alternative was to use a τ_{max} along the soil/grout interface. Furthermore, Bastick argued that local equilibrium methods such as Juran's should be avoided, and full-scale pullout tests should be conducted.

Plumelle and Schlosser (1990) presented the results of Clouterre, the French soil nailing research program. It showed that although bending stiffness can play an important practical role in maintaining face stability, axial reinforcement force provides the overall ground stability.

At the conference, Jewell attempted to provide a definitive analysis of the various design methods. This paper discussed lateral nail stresses, axial nail force only methods, and Juran and Schlosser's approaches linking lateral soil stresses and the nail forces. Through Jewell's analysis, the conclusion was reached that in order for the combination of forces at the point of maximum shear to become critical, the maximum bearing stress in the soil would have to be on the order of the yield stress of the bar. Jewell also pointed out that nail reinforced walls fail long before the limiting shear force in the nail can be mobilized. Jewell cited Gässler's (1987) test wall data to show that at failure, defined as the point of maximum overall soil shearing resistance, no displacements were measured along any one slip surface, only local shear displacements. No displacement was recorded along a slip surface until well after failure; therefore, no shear contribution from the nail was effectively mobilized. It is therefore prudent to rely solely on the axial capacity of the bar. This was also the recommendation made by Nielson (1984) for the dowel action of reinforcing steel in concrete. The Gässler-Gudehus (1981), Shen et al (1981), Gässler (1988), and Stocker-Riedinger (1990) methods were all recommended. Acceptable failure surfaces were considered to be log spiral rigid body rotations and two-part wedges. The method of slices was not recommended because of the questionable allocation of reinforcement forces to the individual slices. For safety factors, Schlosser's (1985) method of partial material factors was considered attractive, as was the more rigorous analysis presented by Gässler (1988) that utilized a statistical approach.

Summary

It is easy to see from the brief review of the development of soil nailing design that a number of issues remain unresolved. Many of the methods and theories presented share common elements, but for every common element there is also a difference. Most of the methods utilize standard slope stability analysis concepts with varying assumptions about the incorporation of interslice nail forces and the benefit of the application of the reinforcing to each slice. Some of the methods arguably claim that the adopted failure mode is kinematically admissible without presenting any rigorous proof. The benefit of the reinforcements is the major point of divergence. Some of the methods combine the contributions from nail shear and axial forces, while others simply utilize the effect of nail tension. Some methods consider internal equilibrium with the aid of face pressure or simply bond stress, while others do not. Given the number of methods and the differences among the methods, it is important to determine the effects of the underlying assumptions on the results of the analysis.

2.3 NAIL LOADS

Below is a summary of the information on nail loads gathered from the existing literature, including case histories involving instrumented soil nails, the magnitudes and distributions of nail loads, and methods of estimating the soil nail forces from measured strain data.

Bodenvernagelung

Performed by the University of Karlsruhe and the specialty contractor Bauer for the Bodenvernagelung project in Germany, this five-year research and development program (initiated in 1975) included theoretical stability analyses, model tests, and tests with seven full-scale walls. These test walls were instrumented and loaded to failure by increasing surcharges (Gassler, 1992).

The results of this project were first presented by Stocker, et al (1979). The distributions of axial nail forces along the nails were discussed for test wall B. The changes in the nail forces with changes in the surcharge load were reported. The upper nails displayed maximum nail

forces at or near the middle of the nail length. The lower nails displayed maximum forces near the predicted critical slip surface for surcharge loads close to the surcharge load in which the wall failed (Stocker, et al., 1979). The authors also noted that soil nails within these test walls did not undergo any significant bending (Gassler, 1990b).

UC Davis

The research team from the University of California at Davis was involved with instrumenting the Good Samaritan Hospital wall with inclinometers. As a follow up of that work, they conducted a research program that involved constructing a full-scale test wall at the UC Davis campus in 1979 (Shen, et al, 1981). The soil nails in one cross-section were instrumented with four sets of strain gauges distributed along the length of each nail. The reported axial nail forces were compared with forces predicted on the basis of finite element analyses performed during the research program.

CLOUTERRE

This work led to publication of the French soil nail design manual (Schlosser, et al, 1992). The results of three full-scale experimental soil-nailed walls were reported in 1990. The test walls investigated three possible failure modes—breakage, nail pullout, and excessive excavation below the reinforcement (Plumelle, et al, 1990). In the first wall, CEBTP #1, the nails were instrumented to measure tensile nail forces. Strain gauges were placed along the nail in pairs attached to the top and bottom of aluminum tubes, which were grouted into the borehole. An aluminum tube encased in concrete grout was tested in the laboratory in axial tension to develop a tensile force-displacement curve. This curve was used to interpret the strain gauge data in order to estimate the nail forces (Plumelle, et al, 1990). This is the first known study that attempted to account for the composite stiffness of the soil nail inclusion. In this case, the grout diameter of the nail was small, and strains were large enough for the grout to have an influence on the nail force. Also, because the nails were designed to fail by breaking, the strains exceeded the elastic range of the aluminum tube, thus making accurate nail load estimation difficult.

The CEBTP #1 wall failed after the ground had been saturated from a water basin placed above the reinforced soil zone. Fortuitously, the observed failure zone coincided with the measured maximum tensile force line. The tensile force in the nails was mobilized in the two excavation stages following nail installation. Bending of the nail was not observed until large deformations had occurred, just prior to complete failure. The maximum measured tensile forces were slightly greater than the predictions based on assumed at-rest soil conditions near the top of the wall and slightly less than those based on assumed active soil conditions near the bottom. Although no tensile force was observed on the bottom nail at the end of construction, three months later a small force was measured, which was possibly due to soil creep. The major conclusions from the three experimental walls were reported by Plumelle and Schlosser (1991)

FHWA sponsored research

The study sponsored by the Federal Highways Administration involved analysis of four case histories: the CEBTP test wall #1, Davis test wall, Paris wall (Cartier and Gigan, 1983), and the first Cumberland Gap wall (1985). The findings of this study were reported by Juran and Elias (1987).

The distribution of horizontal displacements and maximum axial nail forces were reported for each case history. (Note that the nail load refers only to the tensile forces in the steel rebar without attempting to account for the surrounding concrete grout.) The similarities in the loads experienced by soil nails and the bracing systems in braced excavations were reviewed in this study. The authors proposed that the apparent earth pressure diagrams for braced cuts (Terzaghi and Peck, 1967) may be used, with some modifications, for preliminary design of soil-nailed walls, provided the wall geometry is similar to the intended geometry of the diagrams (Figure 2.1). The trapezoidal shape of the distribution used for stiff clays by Terzaghi and Peck (1967) was proposed regardless of soil type. In the report, the empirical diagrams were plotted with the non-dimensional nail forces obtained from measured data. The nail force was normalized by the soil unit weight, wall height, vertical nail spacing, and horizontal nail spacing.

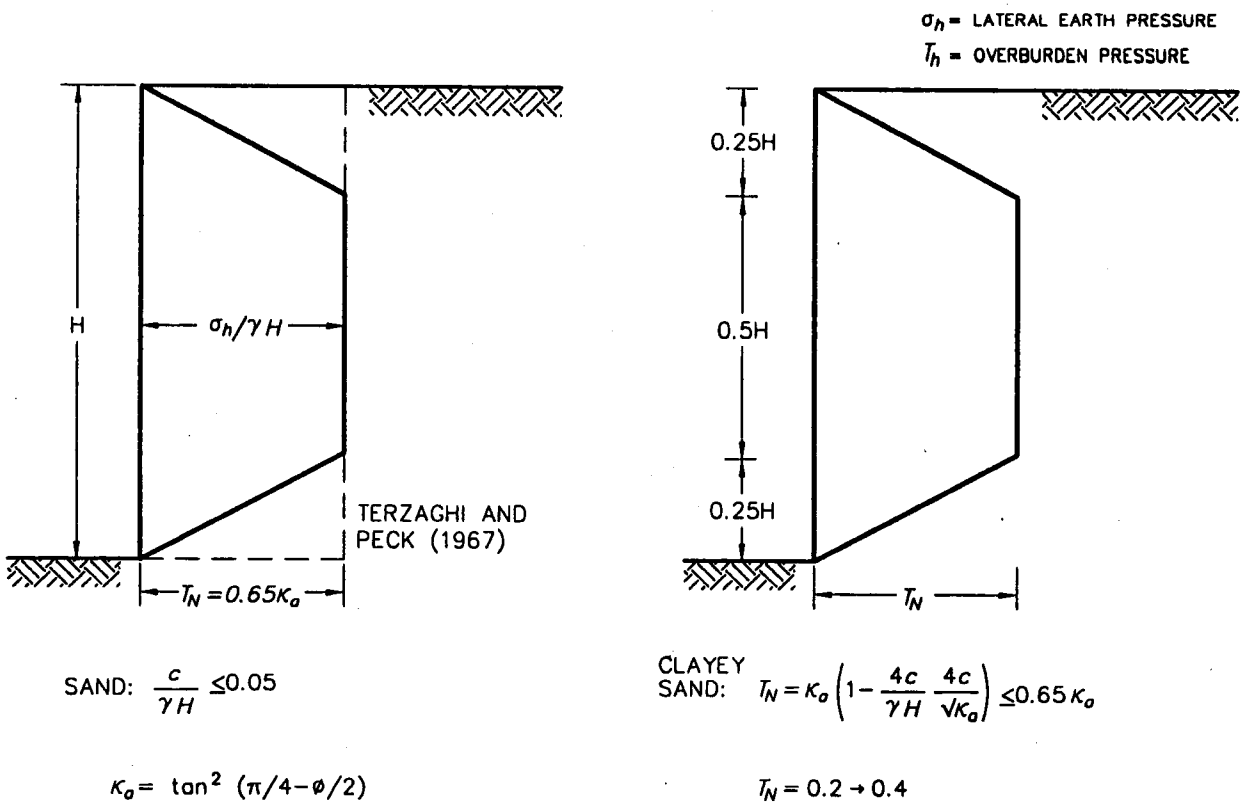

Figure 2.1. Empirical earth pressure diagram

The authors also observed that long-term soil creep was noted in the strain data. For example, for the Cumberland Gap 1985 project, displacements measured by inclinometers stabilized within two to three months after construction, while tensile forces continued to increase with time. The authors claimed that this was due to creep of residual soils.

A later report for the FHWA (Elias and Juran, 1990) discussed similar research results. Four case histories were presented: CEBTP #1, San Bernadino, I-78 Allentown, and the second instrumented soil nail wall at Cumberland Gap (1988). The maximum nail forces were compared with the empirical diagram. (The data from the last three walls were reinterpreted in this study.)

In the discussion of the San Bernadino wall, the authors attributed the low nail forces (considering only the steel rebar) to the large diameter borehole (203 mm) and noted that the large grout column was capable of carrying significant tensile loads while only the balance needed to be carried by the steel rebar. They also contended that the composite force could only be analyzed if a crack occurred right at the gauge location and that the difference in strain readings before and after cracking could be used to back-calculate the composite stiffness. Because the strain data at San Bernadino did not indicate possible cracking, no interpretation was attempted by the authors.

Recent Developments

The performance of the *Polyclinic* soil nail wall in Seattle, Washington, designed and instrumented by Golder Associates, was reported in a paper by Thompson and Miller (1990). As with the San Bernadino wall, the instrumented nails consisted of strain gauges attached to the rebar and grouted in a 203-mm diameter borehole. A combined influence of the concrete grout and steel was noted. First, some of the strain histories appeared to indicate cracking of the grout, as Elias and Juran had hypothesized. Second, the strain history plots showed a pattern of possible soil creep after construction ended. However, the nails were constructed in very dense glacial outwash sands and gravels, and no changes in deformation were recorded by the inclinometers after construction had ended. The authors concluded that because wall

deformations did not increase, it is most likely that the increase in measured strain was due to the redistribution of the load from the concrete to the steel because of creep of the concrete grout. They suggested that, although concrete has a lower modulus than steel, the large grout area allowed the concrete column to carry a large proportion of the load prior to cracking.

The nail loads were estimated from the strain data by two approaches. For the upper bound estimate, the creep effects in the concrete were ignored, and reasonable concrete modulus values were applied on the basis of curing age. Then by assuming that the measured strains were uniform across the nail section, a composite nail load was calculated. For a lower bound estimate, they assumed the jumps in the strain histories represented a crack in the grout at the gauge location. The authors assumed that the strains prior to cracking could be related to a composite stiffness, and the strains measured after cracking related only to the steel stiffness. The nail loads for the remaining strain data were determined using the back-calculated composite stiffness.

The instrumentation data from this wall was evaluated by a simplified kinematical soil-nail interaction model by Byrne (1992). This simplified soil-nail interaction model was able to reasonably predict maximum nail load distribution and locations of maximum straining immediately after construction and nine months later. The model showed that nail loads varied little over the nine months. However, this result was achieved by assuming additional strains, due only to concrete creep, after the end of construction. This was the first attempt to include creep in estimating soil nail forces.

The research conducted for an instrumented soil nail wall in *Guernsey*, U.K., included laboratory testing to simulate a soil nail in axial tension. A pair of strain gauges were attached to a steel bar encased in grout. The test specimen was constructed with the same materials that were used for soil-nailed wall construction. The ends of the steel bar were subjected to axial tension while strains were measured from the embedded strain gauges (Farham, 1992). The resulting applied load versus measured strain plot, not withstanding some testing problems (the chosen initial strain reading probably did not correspond to zero stress), displayed two different

slopes. The initial slope was high, representing the stiffness of a composite nail. After severe grout cracking, the slope decreased to the stiffness of the steel bar.

As part of an instrumentation program for a soil-nailed wall built under a bridge abutment near Portland, the Oregon Department of Transportation (ODOT) performed similar laboratory tests to simulate a soil nail in axial tension (Sakr and Barrows, 1991). Researchers instrumented steel reinforcing bar encased in grout with a pair of strain gauges and loaded it in axial tension by pulling on the bar ends while the strain measurements were recorded. The stress-strain plot displayed four distinct strain zones characterized by different slopes. The first zone, from 0 to 134 microstrain, represented a composite nail stiffness. The second and third zones showed softening due to concrete cracking. Finally, the fourth zone, not reached until 1,000 microstrain, represented the steel bar stiffness alone. The laboratory results were applied to the soil nail strain data in order to estimate nail loads.

Summary

The main topics of the nail load review included the reinforcing mechanism of soil nails, measured and predicted nail force magnitudes and distribution along the nail, and proposed and applied methods of interpreting strain gauge data. The most important points of this review are as follows:

- Soil nail forces develop by relative movement or shear between the initially passive inclusion and the deforming soil mass.
- Soil nails act mainly as tensile reinforcements, and their bending resistance may be ignored except at failure.
- The maximum tensile nail force is not located at the wall face but at some location behind the face where maximum straining of the soil occurs.
- A soil nail is a composite reinforcing member, and both the grout and steel may contribute to the stiffness of the nail.
- Strain measurements of the steel bar require interpretation of the grout influence to determine the total soil nail forces.

The above summary relates to experimental or actual soil nail walls instrumented with strain gauges. Previous researchers have proposed either of the following procedures to relate the measured strains to the nail loads. These are a) ignoring the concrete grout and reporting only the steel loads and b) performing laboratory tests by pulling on the ends of an instrumented steel bar encapsulated in grout, and correlating the composite stiffness measured in the laboratory with the measured strain data to estimate composite nail loads. An empirical method of predicting soil nail forces derived from instrumented soil nail results was also advocated.

CHAPTER 3

INTERPRETATION OF STRAIN GAUGE DATA

One of the major objectives of this study was to examine the distribution and magnitude of the soil nail forces in several soil-nailed walls instrumented with strain gauges. To do this, it was necessary to develop a method of interpreting the strain data measured on the steel reinforcing bars. This chapter discusses the method that was developed in this study to estimate the working nail loads for soil-nailed walls on the basis of the record of their performance.

The method of data interpretation was designed to yield the axial tensile forces that develop in the soil nails. It has been concluded that soil nails act primarily in axial tension, and bending resistance is not mobilized until failure is eminent (Chapter 2). The soil nails in the case studies were instrumented with strain gauges attached to the steel bar at various locations along the nail length. Figure 3.1 displays a typical cross-section of an instrumented soil nail. Commonly, strain gauges were attached in pairs, as shown in the figure, so that the average axial strains could be determined. If a particular instrumentation program did not install strain gauges in pairs, the measured strains were assumed to represent average axial strains. Whether axial strains were measured or assumed is noted later as the results are presented.

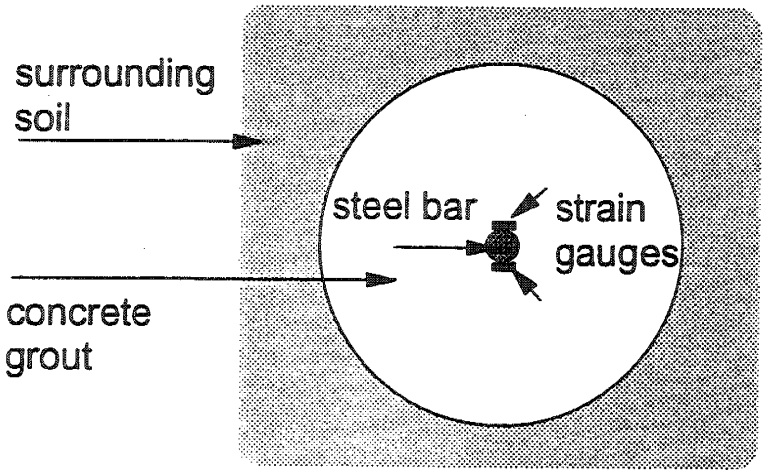

Figure 3.1. Typical soil nail cross-section

As shown in Figure 3.1, the soil nails can be viewed as composite structural members consisting of steel rebar and concrete grout. The strain gauges measure the strain in the steel rebar at the grout-steel interface. Calculating the axial load in the rebar at the gauge location from these data is relatively straightforward, as the steel bar can be assumed to behave as a linear elastic material. However, in many cases the steel load alone cannot account for all the axial forces required to maintain stability of the wall (Elias and Juran, 1990, Thompson and Miller, 1990, Sakr and Barrows, 1990). When the soil nails are placed in a large diameter borehole, the surrounding concrete grout may carry a significant portion of the total axial nail load. This was evident in the San Bernadino and Polyclinic soil-nailed walls, where 200-mm diameter nails were installed with 25-mm to 32-mm rebar (Elias and Juran, 1990, Thompson and Miller, 1990).

However, the basic difficulty in estimating the nail loads is to determine how the concrete grout contributes to the axial stiffness of the soil nail. First, the mechanical behavior of concrete is not linear elastic. Second, the time-dependent, nonlinear effects of curing and creep may introduce further complexities. In addition, unlike steel, the material is brittle and undergoes cracking at a relatively smaller load and strain level.

The method presented below accounts for both concrete curing and creep to estimate an effective modulus for the grout and to determine the tensile loads in the grout. In the event of cracking, the load carrying capacity of the grout is assumed to be limited by the ultimate tensile strength of the grout. The method derived in this study interprets concrete grout response from the measured strains at the grout-steel interface and estimates the actual force developed in the composite soil nail.

The mechanism of mobilizing the soil nail reinforcing action is reviewed in Section 3.1. This provides the background for understanding soil nail behavior and the assumptions involved in estimating nail loads from the method developed in this research. The method is explained in Section 3.2, along with the important mechanical characteristics of curing, creep, and cracking of

the concrete grout. Section 3.3 explains why the development of such a method was necessary in the context of the other methods described in Chapter 2.

3.1 DEVELOPMENT AND DISTRIBUTION OF NAIL FORCES

An idealized distribution of the axial force along the length of a soil nail is shown in Figure 3.2. Because the soil nails are installed passively, relative deformations between the soil nail and the surrounding soil must occur for the nails to act as reinforcements. As the lateral confining pressure on the soil adjacent to the cut is removed by excavation, the soil within the active zone tends to expand and deform towards the excavation. The resistance to this deformation develops at the soil-grout interface in the form of shear forces around the grout circumference. These shear forces are balanced by the axial forces within the soil nail. As explained earlier, this axial force is shared by the steel section and the concrete grout.

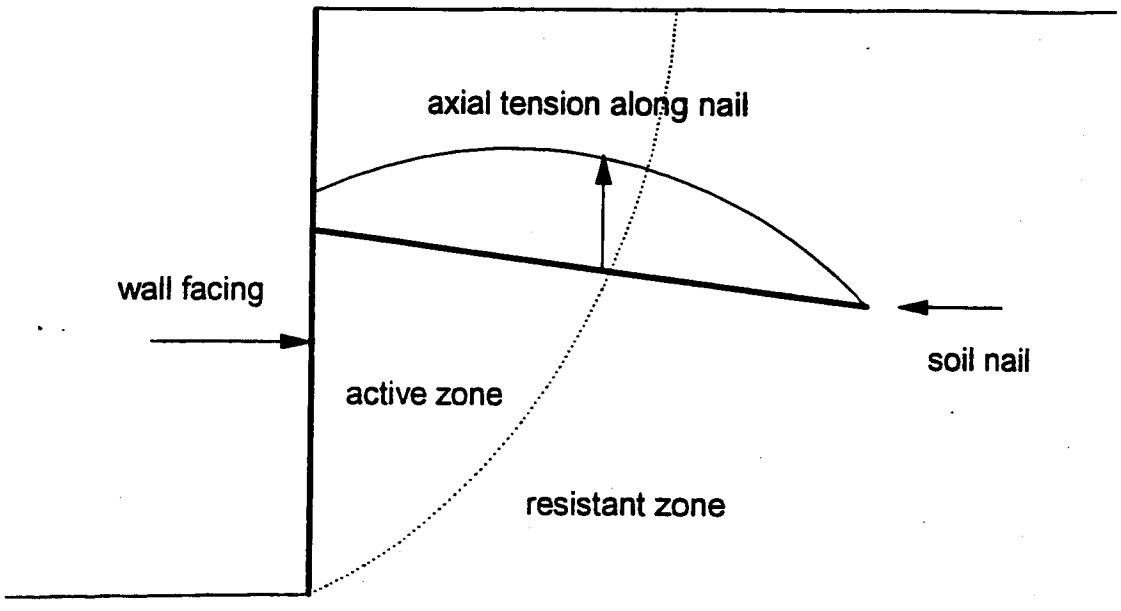

Figure 3.2. Idealized soil nail reinforcement

Because the shear stresses act along the circumferential area of the nail, the axial force at the ends of the nails must be zero. The force at the wall face may be zero or larger, depending on the characteristics of the facing elements. Presumably, the soil nail may develop its maximum axial force where shear stresses at the soil-grout interface reverse directions. The location of maximum force may coincide with the divide between the active soil wedge and the stationary soil mass. However, the actual magnitude and location of maximum nail force varies with the soil deformation pattern, construction sequence, and required reinforcement.

3.2 ESTIMATING AXIAL NAIL FORCES

The hypothetical load-deformation behavior of a composite cross-section in axial tension is shown in Figure 3.3a. Phase 1 reflects the composite behavior while the concrete grout remains intact. The contribution of the grout gradually decreases throughout Phase 2 as the grout undergoes cracking until the grout is no longer effective in Phase 3. It is clear from Figure 3.3 that the major issues in the development of a method for estimating the total nail forces were the composite stiffness during Phase 1, the strain level at the initiation of grout cracking, and the ultimate tensile capacity of the grout. The following sections are devoted to the considerations necessary to define a composite stiffness and to considerations related to cracking.

Note that the following assumptions were necessary: 1) strains measured at the grout-steel interface are uniform across the entire cross-section; 2) strain compatibility exists at the grout-steel interface when the tensile stress is low enough for the grout to remain intact.

Elastic Grout Properties with Curing Time

To determine the load carried by the concrete grout, the elastic modulus and tensile strength of the concrete must be known or assumed. However, these properties change with concrete curing time (Figure 3.3b). The nails must perform as reinforcements within a short period after installation and before the concrete has been fully cured. The loading on the nails continues to accrue until wall construction has been completed. Therefore, an appropriate elastic modulus and tensile strength, based on grout age, should be applied to the measured strains.

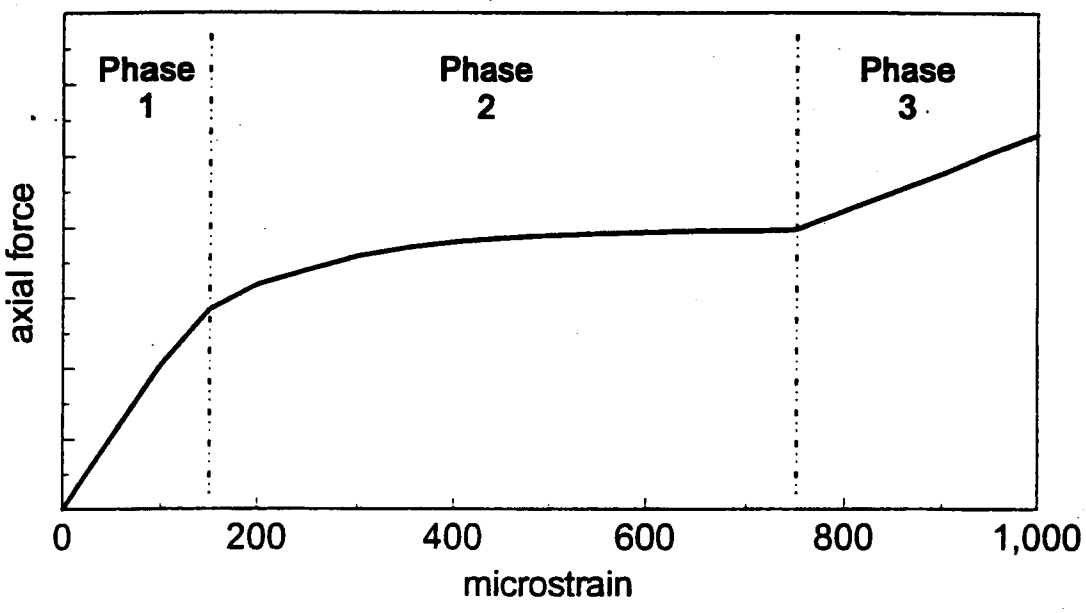

Figure 3.3a. A hypothetical laboratory load-deformation plot of a composite soil nail in axial tension

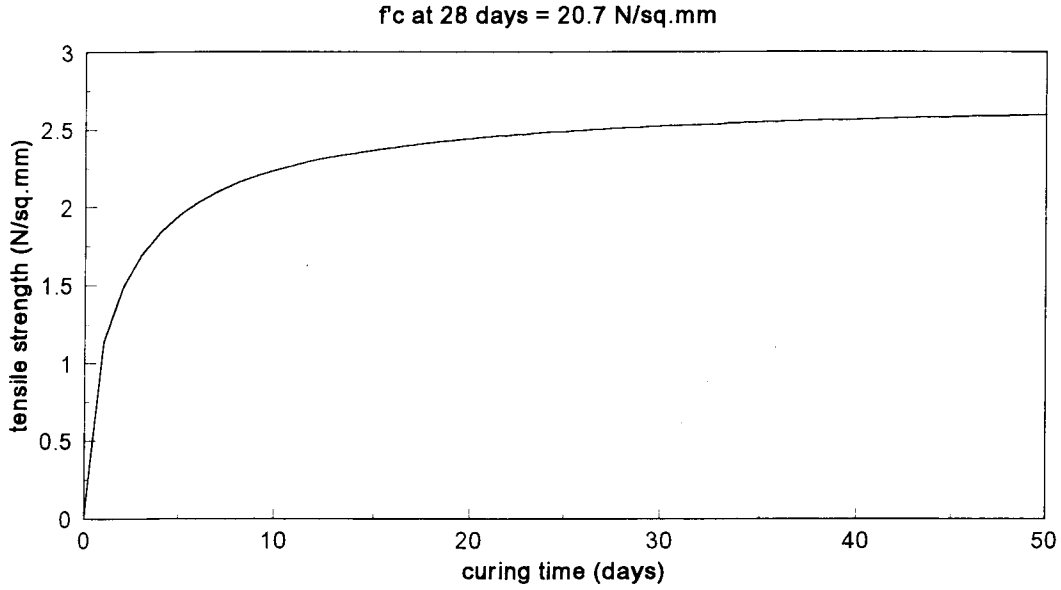

Figure 3.3b. Concrete tensile strength with curing age

To account for the variable loading conditions inherent in the sequence of construction, the elastic modulus of concrete must be estimated for an average curing age during construction for each nail. Because external loads are applied to the nail throughout the construction period, the tensile strength must be estimated for a curing age corresponding to the end of construction. External load changes after the end of construction can be considered to be insignificant unless specifically noted.

The average concrete grout age was determined between the time of nail installation and the end of construction (EOC), as shown in Figure 3.4. By considering the construction schedule and the strain history of the last instrumented nail installed, the EOC was chosen to be the date that strain changes leveled off, usually two weeks after the last instrumented nail had been installed. This allowed time for the facing to be constructed and completion of any other activities that may have influenced external nail loads.

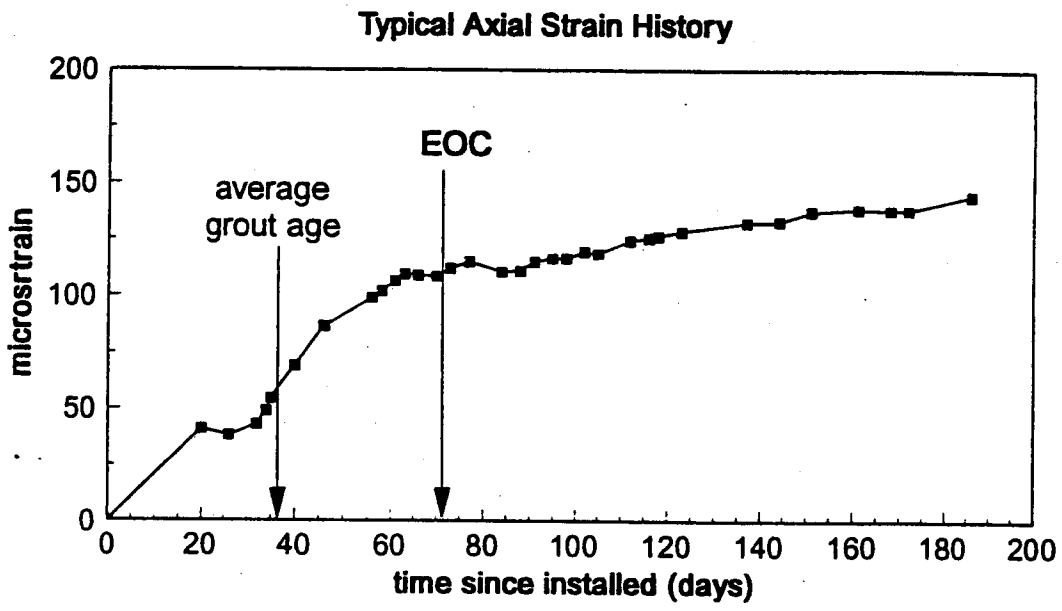

Figure 3.4. Determination of average grout age

Because the grout properties were not reported for any of the instrumented soil-nailed walls reviewed for this study, the empirical relationships published by the American Concrete Institute (ACI) were adopted for estimating the necessary concrete properties (ACI, 1992a). These relationships are given by Equations 3.1 through 3.3. Equation 3.1 provides the compressive strength of concrete, $(f_c')_t$, for any time based on a known 28-day strength, $(f_c')_{28}$, while Equation 3.2 relates the elastic concrete modulus, $(E_c^e)_t$, to the compressive strength. Equation 3.3 relates the direct tensile strength, $(f_t')_t$, to the compressive strength (ACI, 1992b).

$$(f_c')_t = (f_c')_{28} \frac{t}{(4+0.85t)} \tag{3.1}$$

$$(E_c^e)_t = 4800(f_c')_t^{\frac{1}{2}} \tag{3.2}$$

$$(f_t')_t = 0.55(f_c')_t^{\frac{1}{2}} \tag{3.3}$$

where t = age of grout in days, and $(f_c')_t$, $(f_t')_t$, and $(E_c^e)_t$ are in N/mm^2.

A typical value of the 28-day compressive strength, $(f_c')_{28}$ = 20.7 N/mm^2 (3000 psi), was assumed for all the cases; the other properties were determined by the above relationships.

Predicting Grout Creep and Stress Relaxation

Creep and/or stress relaxation phenomena are known to occur in concrete. Creep strain is defined as the additional strain that develops over time after a constant load has been applied and maintained. Stress relaxation, on the other hand, is gradual reduction in stress over time when a specimen is held at a constant strain. Despite no apparent external load changes, the measured strains in the nails continued to increase gradually after the end of construction. A typical example of this is shown in Figure 3.5 for the Polyclinic wall. It is likely that the load initially carried by the grout was gradually being transferred to the steel rebar because of creep (Byrne, 1992).

The mode of load transfer is presented in Figure 3.6 for a simple loading situation. When an axial tensile load is applied to a soil nail, as shown by position **a**, elastic strain occurs in both

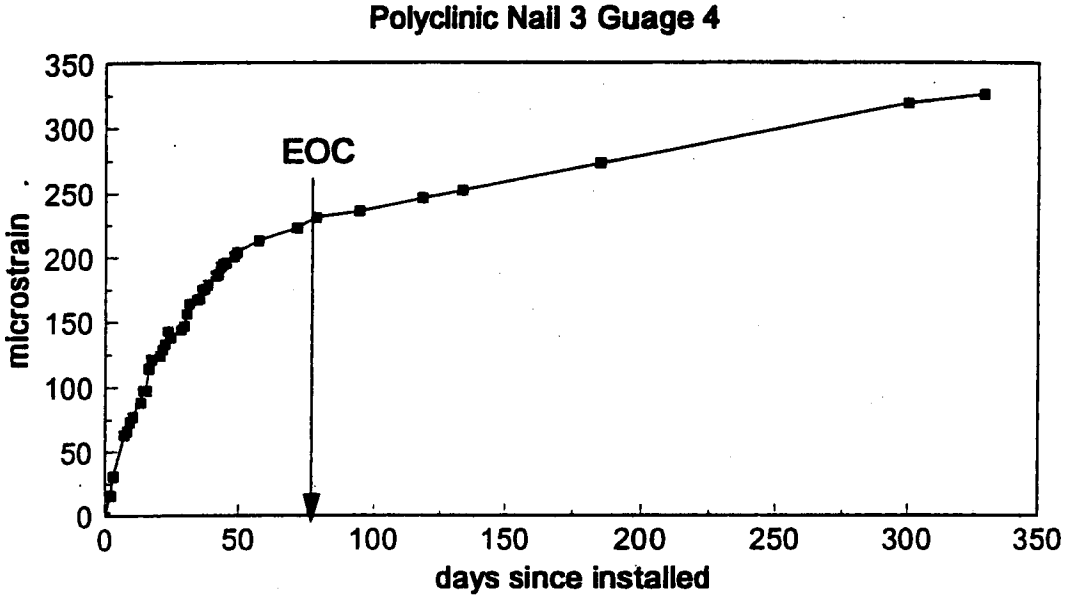

Figure 3.5. Long term strain increases that resemble creep

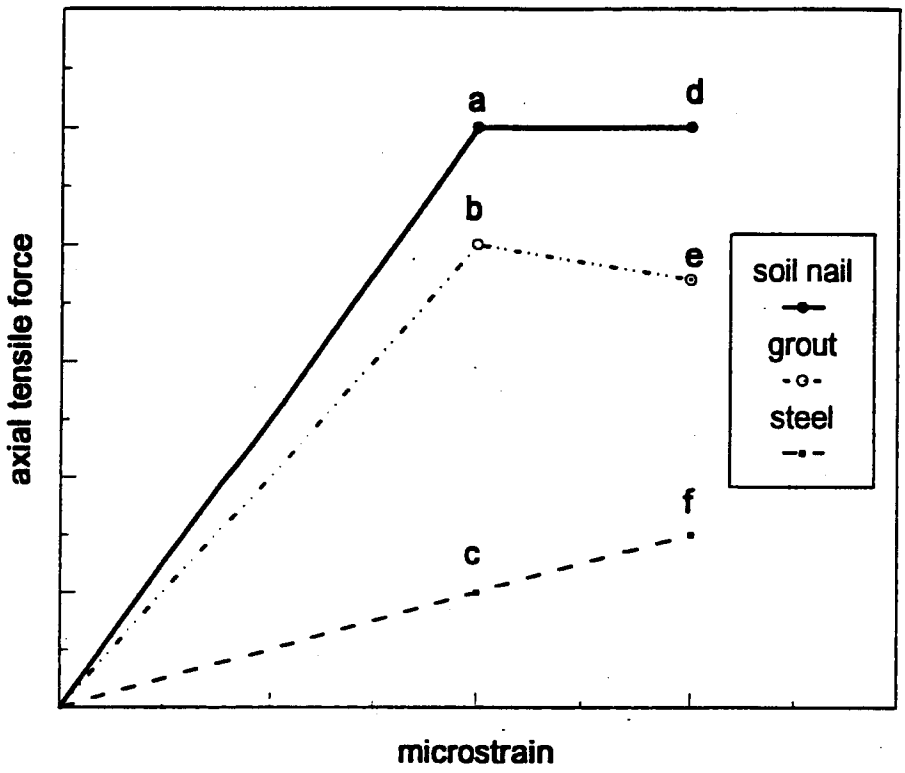

- **a:** initial soil nail force
- **b:** initial grout tensile force
- **c:** initial steel tensile force
- **d:** soil nail force after grout creep and stress relaxation
- **e:** grout tensile force after creep and stress relaxation
- **f:** steel tensile force after grout creep and stress relaxation

Figure 3.6. Response of soil nail, grout, and steel to grout creep and stress relaxation

the concrete and steel sections, as shown by positions **b** and **c**. If the load is maintained, the concrete grout will respond with a combination of creep and stress relaxation, and the final grout load is at position **e**. As the concrete grout creeps, the steel load increases to position **f**, since steel behaves as a linear elastic material. The total load in the soil nail remains constant, as shown between positions **a** and **d**.

To estimate the grout load after creep and stress relaxation have occurred, the ACI-209 estimating procedure was adopted (ACI, 1992a). Although this procedure was originally intended for concrete compressive loads of up to 40 percent of the ultimate strength, and soil nails are loaded in tension with loads often near 100 percent of the ultimate strength, no other generally accepted creep prediction methods were more suitable to the conditions of a soil nail. The limited research of concrete creep in tension indicates that it is similar to creep in compression for stresses at the same proportion to the ultimate strength (Neville, 1970). For stresses greater than 40 percent of the ultimate strength, the creep rate is higher than predicted by the procedure (ACI, 1992, a).

The ACI-209 procedure is given by the relationships presented in Equations 3.4 and 3.5. Equation 3.4 defines a creep ratio, v_d. The creep ratio is calculated from Equation 3.5.

$$v_d = \frac{\varepsilon_c}{\varepsilon_e} \tag{3.4}$$

$$v_d = \frac{Cd^{0.6}}{10 + d^{0.6}} \tag{3.5}$$

where v_d = creep ratio after d days

ε_c = creep strain

ε_e = elastic strain

d = duration of load in days

C = constant

The constant, C, depends on the moist cured concrete age at the time of loading, the surrounding humidity, and the thickness of the concrete member.

The creep ratio is used to determine an effective concrete modulus, $(E_c^s)_d$, as given by Equation 3.6. Since creep depends on load duration, for each date strains are recorded there is a corresponding effective concrete modulus. The effective modulus was used with the measured strains to determine grout load.

$$(E_c^s)_d = \frac{(E_c)_t}{1+v_d} \tag{3.6}$$

where t = average grout age in days

d = duration of load in days

The variables, t and d, are displayed in Figure 3.7. Figure 3.8 illustrates how the effective concrete modulus is used to determine the concrete grout load. For a given measured strain, the effective modulus is used to determine the final stress. The final stress is multiplied by the grout cross-sectional area to yield the grout load. The soil nail load is the sum of the grout load and steel load.

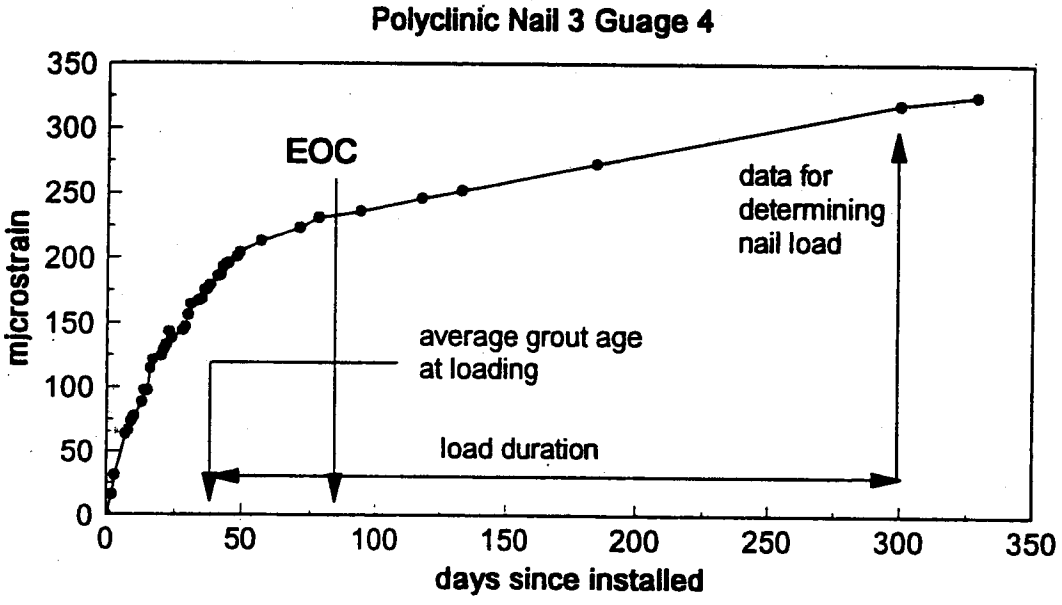

Figure 3.7. Typical stress-strain plot noting required time factors for estimating concrete grout creep

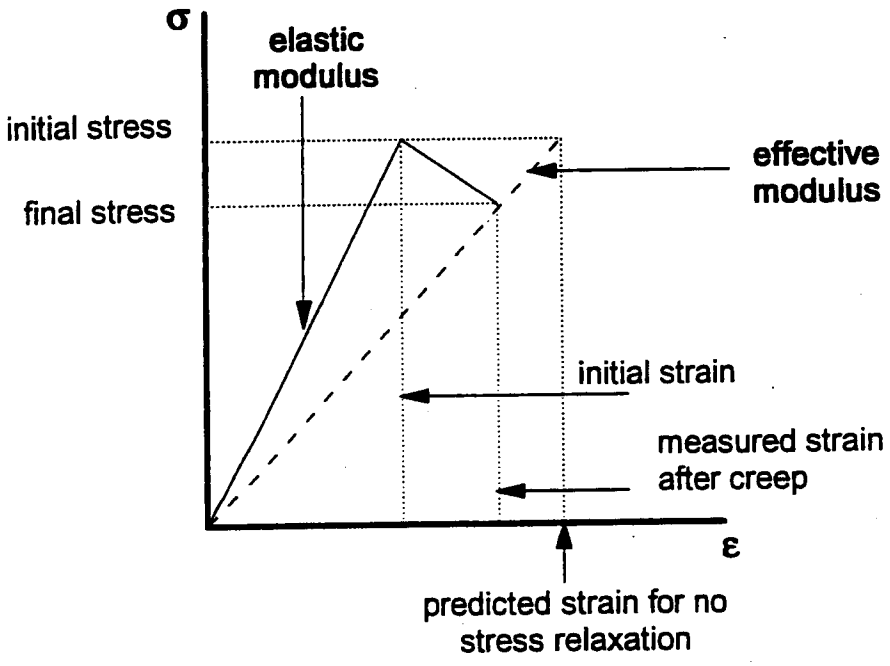

Figure 3.8. Idealized concrete grout stress-strain plot displaying effective modulus method

After estimating nail loads from strain data collected at various times after the end of construction for several instrumented walls, the researchers concluded that the ACI-209 method under-predicted the creep rate for soil nails. Nail loads estimated from data collected long after construction were larger than estimated nail loads using data collected at the end of construction, even though there was no evidence of external load changes to the nail. This indicated that concrete grout creep and stress relaxation occurred faster than was predicted.

For these reasons, in-service nail loads were estimated from data collected at the end of construction (EOC). By using data taken soon after all external loads had been applied to the nail, concrete grout creep had less influence on the estimated nail loads. The larger nail loads, estimated from strain measurements taken long after the end of construction, could be considered an upper bound nail load. The following section will show that when the grout cracks, a larger upper bound estimate is necessary.

Cracking of Concrete Grout

Figure 3.9 displays the stress distribution in a soil nail as the grout cracks. Far from any cracks, there is stress in both the steel and concrete. At a crack, there is no stress in the concrete. Near a crack, where bond stress develops between the concrete and steel, there is a transition zone in which there is more stress in the steel and less stress in the concrete. These three possible cases need to be defined to properly interpret the strain data.

Figure 3.10 is an example of how these three cases were defined for this study. The concrete grout stiffness was determined using an appropriate effective modulus for each date that strains were measured after the end of construction. The grout remains intact while the grout load, calculated with the measured strain, is less than the limit grout load defined by Equation 3.7. The limit nail load before cracking is calculated by Equation 3.8.

$$(P_c)_{\lim} = (f_t^{'})A_c \tag{3.7}$$

$$(P_{sn})_{\lim} = (P_c)_{\lim} + \varepsilon_{\lim} A_s E_s \tag{3.8}$$

where $\varepsilon_{\lim} = \dfrac{(f_t^{'})}{(E_c^s)_{EOC}}$

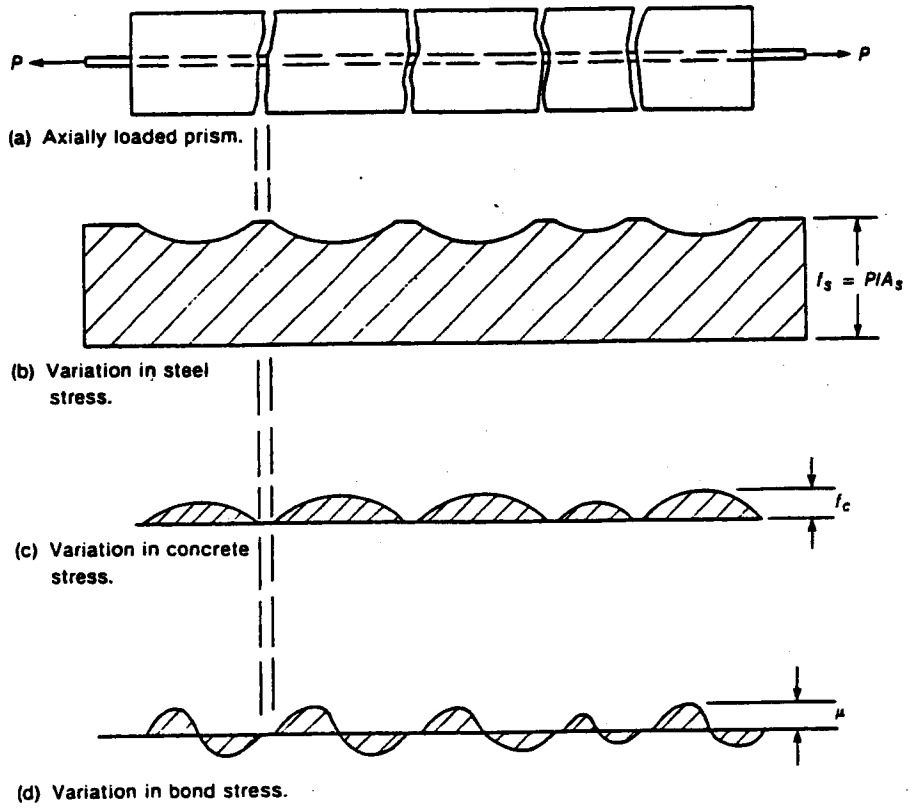

Figure 3.9. Steel, concrete, and bond stress in a cracked prism

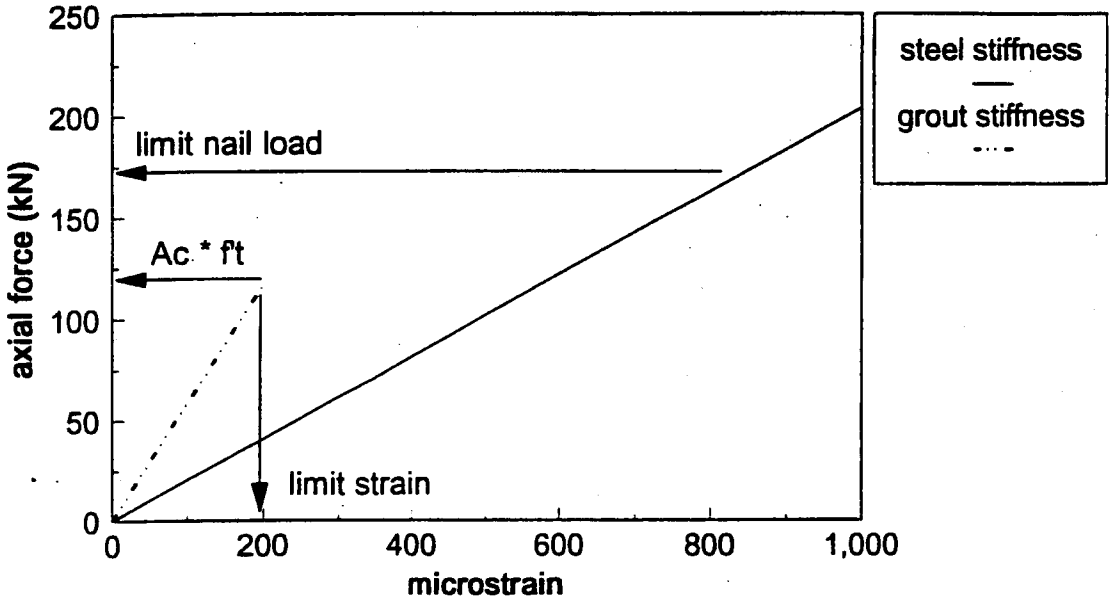

Figure 3.10. Typical stiffness relationship with limit strain and limit composite nail load noted

To estimate in-service nail loads, strain data collected at the end of construction were interpreted, as explained in Section 3.3.2. The grout load is calculated using the measured strain by Equation 3.9. The estimated in-service nail load is determined by Equation 3.10.

$$P_c = \varepsilon E_c^s A_c \tag{3.9}$$

$$\begin{aligned} P_{sn} &= P_s + P_c = \varepsilon(E_s A_s + E_c^s A_c) \quad \text{if } P_c \le (P_c)_{\text{lim}} \\ P_{sn} &= (P_{sn})_{\text{lim}} \quad \text{if } P_c > (P_c)_{\text{lim}} \end{aligned} \tag{3.10}$$

If P_c is greater than $(P_c)_{\text{lim}}$, the assumption of strain compatibility between the grout and steel is no longer valid because the grout load cannot be greater than the limit grout load. A crack has probably formed near the strain gauge, and bond stresses have developed between the steel and grout interface. In this case, the estimated nail load is the limit nail load.

The estimated nail load is constrained by lower and upper bounds. Because strain gauges are attached to the steel bar and steel behaves as a linear elastic material, the steel load can always be determined. Therefore, the lower bound is the largest steel load calculated from strain data collected any time after the end of construction. The upper bound is the largest composite nail load calculated from strain data collected any time after construction and is given by the following:

$$(P_{sn})_{\max} = (P_s)_{\max} + (P_c)_{\max} \quad \text{when} (P_c)_{\max} \le (P_c)_{\text{lim}} \tag{3.11}$$

Note that if the grout has cracked, the upper bound determined by Equation 3.11 assumes that the grout continues to carry its limiting load. Figure 3.11 displays the estimated nail load, as well as the lower and upper bounds for a typical nail calculated from only strain data collected at the end of construction. The three cases displayed in Figure 3.9 are clearly interpreted by the three slopes of the estimated nail load in Figure 3.11.

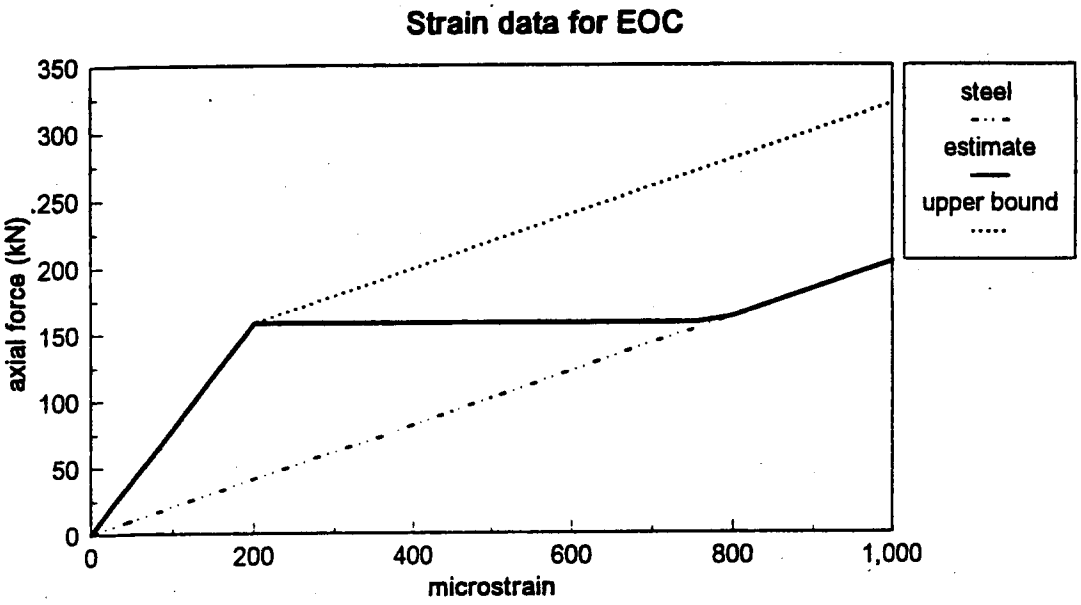

Figure 3.11. Estimated nail load, lower, and upper bounds for a typical nail

3.3 COMPARISON WITH OTHER METHODS OF ESTIMATING NAIL LOADS

In the previous chapter, two other approaches for calculating composite nail loads were discussed: estimating the composite stiffness with the measured strain data from which the occurrence of a crack can be recognized, and estimating the stiffness from the laboratory test data of a specimen with materials and dimensions similar to those of the soil nail. A discussion is necessary to explain why these methods were not used and why the present method was developed.

Among the case histories, only one (Polyclinic) set of data could be found with strain histories that showed definite signs of grout cracking. Although many other case histories reported strains large enough to have caused (at least to be interpretated as to have caused) grout cracking, no jumps in strain were visible. Hence, the first method could not be applied to all case histories. Again, there is no way of knowing if a crack has occurred at the gauge location. If **a (?)** crack does not occur right at the strain gauge, grout stress may be only partially released at the gauge, and this **first (?)** approach will under-estimate the composite nail stiffness (Figure 3.9). Additionally, if changes in the external load have occurred during this period of cracking, strains before and after cracking should not be assumed to be due to the same composite nail load.

Estimating nail loads by using laboratory measured stiffness is a completely different approach from the present method. When strains are correlated with laboratory test information, no assumptions of material properties or response are necessary. A known direct axial tensile load is applied and can be measured with strain gauges attached just as they are in the soil nails. The grout strength and strain relations are tested directly on the same materials used for the in-service soil nails. The changes in stiffness due to grout cracking can be recorded, as a large loading range can be applied.

The first limitation of this method is the fact that the laboratory loading mechanism is somewhat different than that the soil nails experience. In the laboratory, the free ends of the

steel bar are pulled, as opposed to the application of shear stresses to the grout exterior circumferential area. The method of loading and the response of actual soil nails are more complex, variable, and difficult to predict than the simple direct tension applied in the laboratory. It would be difficult to simulate the grouting, casting, and curing of a soil nail in the laboratory. Another important limitation is that the laboratory testing occurs rapidly at a single concrete age and hence, can not account for a soil nail loaded in stages at different curing ages, nor can it account for the creep and stress relaxation of the concrete grout.

The main reason for developing the present method was to allow an assortment of case histories to be analyzed a single, consistent approach. The composite stiffness could not be found for most of the instrumented soil nail walls because jumps in the strain histories were not observed. The method based on the laboratory testing is a site-specific method. Therefore, a method that could account for concrete creep was desirable so that the long-term strain measurements could be interpretated.

CHAPTER 4

NAIL LOAD ESTIMATES FOR IN-SERVICE WALLS

A procedure for estimating soil nail loads from the interpretation of strain gauge data is described in the previous chapter. This procedure was applied to data sets from several soil-nailed walls instrumented with strain gauges, and the resulting estimated nail loads are reported in this chapter. For each case history, the soil-nailed wall and instrumentation program is described, and the estimates of axial tensile forces in the nails, after the end of construction, are presented.

Section 4.1 presents examples of interpreting the strain data using the procedure described in Chapter 3. The examples illustrate how grout creep and cracking affect the estimated nail loads and the upper bounds of the estimates. Section 4.2 describes each of the instrumented soil-nailed walls and presents the estimated nail loads. In Appendix 2, the values of the estimated axial nail force, the steel bar force, and the upper bound estimate for each strain gauge location along the instrumented nails are reported.

4.1 EXAMPLES OF STRAIN DATA INTERPRETATIONS

Figure 4.1 (A) illustrates the interpretations of strain data for the Guernsey wall which, had small diameter (115-mm) soil nails. The strain gauges, located 3 m and 7 m from the face, recorded strains high enough that the calculated composite load exceeded the assumed limit nail load. This was interpreted to mean that grout cracking had occurred near the strain gauges, and the limit nail load was considered to be the estimated nail force. The upper bound estimate assumes the grout continued to carry a load equivalent to its ultimate tensile strength. It represents the sum of the measured steel load and the assumed limit grout load.

The strain gauge located at 5 m from the face recorded high steel strains. In this case, the measured steel load exceeded the limit nail load; hence, the measured steel load was the

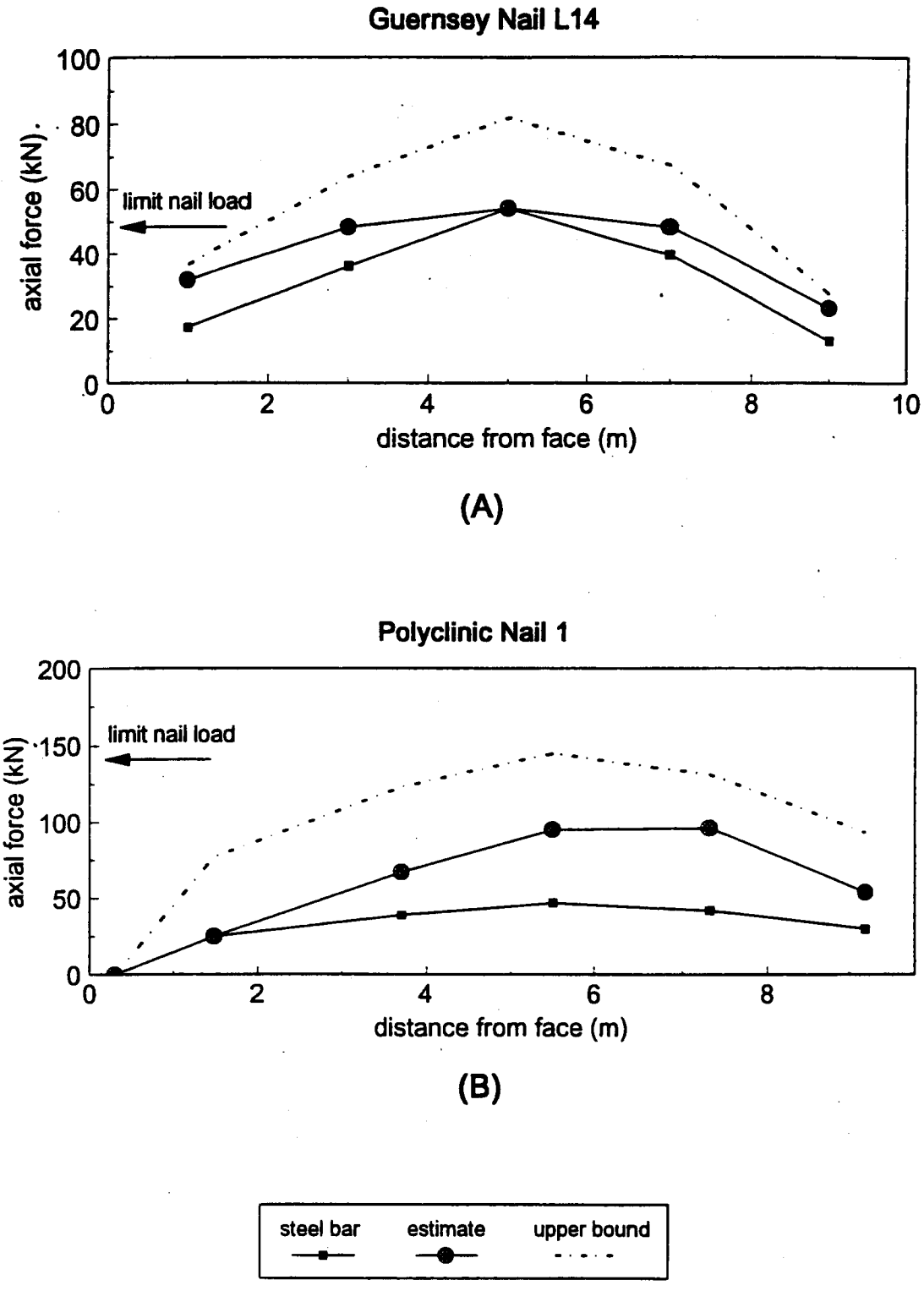

Figure 4.1. Examples of interpreted nail forces

estimated nail load, which implies that the grout no longer contributed tensile strength to the nail at this location. Again, the upper bound represents the sum of the measured steel load and the limit grout load.

Figure 4.1 (B) illustrates how strain data were interpreted when the grout appeared to creep at a faster rate than predicted by the creep ratio. This figure is from the Polyclinic Wall, where large diameter (229-mm) soil nails were used. The strain gauges along the nail measured relatively low strains. The calculated composite load was less than the limit nail load for the data collected at the end of construction. Because there was no evidence of a change in external loads, the estimated nail forces at these locations were the composite nail loads calculated from data collected at the end of construction. However, when data collected long after completion of construction were used, higher nail forces were calculated, implying that the method of predicting creep under-estimated the actual creep rate. Therefore, the upper bound estimate was defined as the largest composite nail load calculated with data from any time. The largest steel load calculated from data collected at any time was considered to be the lower bound at each gauge location.

4.2 RESULTS OF INSTRUMENTED SOIL-NAILED WALLS

The working nail loads were estimated for ten instrumented soil-nailed walls from which strain gauge data were available. The strain histories allowed the quality of the data to be assessed and provided the necessary time parameters, such as grout age for calculating curing and creep, and an appropriate end of construction (EOC) date to be determined. Other case histories that did not provide strain time histories, important construction dates, or only reported estimated nail loads were not used for this study.

The important characteristics such as type of structure, soil type and stratigraphy, and the extent of instrumentation are first described. These are followed by an assessment of the data quality and estimates of in-service nail forces. The results for each wall are presented in a figure that includes a schematic drawing of the cross-section and a plot of the maximum nail load in

each nail. The axial nail force distribution is drawn above each instrumented nail on the cross-section, and the estimated maximum nail loads for each instrumented nail are graphed against the depth of excavation. Similar to the work of Juran and Elias (1991), an empirical diagram of the apparent earth pressures is also plotted to provide a relative measure of the maximum nail loads so that walls with different geometry may be compared qualitatively. This empirical diagram was calculated from the reported design soil parameters. The value of the coefficient of active lateral stress, K_a, was adjusted to account for face slopes and backslopes, and uniform surcharges were modeled as an equivalent height of soil added to the wall height.

Table 4.1 presents the geometry and structural characteristics of each wall analyzed in this study. The details of the geometry and/or structure are provided, as deemed necessary, under the discussion of each wall.

Swift - Delta Station 1

This wall was constructed below an existing bridge abutment. The designers modeled the abutment as 3 m of soil above the wall without nail reinforcement. The bridge was supported by one row of 355-mm steel pipe piles located 0 to 1 m behind the soil nail wall facing and extending below the toe of the wall. The nails were installed between bridge piers, which dictated the 1.4-m horizontal spacing. As shown in Figure 4.2, the bottom nail was inclined at 25° below the horizontal. Although the figures in the paper by Sakr and Barrows (1991) show a slight inclination of the wall face, a vertical face was assumed for this study because no details regarding face inclination were provided in the report.

The soil was a fill characterized as medium dense, damp to moist, poorly graded sand. The groundwater table was located 2 m to 3 m below the base of excavation. The design soil parameters were $\phi = 33°$, $c = 4.8$ kN/m^2, $\gamma = 18$ kN/m^3, and $K = 0.43$ (Sakr and Barrows, 1991).

Each of the five nails were instrumented at five locations. A strain gauge was installed on the top and bottom of the steel bar at each location. After assessing that both gauges were working properly, the average of the top and bottom measurements was used as the axial strain.

Table 4.1. Geometry and structure characteristics of analyzed soil nail walls

	Swift-Delta Station 1	Swift-Delta Station 2	Polyclinic	Peasmarsh	Guernsey
Height (m)	5.3	5.6	16.8	11	20
Face slope (deg)	0	0	0	20	30
Back slope (deg)	55 kN/m2 surcharge	27	0	0	0
Type of Facing	shotcrete	shotcrete	shotcrete	geogrid	geogrid
Nail Length (m)	6.4	5.2	10.7	6 - 7	10
Nail Inclination (deg)	15	15	15	20	20
Nail Diameter (mm)	127	127	229	127	115
Steel Diameter (mm)	29	29	36	25	25
Spacing, H x V (m)	1.4 x 1	1.4 x 1	1.8 x 1.8	1.5 x 1.5	1.5 x 1.25

Table 4.1. Geometry and structure characteristics of analyzed soil nail walls (Continued)

	IH-30, Rockwall Section A	IH-30, Rockwall Section B	San Bernadino	Cumberland Gap 1988	I-78, Allentown
Height (m)	5.2	4.3	7.6	7.9	12.2
Face slope (deg)	0	0	6	0	3 m bench
Back slope (deg)	0	75 kN/m2 surcharge	5	33	33
Type of Facing	shotcrete	shotcrete	shotcrete	shotcrete	concrete panels
Nail Length (m)	6.1	6.1	6.7	13.4	6.1 - 9.2
Nail Inclination (deg)	5	5	12	15	10
Nail Diameter (mm)	152	152	203	114	89
Steel Diameter (mm)	19	19	25	29	25 - 32
Spacing, H x V (m)	.75 x .75	.75 x .75	1.5 x 1.5	1.5 x 1.2	1.5 x 1.5

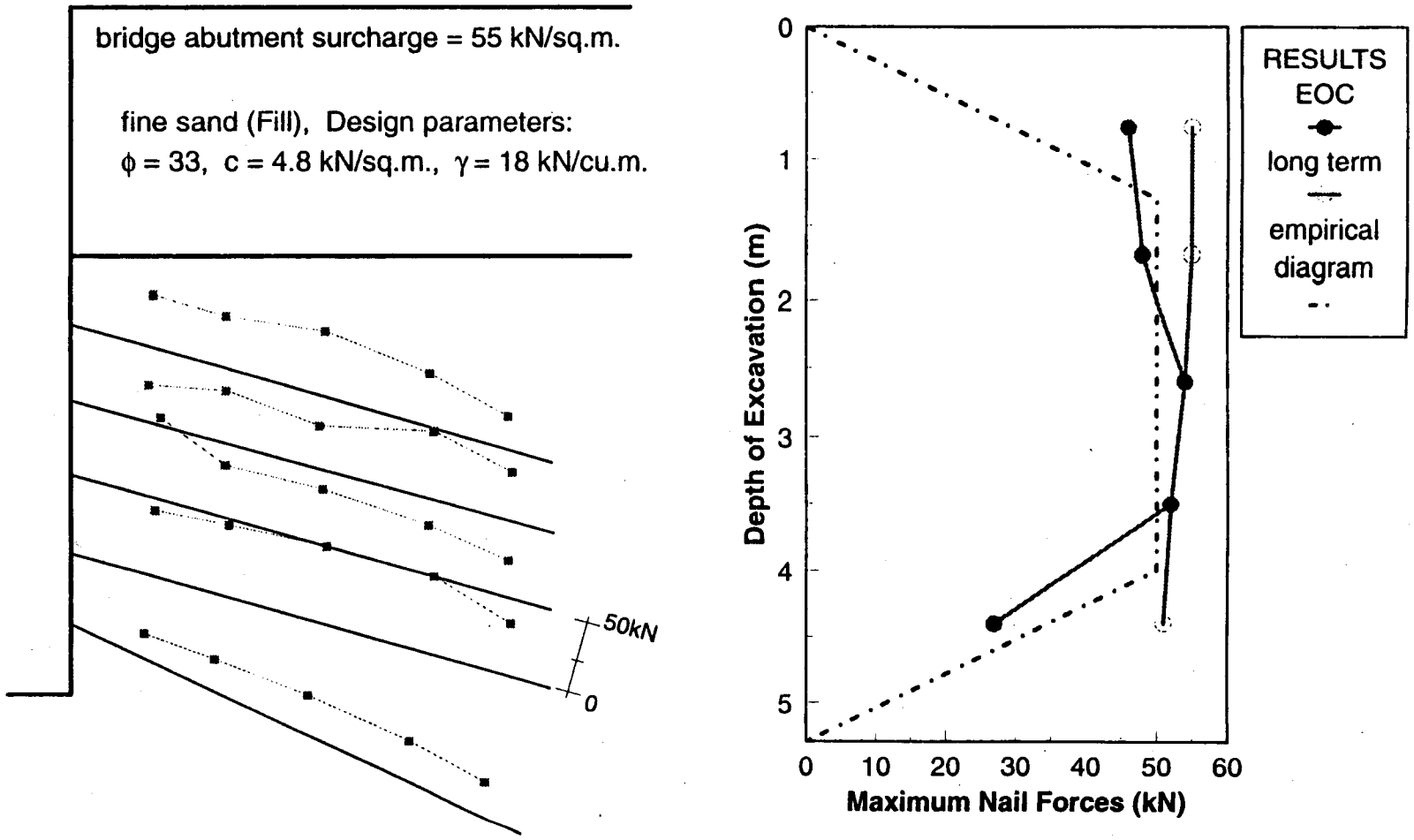

Figure 4.2. Swift-Delta Soil Nail Wall Station 1 axial nail force results

The strain data were recorded at least once a week during construction and then once every month for one and a half years after construction. The pairs of gauges located near the wall showed signs of bar bending. It is not known whether the strain readings were adjusted for temperature.

Inclinometers recorded movements for a long time after completion of construction, indicating possible soil creep. This made estimating in-service nail loads difficult. As explained in Chapter 2, the concrete creep model tends to cause long-term nail forces to be over-predicted. If the soil creeps, actual nail forces in the nails increase, and long-term nail forces have to be estimated. Therefore, the results presented in Figure 4.2 include two sets of maximum nail loads—estimated maximum nail loads at the end of construction, and the largest estimated maximum nail loads calculated from data collected any time after construction.

The estimated maximum nail loads were slightly higher than the empirical diagram predicts. The magnitudes were similar to the loads estimated by the Oregon Department of Transportation using a laboratory stiffness correlation (Sakr and Barrows, 1991). This is notable, as the two methods approach the composite stiffness effect in completely different ways. The axial force distributions along the nails were relatively uniform.

Swift - Delta Station 2

This station was not located beneath the bridge abutment, but approximately 15 m to the west. There were no piles or surcharge except for the 27° backslope. The wall was constructed with the same materials.

Explorations near Station 2 encountered fill soils that consisted of silty fine sand with rock and debris to 2 m. Clayey silt was present from 2 m to 3 m. Below 3 m was the same sand fill that was present at Station 1. Groundwater was 2 m to 3 m below the base of excavation. The design soil parameters were the same as those reported for Station 1.

Instrumentation was the same as that for Station 1, except only four locations on each nail were instrumented because the nails were shorter. The strain data were collected in the same manner as that for Station 1.

Inclinometer measurements indicated soil creep at this station also; therefore, estimated maximum nail loads at the end of construction and long-term maximum nail loads are plotted in Figure 4.3. The estimated maximum nail loads were approximately the same as those for Station 1, which means they were higher relative to the empirical diagram. This may be because of the low load carried by the first nail, the different fill materials, and/or the increased depth of excavation below the bottom nail. The axial force distributions along the nails were relatively uniform, except for the peaks in the second and third nails. These peaks appeared to be located near the top and bottom contact of the clayey silt layer.

Polyclinic

The geometry and structural parameters listed in Table 4.1 were stated in the data package received from Golder Associates. These were used for the nail load estimations. Note that Thompson and Miller (1990) stated the nail diameter as 203 mm and the steel diameter as 32 mm. These values would reduce the loads by the change in grout and steel areas. Nail 1 was installed at an inclination of 20° below the horizontal, as shown on Figure 4.4, to avoid existing utilities.

The soil consisted of a fill for the top 2.4 m, underlain by overconsolidated glacial outwash sand and gravel. Below the bottom of the wall, explorations encountered lacustrine fine sand and silt. The groundwater table was below the depth of excavation. Design soil parameters were $\phi = 40°$, $c = 9.6$ kN/m^2, and $\gamma = 21.2$ kN/m^3 (Thompson and Miller, 1990).

Five of the nine nails were instrumented with four to six strain gauges. The instrumented nails are labeled on the wall cross-section in Figure 4.4. A single strain gauge per nail location was installed at the 3 o'clock position of the rebar. The strain readings were corrected for temperature changes. The data were recorded every workday during construction and six data sets were recorded after construction, the last set recorded nine months after the end of construction.

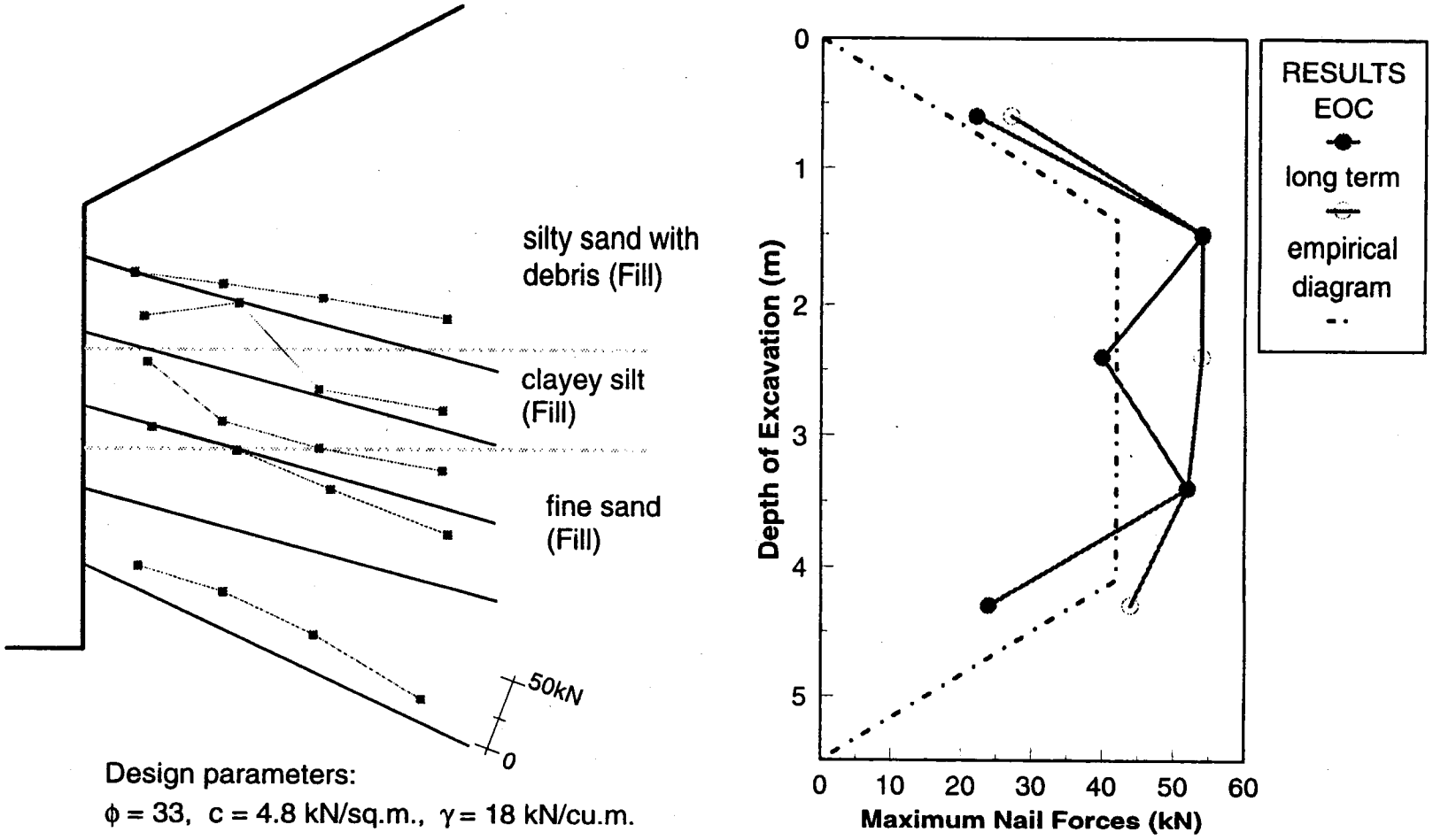

Figure 4.3. Swift-Delta Soil Nail Wall Station 2 axial nail force results

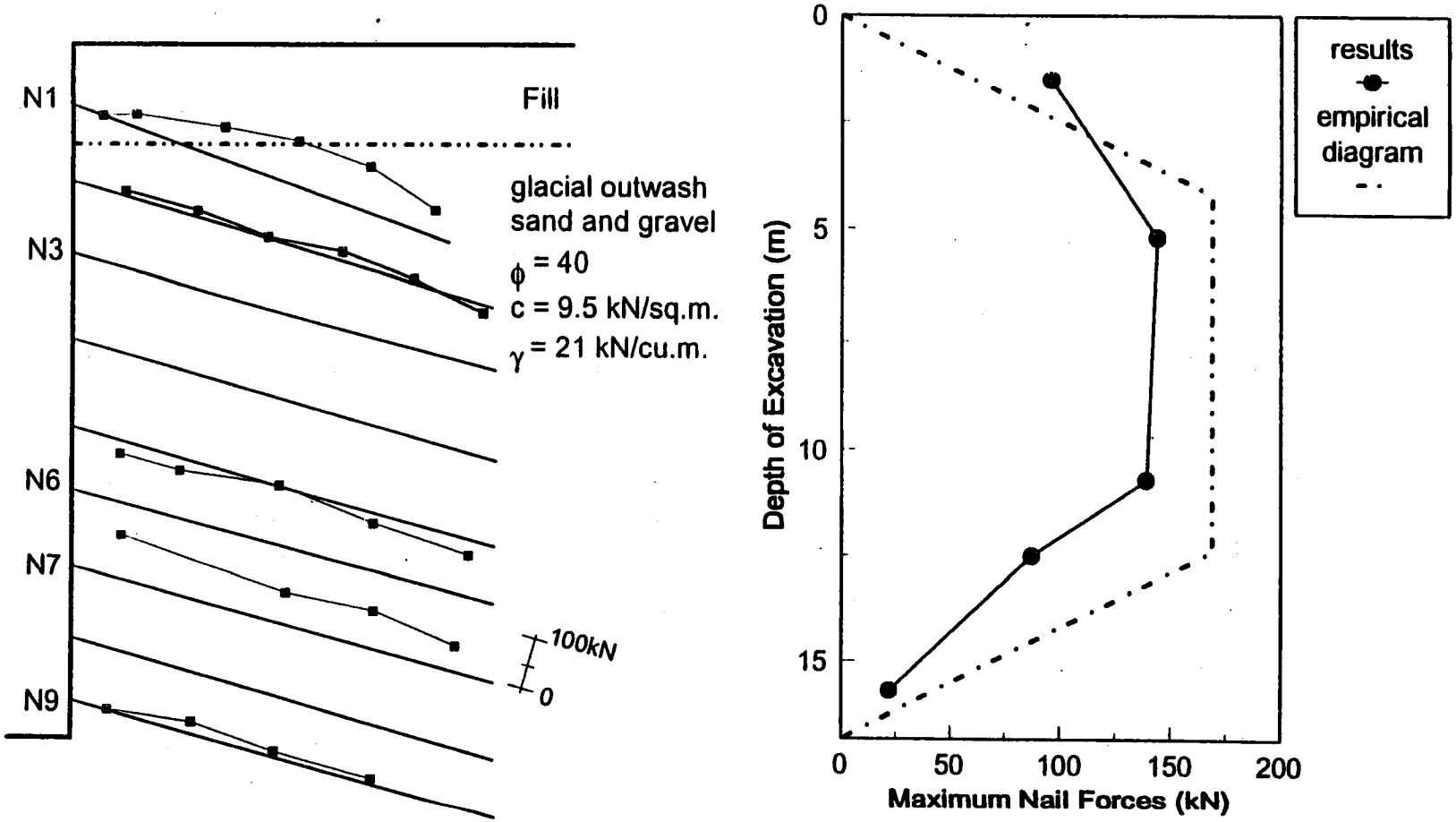

Figure 4.4. Polyclinic Soil Nail Wall axial nail force results

The measured strains were assumed to be axial. Possible bending of the nails cannot be accounted for, as only one gauge was installed at each location along the nail. In each of the instrumented nails the strain gauges installed nearest the face were most likely to have measured bending effects. Their strain history patterns were inconsistent with other gauges and most showed relatively high loads except for those installed on Nail 1, which indicated compressive strains. The influence of the facing probably caused bending of the rebar in this nail. Most of the gauges measured gradual strain increases with time after construction. The strain increase was most likely due to concrete grout creep, as the inclinometer data indicated no movements during this time.

The results are presented in Figure 4.4. The maximum nail loads were similar to estimates made by Thompson and Miller (1990) and Byrne (1992). Except for the top nail, the estimated maximum nail loads were less than those predicted by the empirical diagram. The axial nail force distribution along the nails appearred relatively uniform. Implied high forces near the face were probably due to bending that could not be measured.

Gauge 2 in Nail 3 and Gauges 2 and 3 in Nail 6 measured jumps in strain that appear to represent the grout cracking very near the strain gauges. In Nail 6, Gauge 2 cracked 100 days after construction, while Gauge 3 cracked during construction. In both cases the estimated composite nail load prior to cracking was comparable to the steel load after cracking. The strain data from these gauges provided an encouraging independent check of the present method of estimating the nail forces. Because of the large nail diameter (thus large grout section), estimated nail forces were much larger than steel bar forces except where apparent cracking was observed, as shown in Figure A2.3. In this case history, it was important to consider the composite nail section when interpreting the strain data.

Peasmarsh

The soil nails consisted of the instrumented steel bar grouted within a thin, corrugated PVC sheath, which was grouted within the borehole. The top two nails were 6 m long, with a

1.5-m horizontal spacing, and the bottom four nails were 7 m long with a 1.75-m horizontal spacing. This is shown on the wall cross-section in Figure 4.5.

The soil consisted of dense, iron cemented silt and fine sand in the top 3.5 m. Stiff, silty clay with bands of claystone was located from 3.5 m to 5 m below the top of the excavation. Below 5 m was interlaminated, very stiff, silty clay with claystone and siltstone. These strata were considered to be horizontal. The groundwater table was not present within the depth of excavation. The design soil parameters were $\phi = 30°$, $c = 0$, and $\gamma = 20$ kN/m^3 (Pedley and Pugh, 1992).

The first, third, and fifth nails were instrumented with strain gauges at five locations along each nail. Data were collected up to one year after construction. The strain histories were received in the form of steel load versus time, which was easily converted to strain histories. The report of the case history (Pedley and Pugh, 1992) did not mention strain gauges used in pairs, but did say only axial tension was observed and no bending. There was no discussion of strain readings corrected for temperature.

The results are presented in Figure 4.5. Except for the top nail, the magnitudes were comparable to those indicated by the empirical diagram. The force distribution shapes reflected the ideal distribution illustrated in Figure 3.2. This result was probably due to the sloped face with geogrid protection, which would cause less disturbance to the facing end of the nails than construction of a vertical shotcrete face.

Guernsey

The nails were installed to reinforce a 20-m slope, in which excavation steepened the bottom 14 m to 70° from the existing 52° slope. At a later time, excavation continued below the toe, and a mini-pile wall was constructed. The nail loads were estimated before the additional excavation in order to analyze a structure comparable to the other soil-nailed walls.

The soil was described as a clayey, silty sand, residual soil underlain by granitic gneiss. The contact was variable and approximately sub-parallel to the original slope. The approximate contact is shown on the wall cross-section in Figure 4.6. The groundwater table was not present

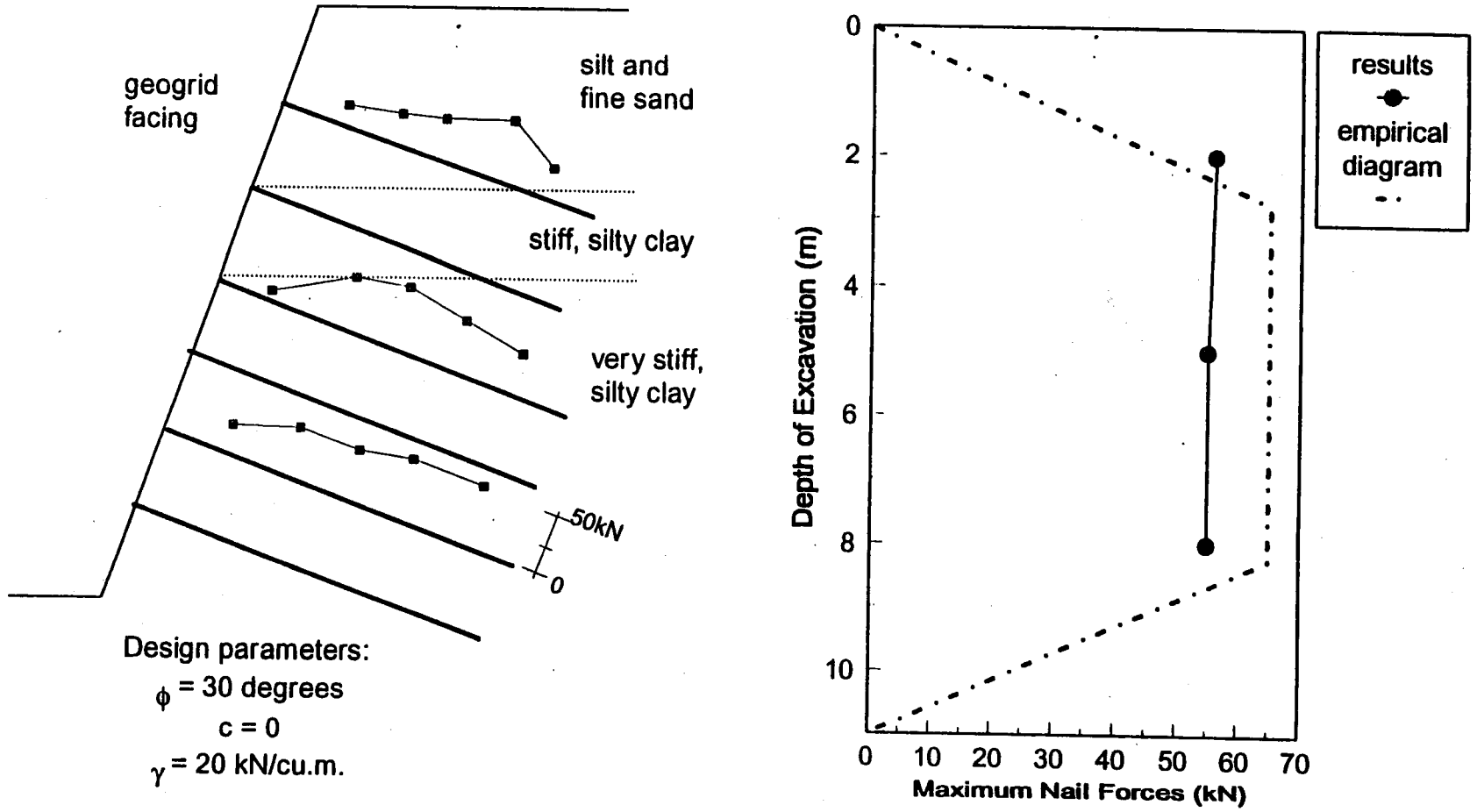

Figure 4.5. Peasmarsh Soil Nail Wall axial nail force results

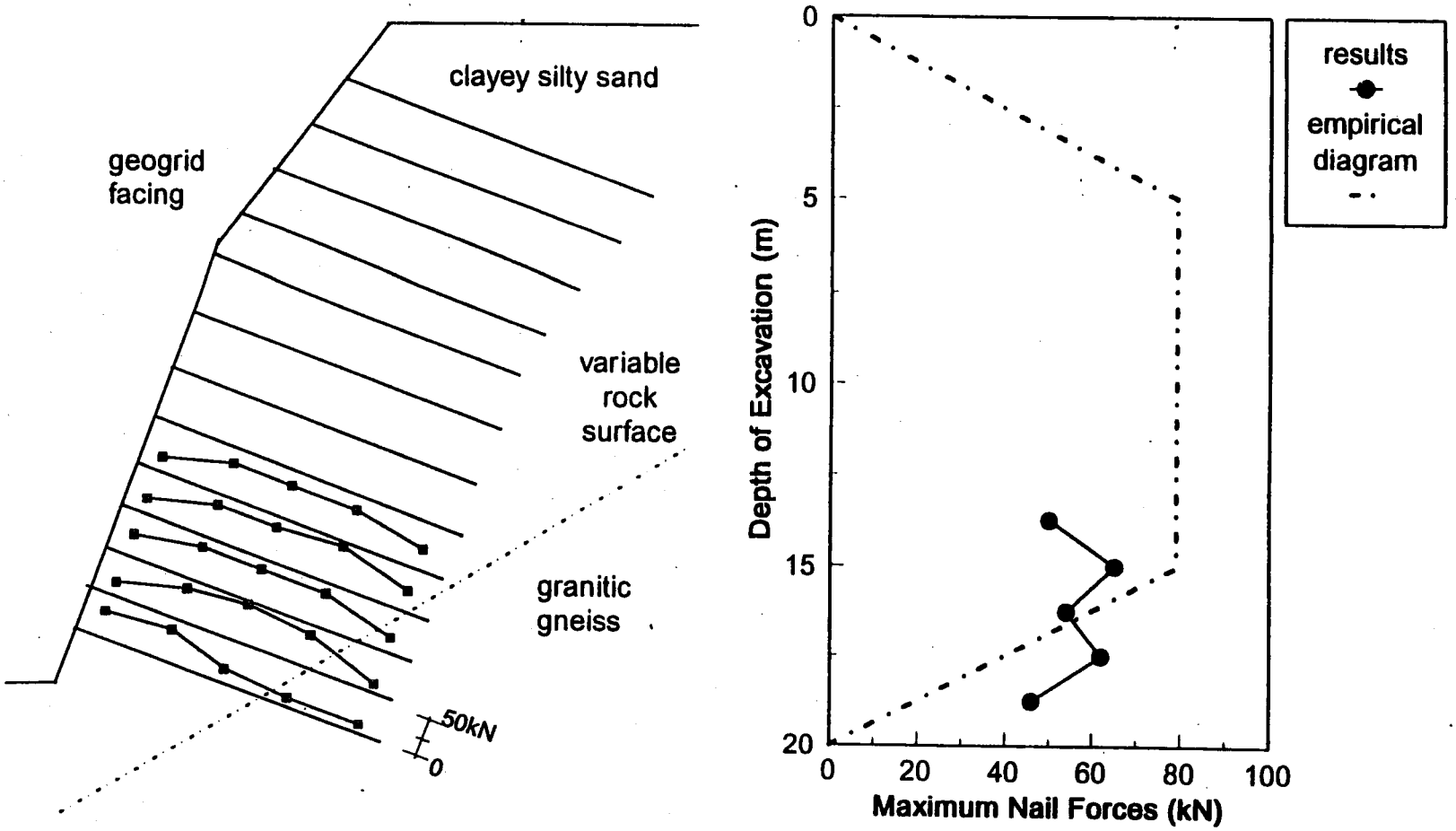

Figure 4.6. Guernsey Soil Nail Wall axial nail force results

within the depth of excavation. On the basis of the above information, the soil properties were assumed to be $\phi = 34°$, $c = 5$ kN/m^2, and $\gamma = 20$ kN/m^3.

The bottom five nails were instrumented with strain gauges installed in pairs at five locations along each nail. The strain readings were collected daily during construction until two weeks after construction. The last set of strain data used in this study was collected one month after the end of construction. The strain data from the two gauges at each location were adjusted for temperature and then averaged to obtain axial strains. The data did not indicate significant nail bending of the nails.

The results are presented in Figure 4.6. The estimated maximum nail loads were less than predicted by the empirical diagram. This may have been because the residual soil was stronger than the assumed soil parameters suggested. The distributions of axial nail force along each nail reflected the idealized shape illustrated in Figure 3.2. This result may have been due to the sloped, geogrid facing, which would cause less disturbance to the nail than shotcrete facings on vertical walls. The bottom nail force distribution peaked close to the face, as would be expected, but this may also indicate that the majority of the nail length penetrated the underlying rock.

IH-30 Rockwall, Texas Section A

The soil was characterized as very soft to soft, moist, clay (CH). The groundwater table was not present within the depth of excavation. The design soil parameters were $c = 13.4$ kN/m^2, $\gamma = 18.9$ kN/m^3, and $K_a = 0.5$.

The strain gauges were installed at two to four locations along each nail. The strain gauges were not used in pairs, so bending could not be detected, and the data were assumed to represent axial strains. Corrections for temperature were not mentioned in any of the information received. The strain readings were recorded every one to four days during construction and weekly after construction for three months.

The data from gauges located 1 foot from the wall face were difficult to interpret because the strain histories had an inconsistent pattern, and some large changes occurred after the end of

construction. These may have been due to bending and/or temperature changes. Because of construction problems, the instrumented nail in the second row (Nail 2) was installed after excavation for the third row of nails. This caused the low maximum nail load evident in Figure 4.7.

The estimated maximum nail loads, presented in Figure 4.7, were slightly higher than loads estimated during design (maximum of 40 kN) and much higher than predicted by the empirical diagram. The empirical diagram was calculated on the basis of a purely frictional soil, using the design K_a. Calculating the diagram for a cohesive soil yielded much smaller values. The force distributions along the nails were relatively uniform; however, the forces near the face may have been influenced by bending, temperature changes, or facing loads.

IH-30 Rockwall, Texas Section B

This cross-section was constructed under a 2.7-m bridge abutment located 3 m back from the top of the wall. The bridge abutment was modeled as a 75-kN/m^2 surcharge. The soil, instrumentation, and assessment of the data were the same as for Section A. Nail 2 in this section was also installed after excavation for the third nail row.

The estimated nail force results, presented in Figure 4.8, were also similar. The estimated maximum nail loads were larger than those the empirical diagram predicted. The distributions of axial force along each nail were relatively uniform.

San Bernadino

Two cross-sections with the same geometry, materials, and soil were identically instrumented. The estimated axial nail force results are presented for both sections (Figures 4.9 and 4.10); for discussion, both sections were considered to be the same soil-nailed wall.

The soil consisted of a highly variable silty, gravelly sand with cobbles and boulders. The groundwater table was not present within the depth of excavation. Laboratory testing results indicated $\phi = 34°$ to $42°$ and c = 7.2 kN/m^2 (Elias and Juran, 1990). The empirical diagram was calculated using the assumed soil parameters $\phi = 38°$, c = 7.2 kN/m^2, and $\gamma = 17.3$ kN/m^2.

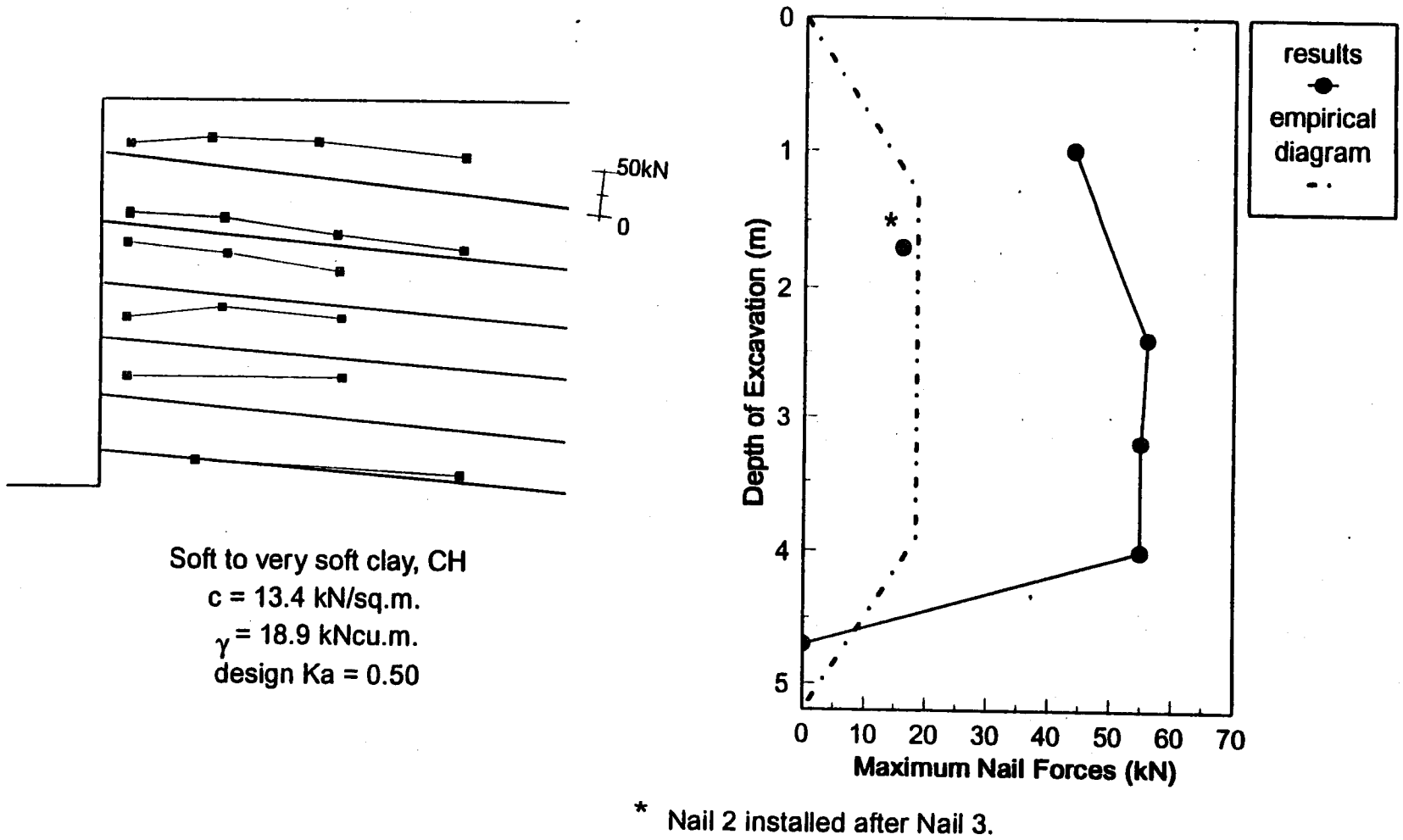

Figure 4.7. IH-30 Rockwall, Texas Soil Nail Wall A axial nail force results

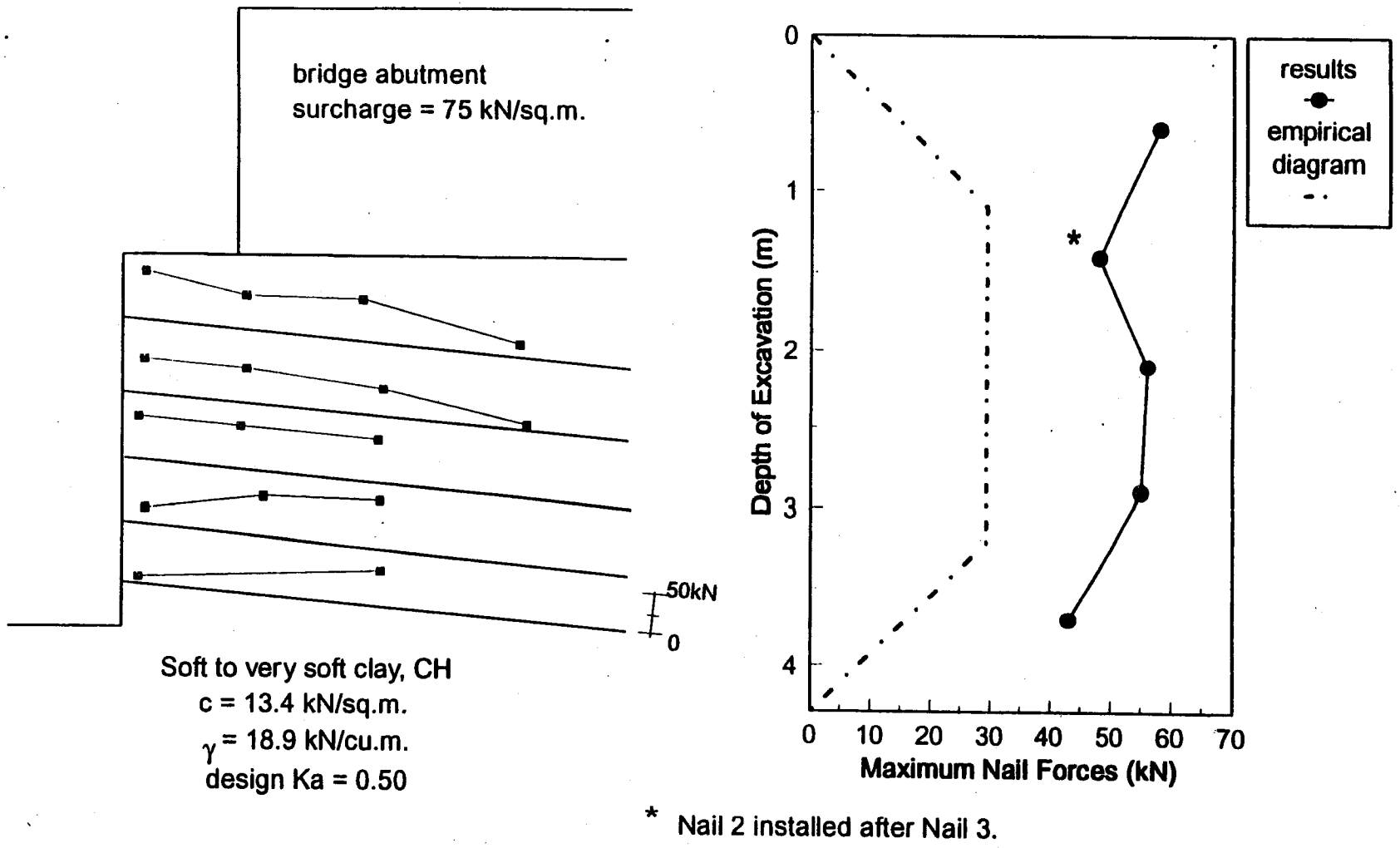

Figure 4.8. IH-30 Rockwall, Texas Soil Nail Wall B axial nail force results

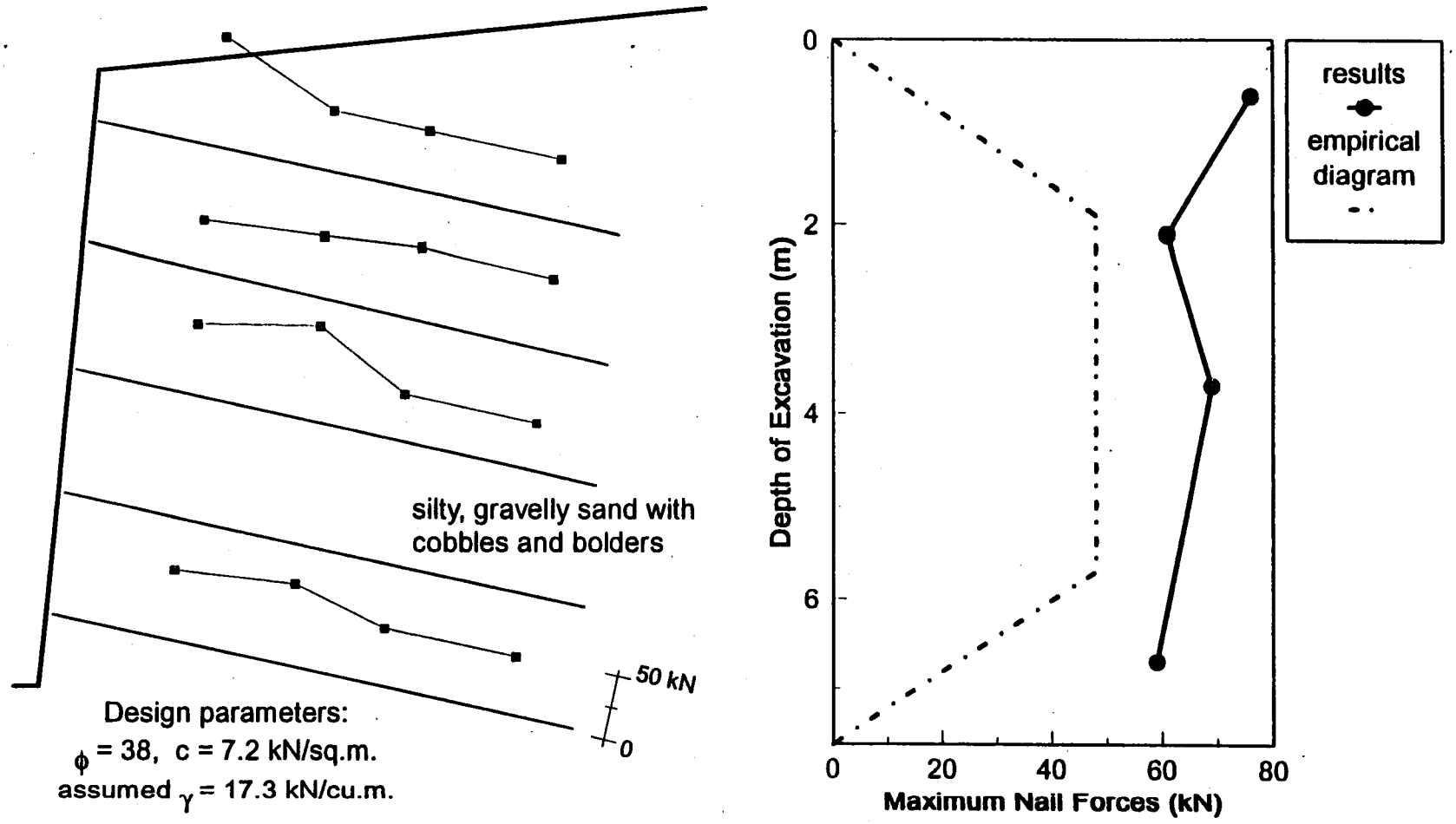

Figure 4.9. San Bernadino, Left Station axial nail force results

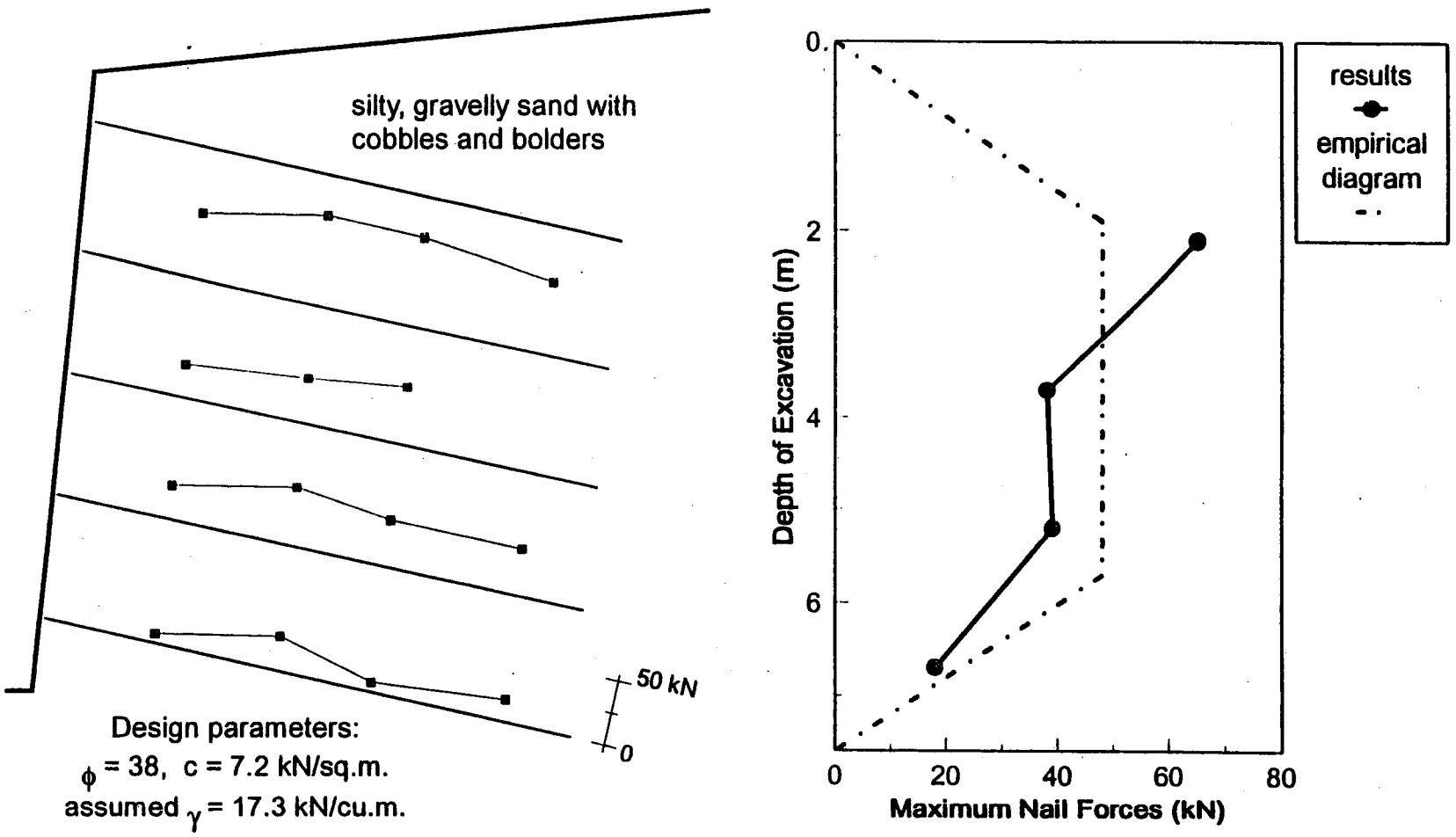

Figure 4.10. San Bernadino, Right Station axial nail force results

The nails were instrumented with strain gauges placed at four locations on four of five nails in each cross-section. In the two gauge locations nearest the face four strain gauges were installed on each rebar at the top, bottom, left, and right positionigure 4.8s. In the other two locations, strain gauges were placed on the top and bottom of each rebar. The strain readings were adjusted for temperature changes. The data were collected only five times during construction. After the end of construction, the strain data were collected on five additional dates, the last being collected approximately two years after construction.

It was beneficial to have two to four gauges per nail location to assess bending and average the readings to obtain axial strains because the strain readings for gauges at one location ranged widely. It was not uncommon to have a 30-microstrain difference among the four gauges. This was not always due to bending. For instance, in one case the right and left gauges read high and the top and bottom gauges read low for data collected long after the end of construction. Recording the strain measurements more frequently would have been useful, as some strain histories appeared erratic, probably because of the large time gaps between data points. The poor data precision observed in this instrumentation program seems to be relatively unique. Ranges in data analyzed from the other walls that contained strain gauges installed in pairs were not large.

The results from this wall, presented in Figures 4.9 and 4.10, were interesting because of the low measured strains and large grout section. On the basis of the present method of determining composite nail forces, no grout cracking should have occurred, and the estimated maximum nail loads represent composite nail loads. Although the results seemed relatively high in comparison to those predicted by the empirical diagrams, they were more realistic than those based on only the steel loads. The uncertainty of the soil properties may have been the reason that the estimated maximum loads appeared relatively high. The distributions of axial force were relatively uniform along most of the nails. High forces measured near the face were probably due to facing loads.

Cumberland Gap, 1988

This soil-nailed wall reinforced soil above a rock excavation. Four months after the soil-nailed wall had been completed, rock excavation continued below the toe of the wall. Strain data collected after the rock excavation were not analyzed in order for the soil-nailed wall to be comparable to the other walls in this study.

The only soil information received was a "heterogeneous mixture of residual soil and weathered rock" with $\phi = 38°$ and $c \geq 7.2$ kN/m^2 (Elias and Juran, 1990). The Cumberland Gap soil-nailed wall, constructed adjacent to this wall in 1985, had a reported soil unit weight of $\gamma =$ 18.9 kN/m^3 (Juran and Elias, 1987). This value was assumed for the 1988 wall. The contact between soil and rock was not known. The empirical diagram was calculated using $K_a = 0.35$ to account for the backslope.

The strain gauges were placed at four locations along each of the six nails. The strain gauges were installed on the top and bottom of the rebar at 0.3 m and 3 m from the face, while one gauge was installed on the top of the rebar at 6 m and 9 m from the face. The available information did not indicate whether the strain data had been adjusted for temperature changes. Data were collected every two to four days during construction and weekly thereafter until the rock excavation began.

The strain gauges 0.3 m from the face measured some bending. After averaging the top and bottom gauge readings to obtain axial strain, the axial force at 0.3 m from the face was the maximum estimated nail force for three of the six nails. It is unfortunate that gauges were only positioned at 3-m intervals along the nails, as the actual maximum nail forces may not have been recorded. The bottom nail was installed 24 days after wall excavation was complete, which accounts for the lack of reinforcement mobilized in this nail.

The results are presented in Figure 4.11. Except for the top nail, the estimated maximum nail loads were less than those predicted by the empirical diagram. The distributions of axial

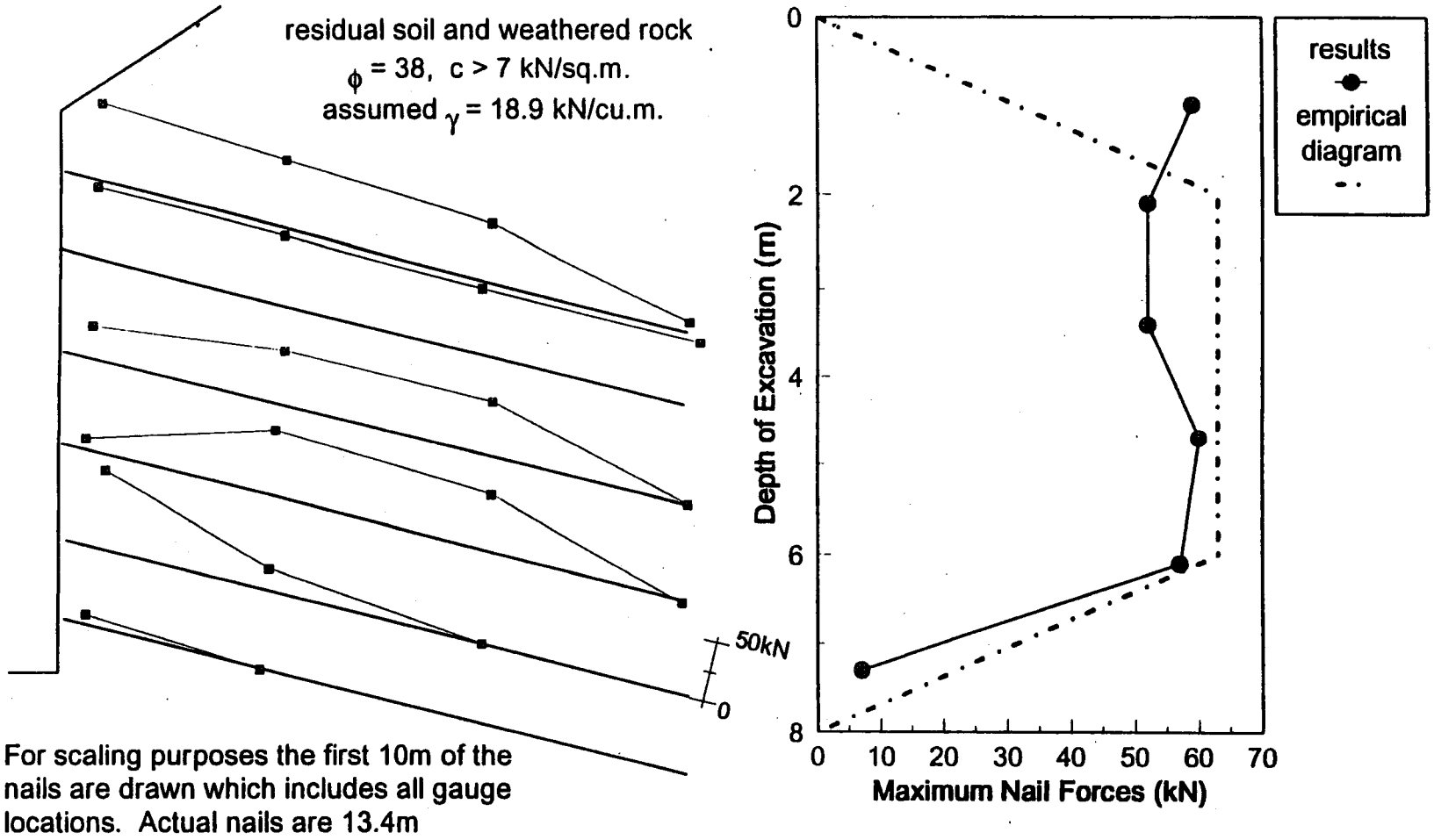

Figure 4.11. Cumberland Gap, 1988 Soil Nail Wall axial nail force results

force along the nails were relatively uniform for the first, second, and last nails. The distributions along the third and fourth nails were characterized by low forces measured at both ends of the nails. Significant nail force was only measured near the face in the fifth nail.

I-78 Allentown

Two cross-sections with the same geometry, materials, and soil were identically instrumented. The estimated axial nail load results are presented for both sections (Figures 4.12 and 4.13); results are combined for discussion.

The soil-nailed wall actually consisted of two 6.1-m vertical tiers with a 3-m bench separating them. The 33° backslope began 3 m back from the top of the wall. The top tier was reinforced with 6.1-m nails using 25-mm diameter steel reinforcing bars. The bottom tier consisted of 9.2-m nails using 32-mm diameter bars. The wall cross-sections are displayed in Figures 4.12 and 4.13. After excavation of each row, a coat of shotcrete reinforced with wire mesh was applied to the face. After the wall excavation had been completed, precast concrete panels, 2 m^2 by 0.165 m thick, were attached to the nails. Drain rock filled the space between the shotcrete and concrete panels where the face had been excavated unevenly.

The soil was characterized as colluvium and highly weathered rock. The wall was constructed in an area originally intended to be a competent rock excavation. The colluvium and highly weathered rock appeared to be created by a natural drainage swale at this location (Leichner, 1989). Laboratory testing produced in $\phi = 39°$ and $c = 86$ kN/m^2. Design soil parameters were $\phi = 37°$, $c = 0$, and $\gamma = 19.6$ kN/m^3. The empirical diagram was calculated using $K_a = 0.35$, which included the backslope but ignored the bench. During nail installation, rock was encountered 1.8 m to 2.4 m from the face in the top tier and 0.3 m to 1 m in the bottom tier.

Four of the eight nails in each section were instrumented with three strain gauges. The gauges were located at 0.3 m, one third the nail length, and two thirds the nail length from the face. Only one strain gauge was installed at each location so bending effects could not be

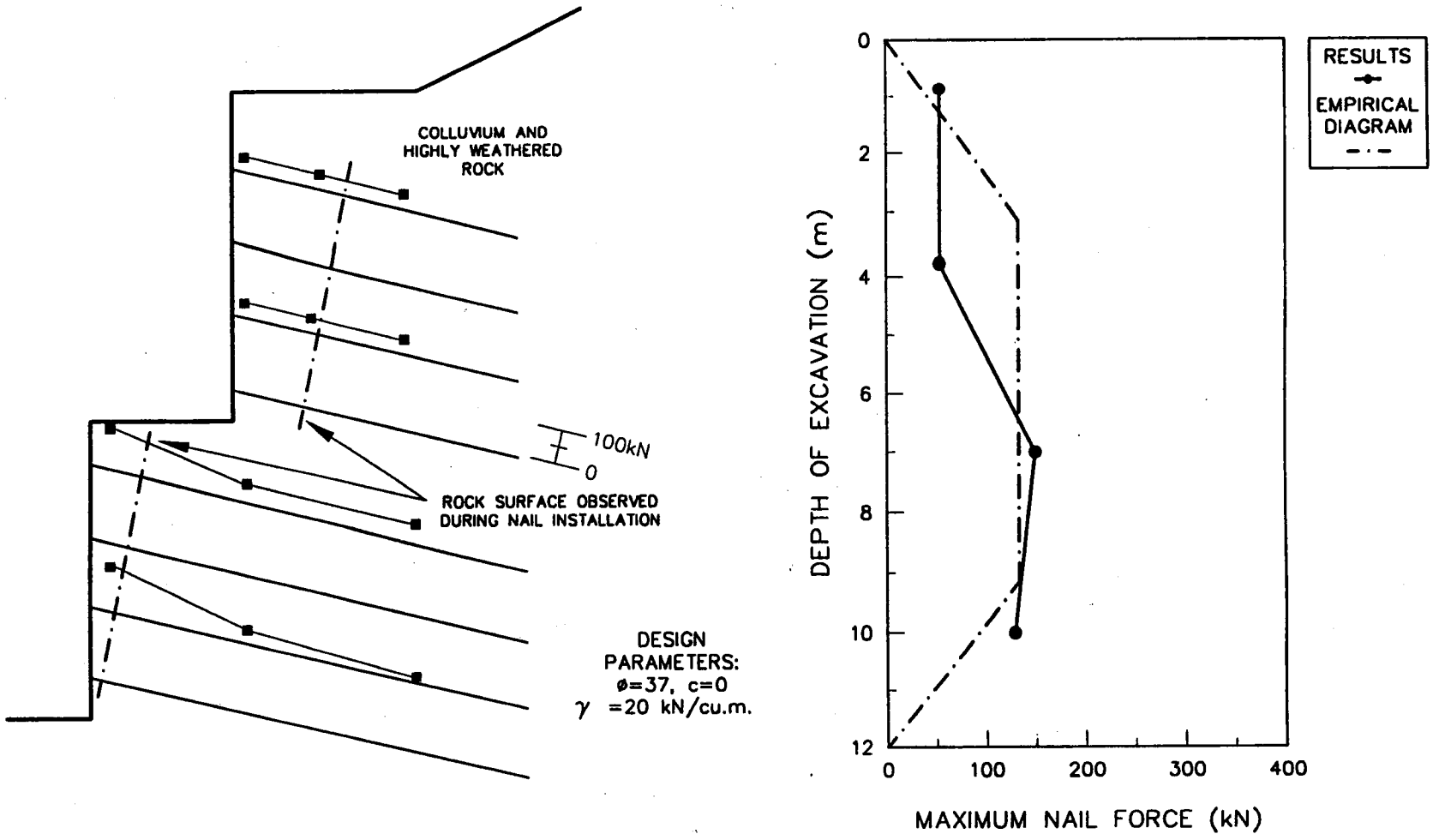

Figure 4.12. I-78 Allentown Grid 24 axial nail force results

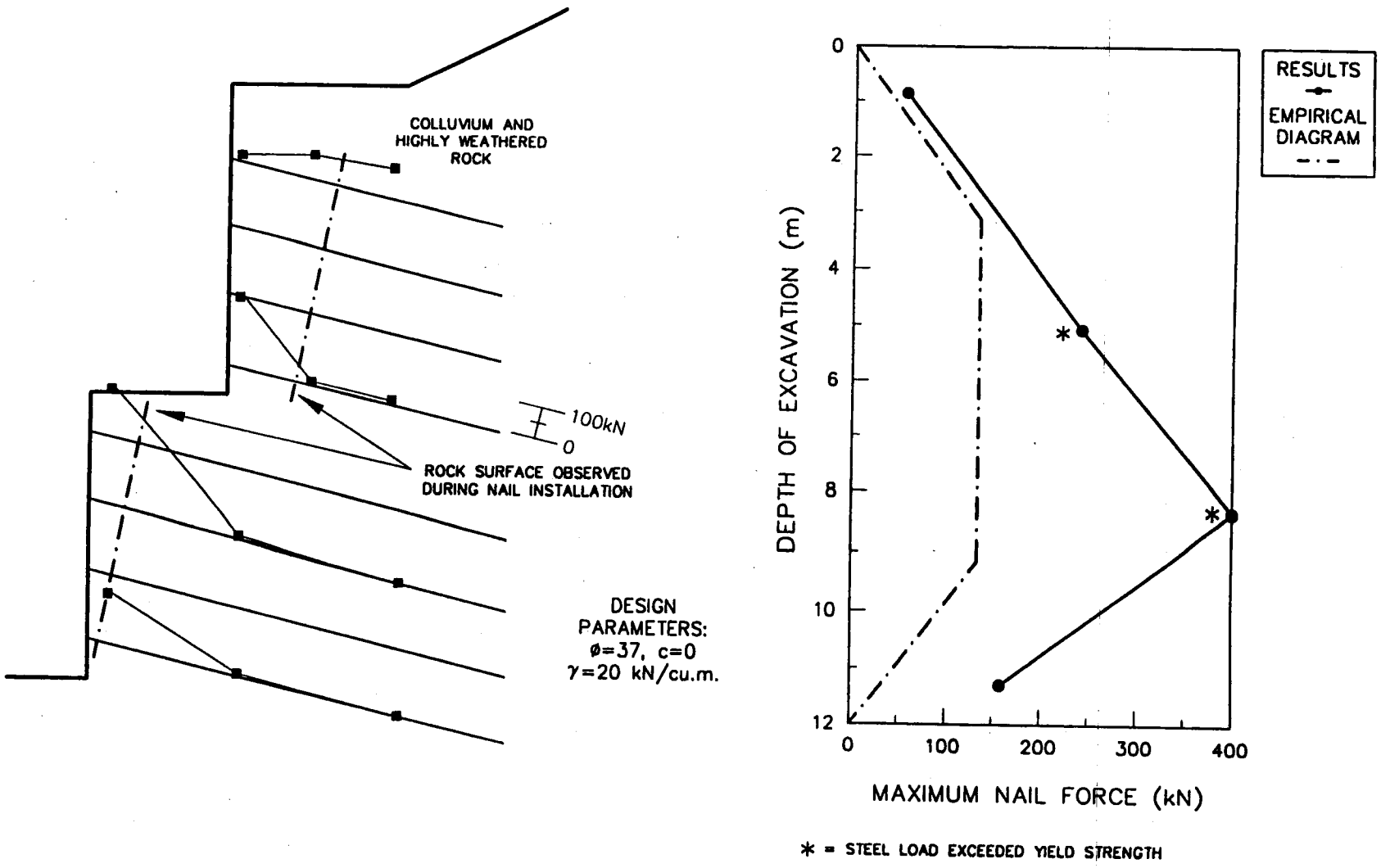

Figure 4.13. I-78 Allentown Grid 33 axial nail force results

assessed. The available information did not indicate whether the strain data had been adjusted for temperature changes.

Because concrete panels were attached to the nails, facing construction most likely influenced the strains measured close to the face, and bending of the steel bar near the face was likely. Because of the type of facing construction, it is not known whether the soil nails were surrounded by soil at the location of the first strain gauge (0.3 m from the face). The gauges further along the nail recorded small strains and were probably located within rock.

The results are presented in Figures 4.12 and 4.13. Except for the top nail in each section, the maximum nail load was measured 0.3 m from the face. In Grid 33, the steel load measured near the face in the middle two instrumented nails exceeded the steel yield strength for the rebar. The large measured strains were probably due to bending. The distributions of axial force along each nail were characterized by high forces close to the face and low forces at the other gauge locations. The low nail forces observed farther along the nails were probably the result of the nails being imbedded in competent rock.

CHAPTER 5

DESIGN ANALYSIS PACKAGES

The design analysis packages reviewed in this study included the programs listed below with their sources. Some of these packages are used for in-house design; others are currently available commercially:

SNAIL	Caltrans, Sacramento, Cal., USA.
NAIL-SOLVER	Oxford Geotechnical Software, Oxford, U.K.
STARS	L'ecole Nat. des Ponts et Chaussees Paris, France.
NAILM	S. D. School of Mines and Technology, S.D., USA.
GOLDNAIL	Golder Associates, Redmond, Wash., USA.
TALREN	Terrasol, Montreuil, France.
CLOUDIM	G.I.T Consultants, White Plains, New York

A brief description of the analysis packages are presented in this chapter

5.1 SNAIL

SNAIL is a soil-nailing design and analysis program developed by the California Department of Transportation (Caltrans). The program uses a two- or three-part bilinear wedge analysis to determine the minimum global safety factor for a given wall cross-section. Presumably, it can be used with both passive soil nails and active tie-backs. In addition, another Caltrans program called *NAILDESIGN* (which is not actually part of the main analysis program) can be used with the data from *SNAIL* to predict nail loads.

The analysis has two modes of operation that differ in their application. In the first mode, ultimate values of bond stress, yield stress, and punching shear are used. The program iterates on a safety factor, which it applies to the material properties C, ϕ, and T, the sum of the mobilized reinforcement tension acting on the wedge. The mobilized tension is defined as the lesser of either the nail force developed on the portion of the nail outside the slip surface, or the force developed on the portion of the nail inside the slip surface combined with the user specified value of punching shear. By using the lesser of these two values, the program examines both internal and external stability in one pass. It assesses stability by calculating the resultant

interslice friction force, which includes the contribution from the interslice nail forces, for both wedges (upper and lower). The program also iterates with the material factor of safety until the difference between the two is essentially zero.

In the second mode, the calculations and iterations are similar, but the user enters pre-factored values of bond stress, yield stress, and punching shear. In this way, different factors of safety with respect to each of the three quantities can be used. If the ultimate values of bond stress, yield stress, and punching shear are pre-factored with the safety factor obtained from a Mode 1 run, then the second safety factor obtained is the same as that obtained from Mode 1. This is because the program iterates by changing only the safety factor on soil strengths. For this study, the second mode of operation was used so that the material safety factors on the bond stress and yield strength could be kept constant at 1.5.

The bilinear wedge analysis is comparatively simple and involves a summation of forces in the normal and tangential directions for each of the two wedges (upper and lower). The forces acting on a given wedge are as follows: the weight of the wedge, including the effects of the water table; the surcharge; psuedostatic earthquake forces; mobilized cohesion on the lower surface, as well as the interslice cohesion; the resultant frictional forces on the base of the wedge; the resultant interslice frictional force, including interslice nail forces; and the sum of the mobilized reinforcement friction forces acting on the wedge. The analysis assumes that the reinforcement acts only in tension, and that the effect of nail bending is minimal.

The analysis allows the user to enter a number of wall parameters and loading scenarios. It is very flexible in this respect and can accommodate cases such as benched walls; two slope angles below the wall toe; varying distributed surcharge loads; a water table; earthquake loading; failure surface emanating from points below the toe of the wall; horizontal forces applied to the wall face; and varying reinforcement parameters such as length, grout diameter, and bond stress. It is limited to two soil types, and the soil boundaries are specified with two sets of x and y coordinates, requiring that highly variable profiles be approximated by the user. Furthermore, the program looks at internal and external wall stability, i.e., a soil wedge pulling away from the

nails (which remain in place) and a soil mass pulling away along with the nails. This is achieved by comparing the required forces for internal stability with an input value for punching shear, expressed in kips. Punching shear is the resultant of the face pressure acting on a section of the wall face, the dimensions of which correspond to the horizontal and vertical spacing between nails. Both punching shear and face pressure are a measure of the structural capability of the facing to resist internal soil failure through pull-away of the wall from the nails and subsequent failure of a wedge of soil. While punching shear is used exclusively in this program, the face pressure is used in other programs. In this study, however, face pressure was used in the plots to facilitate the comparisons. The user's manual is straightforward and includes easily understood definitions of the required input parameters.

The method of search to determine the global safety factor for a homogeneous soil profile is presented in Figure 5.1. The input search range is divided into ten equal parts, or ten nodes. The search intervals begin from the wall crest, if not otherwise specified by the user. For cases with wall batter, the horizontal distance from the wall toe to the wall crest is subtracted from the search limit, and the remainder is divided into ten parts. For a given node, lines are drawn from the toe and the backslope node to every intersecting grid point; each point represents a possible failure plane. A quick check will show that there are possible failure planes for each node, and hence, the program checks possible failure planes with the ten nodes.

A typical output (Figure 5.2) includes a graphical representation of the wall cross-section, displaying the slip surface with the lowest overall factor of safety. This can be printed using the printscreen utility of DOS. The results of the calculation, along with the input parameters, can also be output.

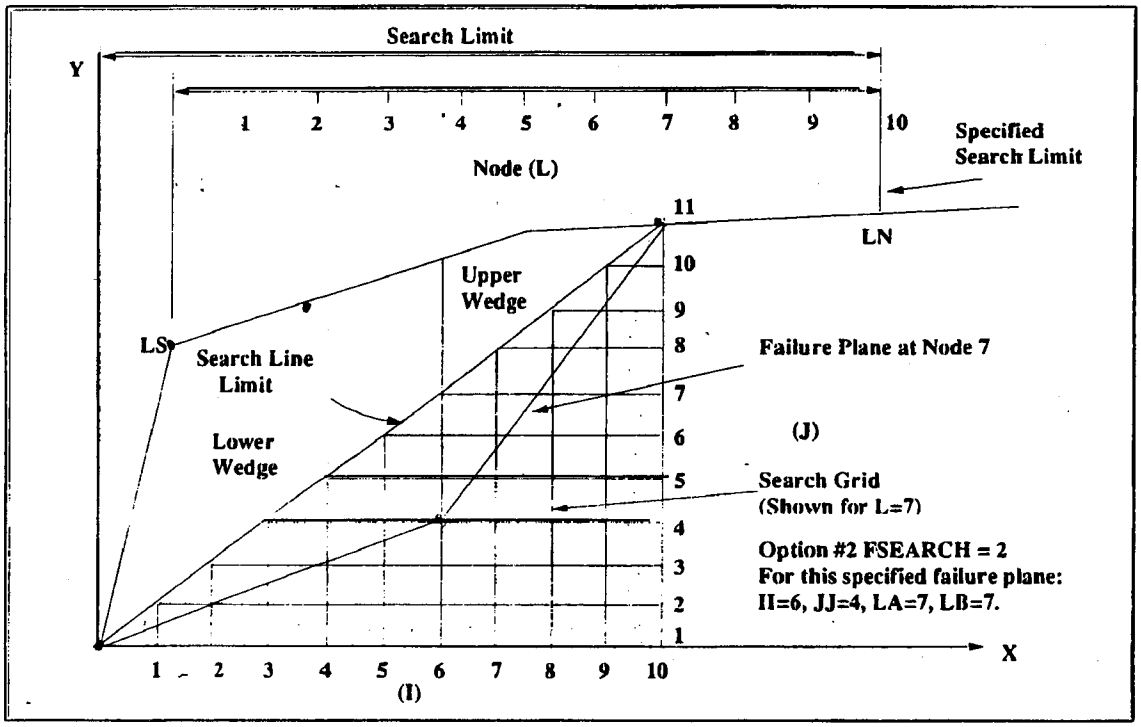

Figure 5.1. Search grid pattern for SNAIL

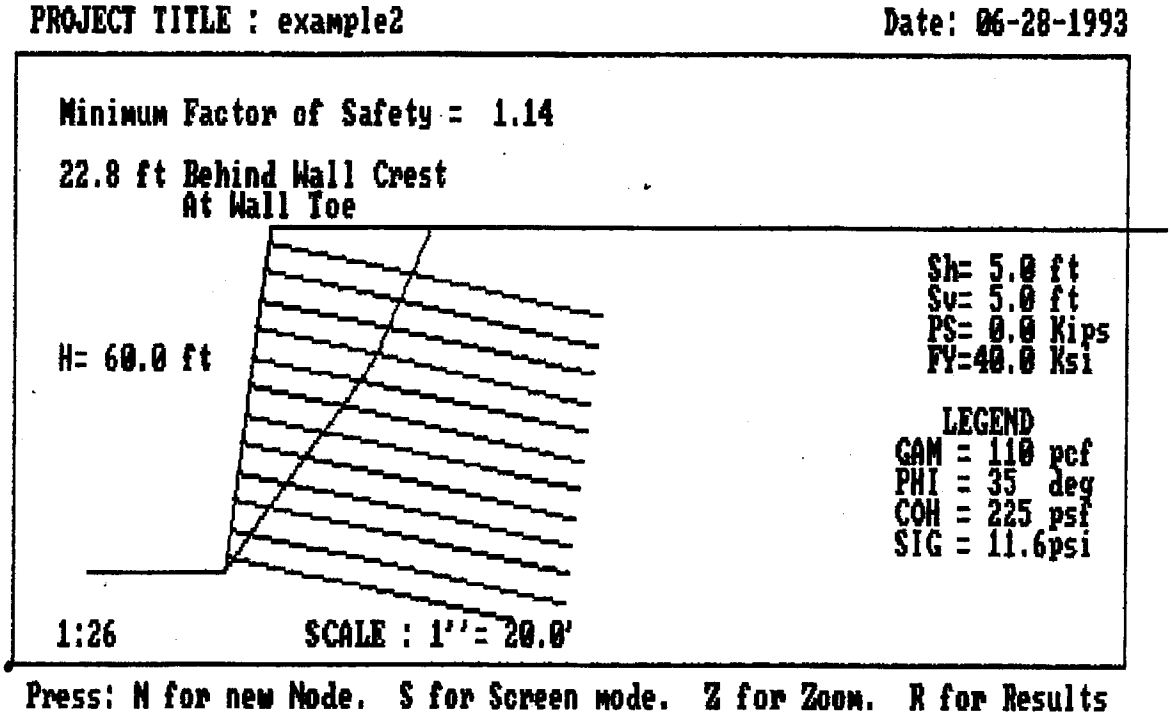

Figure 5.2. Output for SNAIL

5.2 NAIL-SOLVER

NAIL-SOLVER is a computer design package developed by Oxford Geotechnical Software and is based on the work by Jewell and Pedley at the University of Oxford. This program also uses a bilinear wedge analysis to evaluate both internal and overall stability of a given soil-nailed cross-section.

The program is somewhat limited in the cross-sections and loading conditions that it can handle. The wall must be a single element, without benches, and cannot involve toe slopes or more than a single slope above the wall. Varying reinforcement parameters, such as spacing, length, grout diameter, and bar diameter, cannot be accommodated. The pullout resistance is calculated using the overburden stress, and a dimensionless bond coefficient, f_b, which represents a percentage of the factored soil friction angle (the given range of f_b is from 0.4 to 1.0). The user enters the horizontal and vertical nail spacing, but if the program reaches the bottom of the wall and finds a space of more than one half the vertical spacing, it will automatically add an additional row of nails.

This program accepts both point and uniformly distributed surcharge loads, but it is unable to handle arbitrarily varying distributed loads. Pore pressures can be input using a non-dimensional pore water pressure ratio, r_u, which expresses the pore pressure as a percentage of the overburden stress. A single r_u value describes a distribution of pore pressures that increases with depth. Note that the program uses effective parameters for cohesion and angle of friction. The soil shearing resistance is described by a secant angle of friction for the effective stress range. For this reason, it is necessary to prefactor the effective cohesion, as the safety factor on peak soil shearing resistance is not automatically applied to the cohesion.

The computational process begins with the calculation of 120 unreinforced trial failure wedges to determine the maximum forces required for internal equilibrium. The program examines wedges intersecting the wall at ten different elevations below the crest. The required

forces for the internal equilibrium are derived from a simple summation of forces, which can be approximated with the use of Coulomb's formula:

$$P_a = \frac{1}{2} K_a \gamma H^2 \tag{5.1}$$

where P_a = active soil force

K_a = active earth pressure coefficient

γ = soil unit weight

H = depth below the wall crest

The user enters reinforcement parameters and the program calculates the maximum required forces for overall equilibrium using a two-part failure mechanism. For each of the bilinear wedges passing from the toe to the ten different elevations at the back of the reinforced zone, the program searches to find the worst inclination of the back wedge. It calculates the required forces by using a summation of forces on the two wedges, satisfying both horizontal and vertical equilibrium. First it assesses them by determining the vertical spacing of the nails on the basis of the entered "trial" spacing. Next, the program calculates bond strength on the basis of the bond coefficient, f_b, and the average of the vertical effective overburden stress and the lateral effective stress acting parallel to the slope. The reinforcing benefit is derived from the portion of the nails outside the slip surface. If a nail passes through the failure plane and into the soil beyond, it is assumed to be able to contribute the lesser of the total yield strength of the nail, or the bond stress integrated over that portion of the nail outside the failure plane. Next, the program makes two checks to compare the required and available forces for internal equilibrium, one during construction (without the next nail installed) and one at the end of construction. Finally, two more passes are made to compare required and available forces for overall equilibrium, during and after construction.

Comparison of this program with other programs is further complicated by the fact that it calculates bond stress being calculated from the effective overburden pressure. First, without a strictly specified value of bond stress, the comparisons are not exact. Second, the material safety

factor applied to ϕ for the soil is also applied to the calculations of bond stress through the use of the factored soil ϕ-value. For consistent comparisons, a procedure that could approximate the design bond stress using nail overburden stress, a lateral earth pressure coefficient, and a bond coefficient had to be developed. The overburden stress was calculated at a point half-way along the length of the middle nail (or between the nails, in the case of an even number of nails), and the following formula was used to calculate the bond stress at a given depth:

$$\tau = \sigma_v' (1 + k_L) f_b \tan \phi_d' \tag{5.2}$$

where k_L = lateral earth pressure coefficient

f_b = bond stress coefficient

ϕ_d' = effective soil friction angle for design.

This formula was set equal to the allowable bond stress used in the other programs, at this middle nail depth, and solved for k_L. This value of k_L was used in the subsequent runs, although in a number of cases its value exceeded one. This was the only way to modify the equation to produce the desired results, as the bond stress coefficient , f_b, was limited to a maximum value of one.

The program allows the user to enter both ultimate and allowable values of yield stress and the soil properties C' and ϕ', and it displays on-screen the calculated material safety factor. In this way it utilizes individual material factors of safety, providing the user with an overall global safety factor at the end of calculations. It should be reiterated that the bond stress is computed with the design value of f'; therefore, the bond stress carries with it the safety factor on soil strength. However, this was not an issue with our comparison, as the average value of bond stress calculated with an artificial k_L included only the safety factor of 1.5 used on bond stress.

The typical output is in the form of graphs of force versus depth below the crest, showing maximum required and minimum available forces previously calculated for both internal and external stability, both during and after construction. The depth below the crest refers to the depth below the crest at which either the internal wedge intersects the wall facing (in the case of

the internal equilibrium plot), or the depth below the crest at the back of the nailed zone that delineates wedge one from wedge two (in the case of the overall equilibrium plots). In all trials, the most critical case (either internal stability at the end of construction or overall stability at the end of construction) was used to produce the global factor of safety equal to one. No output specifying the location of a failure surface is given, and therefore no failure surface for this program is shown on the comparison plots (Figure 5.3).

5.3 STARS

STARS is a program developed by a joint venture known as C.N.R.S., which includes the Laboratoire Commun a l'Ecole Polytechnique, l'Ecole Superieure des Mines de Paris, and l'Ecole Nationale des Ponts et Chausses. It is currently available in a version 2.0.

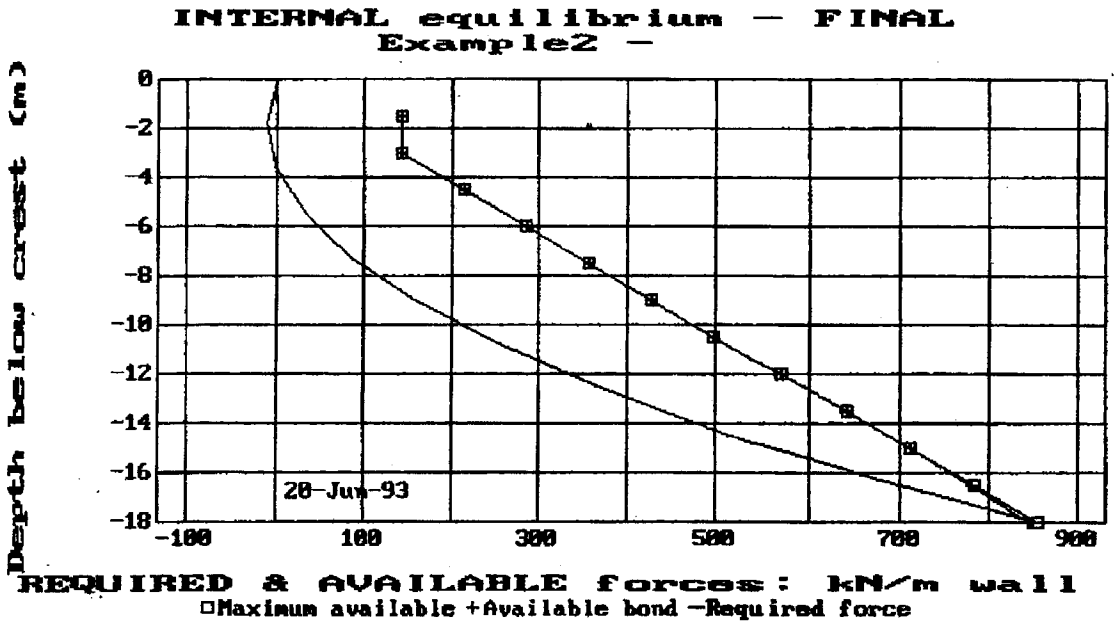

Figure 5.3. Output for NAILSOLVER

STARS uses a moment balance approach, coupled with a log spiral failure surface, to calculate an overall, or global, safety factor. The program has an excellent user interface with on-screen graphics and brief descriptions for all entered parameters. The program can handle different reinforcement parameters, allowing the user to enter the individual nail properties. It can handle varying distributed surcharges, point loads, toe slopes, multiple sloping soil layers, and a simple non-sloping bedrock surface. It can also be used with tie-backs or a combination of tie-backs and nails. Water tables and multiple ground surfaces behind the wall are not accommodated. Furthermore, the program will not allow backslopes with angles greater than the allowable ϕ value of the top soil layer. A significant advantage of the program, however, is that it will directly assess overall stability during construction and after construction, as well as the stability of deep-seated failure surfaces not passing through the toe.

The program starts at the upper nail level and searches for the surfaces that intersect the wall face just below the nail, with no assumed benefit from the nail. This is often a critical period during construction, when the cut has been made and the nail has yet to be installed. The program successively proceeds to the next nail levels until it reaches the bottom of the wall. Different soil layers with different ϕ values produce slightly different log spirals, and hence, the program creates a composite surface.

The resisting and driving moments for each trial slip surface are calculated in the same manner as in many slope stability programs. The program calculates the driving moment by considering the weight of the soil and any surcharges present. It considers surcharges at the toe of the slope that increase resistance as negative driving moments. It calculates the resisting moment by integrating the contribution of the soil shearing resistance to the resisting moment along the length of the slip surface. The resultant of the frictional forces acting on the slip surface, both normal and shear, passes directly through the center of the log spiral without contributing anything to the moment. As shown in Figure 5.4, the component of the remaining resisting force perpendicular to the moment arm (C cosϕ) is then multiplied by the moment arm and integrated along the slip surface.

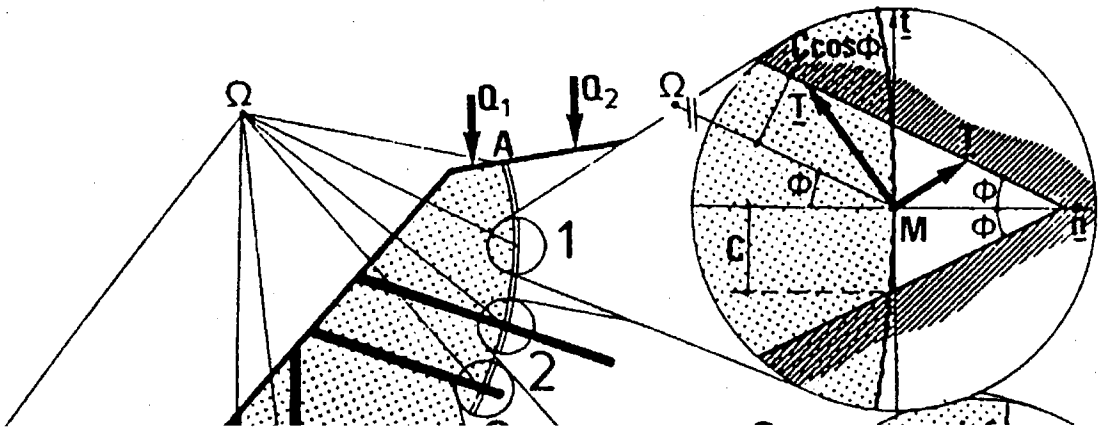

Figure 5.4. Assumed tension and cohesion on log spiral surface for STARS

Every time reinforcement is encountered, *STARS* simply adds its contribution to the resisting moment in the following way. If the reinforcement is positioned across the slip surface so that it is working in compression, or if it is aligned along the ray of the log spiral, its contribution is considered to be zero. If the reinforcement is positioned so that it is working in tension, it is assumed to be contributing the lesser of either the maximum yield stress of the nail or the lateral soil/grout interface friction over the length of the nail outside the log spiral. The contribution perpendicular to the log spiral radius of this vector N is multiplied by the moment arm to give its resistance. The internal stability is not checked by the current version of the program.

The overall factor of safety displayed after calculation is a straightforward M_r/M_d, where M_r is the resisting moment and M_d is the driving moment. The program does allow the user to

enter individual material safety factors on lateral interface friction, yield strength, soil strength, and surcharges.

The output consists of a DOS printscreen capture of the wall cross-section depicting the various critical slip surfaces intersecting the slope at each of the nail levels and at the toe. In addition, if it has been previously calculated, the critical deep-seated slip surface will be shown. Also output is a summary of the input data and the results of the calculations. The output results are limited to the depth below the crest of the failure surface intersection and overall or global safety factor ("factor of confidence" in Figure 5.5). Note that a math coprocessor is required to run this program.

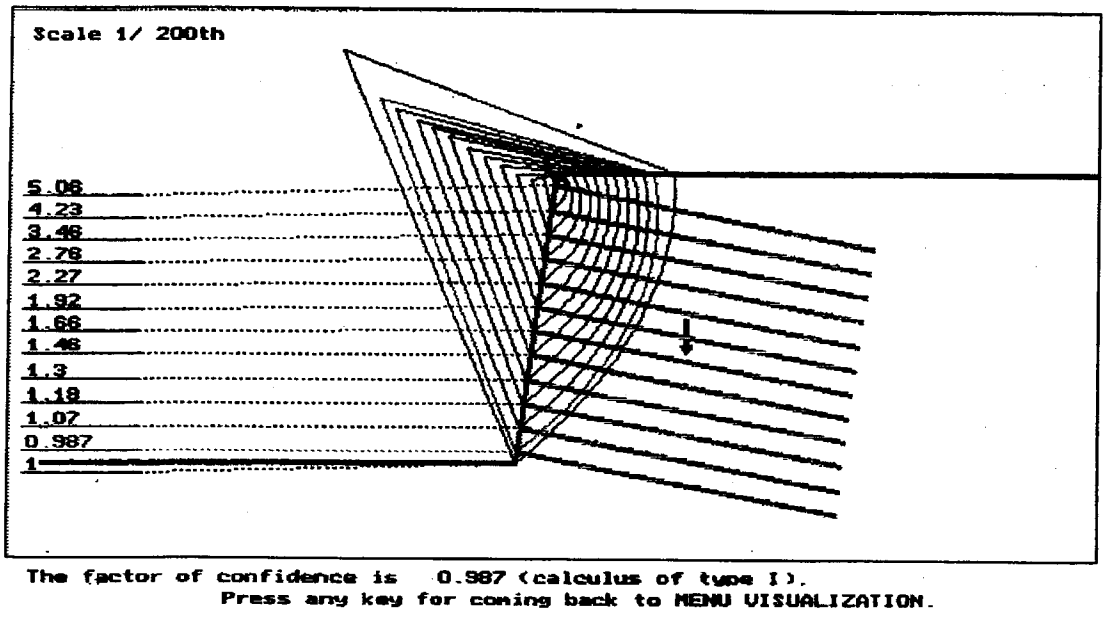

Figure 5.5. Output for STARS

5.4 NAILM

NAILM was developed by Prof. Sanchul Bang at the South Dakota School of Mines and Technology. This program is based on the Davis method and uses a parabolic slip surface to describe the failure (Shen et al., 1981a, 1981b). Although a more current version (*NAILM11*) of the program is supposedly available, the version of the program available during this evaluation was *NAILM9*. Note that the discussions in this report apply only to *NAILM9*.

The program can handle different horizontal soil layers, simple distributed surcharges over the entire backslope, point loads, earthquake loading, and varying nail lengths. The program allows one to use either pullout test data or a bond stress calculated from overburden stress. It cannot accommodate varying nail pullout resistance or varying nail parameters such as grout diameter, yield stress, and bar cross-sectional area. This version of the program is also unable to handle water tables, stepped walls, or toe slopes.

The program asks for a user-input search limit. It then divides this distance into even increments and proceeds to run parabolas from the toe to each of these points. Each parabola is divided into two parts—a reinforced slice and an unreinforced slice (Figure 5.6). If the parabola passes beyond the length of the uppermost nail, the X coordinate of the division between the reinforced slice and the unreinforced slice is the coordinate of the end of the uppermost nail. If the parabola passes completely through the nailed zone, the X coordinate of the slice division is that point where the failure parabola intersects the uppermost nail.

The reinforcement contribution is determined simply as the pullout resistance developed over the length of the nail beyond the slip surface. The stability calculation involves a straightforward summation of forces with a slight difference in the definition of the safety factor. Instead of the standard resisting forces divided by the driving forces, the overall or global safety factor is defined as the component of the total resisting force in the direction of the driving force divided by the total driving force, resulting in a value that is consistently lower than that of the other approaches.

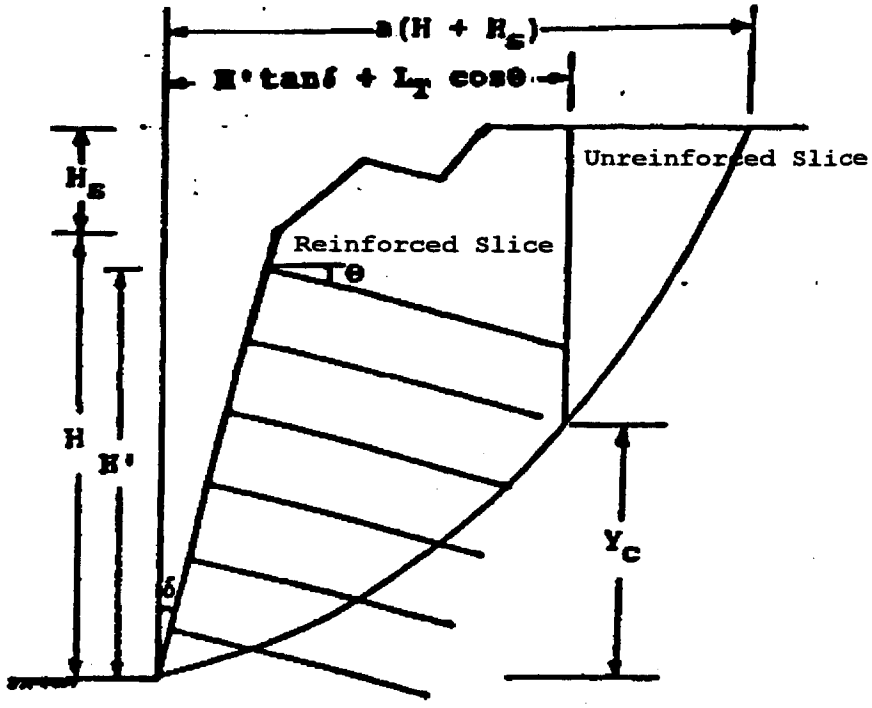

Figure 5.6. Assumed failure surface for NAILM9

The program does not make direct allowances for individual material safety factors; however, to allow comparison with other programs, the input values of bond stress and yield stress were prefactored, and the overall safety factor was made to equal one by changing the material safety factor on the soil.

Data are entered in response to program prompts and are stored in a data file. There are separate files for data entry and output; viewing the input or output files requires exiting to the text editor. Output from this program is a standard printout of the input parameters, the slip surface and lowest safety factor from the results of the searches, and the location of this surface behind the crest. To compare the surface with that of other programs, hand calculations were made using formulas given in Bang et al. (1991) to delineate the parabolic surface on the cross-section.

5.5 GOLDNAIL

GOLDNAIL, a program based on the limiting equilibrium approach using a circular failure surface and the Janbu method of slices (Janbu, 1973), was developed by Golder Associates. It can accommodate passive soil nails as well as active tiebacks. It has the capability not only to analyze any given design but also to develop designs and predict nail loads.

It can accommodate varied back slope geometry. It can handle multiple and varied soil layers, water tables, earthquake loadings, varying distributed surcharges, point loads, and varying nail parameters. It is unable to directly handle benched walls or toe slopes. These last two can be accommodated by making certain assumptions about the wall modeling, such as by using an equivalent sloped wall facing to model a benched slope. This is true with many of the other programs that cannot directly accommodate benched walls.

The user interface is somewhat tedious in this program. Although the input data can be viewed on-screen in the program, to view or print a given output file, one must enter the DOS text editor and edit the output file. It is possible to examine the internal stability of the wall and

incorporate the use of a face pressure value, entered in psf by the user. This face pressure value is a measure of how resistant the facing is to having the bars punch through the wall. This is important because the adhesion between the nail and a thin failure wedge behind the wall is minimal.

It is important at this point to distinguish between the program's two modes of operation. In mode one, the design mode, all information about the wall geometry, soil properties, and desired safety factor on the soil is entered. The program then determines the required nail lengths, loads, and face pressure required to meet this safety factor. The program does this by stepping through a number of slip surfaces that pass through the wall toe, or through a user-specified point. The circles are bounded by the inclination of the wall facing and by the two minimums of the parameters α and β specified by the user. α is the minimum tangential orientation of the slip circle at the wall toe. β is a minimum angle measured from the horizontal, at the wall toe, whose intersection with the back slope specifies the search limit. This value is used to define a range for the radii of the trial slip circles. The program then steps through the angles α and β and begins to construct circles from the toe to each node. The first pass assumes that the nails have sufficient pullout capacity beyond the failure surface and determines the minimum value of face pressure necessary to obtain the user- specified safety factor on the soil. The second pass then uses this value of face pressure to determine the length of nail required by systematically adding an incremental length to each nail until the specified safety factor has been met. Finally, using the determined values of face pressure, nail length, and factored adhesions, the program calculates the nail loads.

In mode two, or the safety factor mode, given wall geometry and soil properties are entered, as are nail properties such as length and maximum load, values for face pressure, and desired safety factor. Here the objective of the program is to identify any slip surfaces that have a safety factor lower than the user-specified safety factor. The maximum nail load is simply entered as the product of the factored yield strength of the steel and the nail's cross-sectional area. It is important to note here that with any limit equilibrium method, assumptions have to be

made regarding the distribution of nail forces along the nail. The program computes each nail's contribution to stability by using a triangular distribution of forces along the nail. If face pressure is included, the nail sees a jump in the force applied at its head. As the analysis considers only tension in the nails, the value used to determine overall stability is the value of tension in the nail where it crosses the trial failure surface. Using this value eliminates the need to use the entire length of the nail outside the slip surface as the contribution to stability. The difference is most evident when one looks at the lower nails in a given wall. Conventional methods dictate that any extensive length of nail outside the slip surface contributes a great deal to the stability; however, it is widely known that the bottom nail has little applied force. The program predicts this, as the nail force contributing to stability is limited by the bond stress acting on the nail between the slip surface and the wall facing. In this way, the program considers face pressure and its effect on the force distribution on the nail. It also eliminates the need for a separate step to check internal stability, as it can consider pullout of the bars and the pull-away of the soil simultaneously (Figure 5.7).

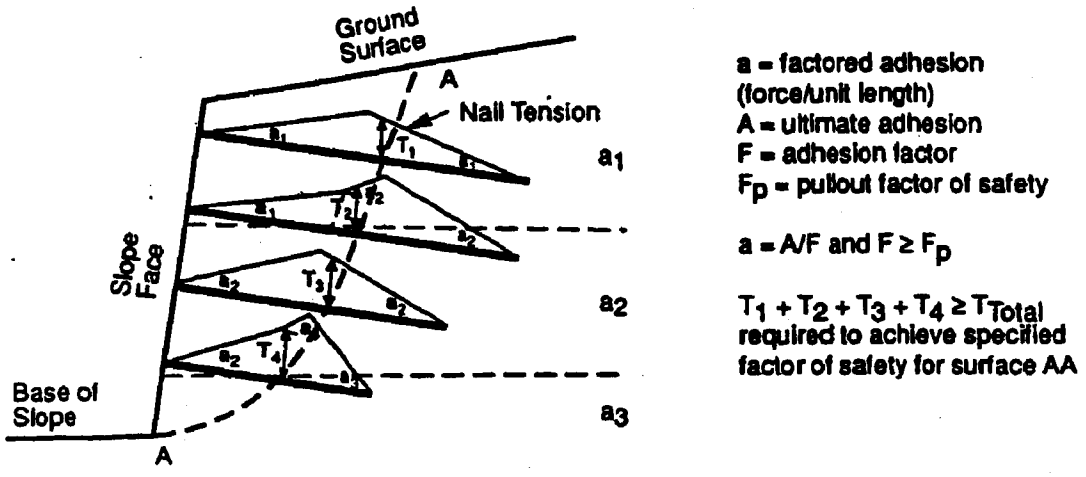

Figure A-1. Nail Tension Distribution - Limiting Equilibrium Analysis

Figure 5.7. Assumed nail tension distribution for Goldnail

Equilibrium of the system is analyzed with a Janbu slices approach. Each slice must satisfy horizontal and vertical equilibrium. The total nail force contributing to equilibrium is known, but how that force is distributed throughout the various slices is not known. Placing fictitious nails so that one nail passes through the center of the base of each slice and using the same procedure as before, the program determines a distribution of nail tension forces. It then divides the actual total nail force into components applied to the base of each slice on the basis of this computed force distribution. The same process is used with interslice nail forces. Three fictitious nails are run through each slice to determine relative magnitudes of the nail interslice forces. All forces acting on the base of a given slice are known, as are the interslice forces and the relative magnitudes of the nail forces. To reduce the number of unknowns, the program assumes that the interslice soil shear forces acting on either side of a slice are equal and opposite in direction, and therefore cancel.

The overall safety factor is defined as the material strength factor applied to the soil strength parameters. The traditional overall safety factor of F_r/F_d (resisting forces divided by the driving forces) is internally set equal to one. This definition of output safety factor was totally compatible with the procedure adopted for the study comparison. It did not require multiple runs per wall to iterate to a value of 1.0 for the overall or global safety factor. To view the slip surface with the lowest factor of safety, it was necessary to lower the factor of safety applied to the soil to just above the lowest factor calculated. This is because, as was mentioned before, the program will only display circles that have a safety factor lower than that specified.

Output from the program includes a DOS printscreen capture of the wall cross-section and failure surfaces (Figure 5.8). Also printed through the DOS text editor are the input parameters and results for each of the weakest slip surfaces run through a given node.

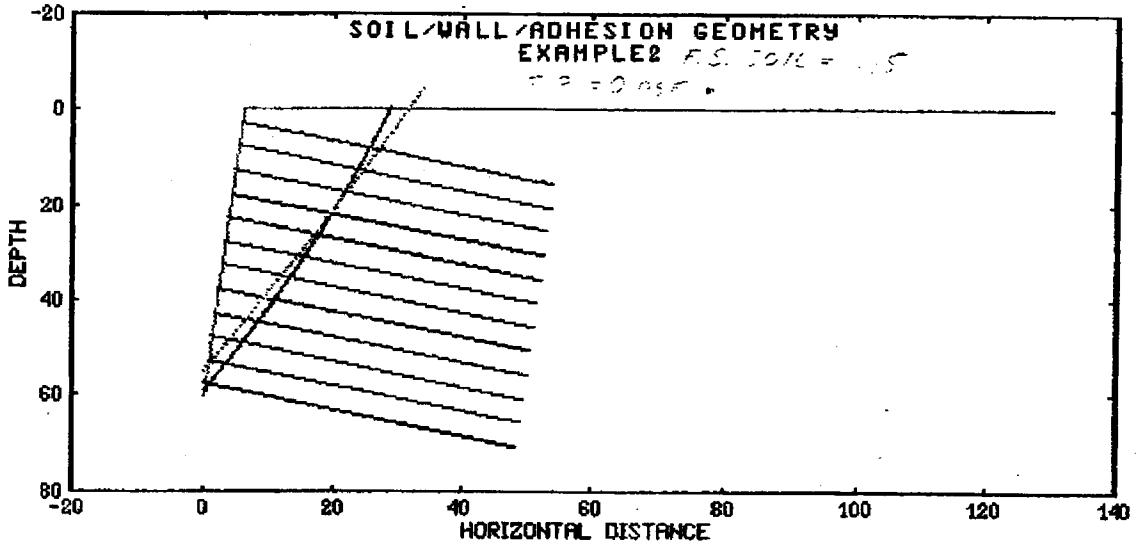

Figure 5.8. Output for Goldnail

5.6 TALREN

TALREN is a general slope stability and reinforced soil design package developed by Terrasol. It is a much more versatile program than the other programs that were evaluated, and in addition to soil nails, it can handle tie-backs, struts, Reinforced Earth strips, geotextiles, piles, micropiles, and retaining walls. It is currently available in version 2.3.

The program can handle any one of a number of inputs for hydraulic conditions, including user specified points on a phreatic surface, specified pore pressures, or a triangular mesh with pore pressures defined at every point. Any cross-sectional geometry, with the exception of overhangs, can be accommodated, as can varying distributed surcharges, linear surcharges, additional applied moments, and seismic loadings. Intrinsic strength curves can be input for a given soil, as can curves for cohesion anisotropy.

User input is complicated by the fact that prompts for data entry are given by a shortened French term (e.g., ESP for horizontal spacing, short for espace in French). Many of the terms in the program are poorly described in the user's manual. The manual is not well laid out, and descriptions of a given input parameter are often hard to find.

TALREN utilizes classical limit equilibrium methods of slope stability to calculate its overall safety factors for a given cross-section. Choices available for calculation methods include the simplified Bishop method of slices, Fellenius' method of slices, or the perturbations method. For the present comparison, the simplified Bishop's method was used. As is standard with this method, the soil is divided into infinitesimally small vertical slices, and the static equilibrium of these slices is evaluated. The global safety factor is assumed constant along the length of the failure surface and is defined as the ratio of the maximum shear strength, τ_{max}, to the mobilized shear stress, τ, along the failure surface.

TALREN is divided into different modules. A separate module allows data entry and provides the data entry format. Another module calculates the stability; yet another provides the graphical representation of the results, and another serves as the "home" menu. The program can calculate the bending and shearing resistance of the soil nails. The calculation requires the user to input a large number of terms to describe not only the nail properties, but the soil and the nail/soil interaction properties.

Failure of the nail is calculated using Multicriteria analysis (Schlosser 1985), in which a limit envelope for the nail is constructed using the curves for the plasticity of the soil, plasticity of the nail, limit lateral friction, and yield stress of the steel.

The critical slip surface is determined through a grid of circle centers for which the user enters where the grid parameters such as location, size, angle between adjacent centers, and number and increment of radii to be searched. A given circle is then divided into slices, and the corresponding assumptions regarding interslice forces are made. If the Simplified Bishop Method has been selected, the interslice shear forces are assumed to be equal and opposite, and therefore cancel. If the center of the circle is below the wall crest, the program creates a

composite surface, rather than allowing an overhang. The composite surface simply consists of a vertical portion grafted onto the remaining "allowable" surface (Figure 5.9). Noted that the program conservatively assumes that the shear forces acting on the vertical section of wall are zero. The manual indicates that in later versions this assumption may be replaced by an active soil pressure distribution acting on the vertical section of the slip surface.

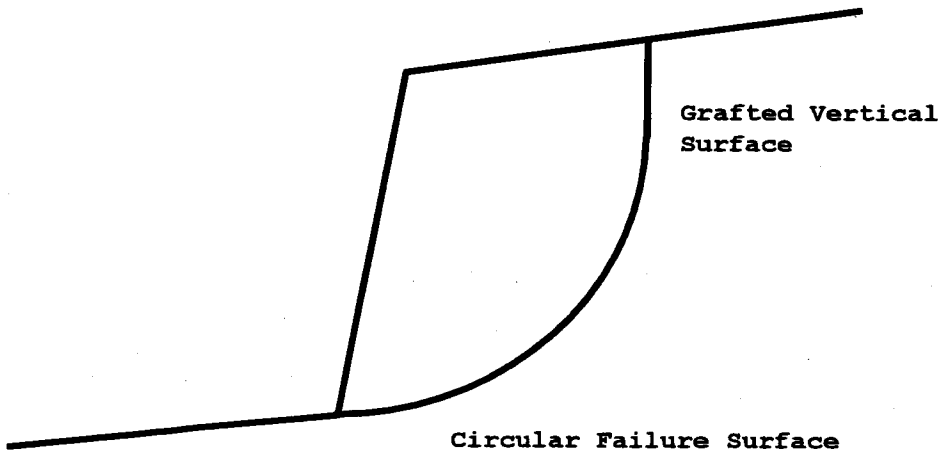

Figure 5.9. Composite failure surface for TALREN

With soil nails, the inclusion is assumed to be working in a combination of tension and shear. As with all limit state analyses, the nails are evaluated using their at-failure strengths. These strengths, as previously mentioned, are determined using Schlosser's Multicriteria envelope. The nail is modeled as an elastically supported beam. In shear and normal space, the Tresca criterion provides a limiting envelope of the form:

$$(T_n^2/R_n^2) + (T_c^2/R_c^2) \leq 1.0 \tag{5.3}$$

where T_n = tension force in the nail

R_n = ultimate tension force in the nail

T_c = shear force in the nail

R_c = ultimate shear force in the nail = $R_n/2$

At the point of maximum moment the nail works in combined bending. Here the developed envelope has the form

$$M_{max} = M_{max0}(1-(T_n^2/R_n^2)) \tag{5.4}$$

where M_{max0} = maximum bending moment of the nail in simple flexure.

This equation is only valid for a rectangular bar and is conservative for circular cross sections such as nails. The soil/inclusion lateral friction is limited by the following:

$$T_n \leq L_a f_{lim} \tag{5.5}$$

where L_a = length of the nail outside the slip surface

f_{lim} = limiting shear force/length of nail

The nail normal reaction is limited by the elasto-plastic rule:

$$P = K_s y \tag{5.6}$$

where P = soil pressure under the nail

K_s = soil modulus of subgrade reaction

y = deflection of the soil

and $P \leq P_L$, where P_L = limit pressure of the soil. (5.7)

TALREN models the nails in two different ways, depending on their transfer length (Table 5.1). It assumes that they can either be modeled as an infinitely long beam or an infinitely

rigid beam. At the point of convergence, the difference between the two analyses differs by 25 percent.

Table 5.1. TALREN Nail Modeling

Bending resistance of the inclusion (M_{max})	Minimum length available on one side of the failure surface	
	"Long" inclusion $L^* \geq 2 \cdot L_0$	"Short" inclusion $L^* < 2 \cdot L_0$
HIGH	$M_{max} > 0.16 \cdot p_l \cdot B \cdot L_0^2$ $T_{cl1} = p_l \cdot B \cdot L_0/2$	$M_{max} > p_l \cdot B \cdot L^* \cdot 2/27$ $T_{cl1} = p_l \cdot B \cdot L^*/4$
LOW	$M_{max} < 0.16 \cdot p_l \cdot B \cdot L_0^2$ $T_{cl2} = 0.24 \cdot p_l \cdot B \cdot L_0$ $+ 1.62 \cdot M_{max}/L_0$	$M_{max} < p_l \cdot B \cdot L^* \cdot 2/27$ $T_{cl2} = 0.10 \cdot p_l \cdot B \cdot L^*$ $+ 4.05 \cdot M_{max}/L^*$

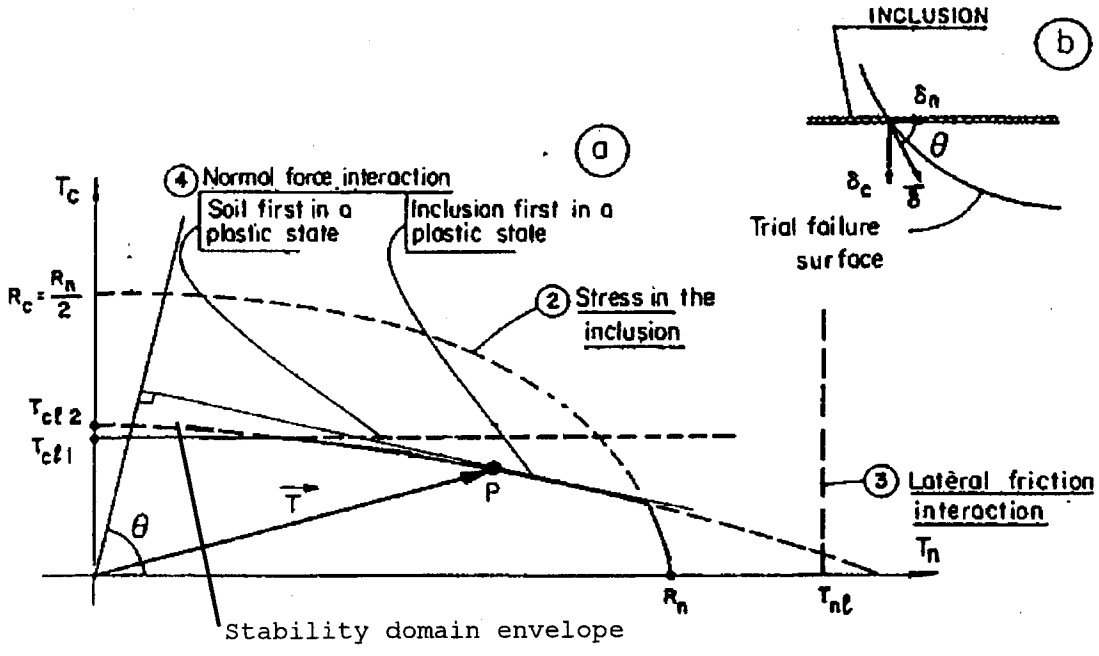

Figure 5.10. Multicriteria envelope used for TALREN

To utilize the envelope to determine the limit state nail forces applied to an individual slice, the program uses Mandel's theory of maximum plastic work (Mandel, 1978). The basic principle of this theory is that at the point of intersection between the nail and the failure surface, the relative displacement between the two parts of the nail, d, is assumed to be tangent to the failure surface (Figure 5.10). Point P in Figure 5.10 corresponds to the point of tangency between the stability domain (as defined in Figure 5.10) and the perpendicular to the δ direction (defined by the angle θ) . T represents the combination of shear and normal forces in the nail; as can be seen in Figure 5.10, T intersects the stability domain at point P, the limiting value of shear and normal forces in the nail.

The program handles the contribution of the nails to the stability of a given slice by applying the normal and tangential reinforcing forces at the failure surface to the base of the slice and along its axis. In addition, in cases of highly heterogeneous soils, the nail forces, both shear and tension, can be distributed over a larger area. This is possible through the specification of a base width of diffusion for the forces L_b and an angle of diffusion ALB (both previously defined), which define how the diffused area expands as it moves from the head of the nail to the slip surface. The computational procedure for the overall stability can be summarized as follows:

a) calculation of the safety factor for the unreinforced soil

b) calculation of the tension and shear forces for each reinforcement, on the basis of the previously calculated factor of safety

c) determination of the distribution of tension associated with (b)

d) calculation of the safety factor for the reinforced soil

e) iteration of steps (b) through (e) until convergence is reached for the factor of safety.

It is necessary to iterate until convergence because calculation of the tension and shear forces in the nails depends on the safety factor for the unreinforced soil. To derive an overall or global safety factor, *TALREN* adds the component of the tension forces supplied by the nails

perpendicular to the slip surface to the resisting moment, and subtracts the shear resistance supplied by the nails from the driving forces.

Output is in the form of plots of the wall cross-section with the slip surfaces depicted, as well as convenient displays of the material safety factors and the soil properties (Figure 5.11). Calculation can also be output in a number of different forms. The program prompts the user to define specifically which output is required; the comprehensive option includes the input parameters, as well as all worst case surfaces for each circle center and the corresponding nail forces. *TALREN*'s calculation results can be output on any number of common printers, although the printout is in landscape format. However, the graphical output requires a plotter, post-script laser printer, or a Laser-jet III or later model for proper results. The program also supports the use of two separate plotting routine programs, which are not included with the basic package. The program has a separate utility (not reachable from the main menus) that allows one to select the printer type, and it provides marginally better resolution than the printscreen utility of DOS, which often results in nearly illegible output of many screen figures.

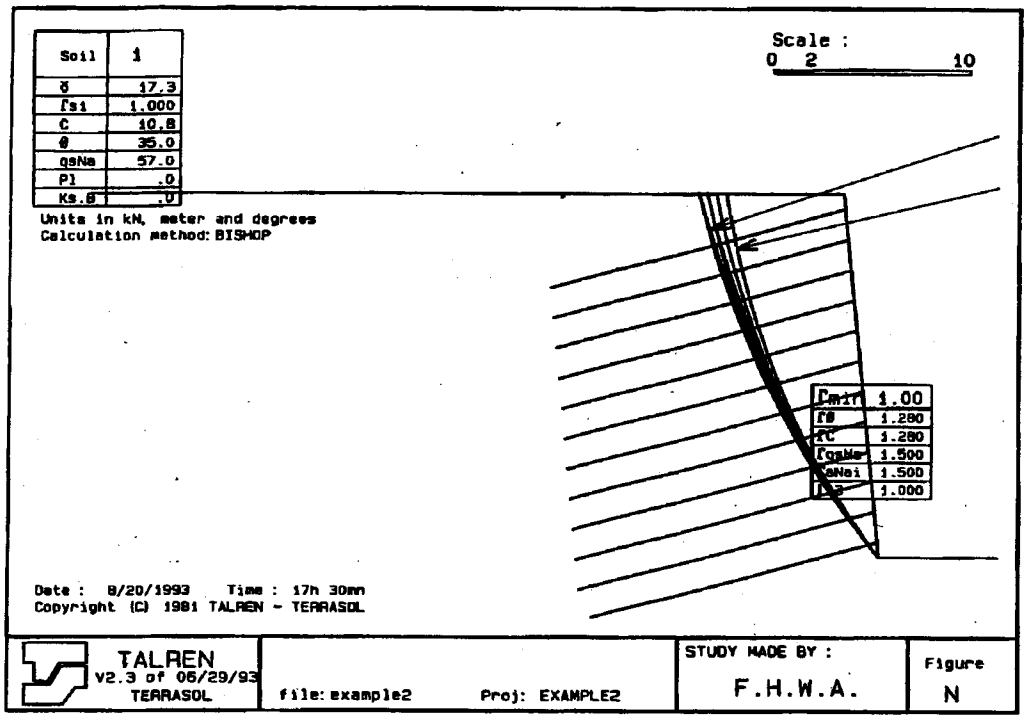

Figure 5.11. Output for TALREN

5.7 CLOUDIM

CLOUDIM is a user-friendly design package for soil-nailed walls developed by a private engineering firm from France. The software is presently marketed in the U.S. by GIT Consultants, of White Plains, New York. The program is written in an interactive programming environment and has an excellent user interface that includes on-screen graphics and mouse/menu driven procedures. The screen display allows the user to input geometry, surcharge, water table, and nail data and to perform the necessary analyses using the mouse. The user can choose between either safety factor evaluation or reinforcement design. The program is simple but quite versatile in comparison to the other programs evaluated.

The program is flexible enough to allow irregular wall cross-sections and any number of irregular soil layers. The program also considers parabolic phreatic surfaces, which are somewhat more realistic than horizontal or inclined water tables.

The program uses the limit equilibrium approach of slope stability to calculate the global safety factor for a given cross-section on the basis of assumed circular failure surfaces. The shear strength of the soil is expressed in terms of a Mohr-Coulomb failure criterion (i.e., $\tau = C + \sigma \tan \phi$). The program calculates the mobilized shearing resistances on the failure surface by applying a material safety factor, F, to the cohesive and the frictional components of the strengths. Two additional constants, λ and μ, are introduced to render the system statically determinate. These constants are related to the normal stress, σ, on the failure plane as follows:

$$\sigma = \gamma h \cos(\alpha)^2 [\lambda + \mu \tan(\alpha)] \tag{5.8}$$

The global factor of safety is defined by the ratio of the sum of resisting moments to the sum of driving moments. The program calculates the two factors of safety simultaneously.

The reinforcement design option does not use the safety factor as the unknown; instead, it finds the nail forces necessary for stability. The failure surface is initially unknown. The user defines a series of trial failure surfaces, and the program computes where the sum of the nail forces is maximum.

Details of the theory behind this program are neither furnished in the user manual nor found in the published literature.

The features of each design program are summarized in Table 5.2.

Table 5.2. Summary of Program Features

Program Features	*GOLD NAIL*	*NAILM*	*NAIL SOLVER*	*SNAIL*	*STARS*	*TALREN*	*CLOUDIM*
Profiles							
Benches	x(1)			x		x	x
Backslopes	x	x		x		x	x
Toe slopes	x			x	x	x	x
Wall							
Face press.	x			x			
Soil/water							
No. of layer	Any	Any	1	2	Any	Any	Any
Irregular profile	x					x	x
Water table	x			x		x	x
Inclusions							
Moment						x	x
Varying length	x	x		x	x	x	x
Pullout test data	x	x		x	x	x	x
Tiebacks	x			x	x	x	x
Loadings							
Non-areal surcharges	x		x	x	x	x	x
Point load		x	x		x	x	x
Varying surcharges				x	x	x	x
Seismic	x	x		x		x	x
Lateral				x			
Failure surface	circle	para -bola	bilinear wedge	bilinear wedge	log spiral	circle	circle
Graphics							
Input data					x	x	x
Cross-section	x			x	x	x	x

Notes: x signifies that the program will accommodate the specific option. (1) will allow the user to enter points defining a benched wall. The program will calculate the safety factors or nail loads based on an equivalently sloped wall face. The output data defining the wall geometry, however, remain as input.

CHAPTER 6

EVALUATION OF DESIGN METHODS

6.1 METHOD OF COMPARISON

The analysis packages presented in the previous section were evaluated by running 15 example problems with the programs (figures 6.1 through 6.15). The design examples included ten hypothetical walls, three in-service walls, and two actual failure cases. The ten example problems were chosen so that the problem features would be varied. The actual in-service walls and failure cases were selected for their data availability. A brief summary of the problems is presented in Table 6.1.

The computed "factor of safety" and the location of the slip surface for each case were compared to evaluate the performance of the programs. To accommodate the different definitions of an overall safety factor, a standardized approach was devised to ensure that the comparison was as consistent as possible. This of course did not include the inherent effect of the assumed slip surfaces. Four general safety factors are applied to nail yield strength, bond strengths (soil/nail), soil strengths, and overall or global stability. The procedure used in this analysis was to set the first two to 1.5 and vary the third until the fourth, or the global stability, was equal to unity.

The analysis by *TALREN* did not include the benefit of nail shear. This was done partly to make the comparison more consistent and partly because of the difficulty in choosing appropriate values for the many input parameters. The additional complication of face pressure had to be included in the analyses with the programs, *SNAIL* and *GOLDNAIL*. The larger was the face pressure, the less critical was the internal stability, and the closer the results of these two programs were to the results predicted by the other programs. The procedure with *SNAIL* and *GOLDNAIL* was to vary the face pressure in a given example to determine its effect until further

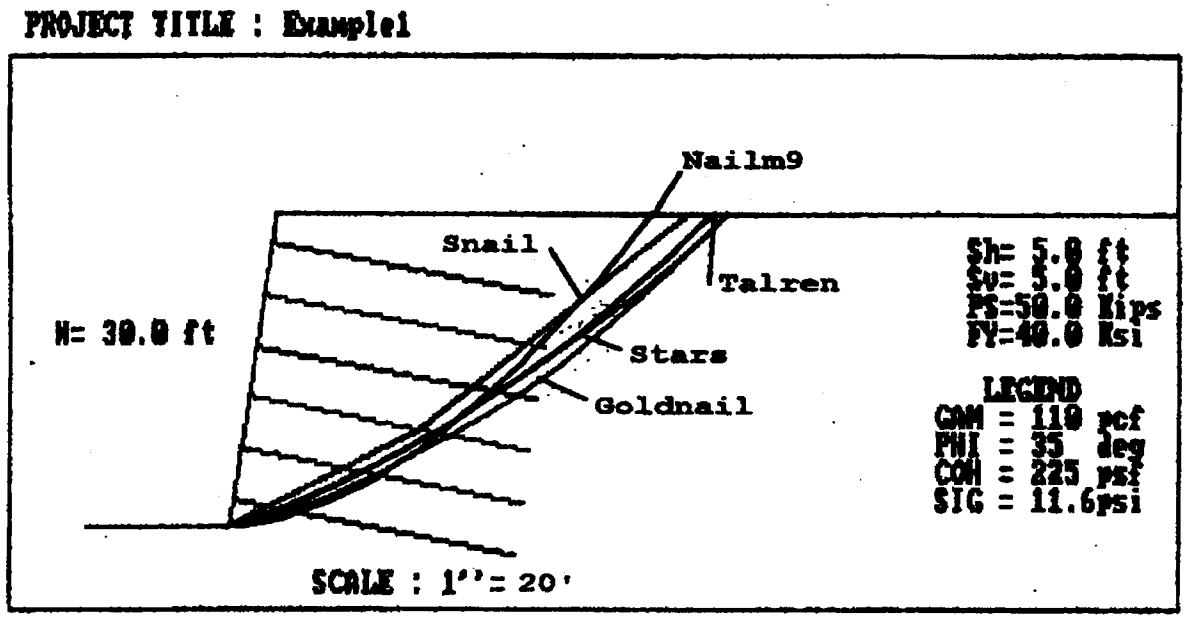

Example 1

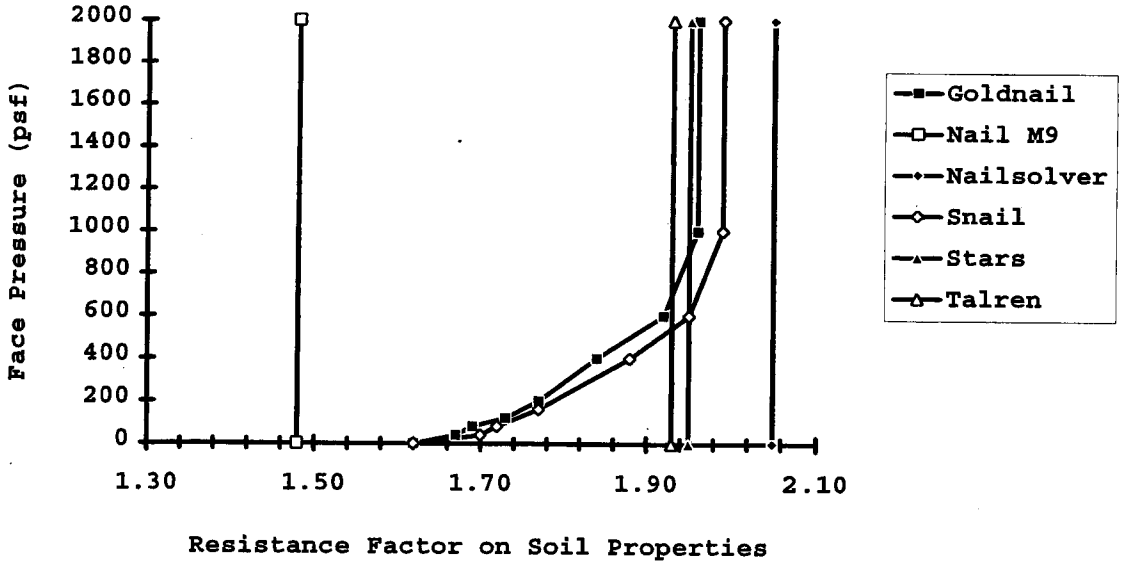

Figure 6.1. Comparison of computed results — Example 1

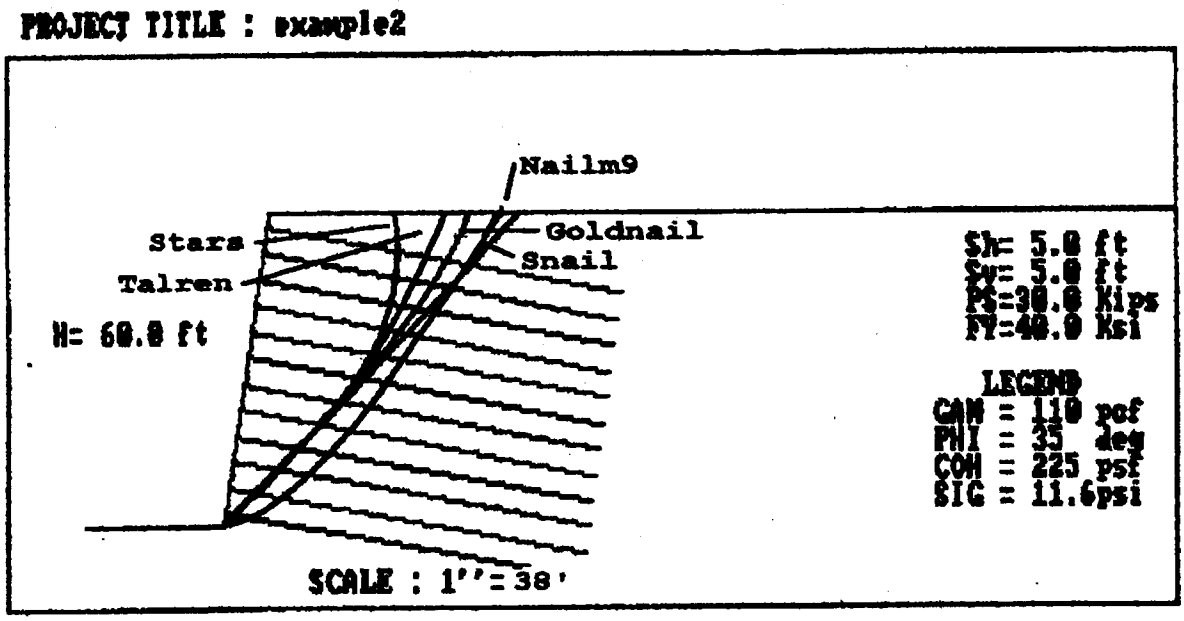

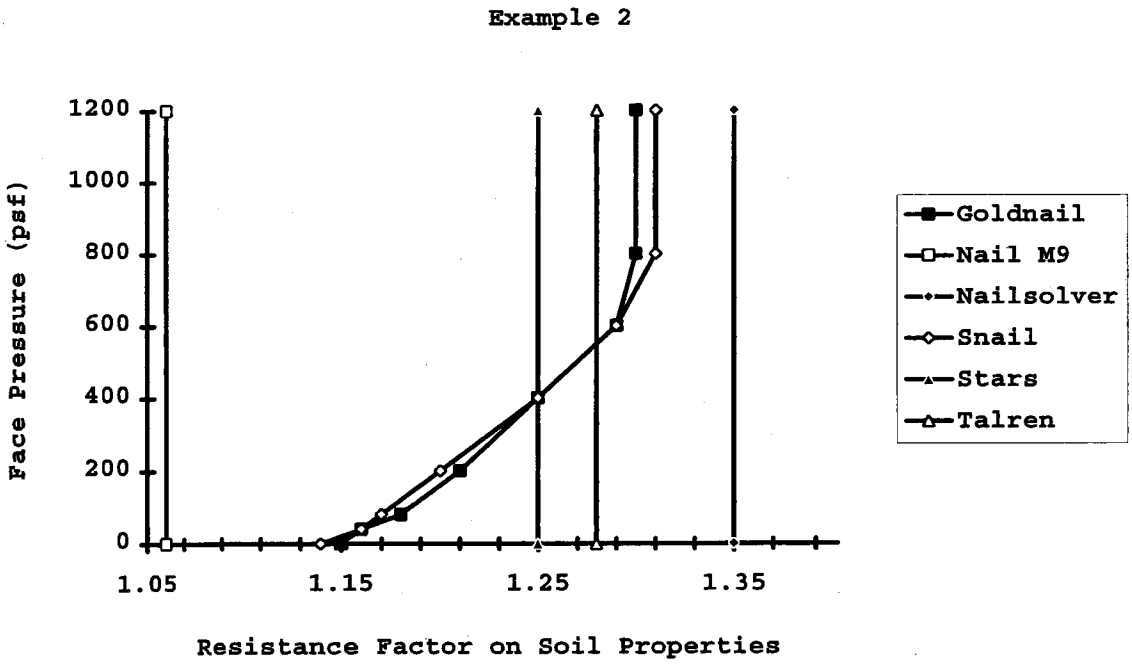

Figure 6.2. Comparison of computed results — Example 2

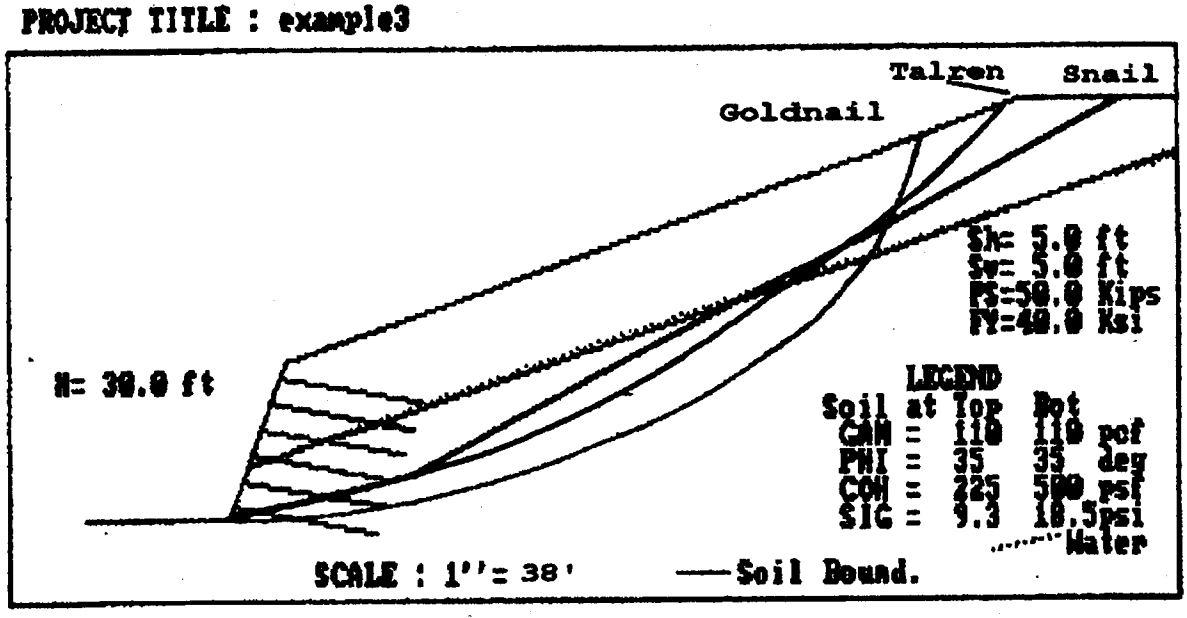

Example 3

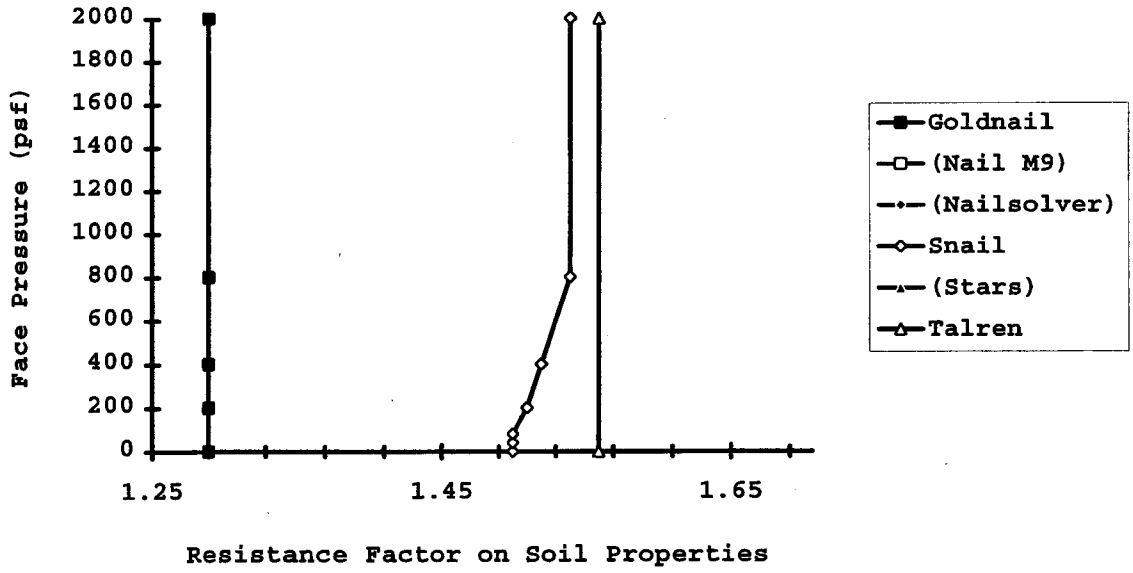

Figure 6.3. Comparison of computed results — Example 3

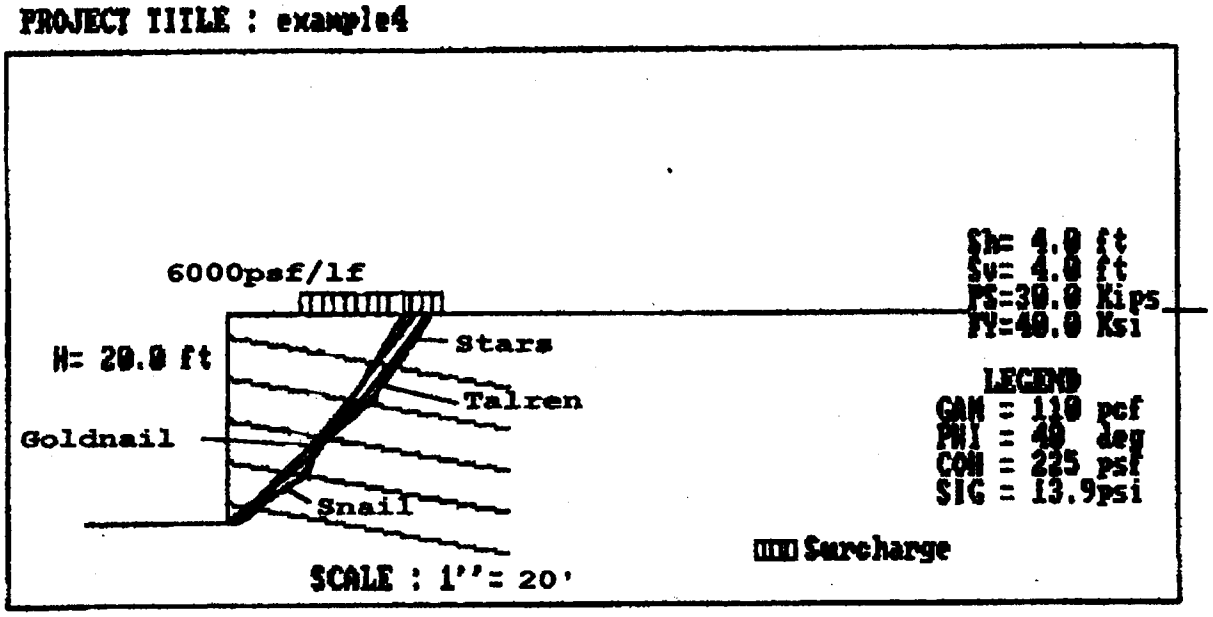

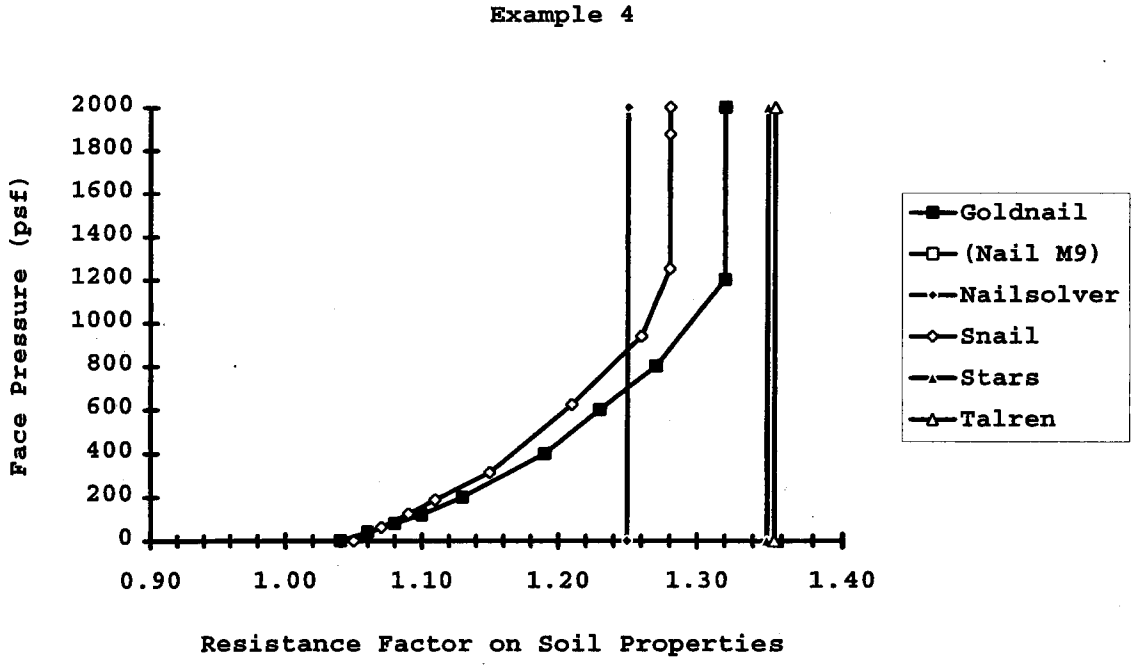

Figure 6.4. Comparison of computed results — Example 4

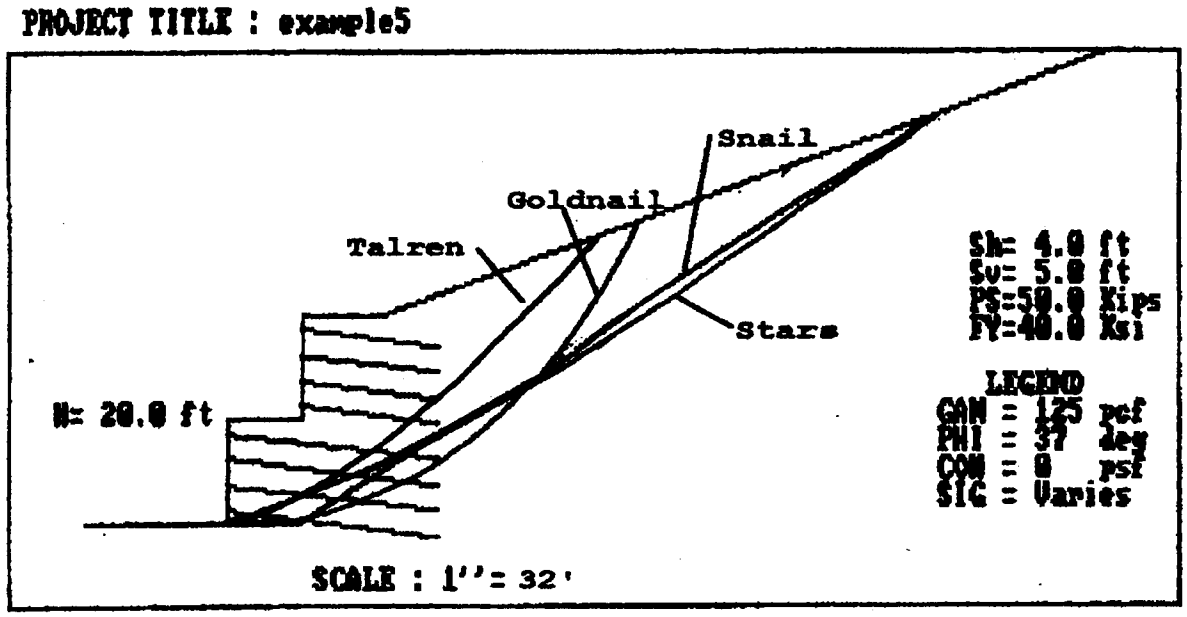

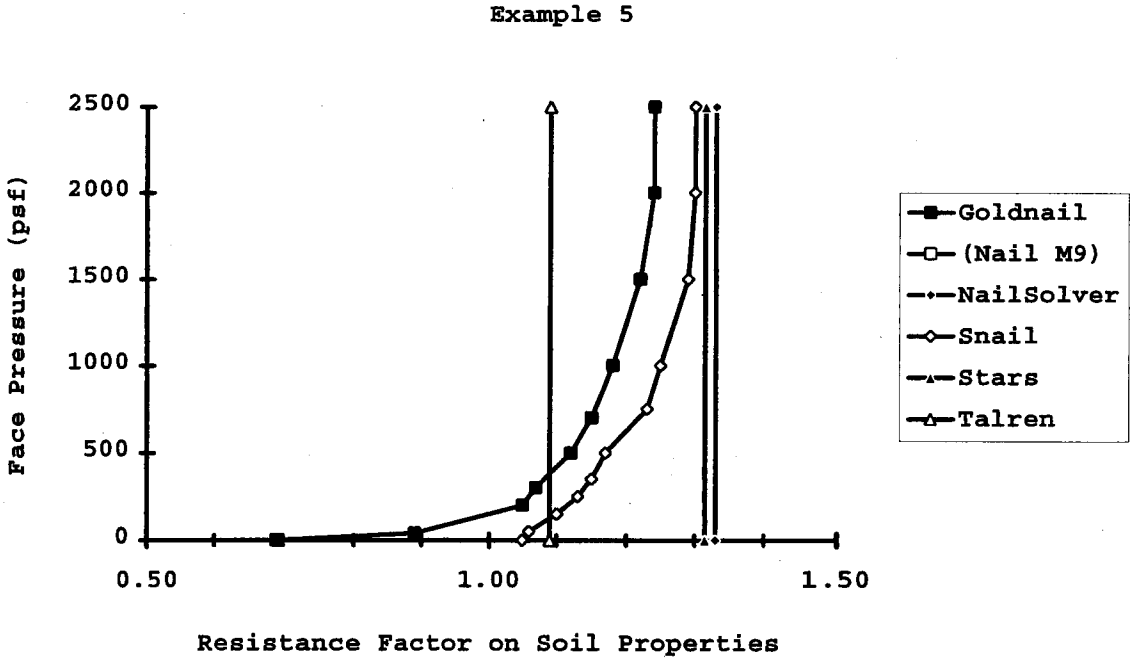

Figure 6.5. Comparison of computed results — Example 5

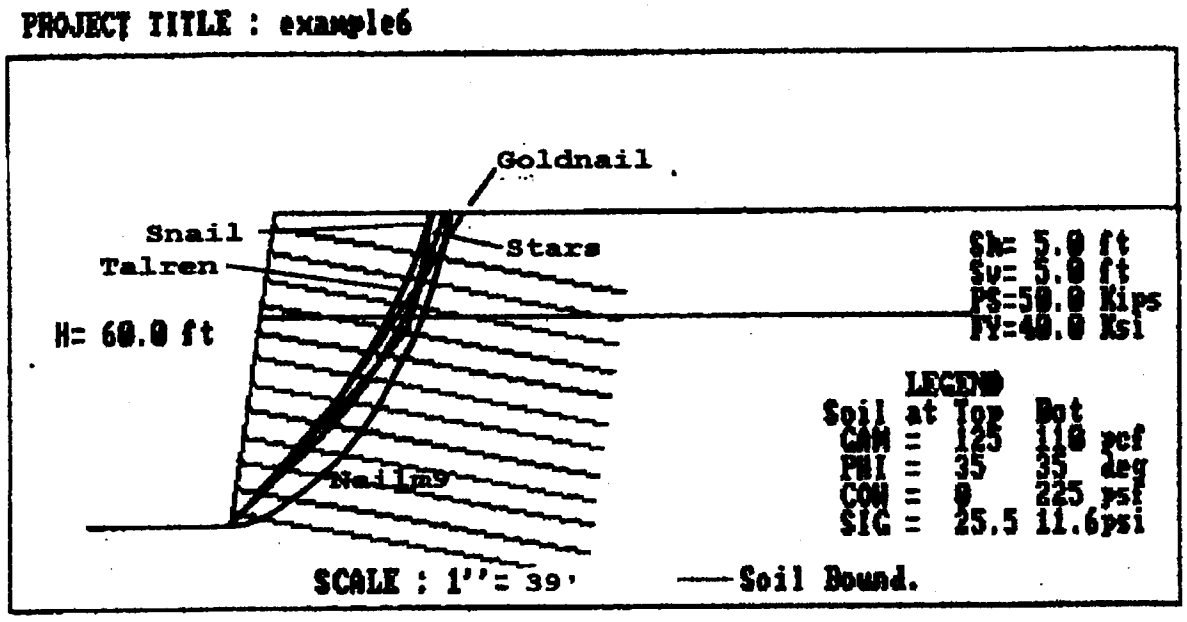

Example 6

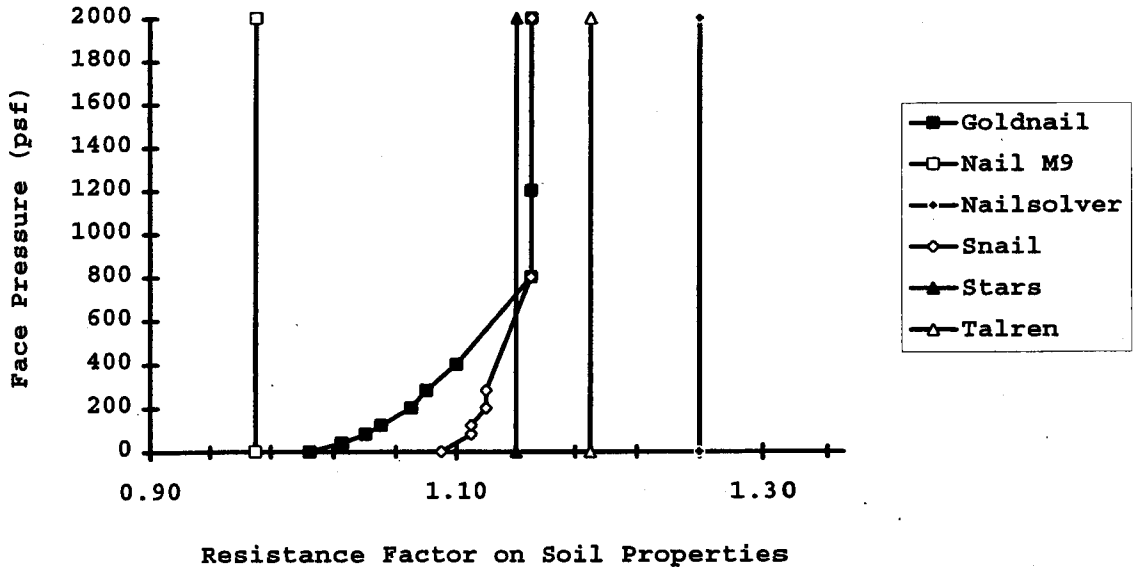

Figure 6.6. Comparison of computed results — Example 6

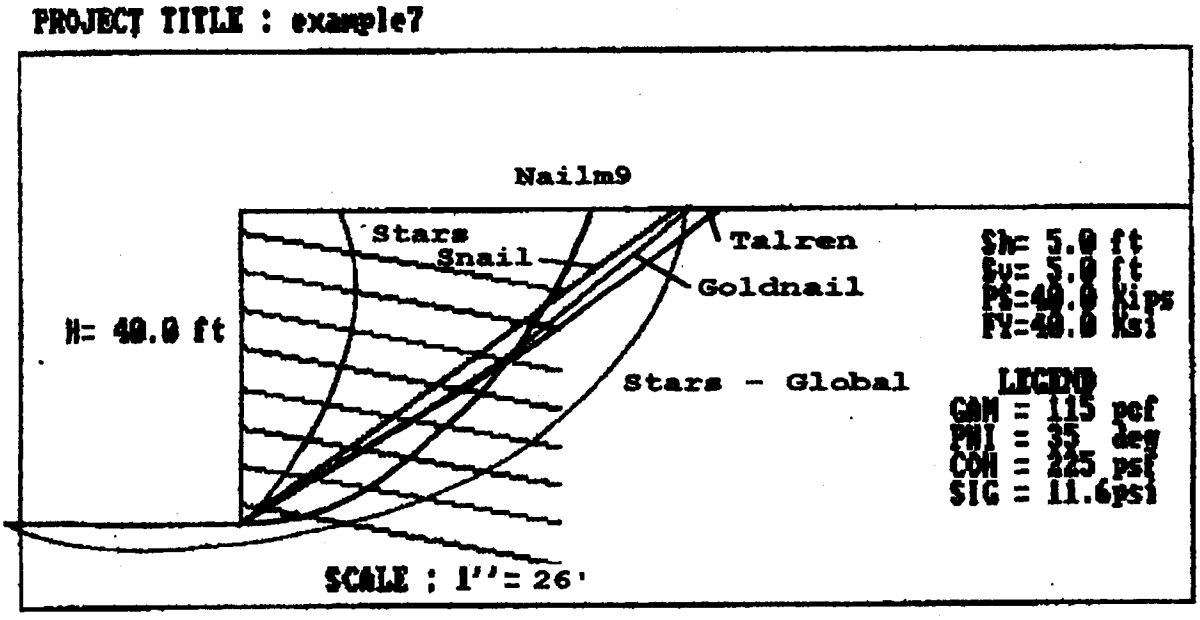

Example 7

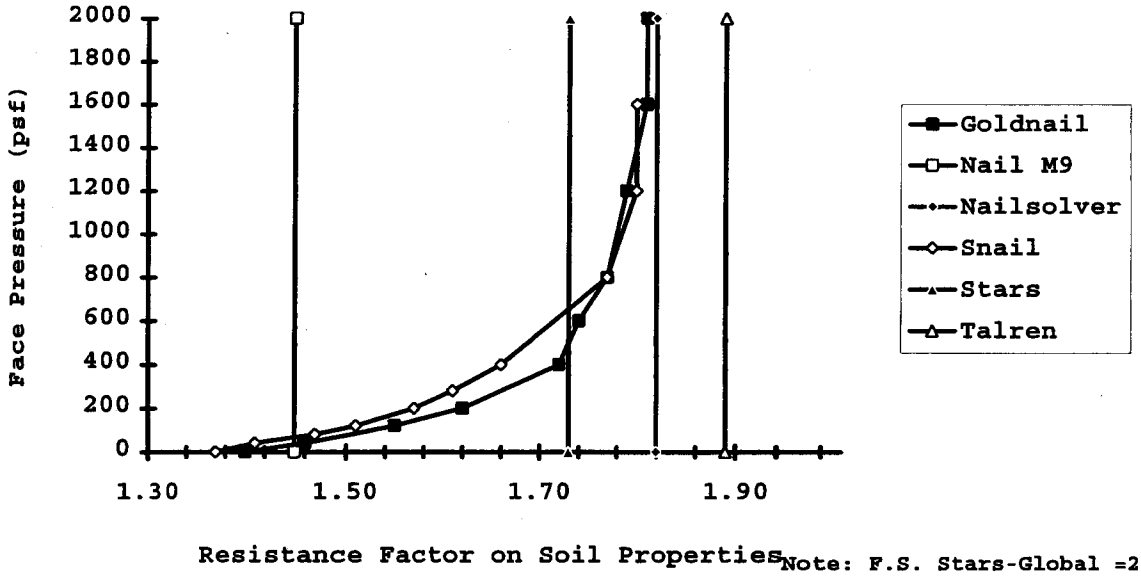

Figure 6.7. Comparison of computed results — Example 7

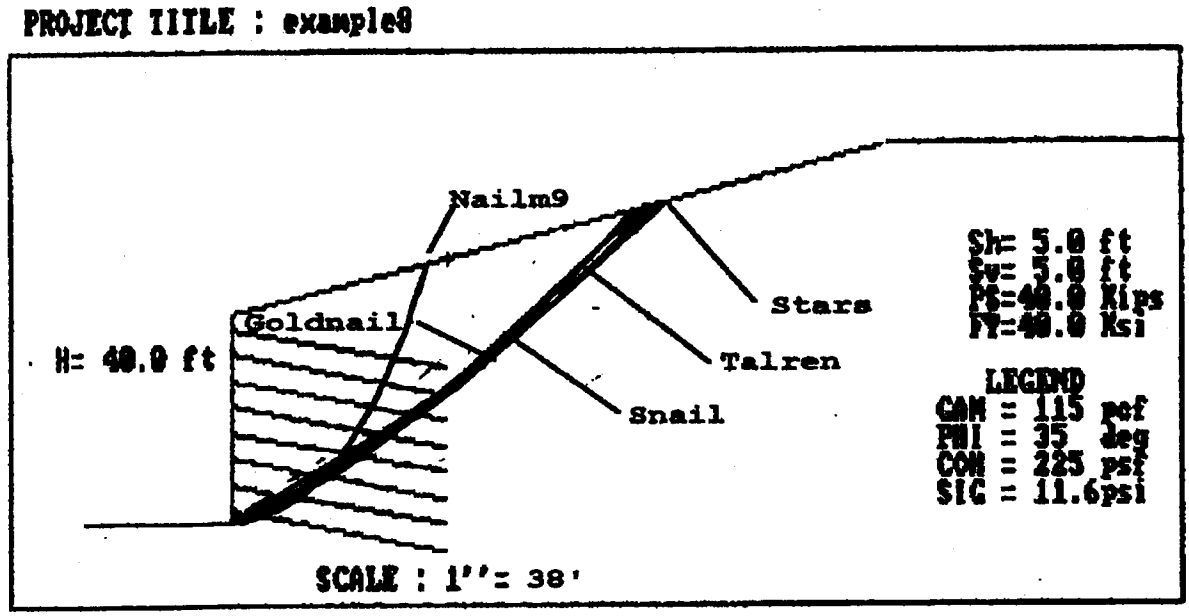

Example 8

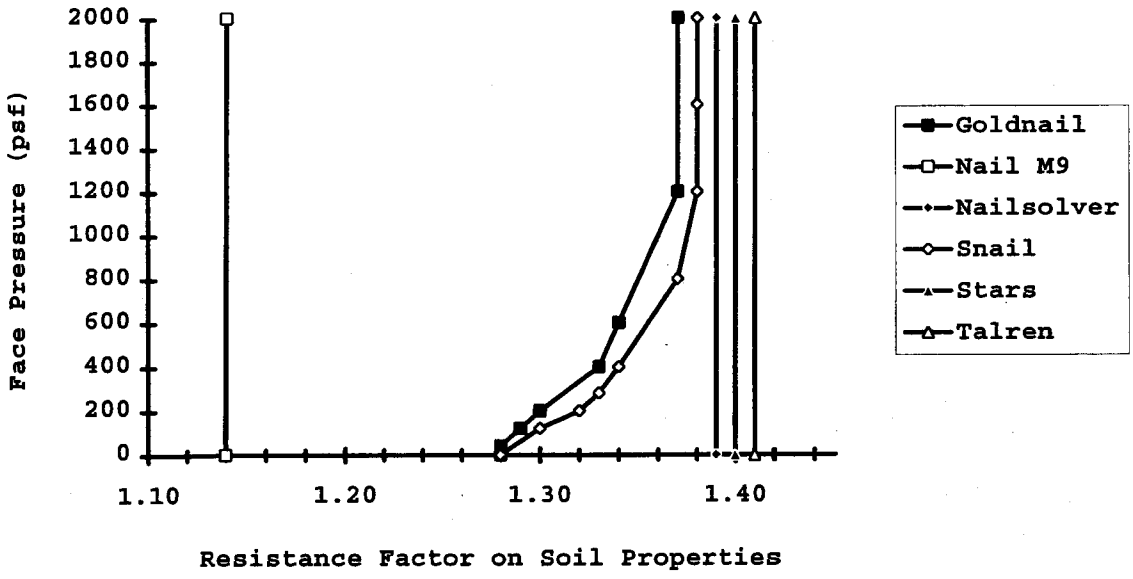

Figure 6.8. Comparison of computed results — Example 8

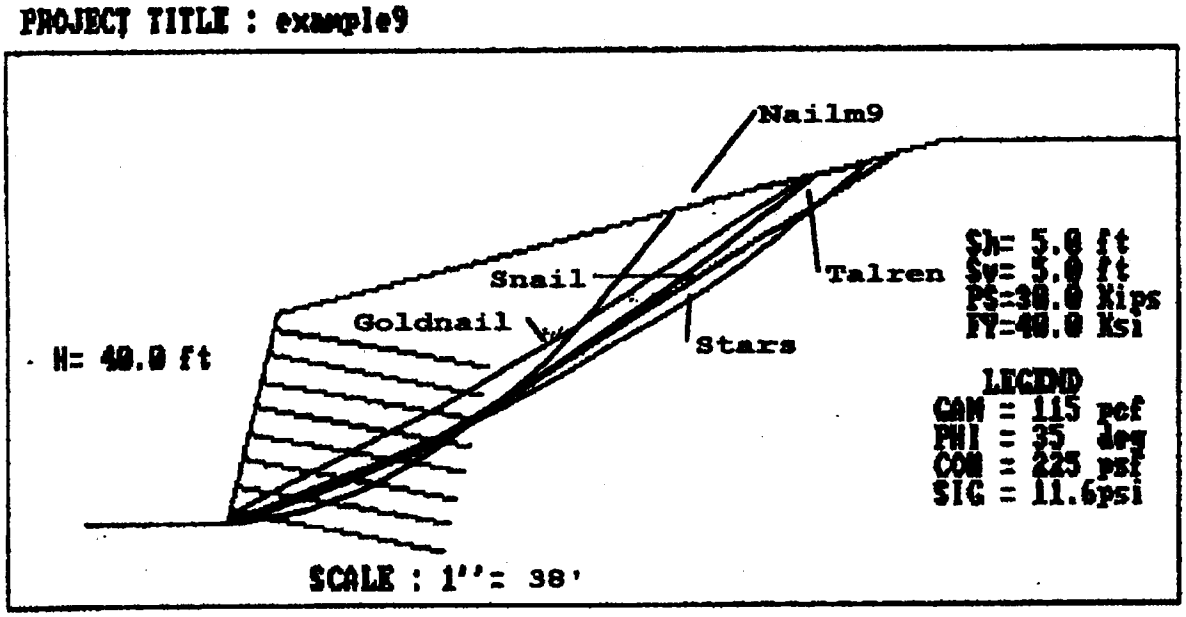

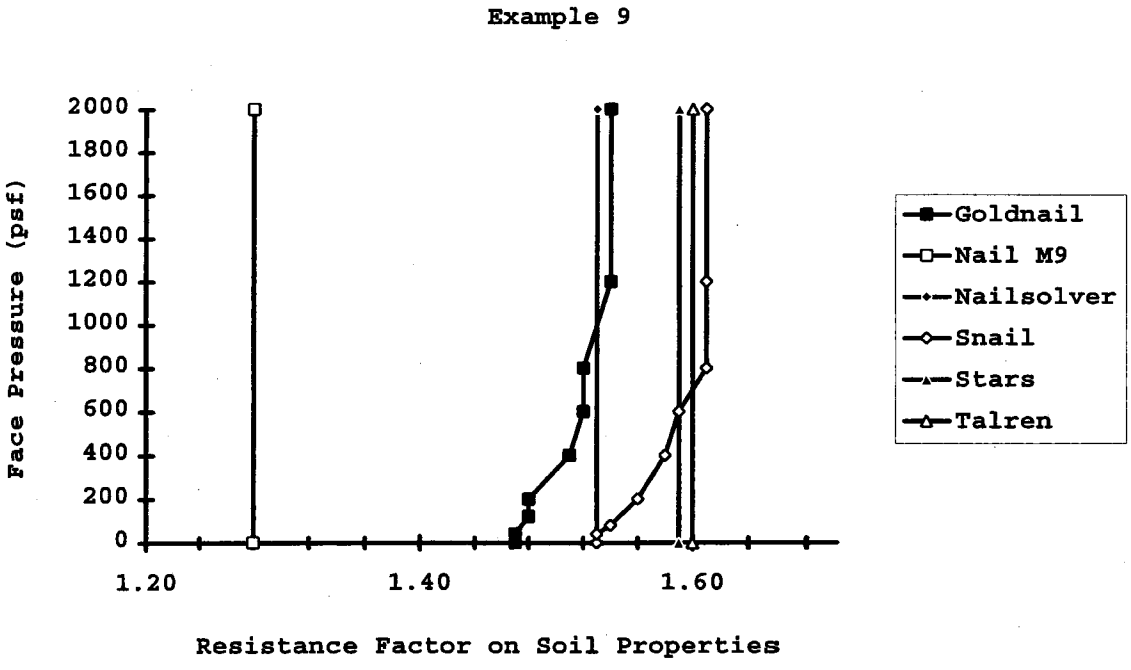

Figure 6.9. Comparison of computed results — Example 9

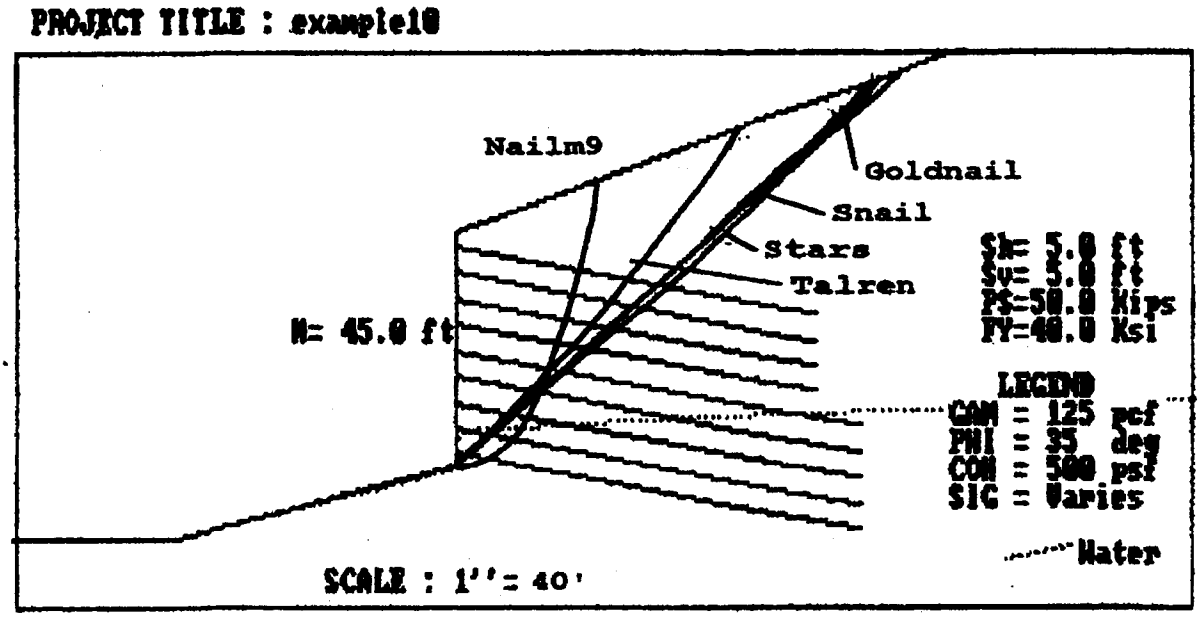

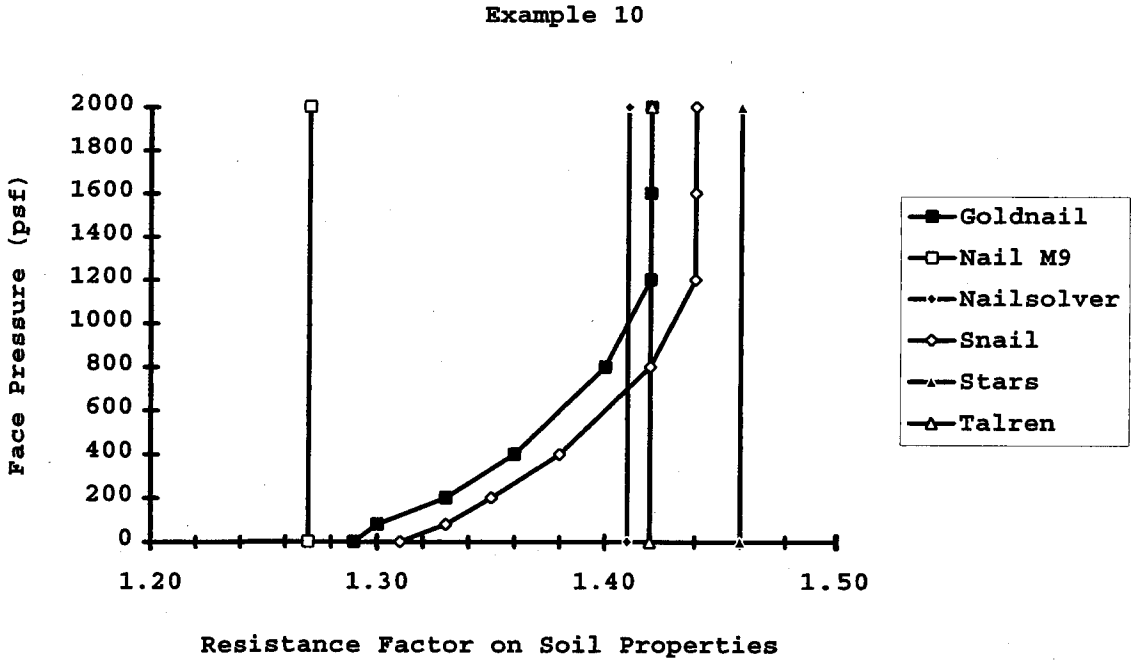

Figure 6.10. Comparison of computed results — Example 10

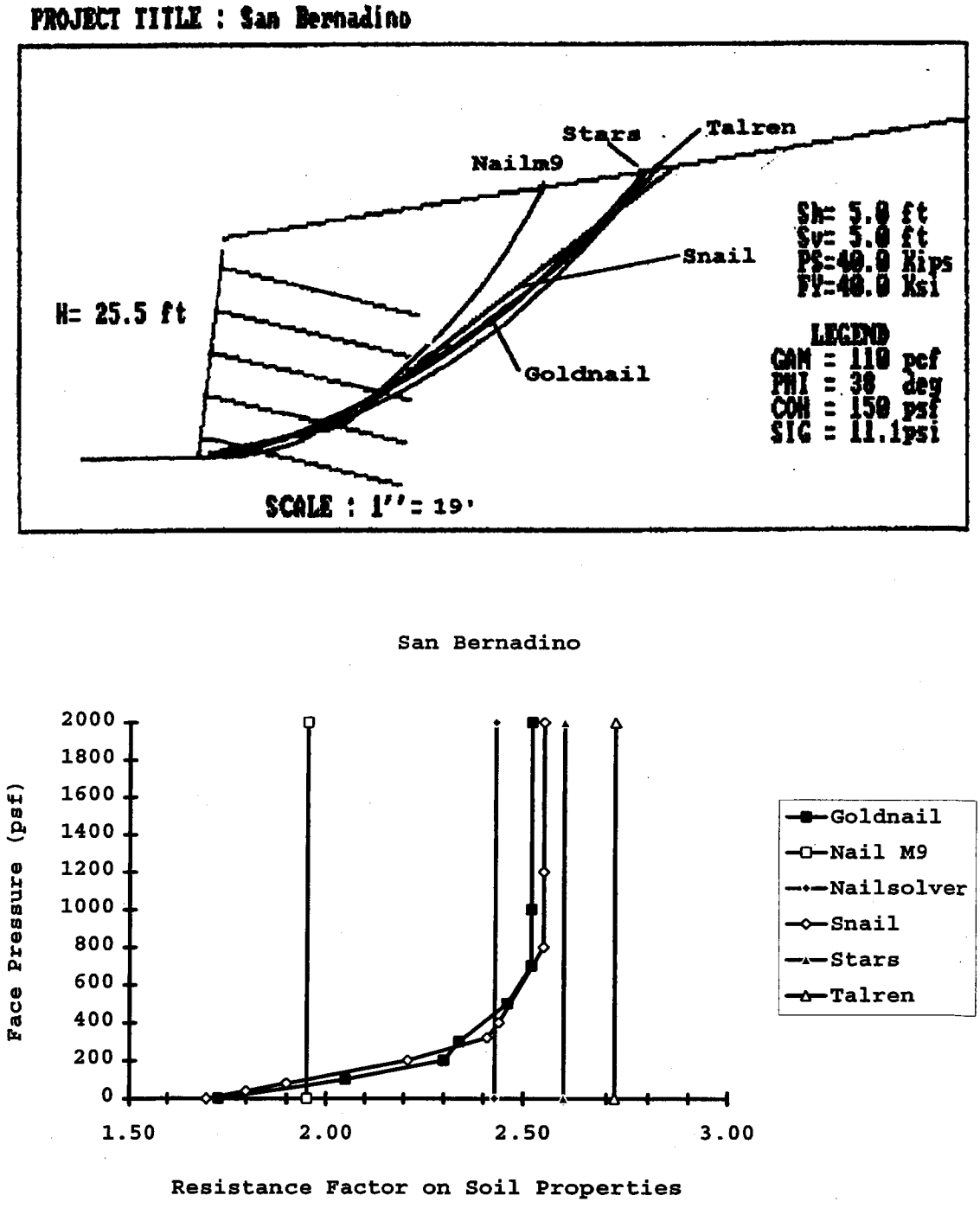

Figure 6.11. Comparison of computed results — San Bernadino Wall

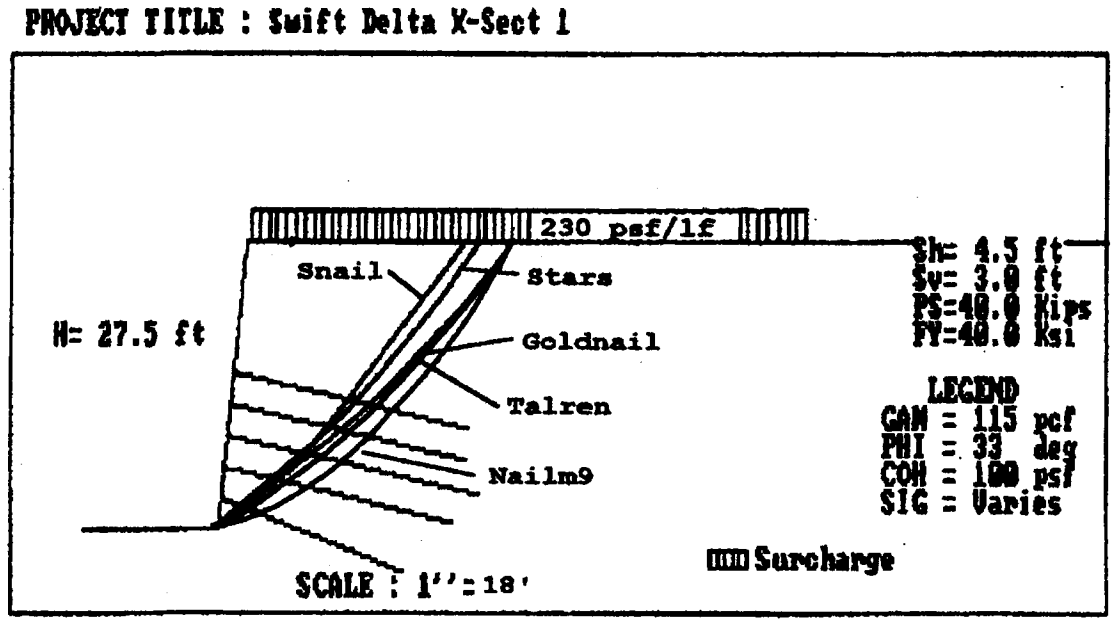

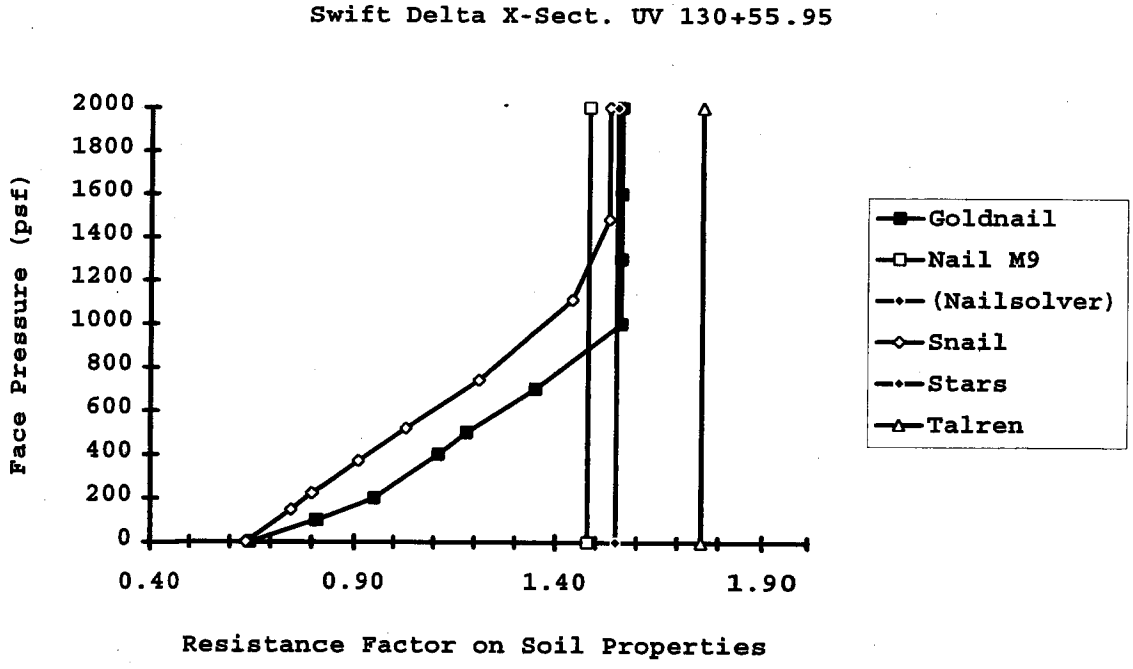

Figure 6.12. Comparison of computed results — Swift Delta 1 Wall

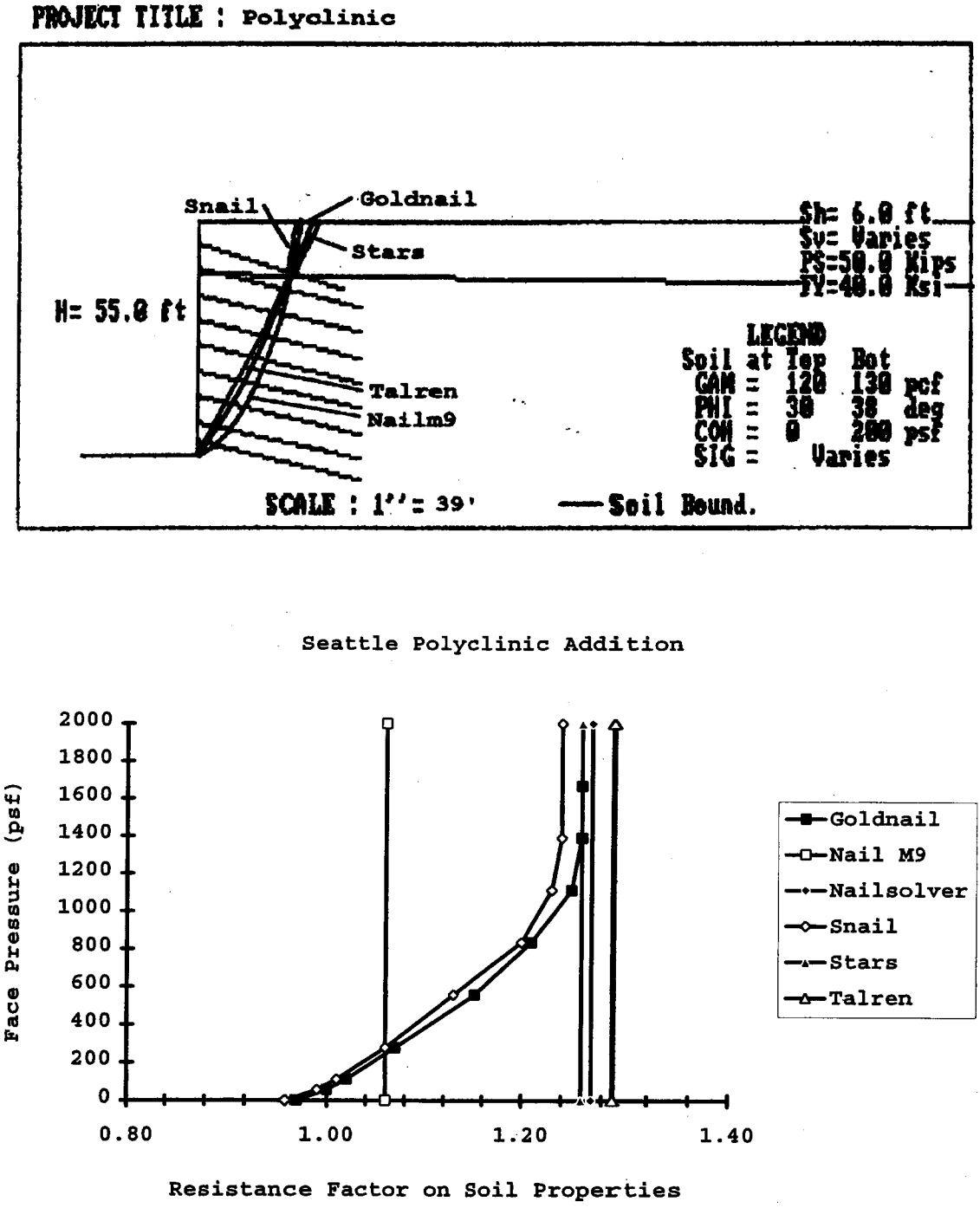

Figure 6.13. Comparison of computed results — Polyclinic Wall

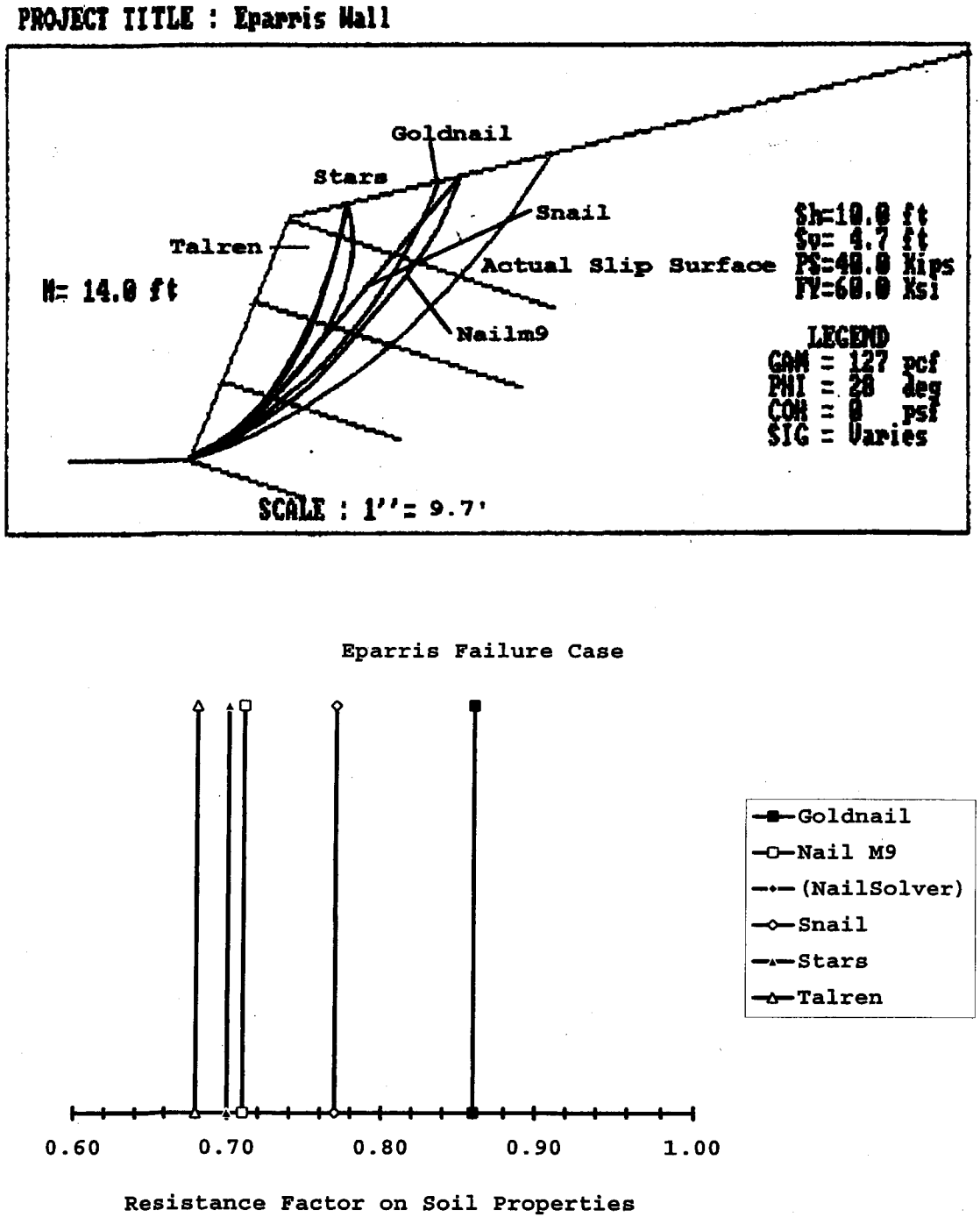

Figure 6.14. Comparison of computed results — Eparris Wall

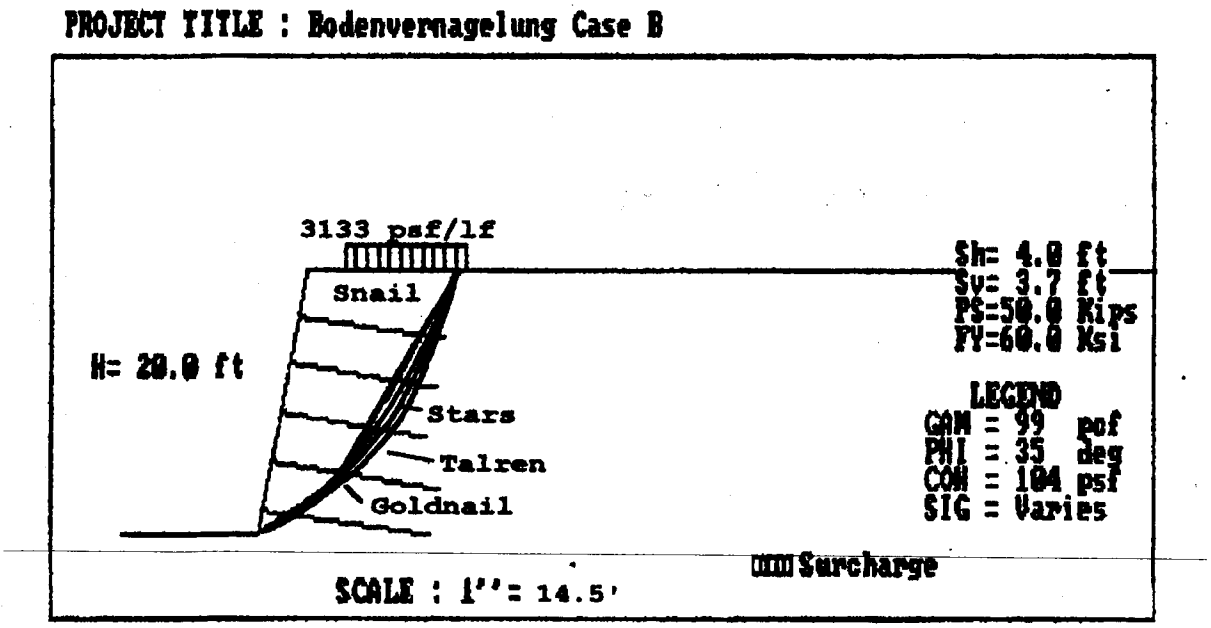

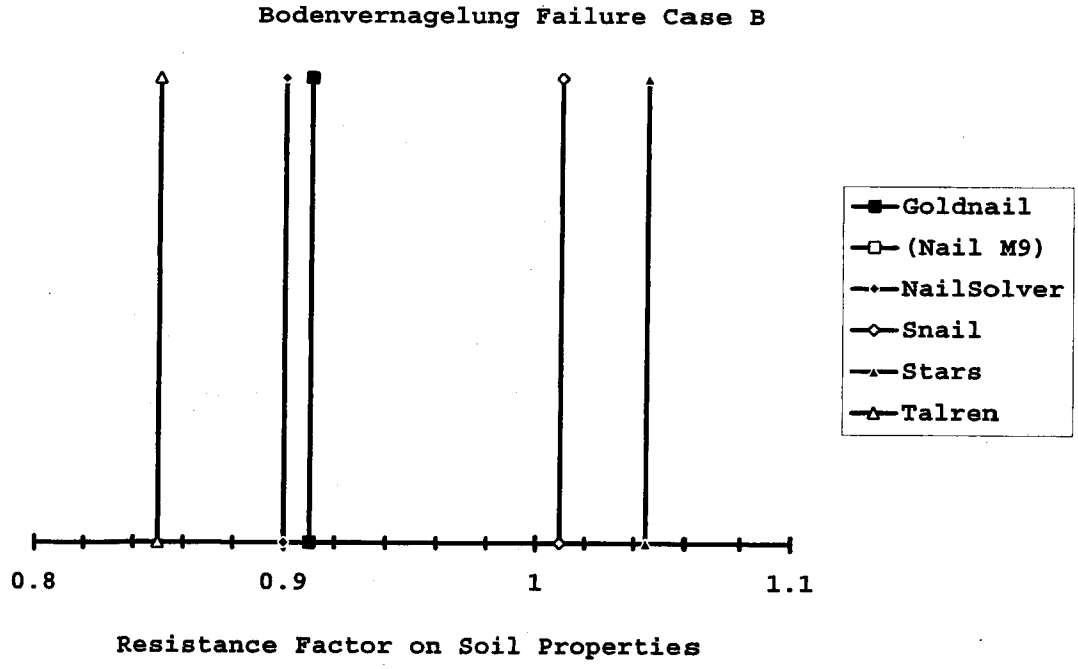

Figure 6.15. Comparison of computed results — Bodenvernag, B Wall

Table 6.1: Summary of Example Problems

Example No.	Brief description
Example 1	30' wall, horizontal backslope, 5.7° batter
Example 2	60' wall, horizontal backslope, 5.7° batter
Example 3	30' wall, sloped backslope, 14° batter
Example 4	20' wall, horizontal backslope, 0° batter, surcharge
Example 5	Benched 40' wall, sloped backslope, 0° batter
Example 6	60' wall, horizontal backslope, 5.7° batter, Layered soils
Example 7	40' wall, horizontal backslope, 0° batter
Example 8	40' wall, sloped backslope, 0°batter
Example 9	40' wall, sloped backslope, 10° batter
Example 10	45' wall, sloped backslope, toe slope, 0° batter
San Bernadino	25.5' wall, sloped backslope, 5.7° batter
Swift-Delta 1	27.5' wall, 4.8° batter, surcharge
Polyclinic	55' wall, horizontal backslope, 0° batter, Layered soils
Eparris	14' wall, sloped backslope, 20° batter
Bodenvernag-elung, Case B	20' wall, horizontal backslope, 9.5° batter, surcharge

variation in the value produced no change in the overall safety factor. The slip surface corresponding to this final value of the safety factor, where face pressure was no longer critical, was compared with the results of the remaining programs.

To facilitate comparisons, a summary of program difficulties or input limitations and additional observations are presented with each example in the following section. If an example is not listed, it indicates that all the programs involved in the comparison could successfully run it. For each of the 15 cases, three sets of plots of the results are included in this section: a general comparison showing factors of safety and slip surface locations (Figs. 6.1 to 6.15) and a set of two plots showing how face pressure/punching shear in *SNAIL* (figures 6.16 to 6.28) and *GOLDNAIL* (figures. 6.29 to 6.41) affected the location of the slip surface (Note: only 13 cases are included in these comparisons, as face pressure was not considered to be critical in the other cases). The programs that were unable to run specific examples are designated by parentheses on the comparison plot legends.

Figures 6.1 through 6.15 represent the most accurate representation of the actual plots described in this chapter. One additional computer program (**CLOUDIM**) was analyzed in a later phase of the research project. Its results were plotted by the principal investigator in a different format than the original plots included in this chapter. These plots are included as Appendix C. Please note that there is some ambiguity in the identification of the individual computer program on some of the plots. No attempt has been made to remove this ambiguity because of a lack of information on the original data from which the plots were developed.

6.2 ADDITIONAL OBSERVATIONS

General

For all of the ten examples and five case studies, trends emerged that are worth noting before beginning any discussion of specific cases. The program *NAILM* predicted safety factors that were considerably less than those predicted by the other packages. This was a result of the

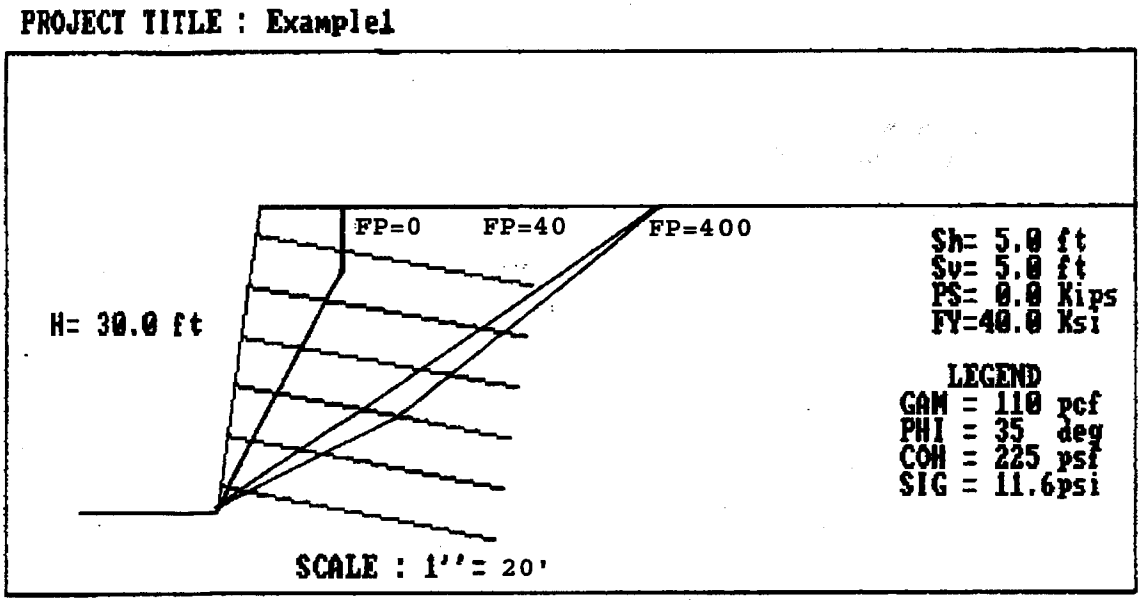

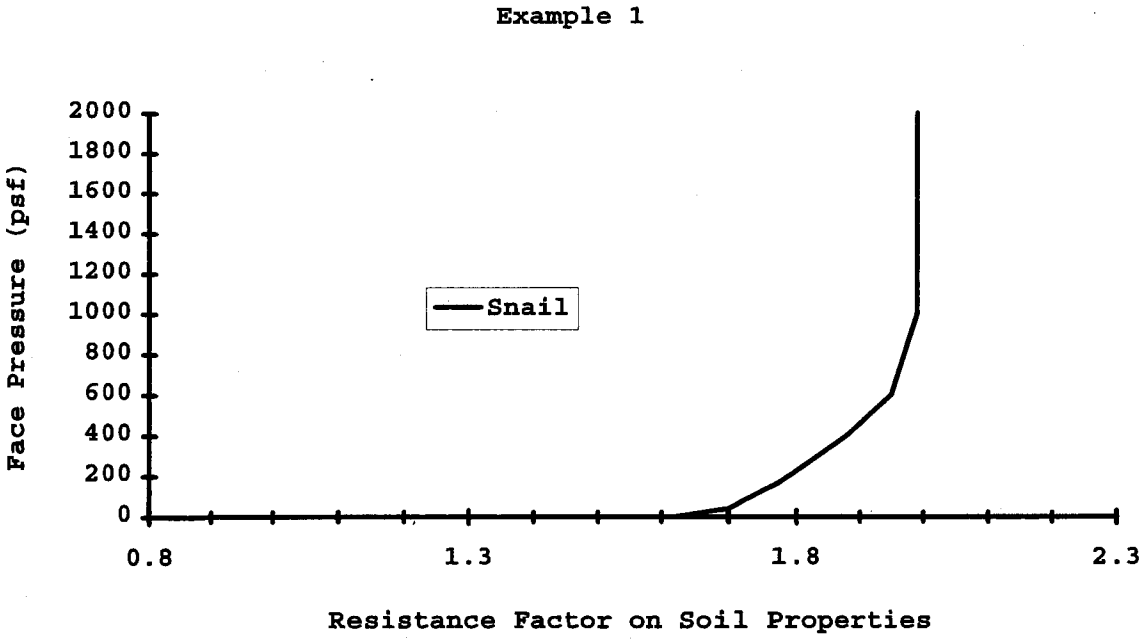

Figure 6.16. Effect of face pressure on SNAIL results — Example 1

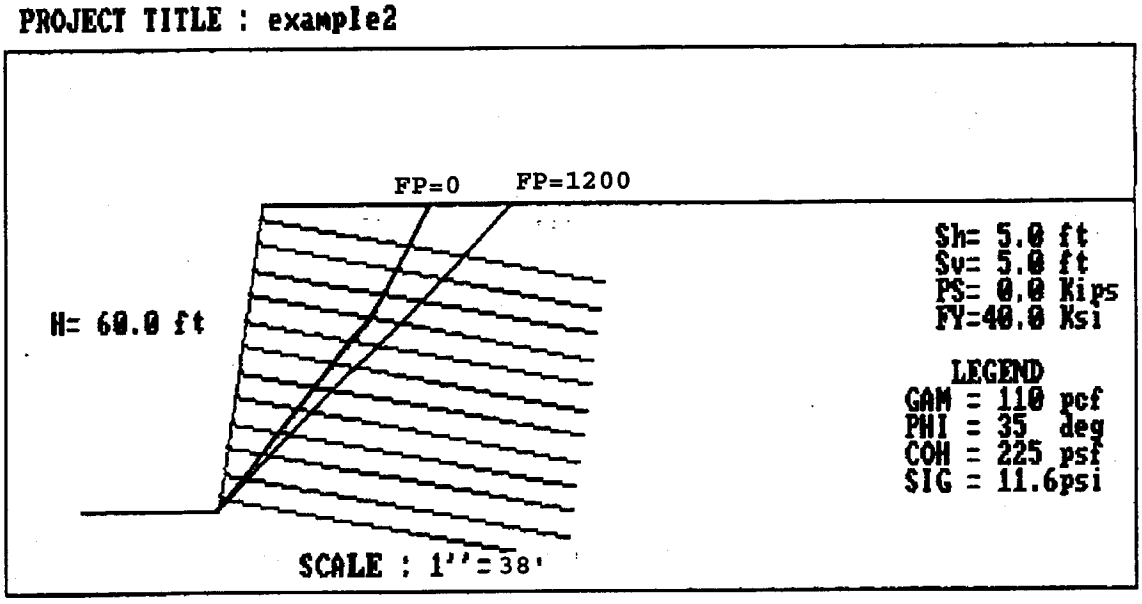

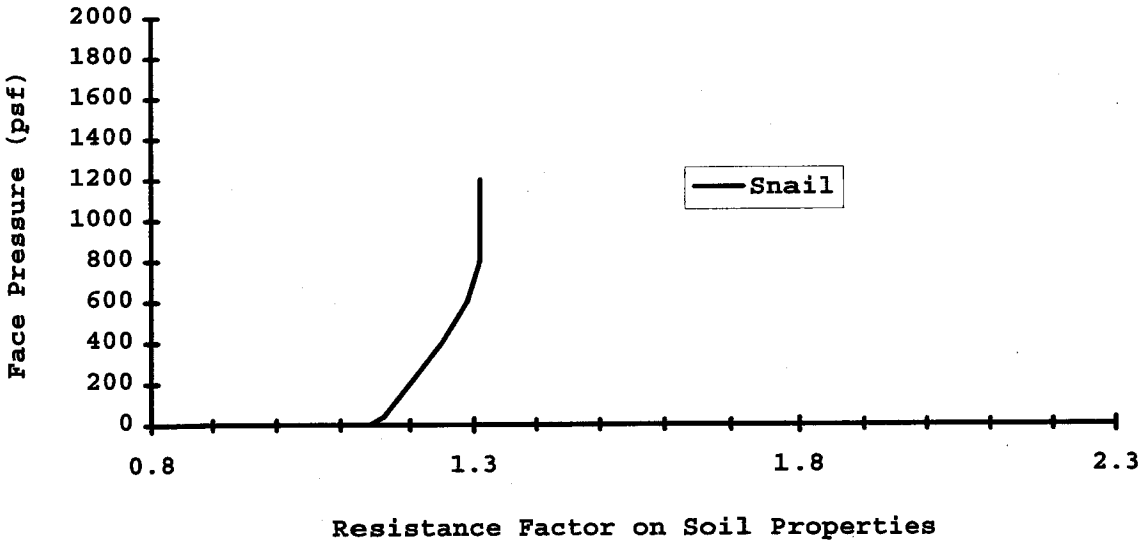

Figure 6.17. Effect of face pressure on SNAIL results — Example 2

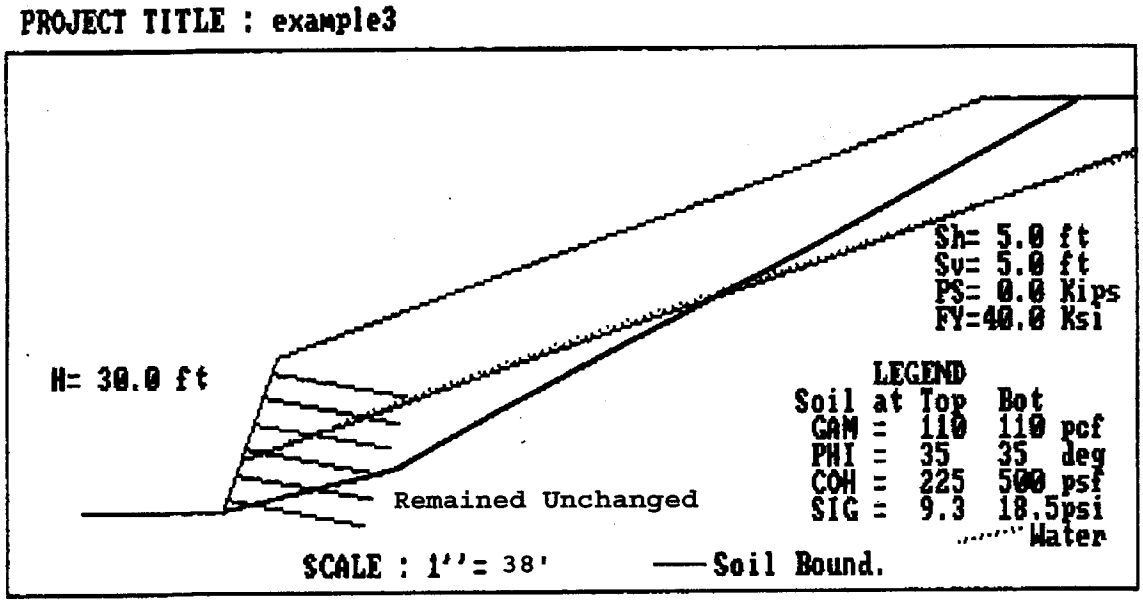

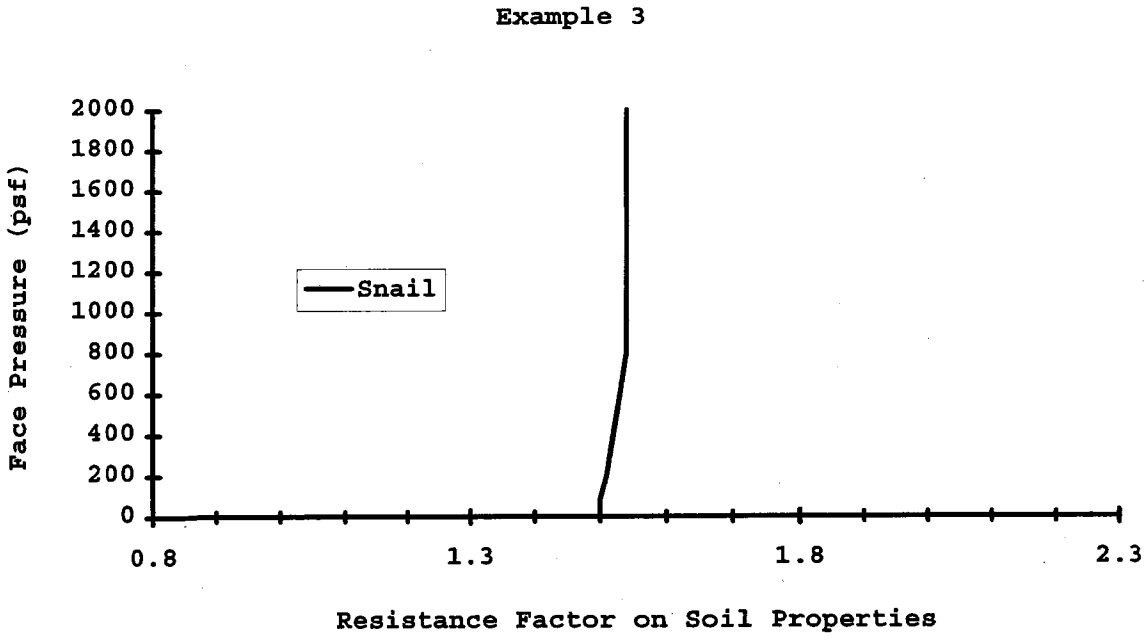

Figure 6.18. Effect of face pressure on SNAIL results — Example 3

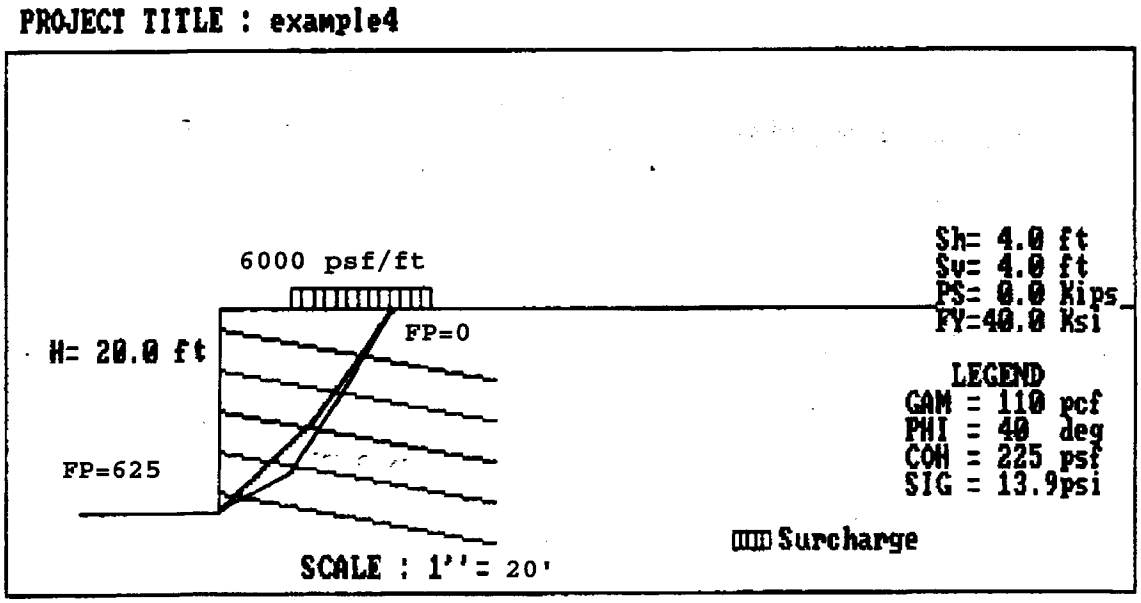

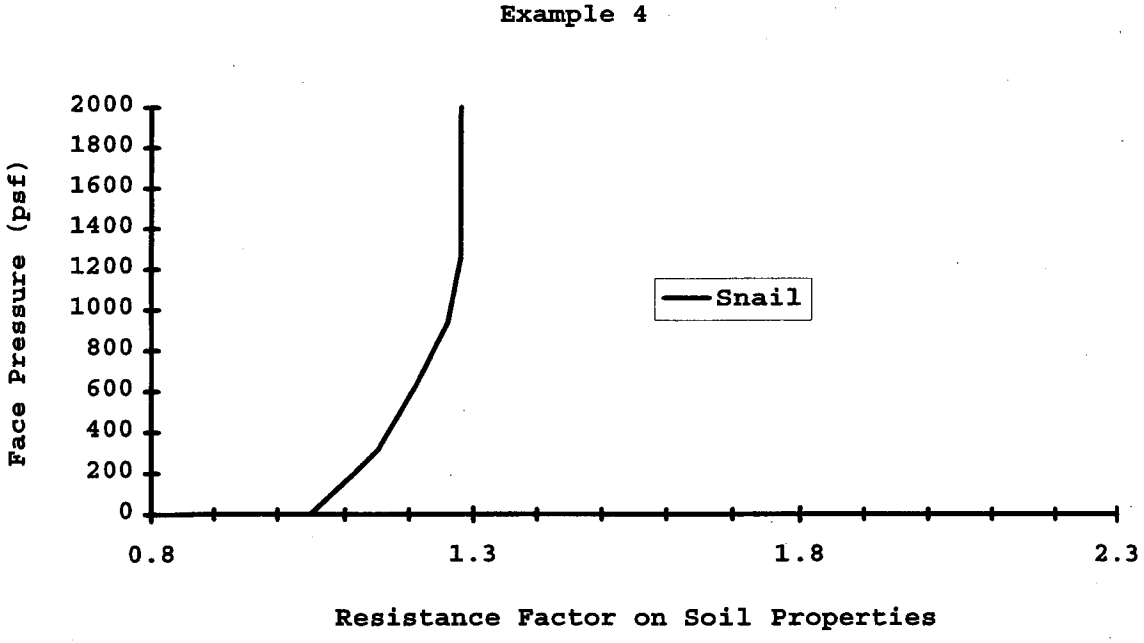

Figure 6.19. Effect of face pressure on SNAIL results — Example 4

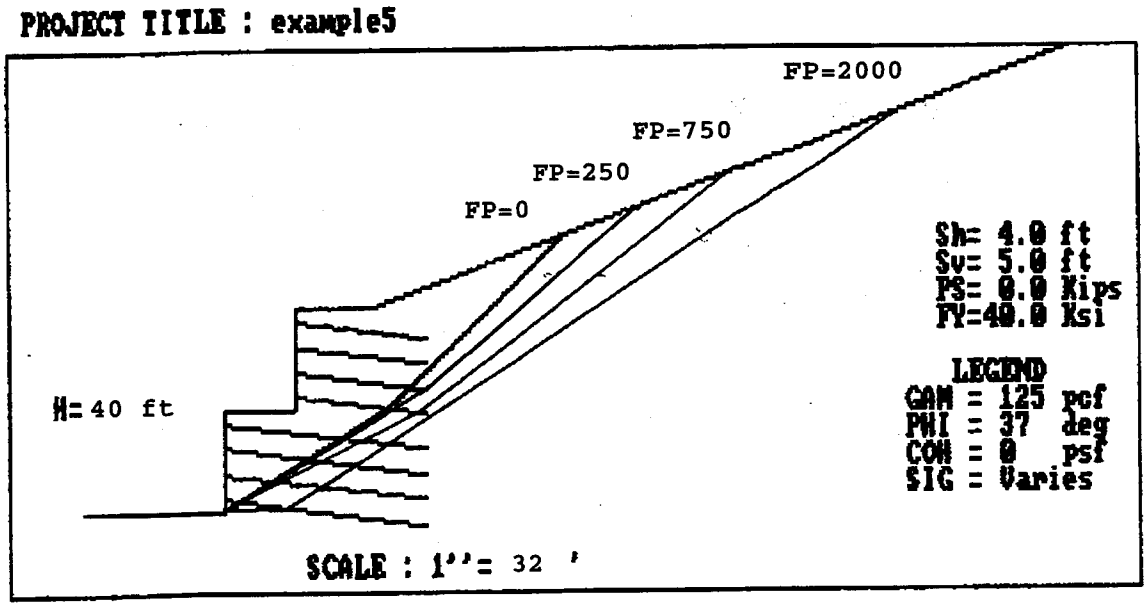

Example 5

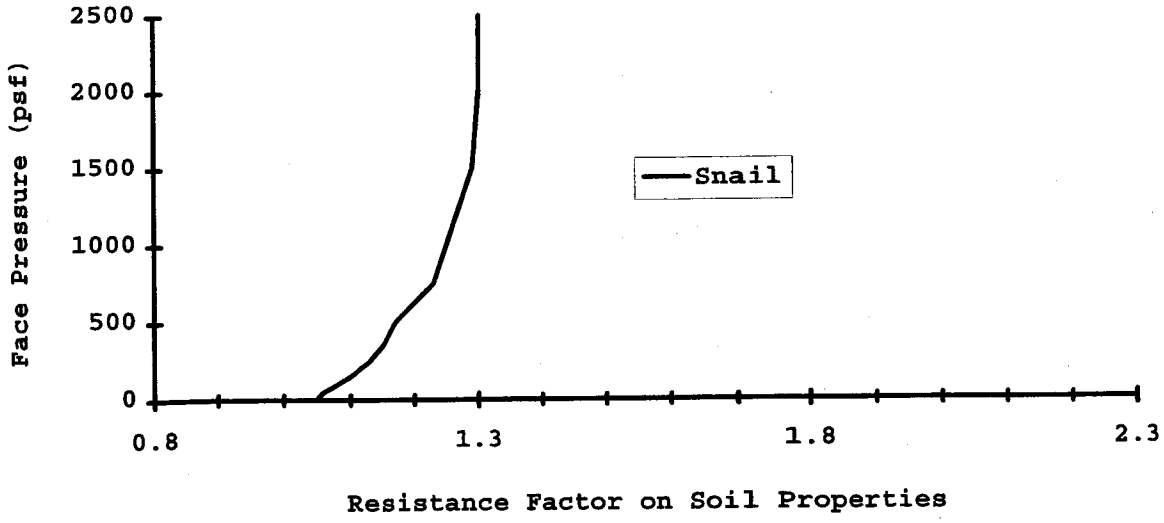

Figure 6.20. Effect of face pressure on SNAIL results — Example 5

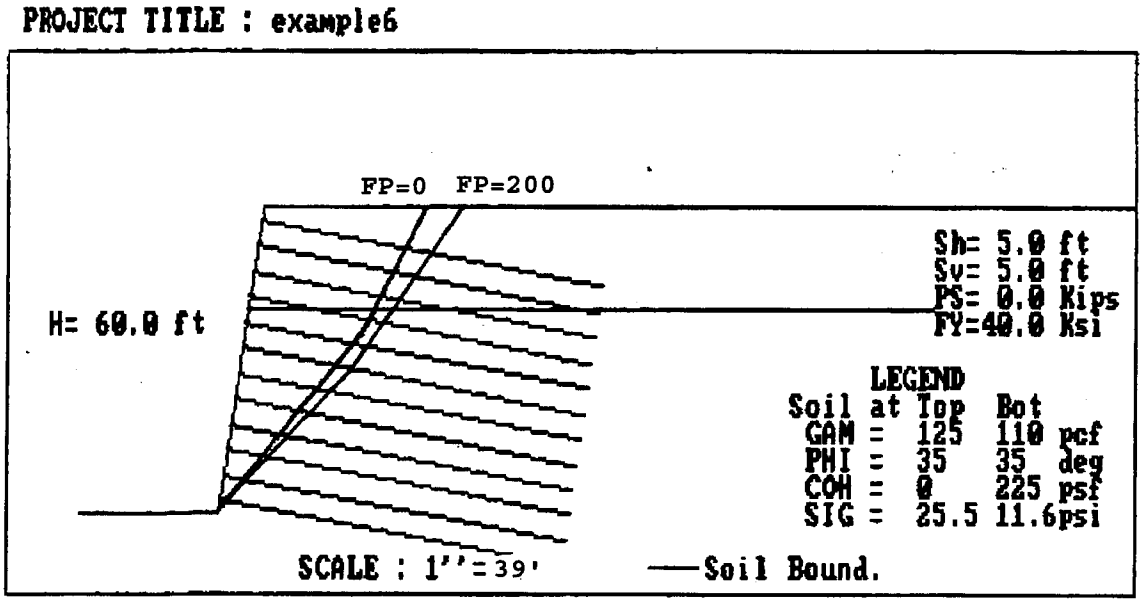

Example 6

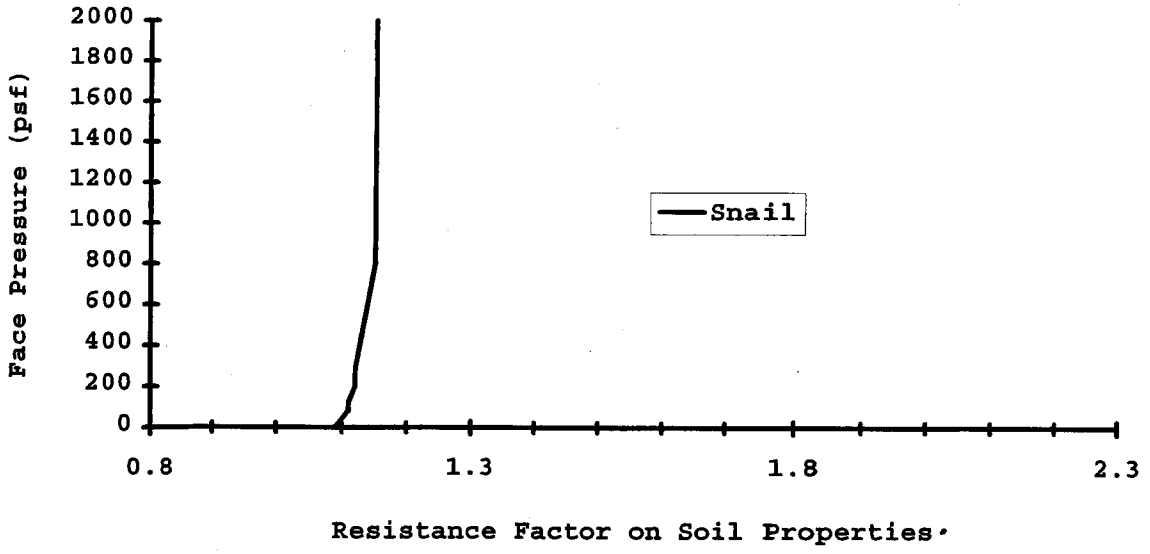

Figure 6.21. Effect of face pressure on SNAIL results — Example 6

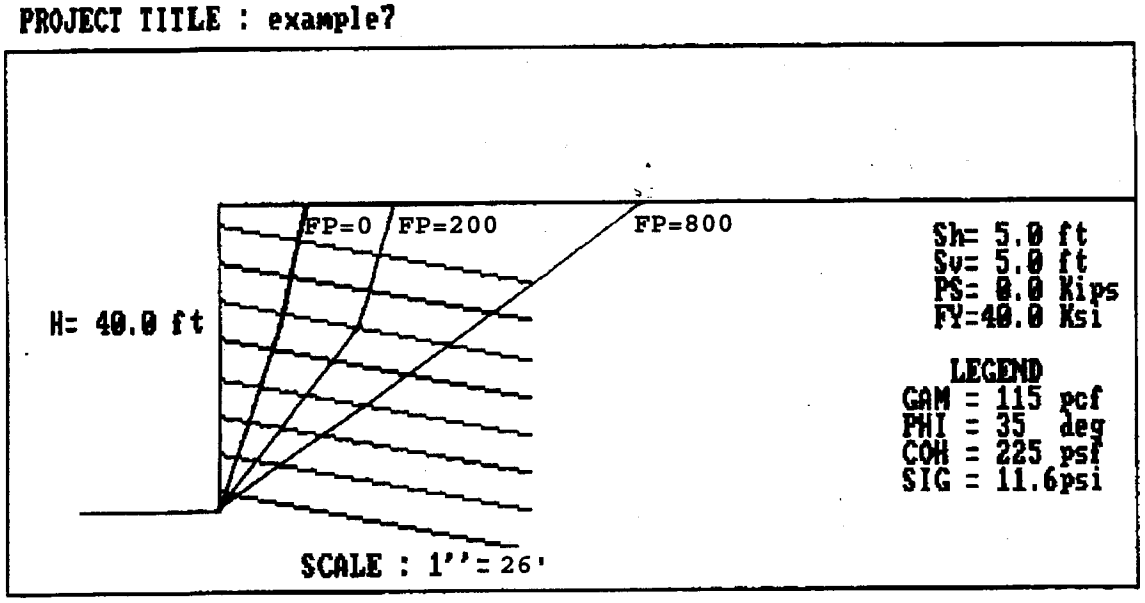

Example 7

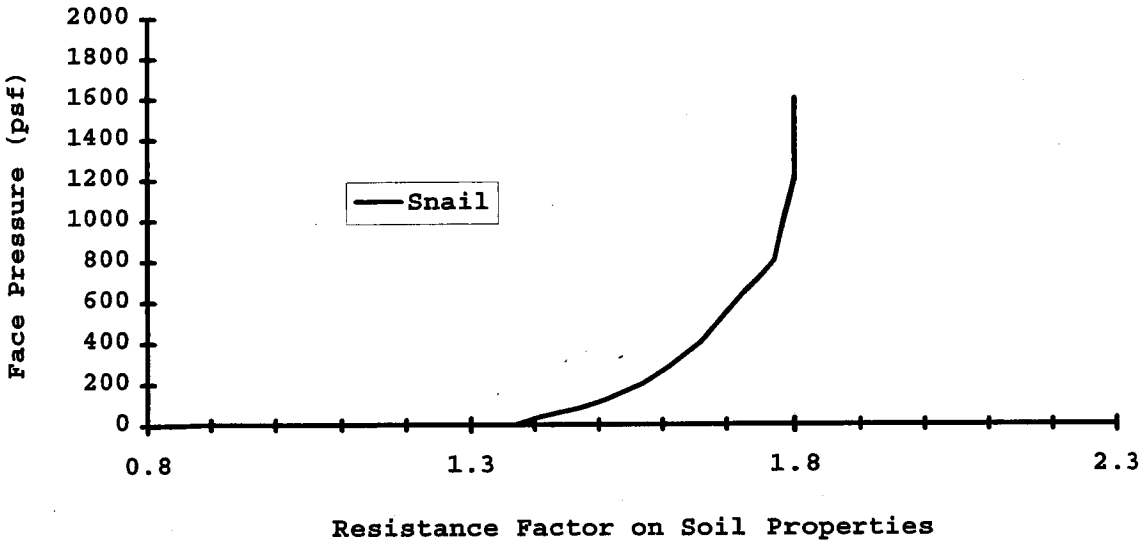

Figure 6.22. Effect of face pressure on SNAIL results — Example 7

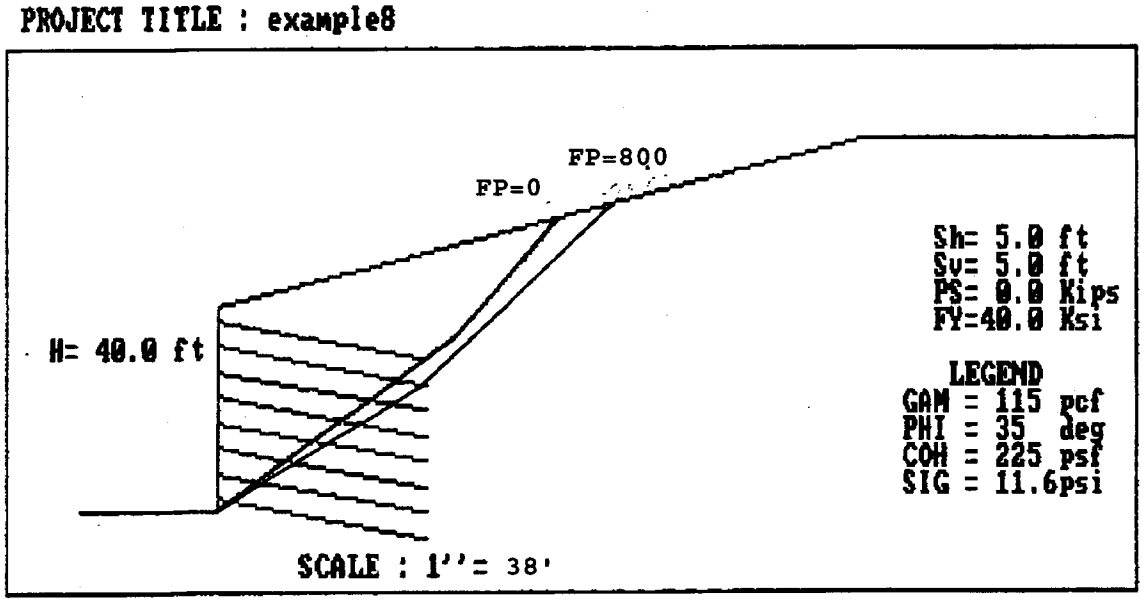

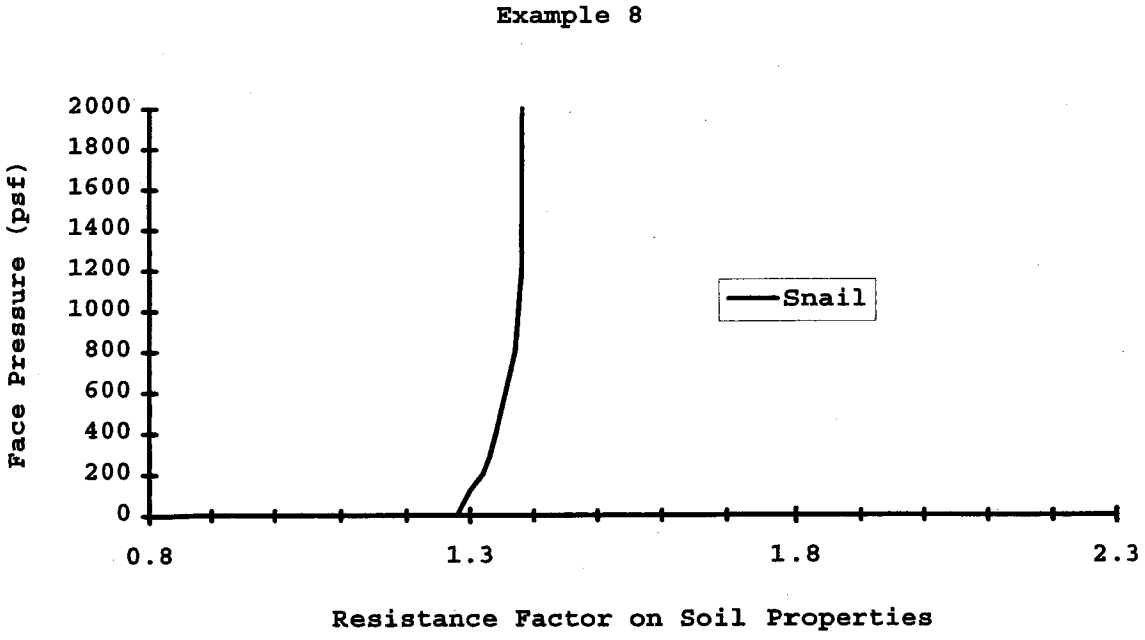

Figure 6.23. Effect of face pressure on SNAIL results — Example 8

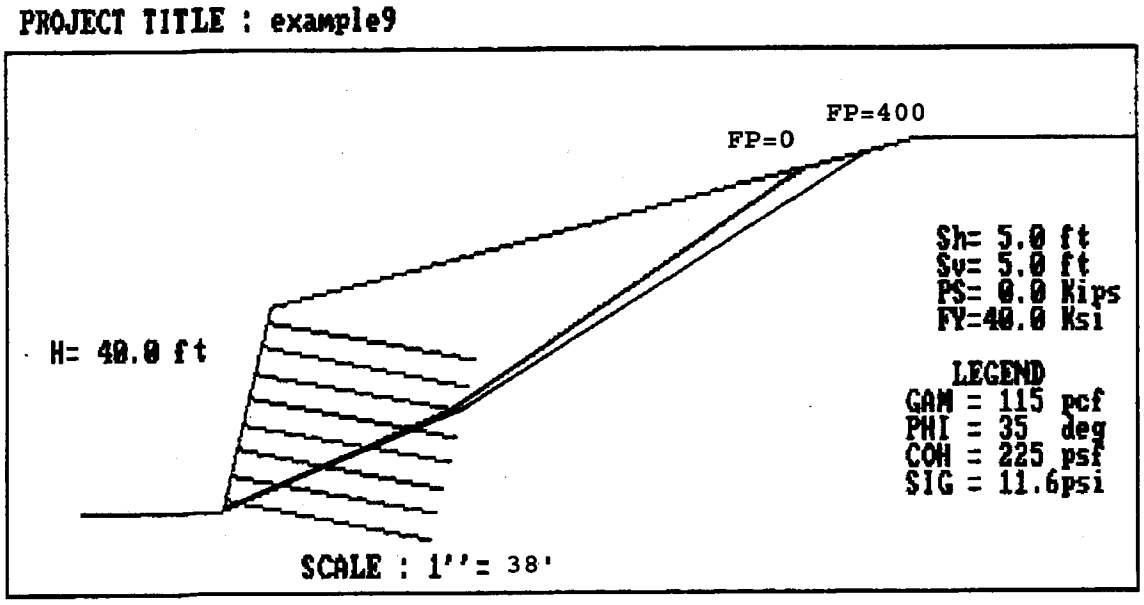

Example 9

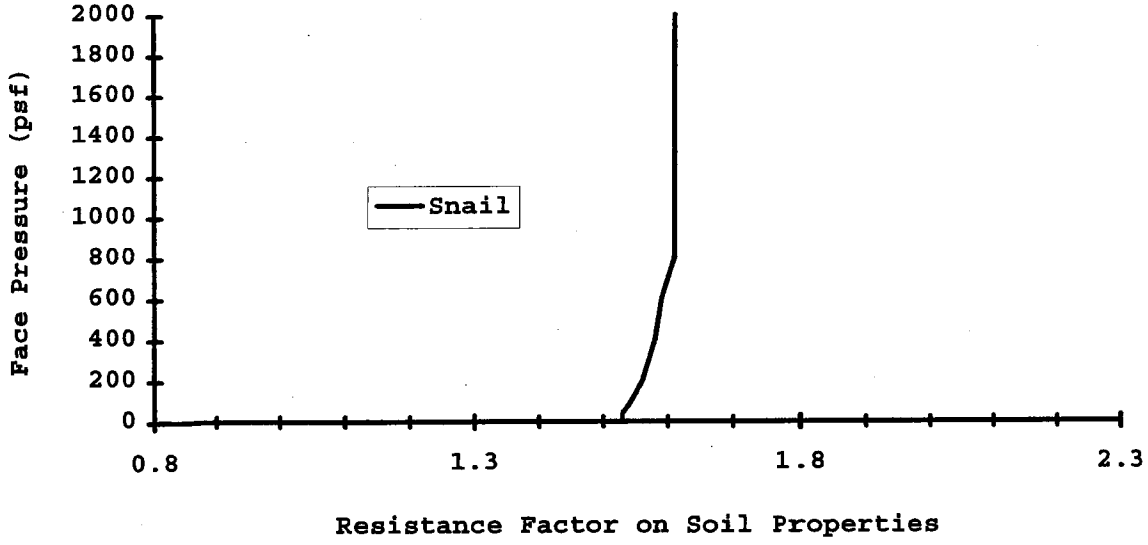

Figure 6.24. Effect of face pressure on SNAIL results — Example 9

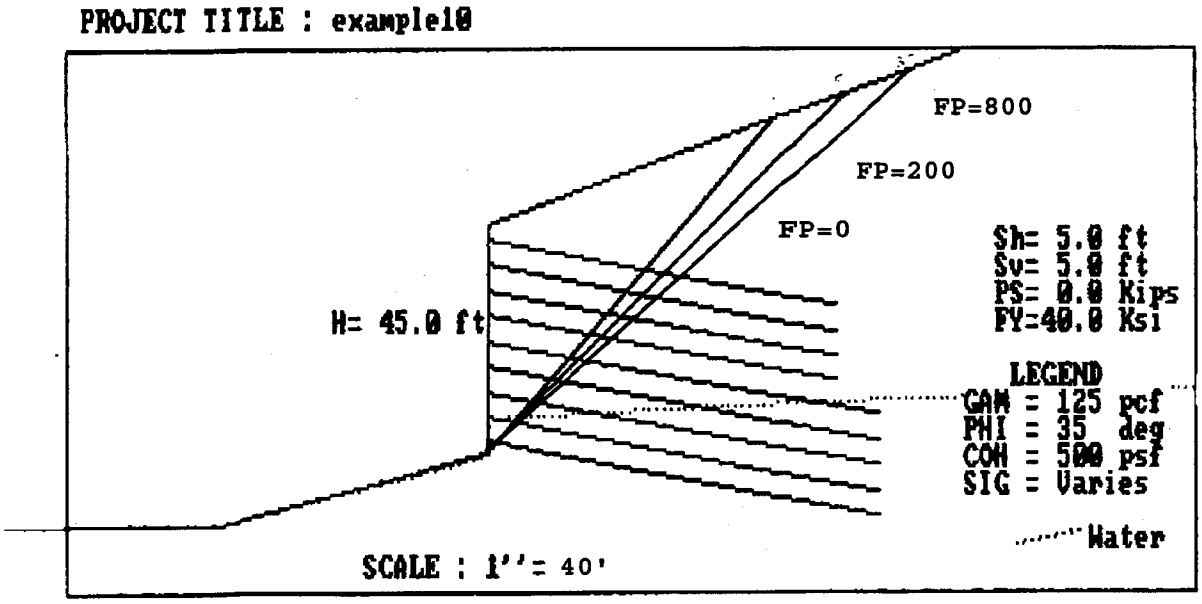

Example 10

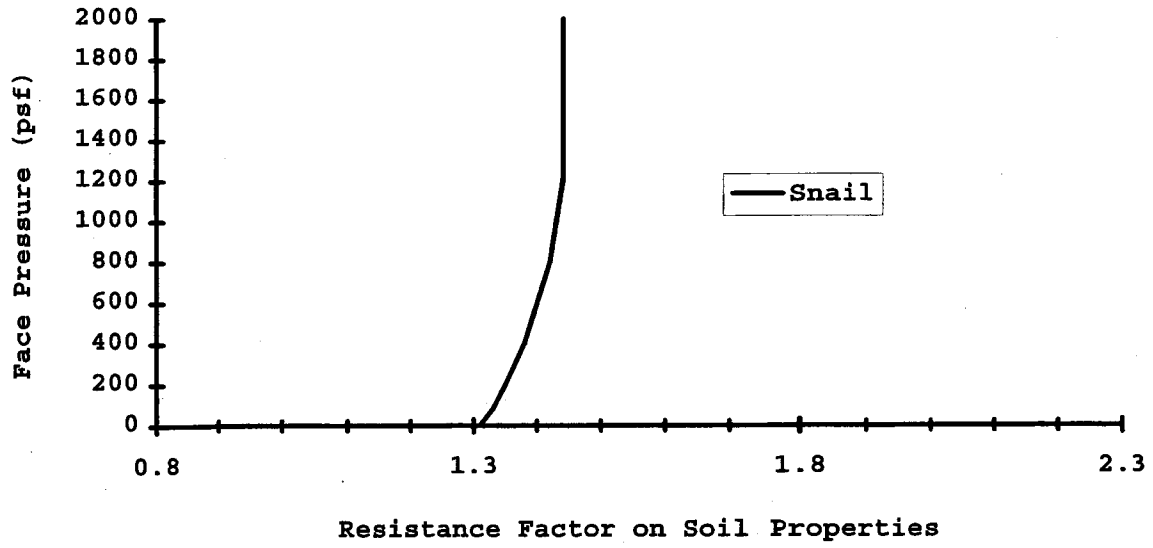

Figure 6.25. Effect of face pressure on SNAIL results — Example 10

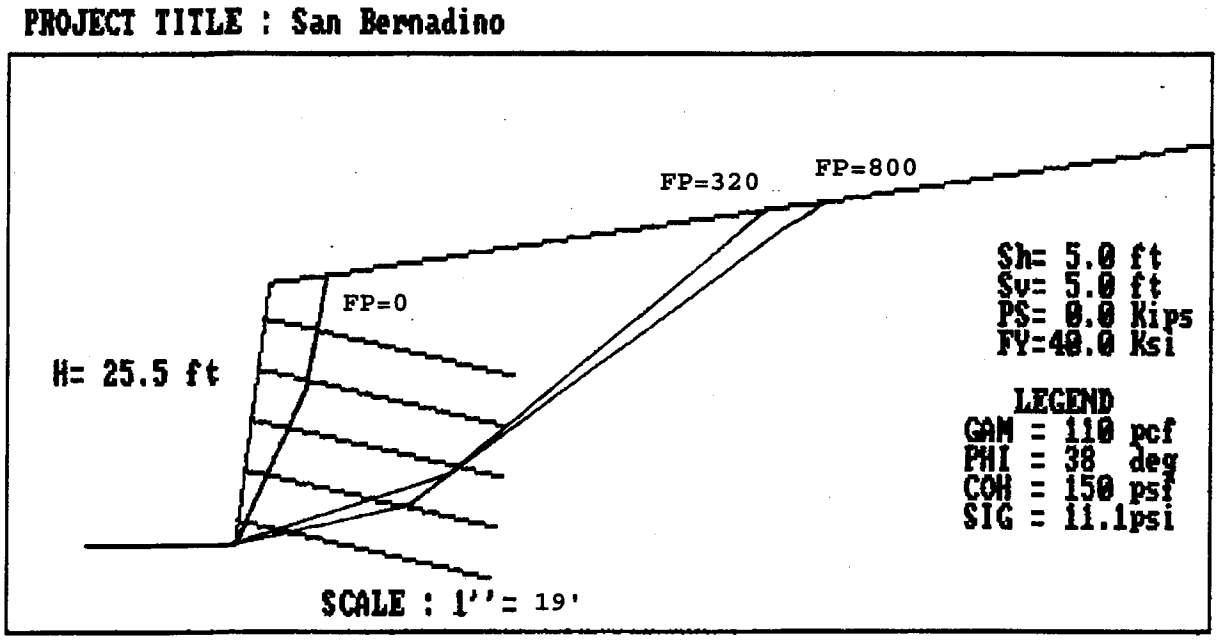

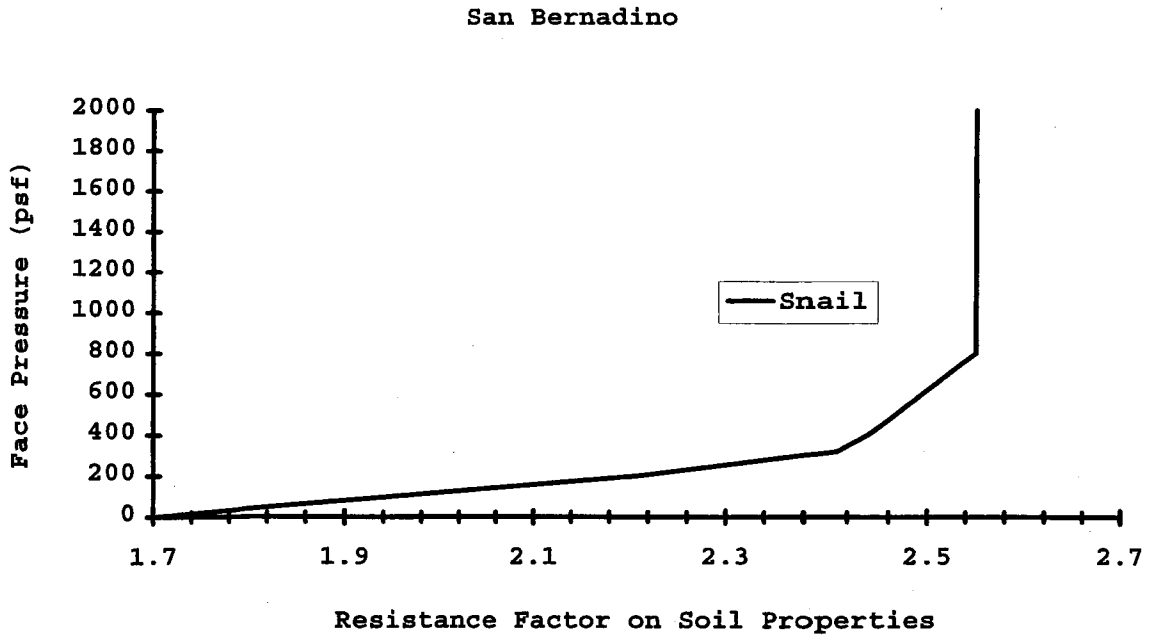

Figure 6.26. Effect of face pressure on SNAIL results — San Bernadino Wall

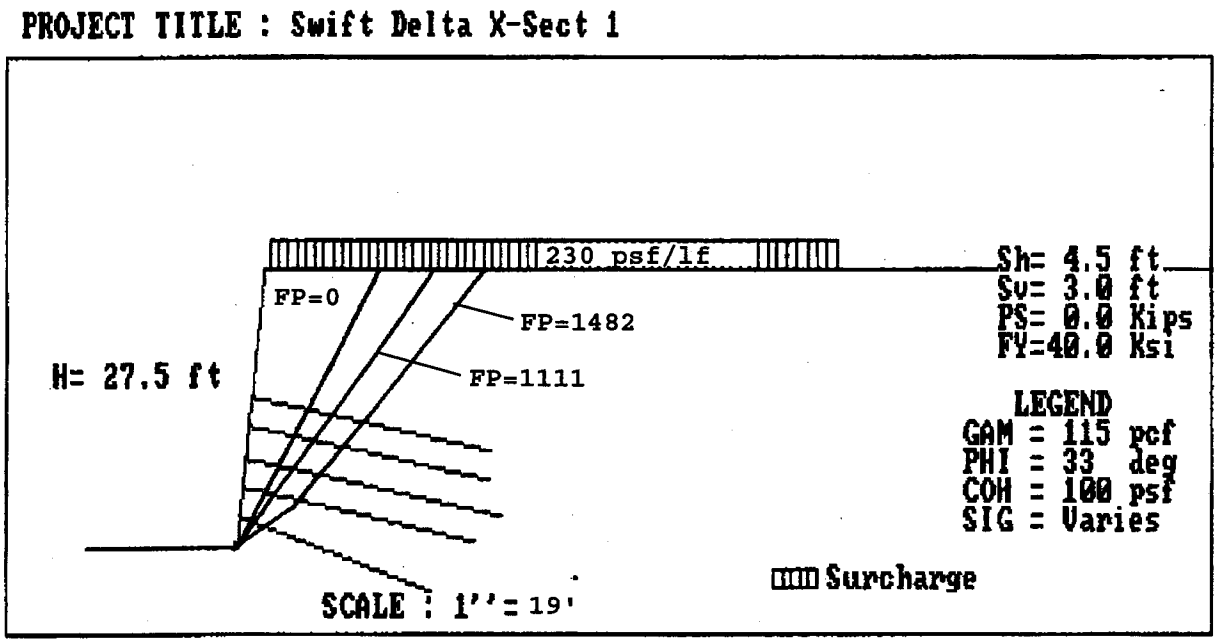

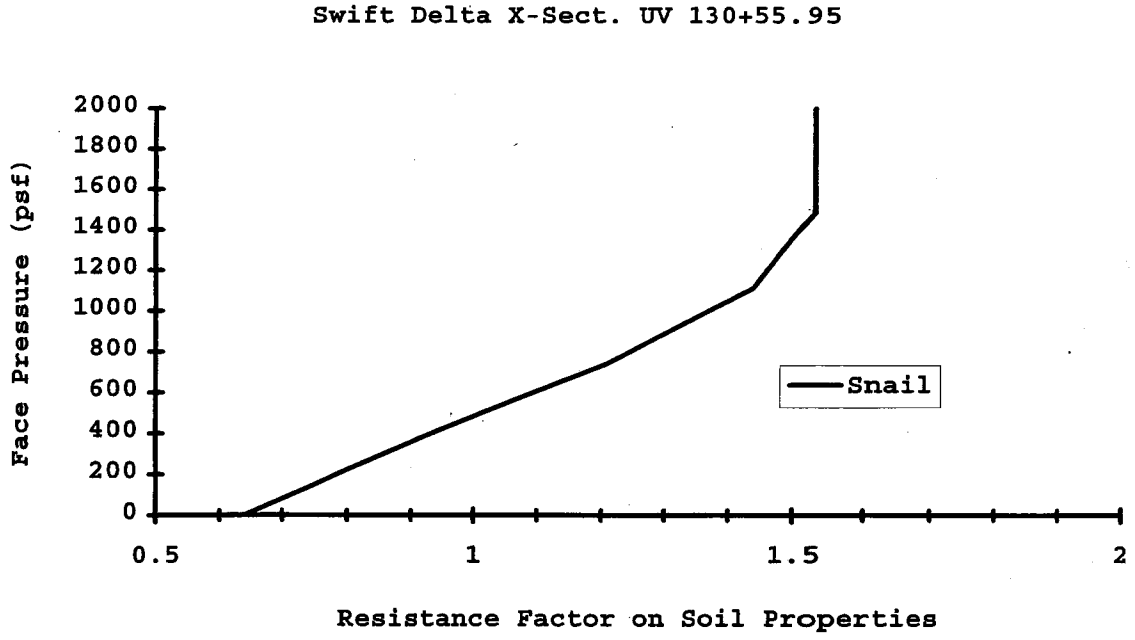

Figure 6.27. Effect of face pressure on SNAIL results — Swift Delta 1 Wall

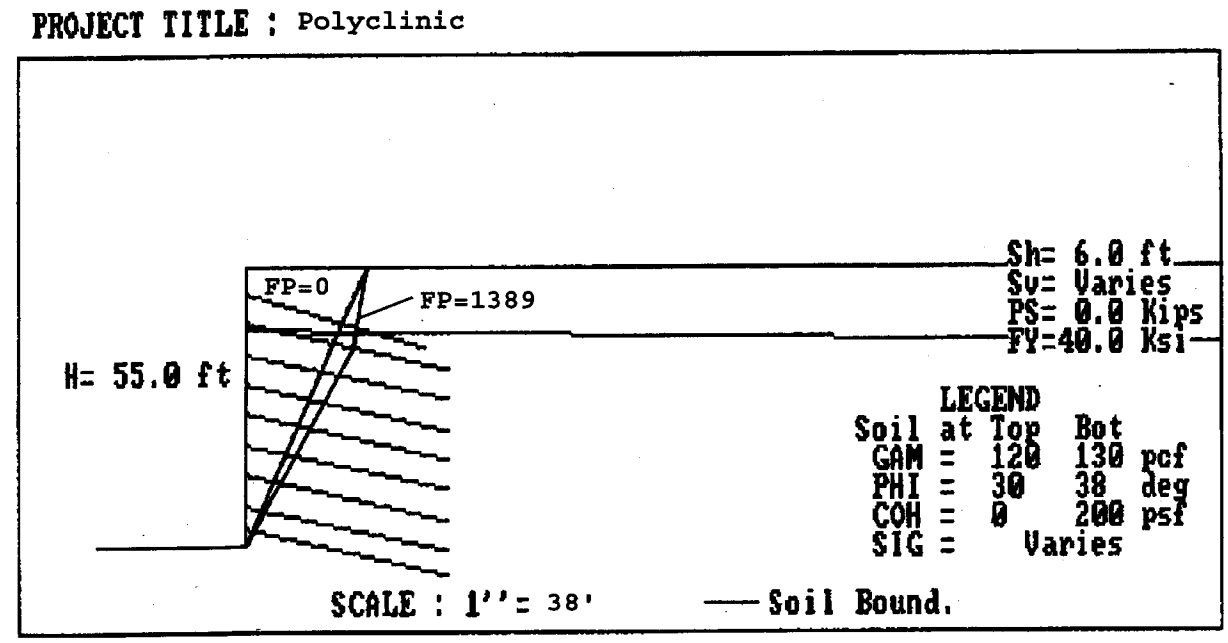

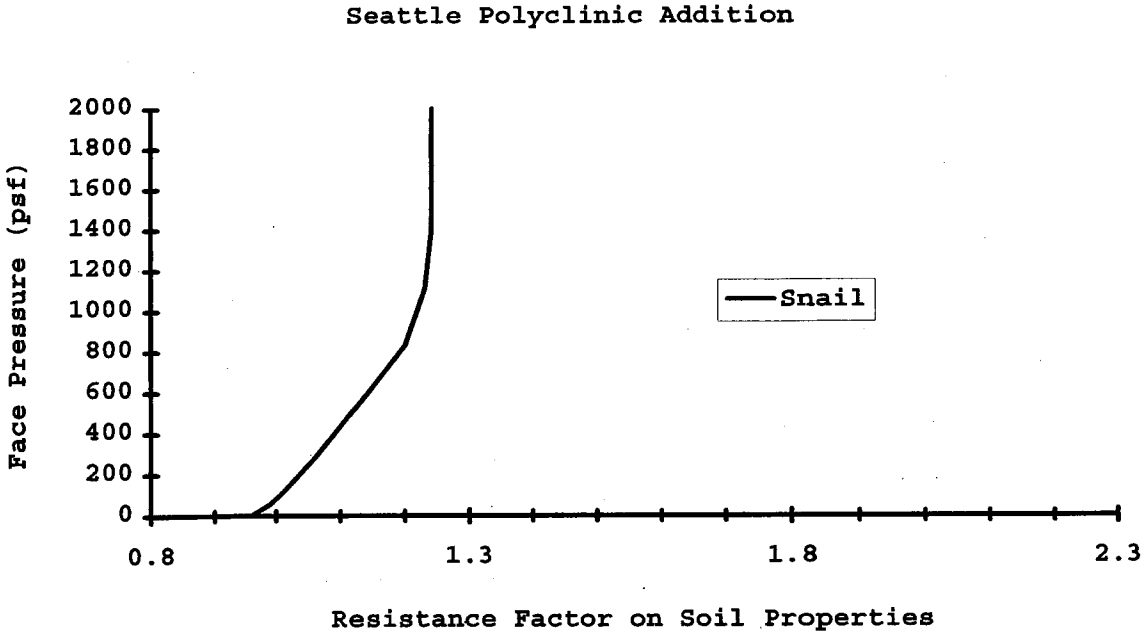

Figure 6.28. Effect of face pressure on SNAIL results — Polyclinic Wall

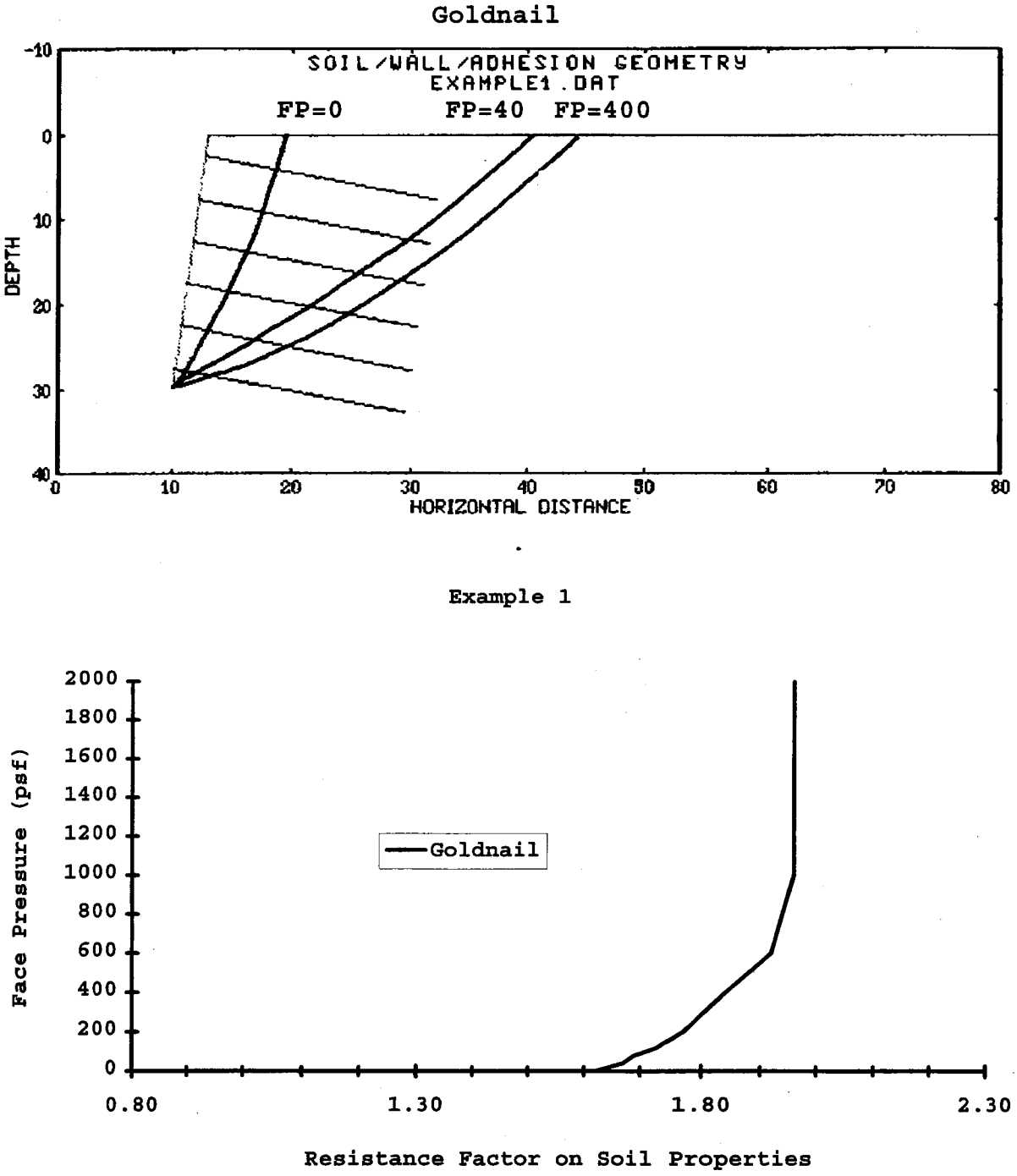

Figure 6.29. Effect of face pressure on GOLDNAIL results — Example 1

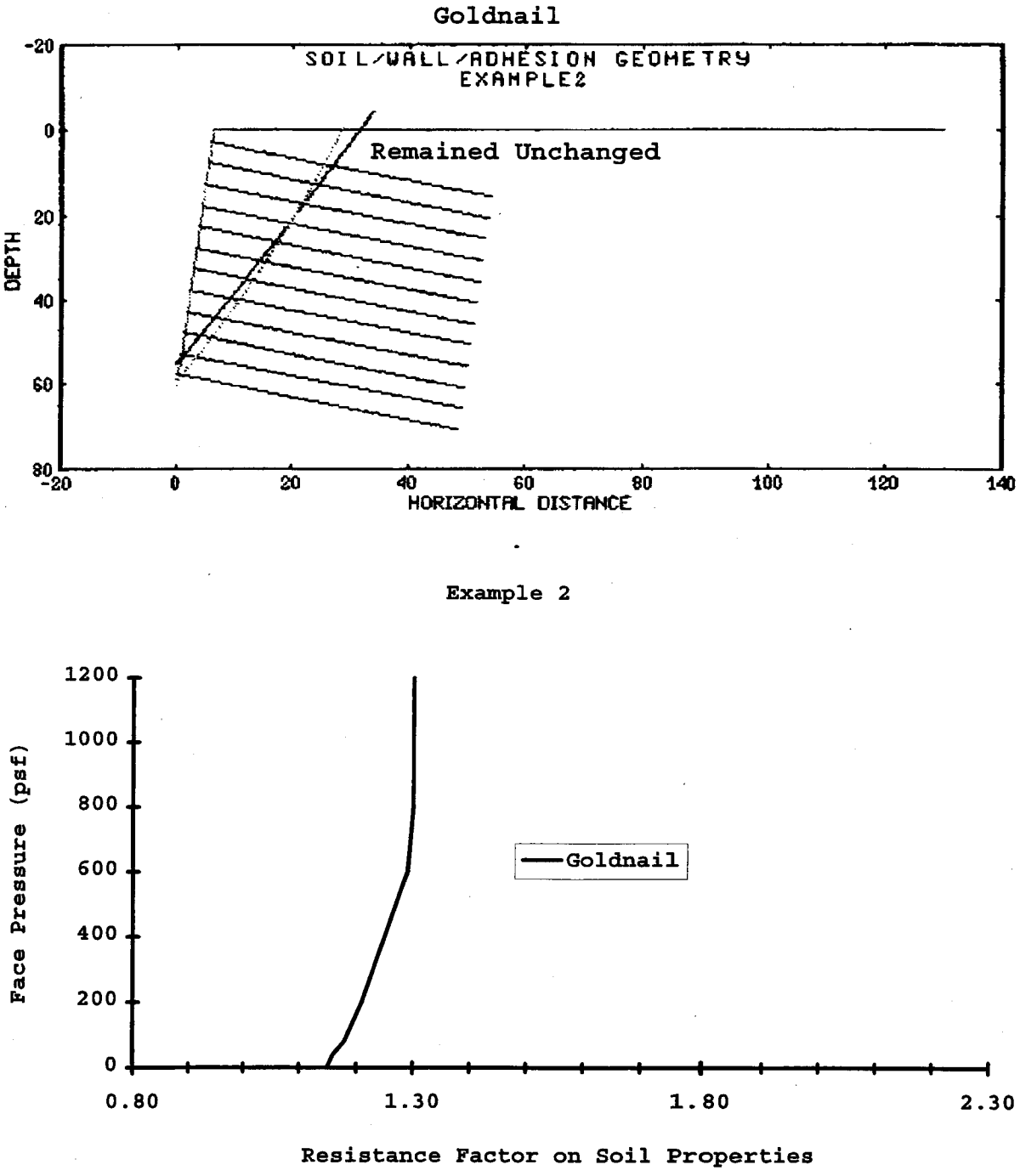

Figure 6.30. Effect of face pressure on GOLDNAIL results — Example 2

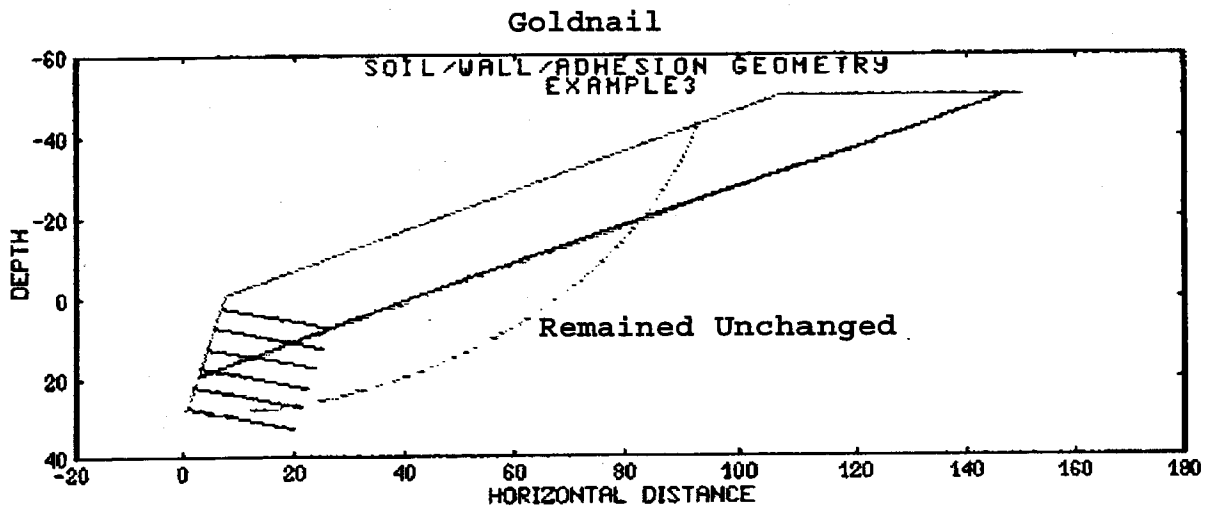

Example 3

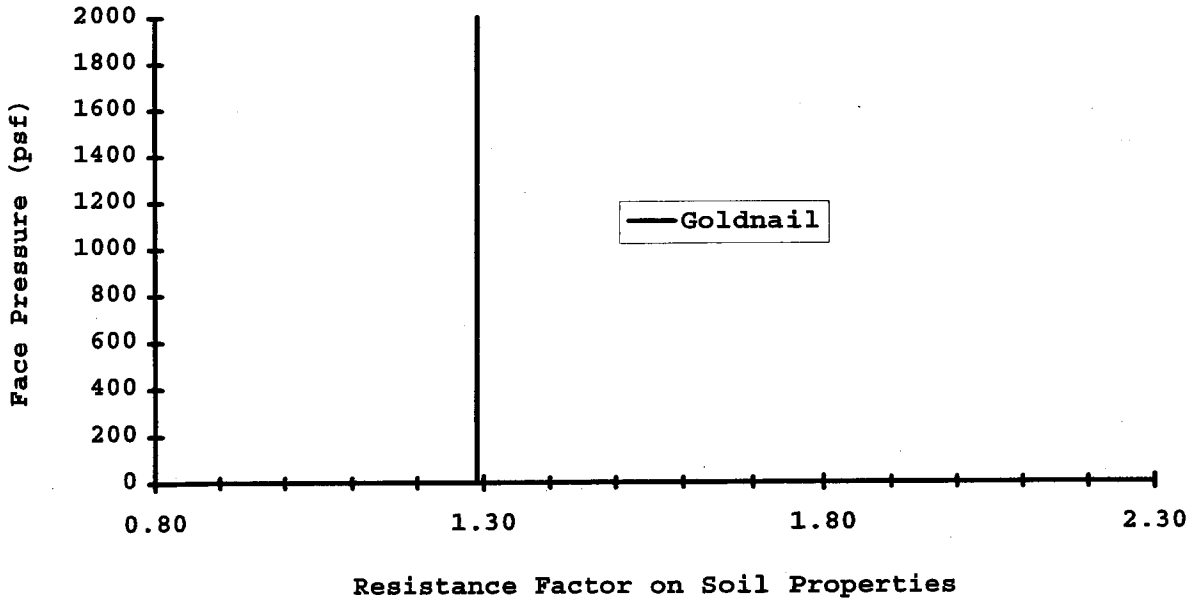

Figure 6.31. Effect of face pressure on GOLDNAIL results — Example 3

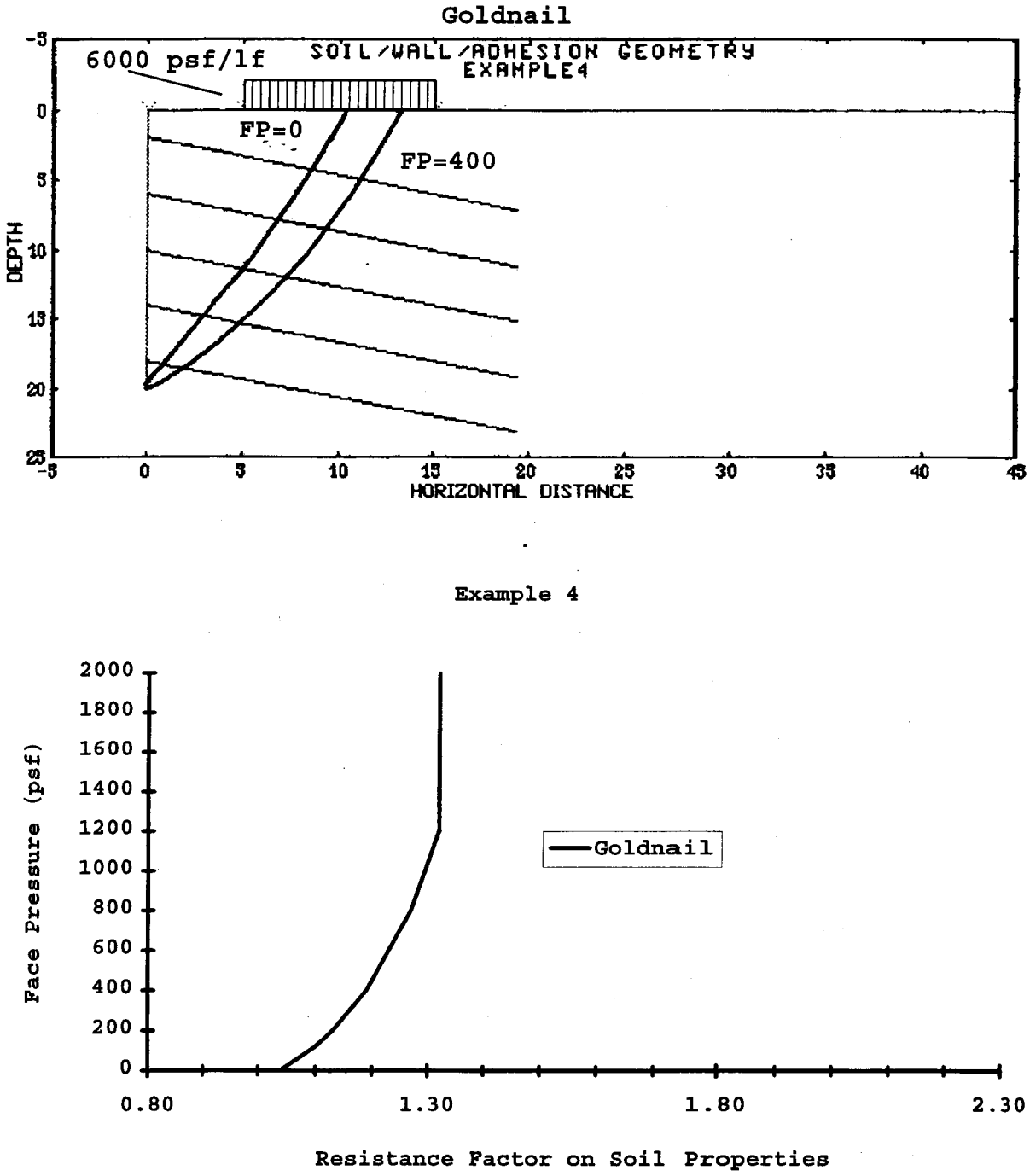

Figure 6.32. Effect of face pressure on GOLDNAIL results — Example 4

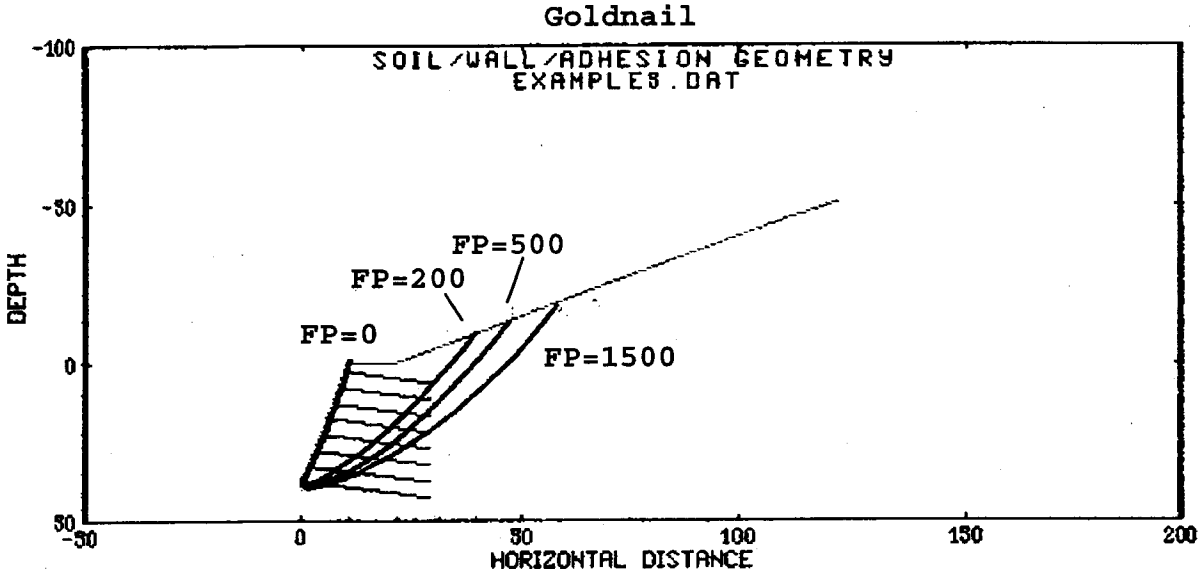

Example 5

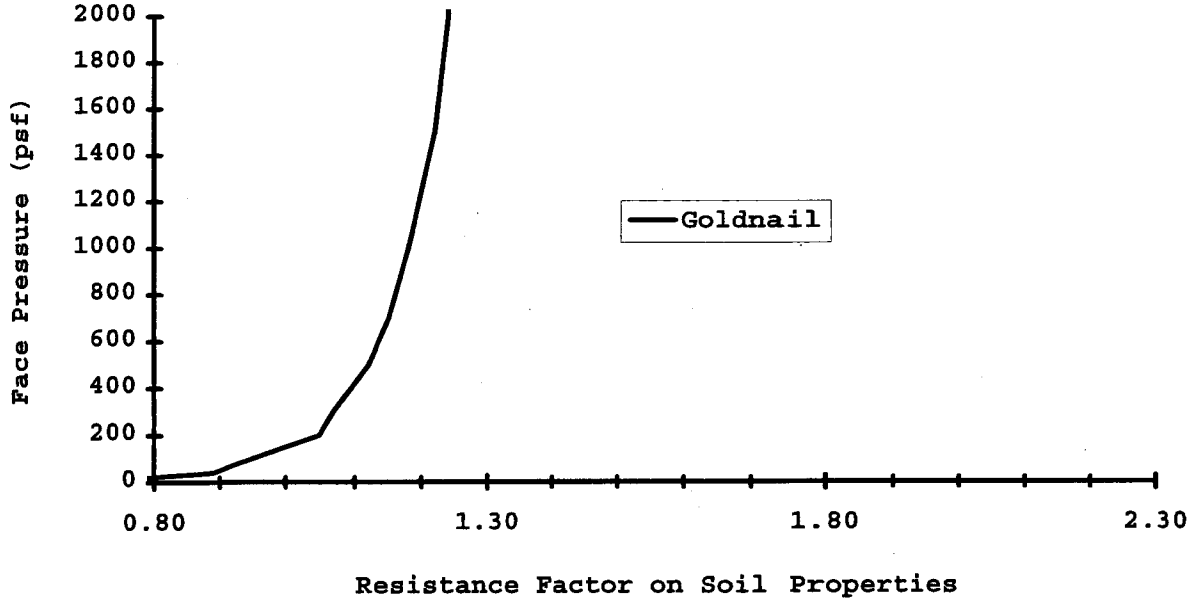

Figure 6.33. Effect of face pressure on GOLDNAIL results — Example 5

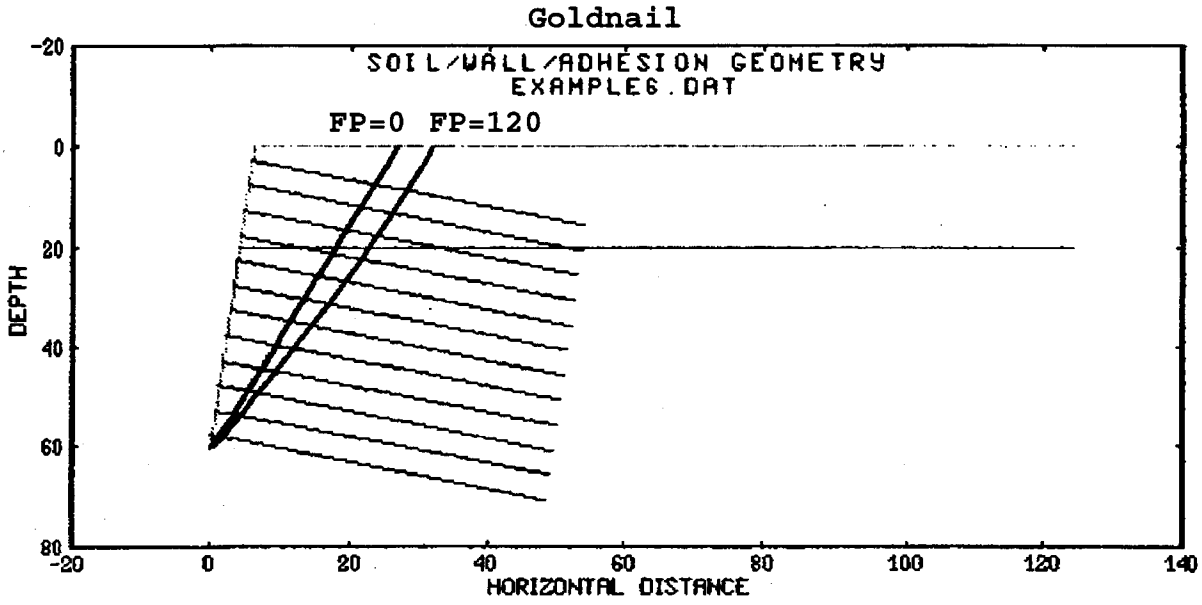

Example 6

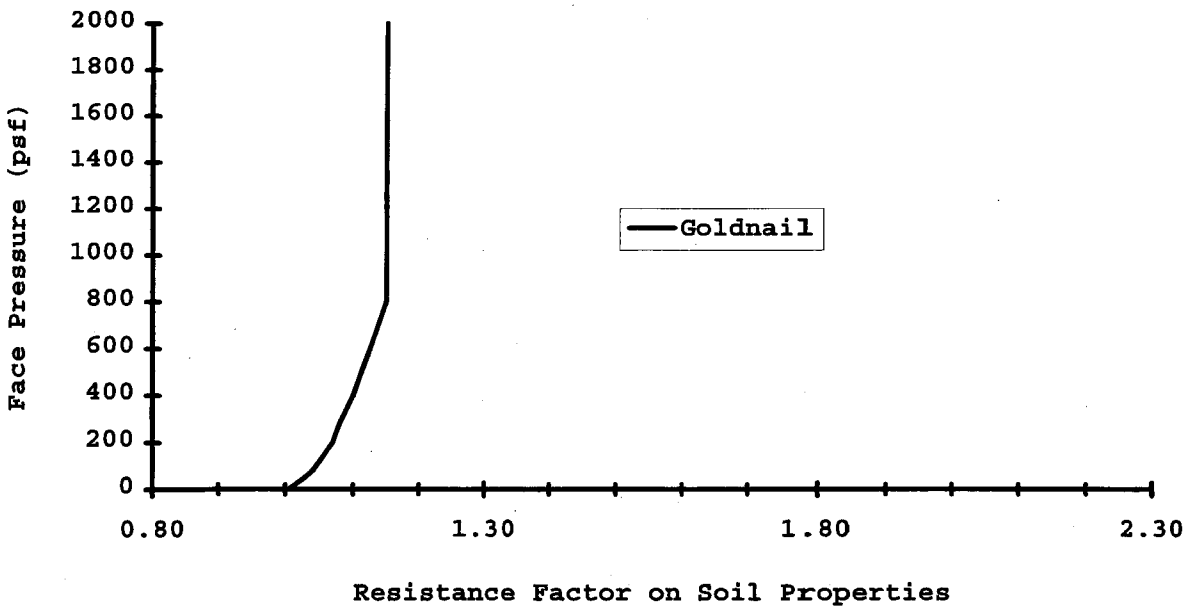

Figure 6.34. Effect of face pressure on GOLDNAIL results — Example 6

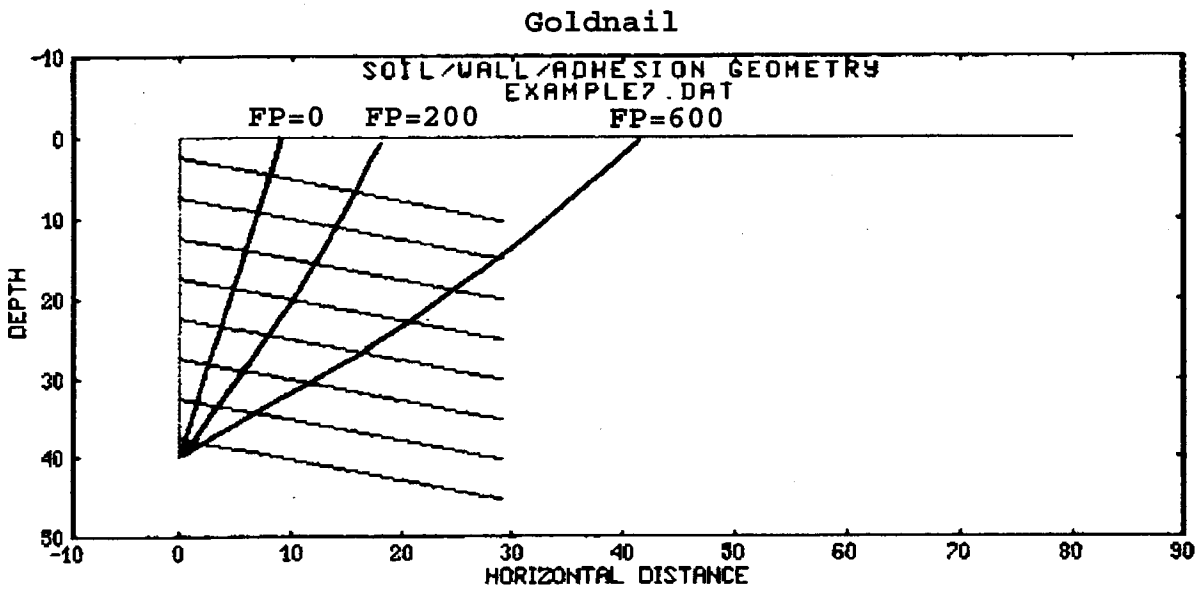

Example 7

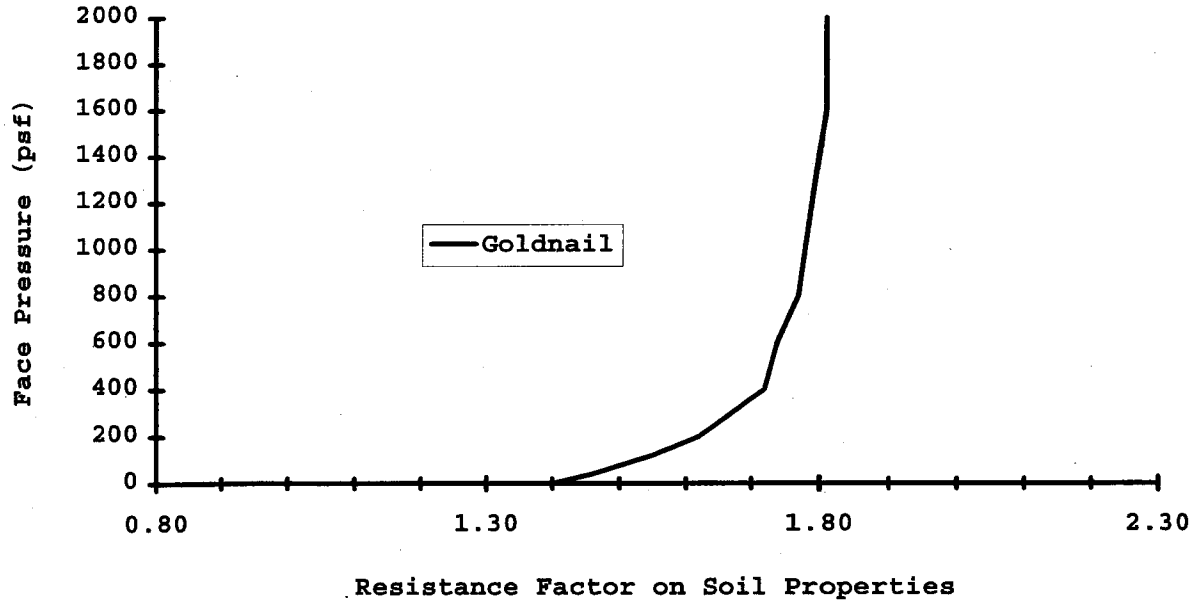

Figure 6.35. Effect of face pressure on GOLDNAIL results — Example 7

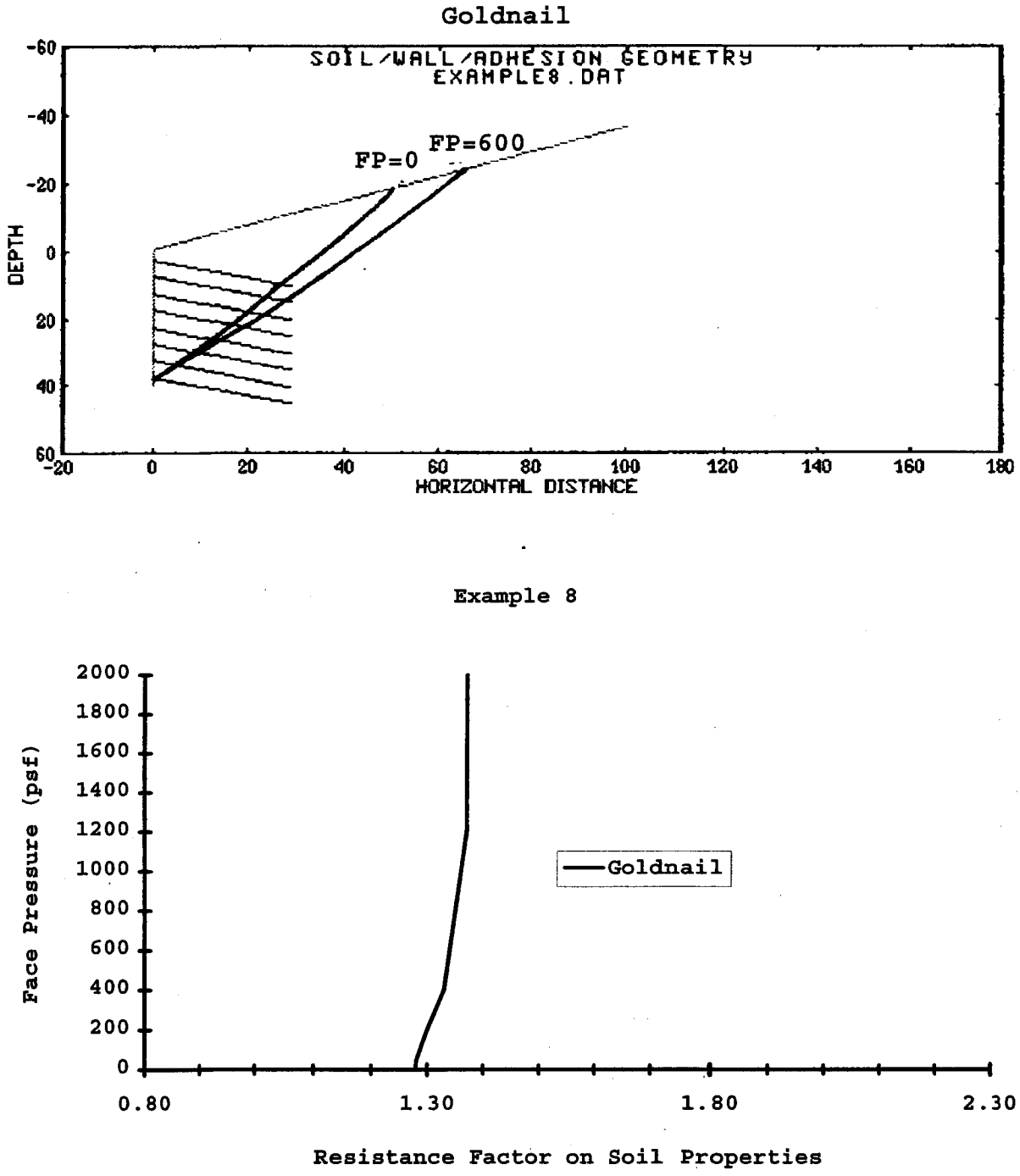

Figure 6.36. Effect of face pressure on GOLDNAIL results — Example 8

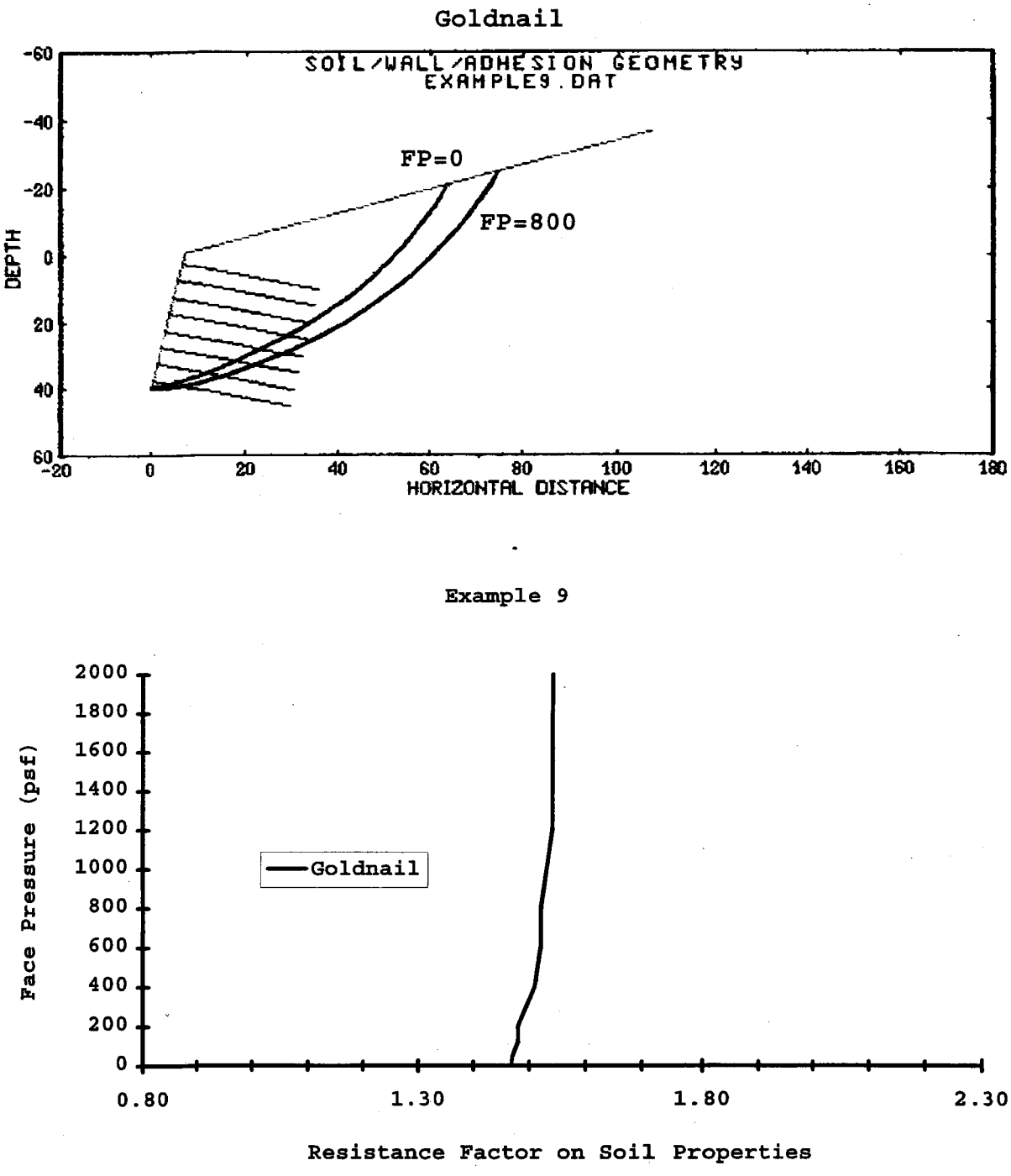

Figure 6.37. Effect of face pressure on GOLDNAIL results — Example 9

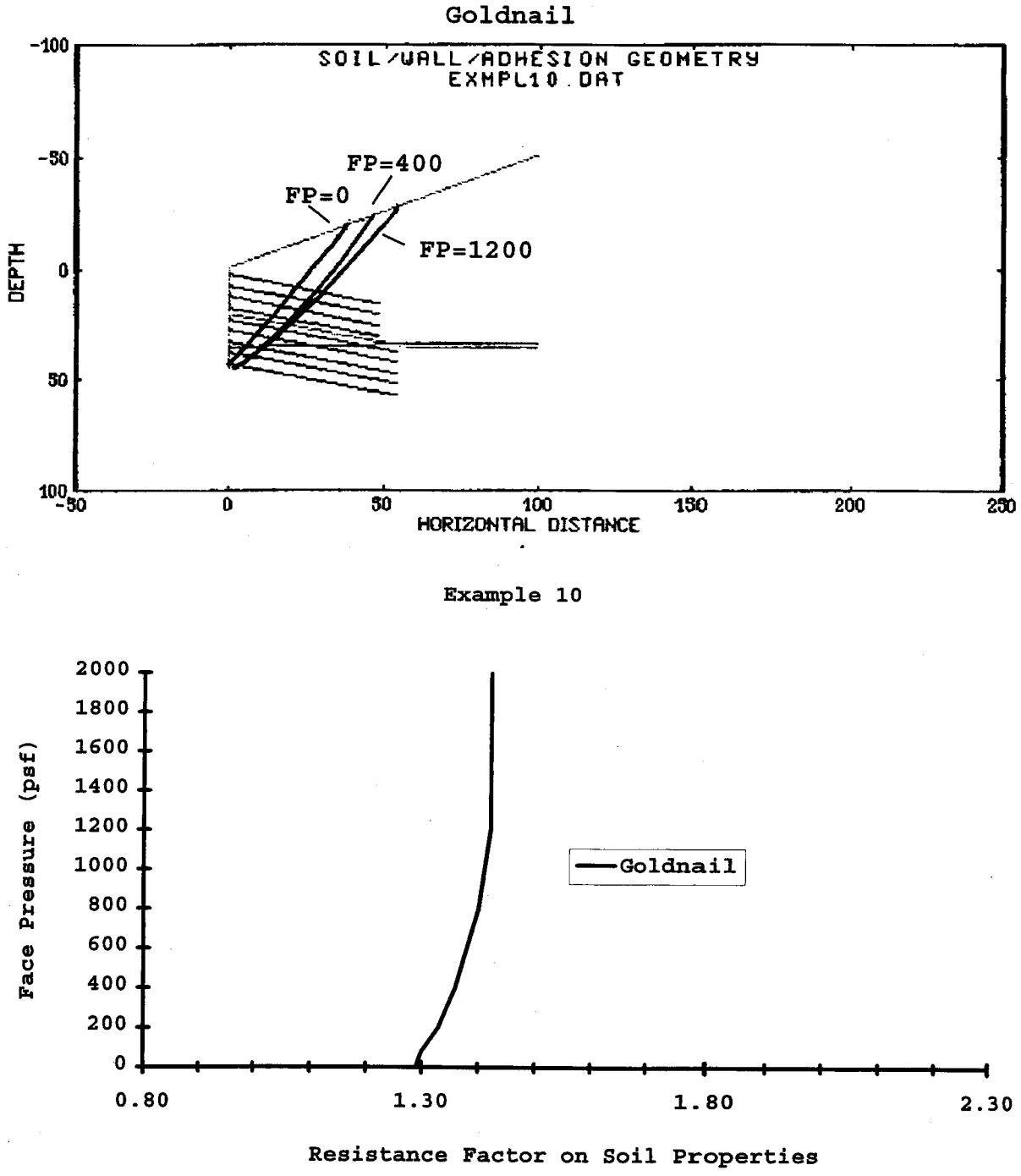

Figure 6.38. Effect of face pressure on GOLDNAIL results — Example 10

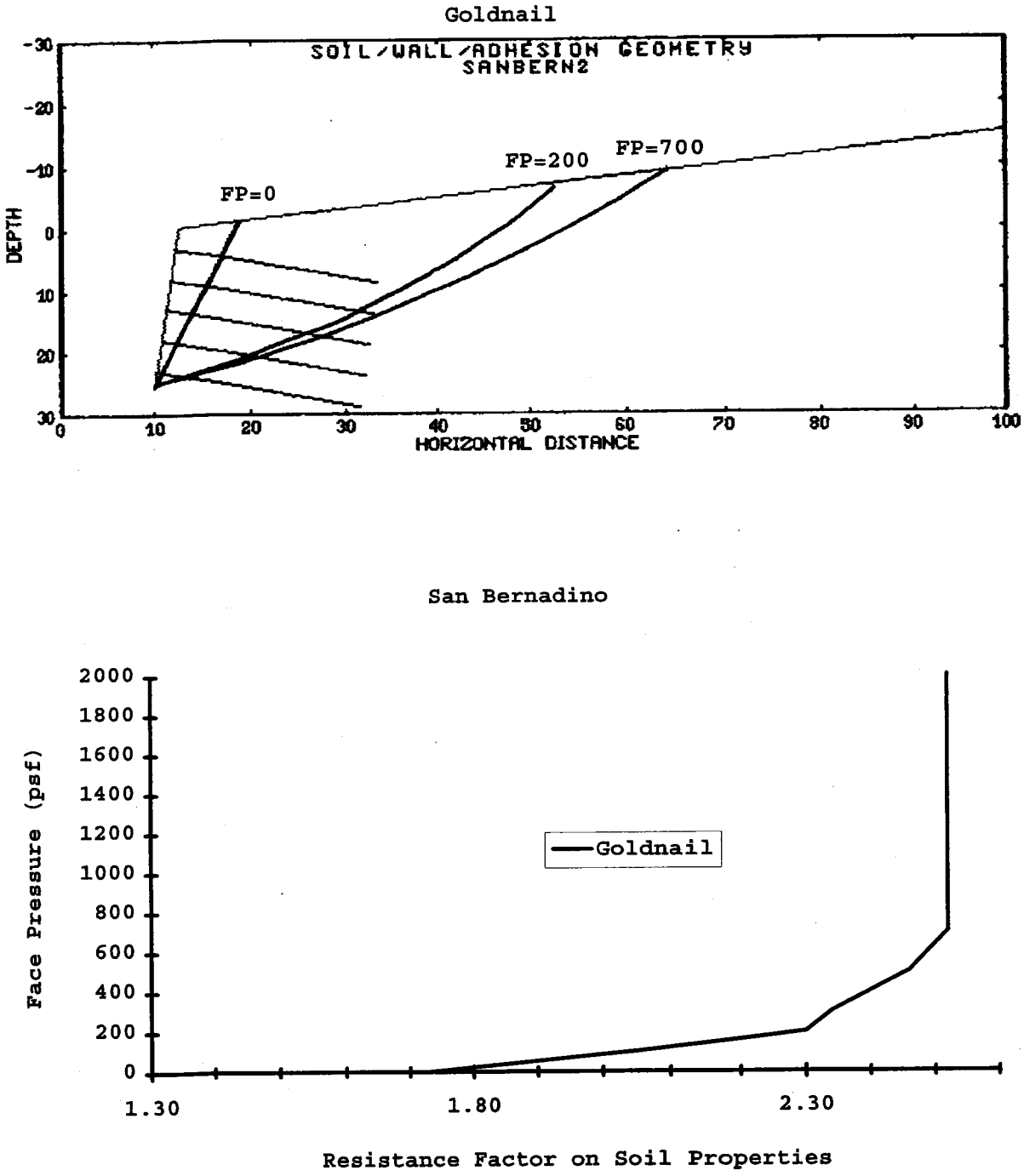

Figure 6.39. Effect of face pressure on GOLDNAIL results — San Bernadino Wall

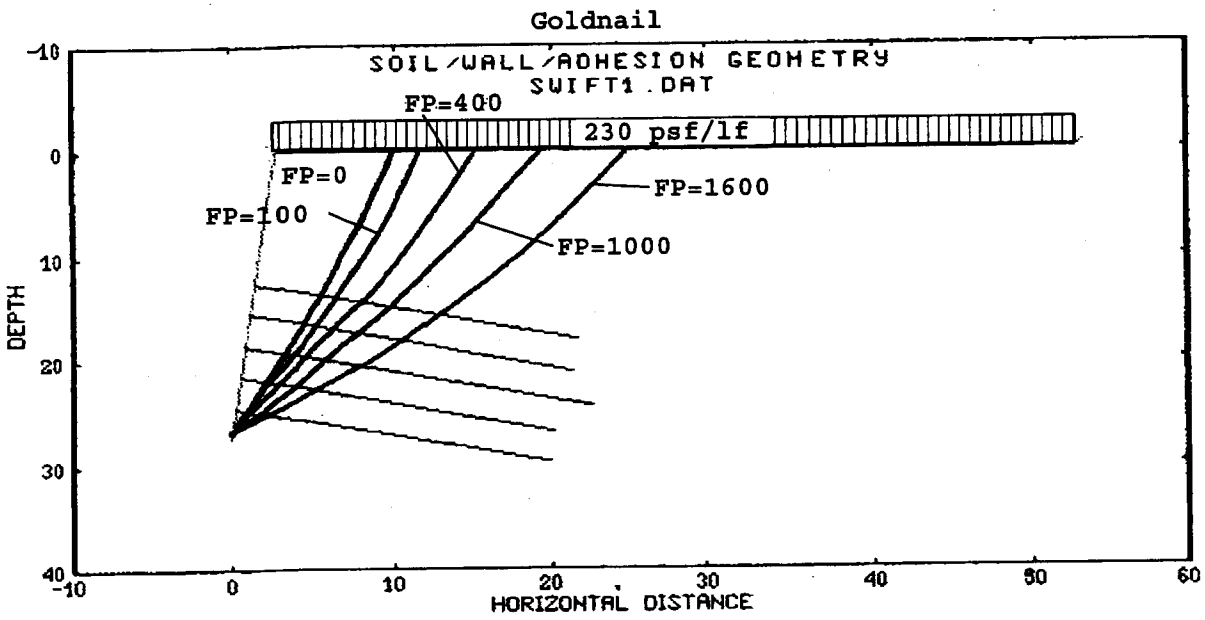

Swift Creek X-Sect. UV 130+55.95

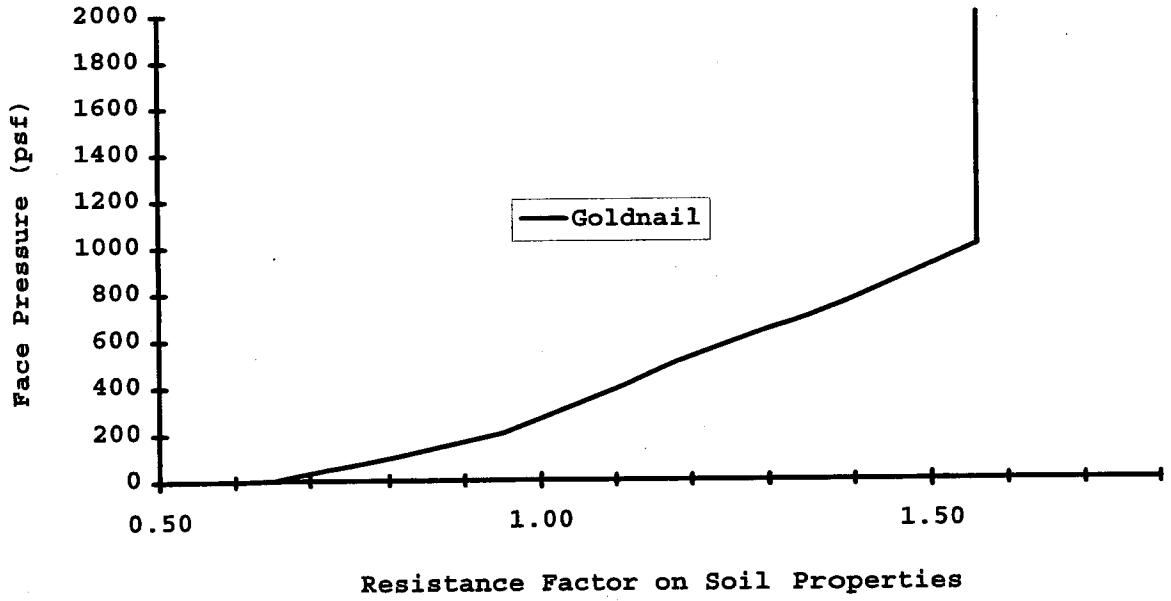

Figure 6.40. Effect of face pressure on GOLDNAIL results — Swift Delta 1 Wall

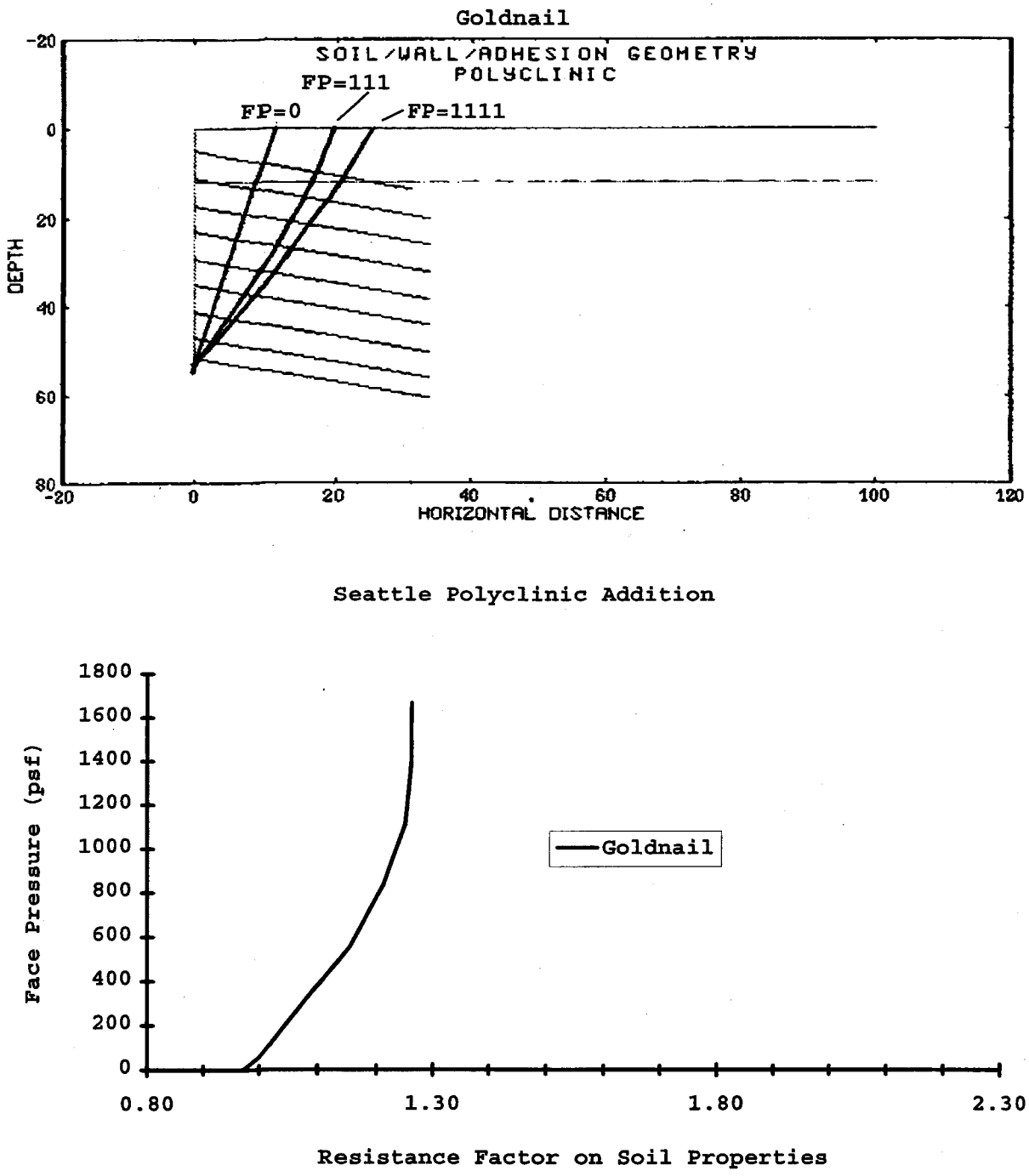

Figure 6.41. Effect of face pressure on GOLDNAIL results — Polyclinic Wall

program's definition of a safety factor. In addition, the safety factor predictions of *GOLDNAIL* and *SNAIL* were almost always bounded by those of the remaining three programs (not including *NAILM*).

Example 2

In this example, one can see an artifact of the use of a log spiral slip surface, the overhanging failure surface for *STARS*. The program does not include a routine to reduce this overhanging surface to a vertical surface, unlike the program *TALREN*.

Example 3

NAILM is unable to handle inclined soil layers or the water table and was therefore not used to run this example. *STARS* refuses to proceed with computations if it detects that the factored ϕ –value for the top layer of soil is less than the backslope angle. Attempts were made to rectify this problem by introducing an infinitely small layer of high friction soil on the backslope. This enabled the program to continue, but the program consistently determined the safety factors to be exceedingly high because the chosen slip surfaces for *STARS* progressed gradually into the backslope and were so deep that they became horizontal at the wall toe.

NAILSOLVER is unable to handle multiple soil layers or a water table. Differences between the output of *SNAIL* and *GOLDNAIL* in this example were due to the different slip surfaces and the dipping of the slip surface under the water table. The cohesive forces acting on the two slip surfaces were similar, but with a deeper slip circle for *GOLDNAIL*, the porewater pressure had a larger effect on reducing the soil's frictional resistance.

Example 4

NAILM cannot handle specific sections of surcharge. It only allows input of a uniform surcharge over the entire backslope surface; therefore, it was not able to run the example.

Example 5

GOLDNAIL cannot accommodate benched walls, so the analysis was based on an equivalent inclined wall. The nail lengths were changed so that their embedded ends would be in the same locations as in the actual cross-section.

An equivalent inclined wall was also used for analysis with *NAIL-SOLVER*, but an 11-foot wide bench at the top of the wall could not be accommodated, as the program only allows one slope angle at the crest. This problem was circumvented by using a negative surcharge on the backslope to simulate the removal of the extra soil weight. Directly behind the wall, where there is in actuality a bench, this program slightly under-predicted the soil gravity load. However, because the critical surface is a bilinear wedge intersecting the back of the nailed zone, the discrepancy made little difference. Also, the program *NAIL-SOLVER* cannot handle varying reinforcement parameters, so the nail length was an average, as was the nail diameter.

STARS also can handle only one slope angle at the wall crest, but two negative surcharges were used, one varying and one constant, to simulate the 11-foot bench and the subsequent reduction in soil height along the backslope.

Example 6

NAIL-SOLVER cannot handle different soil layers, so average values for cohesion and unit weight were used. *NAILM* cannot handle differing pullout resistance values, so a weighted average for the two soil layers was used.

Examples 7, 8, and 9

These three examples are interesting in that they demonstrate the effect of varying the wall inclination and the angle of the backslope. Example 7 was a vertical wall with a horizontal backslope and safety factors near 1.8. In Example 8, the wall remained vertical, but the backslope was inclined. The result: the slip surface change very little, but the safety factors dropped to about 1.4. With Example 9, the wall and the backslope were inclined, the slip surface moved away from the crest, and the safety factor was raised to 1.6.

Example 7

There is a question with the results from *STARS*; unless one looks at the deep seated slip surface, its prediction of the failure surface is radically different from that of the other programs. For this case the factor of safety was higher, and the slip surface was away from the crest. The program has the option of computing the stability of surfaces that are not required to pass

through the toe. The problem may have been the result of the large safety factor applied to the soil strength, which rendered the soil predominantly cohesive, with little frictional strength.

Example 10

GOLDNAIL is unable to handle toe slopes below the wall, so the analysis was done disregarding the toe slope. Also, to handle the different adhesion values of the nails, an elaborate interface between the two soil types was used to correctly assess the pullout resistance of each of the nails. The strength and unit weight of the soils were unaffected.

STARS was unable to accommodate the water table in the profile, so the run was made without it. The overhanging slip surface, previously mentioned, developed as the factored ϕ angle dipped below the slope angle. This addition of a thin frictional layer was successful in allowing the run.

NAIL-SOLVER is unable to handle varying nail parameters, such as length, so an average value was used. It is also unable to accommodate a water table. *NAILM* can not handle varying pullout resistance; therefore, a simple average value was used.

San Bernadino Wall

All the programs except *NAIL-SOLVER* handled this problem without any difficulty. *NAIL-SOLVER* is unable to allow anything but uniform spacing of the nails. As a consequence, the depth to the first nail was not 3 feet, with the lower nails at 5-foot vertical spacing; instead, it had to be made 5 feet with 5-foot spacings below. This difference altered the wall geometry, but with negligible effect on the results.

Swift Delta Wall (CrossSection 1)

SNAIL, *GOLDNAIL*, and*TALREN* all handled the wall without difficulty. The varying reinforcement parameters and surcharge provided no difficulties. The key to designing this wall was to model the bridge abutment as an additional 10 feet of wall and to add an additional 2 feet of live load surcharge to simulate traffic. *STARS* would not allow the extra 10 feet of wall above the top of the actual wall, so additional nails with no bond strength and no yield strength were added to the top 10 feet.

NAILSOLVER was not applicable here, as it only allows regular nail spacings and would not allow the placement of fictitious nails in the top 10 feet. *NAILM* was able to analyze the wall by using an average nail length and by analyzing the bottom nail at 15° below horizontal, instead of the actual inclination of 25°.

Polyclinic Wall

This wall was characterized by varying nail parameters, such as bond strength, nail length, yield strength, and inclination. Thus, only *GOLDNAIL*, *SNAIL*, *STARS*, and *TALREN* could accurately represent the as-built condition without making further assumptions.

NAILSOLVER, with its required regular nail spacing, added an additional nail to the bottom of the wall. It also required the use of one set of soil strength parameters. The soil strengths used were those of the larger lower layer because the largest length of the failure surface would pass through that layer. A weighted average of the unit weights of the two layers was used.

NAILM required the use of an average nail cross-sectional area and the pullout strength of the lower soil layer. The top nail's different length was handled through the use of the stepped nail length option (in which groups of nails are specified with a common length).

Eparris Wall

None of the programs were able to predict the actual slip surface location. This may be a result of poor soil characterization or incorrect reinforcement parameters. *TALREN* was the most notable in its prediction, as it predicted a slip surface with a grafted-on vertical section to avoid an overhang. Repeated attempts to correct this prediction failed.

NAILSOLVER was unable to handle this failure case because of its limitations on varied nail length parameters. It is unable to accommodate multiple nail lengths and bar diameters, and was therefore not used in the comparison. *NAILM* required the use of an average nail cross-sectional area, but it was able to handle the differing nail lengths.

Bodenvernagelung Wall (Case B)

All the programs predicted the correct failure surface for this failure case. This result may have been due to the excessively large surcharge controlling the location of the slip surface exit point.

NAILM was unable to handle the specific surcharge applied to the backslope. As was mentioned before, it can only accommodate linear surcharges applied to the entire backslope; thus the program was not used in the comparison.

CHAPTER 7

CONCLUSIONS

7.1 ANALYSIS PACKAGES

The program assumptions, which may include the type of slip surface and nail modeling, made very little difference to a) predicted factors of safety and, b) predicted slip surface location. However, from the user's viewpoint input flexibility, ease of data entry, and the quality of output varied considerably.

In a somewhat subjective rating or evaluation of specific program features, the preferred features of each would be as follows:

- Flexibility of input - *TALREN*, and *CLOUDIM*
- On-screen display of data during data entry - *STARS* and *CLOUDIM.*
- Input of a face pressure parameter- *GOLDNAIL* and *SNAIL.*
- Toe search capability - *SNAIL*, *TALREN*, and *STARS.*
- Output quality - *TALREN* (with the correct printer), *CLOUDIM*
- Ease of data modification - *STARS*, *SNAIL*, and *CLOUDIM.*
- Calculation methods - *SNAIL*, *GOLDNAIL*, and *TALREN.*

7.2 NAIL LOADS

In the past, instrumented soil nailing projects have generally reported the tensile force in the steel bar as the nail load without considering the load carried by the surrounding concrete grout. For many soil-nailed walls, including the walls analyzed for this study, the surrounding grout supports a significant portion of the total load carried by a typical soil nail, and therefore, reporting only the steel force as the nail load is misleading. The composite nail stiffness must be considered to improve the estimate of the total nail forces. Some previous works have attempted to account for the composite action of the nail by correlating the strain measurements to the laboratory-determined nail stiffness.

The proposed method for estimating the total nail forces by considering the composite nail section may be applied to any instrumented soil nail; it requires only the measured strain history and the cross-sectional areas of the steel bar and surrounding concrete grout. Thus, it is possible to estimate the development of the axial force in a soil nail with time.

The nail forces estimated for the analyzed case histories compared reasonably well with the required reinforcement for active soil conditions predicted by classic soil mechanics. Additionally, the results compared well with reported nail forces estimated by site specific methods that considered the composite action of the nail (Sakr and Barrows, 1991, Thompson and Miller, 1990, Byrne, 1992).

In some of the case histories analyzed in this study, strain measurements were high enough that the concrete grout had little influence on the total nail force. Although the load carried by the grout depends on the magnitude of strain and the area of the grout section, for small diameter nails the steel force represented the nail load reasonably well. Given the instrumented nails analyzed in this study, for which the diameters ranged from 89 mm to 229 mm, estimation of nail forces must incorporate the composite action of the nail for soil nails with diameters of larger than 100 mm.

A number of trends became evident when the nail forces in the soil nail walls analyzed for this study were compared. The distribution of axial tensile force along the lengths of the nails was relatively uniform, with a slight decrease near the far ends of the nails. In most cases, the strains measured near the face were not very reliable because of the affects of bending, facing loads, temperature changes, and/or freezing. Consequently, conclusions regarding face pressure are not very meaningful.

The distribution of maximum nail force down the wall depth was also relatively uniform, except that the estimated maximum nail forces were usually smaller in the bottom row or bottom two rows of nails. This is expected, as the nails are tensioned as excavation continues below the nail level, and usually there is no further excavation after the bottom row of nails has been installed.

The magnitude of the working nail loads for the walls analyzed in this study were compared to their respective empirical diagrams. In this manner, the nail loads estimated from strain measurements were compared to nail loads predicted on the basis of design soil properties and wall geometry. The soil-nailed walls constructed in residual soils and overconsolidated soils generally required less reinforcement than that predicted by the empirical diagram. Relatively low reinforcement was required for Polyclinic, Peasmarsh, Guernsey, and Cumberland Gap. Results from I-78, also constructed in residual soils, were questionable because of probable bending and facing loads, and therefore were not considered in this comparison. The soil-nailed walls constructed in normally consolidated soils and fill generally required more reinforcement than that predicted by the empirical diagram. In particular, the IH-30 walls, constructed in soft clay, required nearly twice the reinforcement predicted by the empirical diagram.

The empirical diagram (Juran and Elias, 1991) evolved from the apparent earth pressure envelope for braced cuts (Terzaghi and Peck, 1967), which was adequately conservative for the design of possible strut loads. However, in all of the walls analyzed for this study, at least one estimated maximum nail load exceeded the empirical diagram prediction. Also, the total estimated reinforcement in a wall cross-section exceeded the total reinforcement predicted by the empirical diagram in six of the ten walls analyzed in this study. Additionally, because of the inclination of the soil nails and the method of loading, soil nails are less efficient at reinforcing in situ soil than horizontal struts bracing sheet piles. Thus, the empirical diagram does not appear to be a conservative design for soil-nailed walls.

REFERENCES

ACI 209R-82 (Re-approved 1986), "Prediction of Creep, Shrinkage, and Temperature Effects in Concrete Structures," ACI Manual of Concrete Practice 1992, Part 1.

ACI 207.2R-73 (Re-approved 1986), "Materials and General Properties of Concrete," ACI Manual of Concrete Practice 1992, Part 1, pp. 207.2R-7-11.

Bang, S., Shen, C. K. and Romstad, K. M., "Analysis of an Earth-Reinforcing System for Deep Excavation," Transportation Research Record, No. 749, 1980.

Bang, S., Shen, C. K., Kim, J. and Kroetch, P., "Investigation of Soil Nailing Systems." Prepared for publication in Transportation Research Record, Nov., 1991, 40 pages.

Baska, D. A., "Design and Construction of a Permanent Soil Nailed Wall in Everett, Washington," ASCE Spring Seminar, March, 1992, ASCE Seattle Section, Univ. of Washington, Seattle, WA.

Bastick, M. J., "Soil Nailing and Reinforced Earth," Performance of Reinforced Soil Structures, Proceedings. of the International Reinforced Soil Conference in Glasgow, U.K., Sept. 10-12, 1990, Paper 12.

Bazant, Z. P. and Panula, L., "Practical prediction of time dependent deformations of concrete," RILEM Vol. II No. 65, Sep - Oct, 1978, pp. 307-328.

Bridle, R. J., "The Analysis and Design of Soil Nails," Performance of Reinforced Soil Structures, Proceedings of the International Reinforced Soil Conference in Glasgow, U.K., Sept. 10-12, 1990, Paper 9.

Bruce, D. and Jewell, R. A., "Soil Nailing: Application and Practice, Part 1," Ground Engineering, Nov., 1986, pp. 10-15.

Bruce, D. and Jewell, R. A., "Soil Nailing: Application and Practice, Part 2," Ground Engineering, Jan., 1987, pp. 21-33.

Byrne, R. J., "Soil Nailing: A Simplified Kinematic Analysis," Proceedings of the 1992 ASCE Specialty Conference on Grouting, Soil Improvement and Geosynthetics, Feb. 25-28, 1992, Geotechnical Special Publication No. 30, Vol. 2.

Byrne, R. J., "Soil Nailing: Kinematical Considerations and a Limiting Equilibrium Design Approach," ASCE Specialty Conference, New Orleans, 1992.

Cardoso, A. S. and Carreto, A. P., "Performance and Analysis of a Nailed Excavation," Proceedings of the Twelfth International Conference on Soil Mechanics and Foundation Engineering, Rio de Janeiro, Brazil, Aug. 13-18, 1989, Vol. 2, pp. 1233-1236.

Structures," Proceedings of the Eighth European Conference on Soil Mechanics and Foundation Engineering: Improvement of Ground, Helsinki, May 23-26, 1983, Vol. 2, pp. 473-476.

Chassie, R. G., "Soil Nailing Overview," ASCE Spring Seminar, Mar. 28, 1992, ASCE Seattle Section, Univ. of Washington, Seattle, WA.

Cotton, D. M., "Soil Nailing: The development of the top down method of permanent wall construction, and local stability problems and resolutions in fill materials, glacial till, outwash, and lacustrine deposits," ASCE Spring Seminar, March, 1992, ASCE Seattle Section, Univ. of Washington, Seattle, WA.

Denby, G., "Two Soil Nailing Case Histories, First Use in Seattle," Proceedings of the 24th Symposium on Engineering Geology and Soils Engineering, Feb. 25th, 1988, Boise, Idaho, pp. 409-423.

Denby, G., Argo, D. and Campbell, D., "Soil Nail Design and Construction of the Swedish Hospital Parking Garage Seattle, Washington," ASCE Spring Seminar, March, 1992, ASCE Seattle Section, Univ. of Washington, Seattle, WA.

Elias, V. and Juran, I., "Summary of Soil Nailing Research Results," U.S. Department of Transportation, Federal Highway Administration, FHWA/RD-90/104, 1990.

England, G. L. and Illston, J. M., "Method of Computing Stress in Concrete from a History of Measured Strain," Civil Engineering and Public Works Review, April 1965, pp. 513-517, 692-694,846-847.

FHWA, Summary of Design Methods Comparison For Nailed Retaining Walls, Preliminary Draft, FHWA demonstration project No. 82, 1991.

Farnham, D. J., "Guernsey: Soil Nail Instrumentation," Trafalgar House Technology, TR. 465, September 1992.

Farnham, D. J., "Guernsey- Soil Nail Monitoring Part 2: Laboratory Testing of Soil Nail," Trafalgar House Technology, TR. 466, September 1992.

Finney, A., "An Evaluation of Soil Nail Analysis Packages," M.S.C.E. Thesis, University of Washington, Seattle, WA, October 1993.

Gässler, G., "Full Scale Test on a Nailed Wall in Consolidated Clay," Proceedings of the International Symposium on Earth Reinforcement Practice, Fukuoka, Japan, November 1988.

Gässler, G., "In-Situ Techniques of Reinforced Soil," Performance of Reinforced Soil Structures, Proceedings of the International Reinforced Soil Conference in Glasgow, U.K., Sept. 10-12, 1990.

Gässler, G., "Soil-Nailing--Theoretical Basis and Practical Design," Proceedings of the International Geotechnical Symposium on Theory and Practice of Earth Reinforcement, Fukuoka, Kyushu, Japan, Oct. 5-7, 1988, pp. 283-288.

Gässler, G., "Vernagelta Geländesprunge - Tragverhalten und Standsicherheit," Doctor Thesis, Publication of the Institute for Soil Mechanics and Rock Mechanics, University of Karlsruhe, FRG, Vol. 108.

Gässler, G. and Gudehus, G., "Soil Nailing--Some Aspects of a New Technique," Proceedings of the Tenth International Conference on Soil Mechanics and Foundation Engineering, Stockholm, June 15-19, 1981, Vol. 3, pp. 665-670.

Gässler, G. and Gudehus, G., "Soil Nailing: Statistical Design," Improvement of Ground: Proceedings of the Eighth European Conference on Soil Mechanics and Foundation Engineering, Helsinki, Finland, May, 1983, Vol. 2, pp. 491-494.

Goldnail User's Manual, Golder Associates, Redmond, WA, Jan., 1993, 20 pages.

Gudehus, G. and Schwing, E., "Soil-Nailing--Design and application to modern and ancient retaining walls," International Geotechnical Symposium on Theory and Practice of Earth Reinforcement, Fukuoka, Japan, 1988, pp. 605-610.

Guilloux, A., Notte, G. and Gonin, H., "Experiences on a Retaining Structure by Nailing in Moraine Soils," Improvement of Ground: Proceedings of the Eighth European Conference on Soil Mechanics and Foundation Engineering, Helsinki, Finland, May 23-26, 1983, Vol. 2, pp. 499-502.

Proceedings of the Twelfth International Conference on Soil Mechanics and Foundation Engineering, Rio de Janeiro, Brazil, Aug. 13-18, 1989, Vol. 2, pp. 1253-1255.

Ho, C.L., Ludwig, H. P., Fragaszy, R. J., & Chapman, K. R., "Field Performance of a Soil Nail System in Loess," Foundation Engineering Proceedings, ASCE, CO Division, Evanstan, IL June 25-29, 1989.

Houghton, D. L., "Determining Tensile Strain Capacity of Mass Concrete," ACI Journal Proceedings V. 73, No. 12, Title No. 84-M29, Dec. 1976, pp. 691-700.

Jewell, R. A., "Soil Nailing," Performance of Reinforced Soil Structures, Proceedings. of the International Reinforced Soil Conference in Glasgow, U.K., Sept. 10-12, 1990.

Jewell, R. A.. "Review of theoretical models for soil nailing," Performance of Reinforced Soil Structures, Proceedings of the International Reinforced Soil Conference, British Geotechnical Society, Glasgow, Sept., 1990.

Jones, C. J. F. P. and O'Rourke, T. D., "Overview of Earth Retention Systems: 1970-1990," Design and Performance of Earth Retaining Structures, ASCE Special Publication No. 25, 1990, pp. 22-49.

Juran, I., Baudrand, G., Farrag, K. and Elias, V., "Design of Soil-Nailed Retaining Structures," Design and Performance of Earth Retaining Structures, ASCE Special Publication No. 25, 1990, pp. 644-659.

Juran, I. and Elias, V., "Behavior and Working Stress Design of Soil Nailed Retaining Structures," Performance of Reinforced Soil Structures, Proceedings. of the International Reinforced Soil Conference in Glasgow, U.K., Sept. 10-12, 1990, Paper 2.

Juran, I. and Elias, V., "Ground Anchors and Soil Nails in Retaining Structures," Chap. 26 in Foundation Engineering Handbook, 2nd ed., Ed. H. Fang, Van Nostrand Reinhold, New York, 1991.

Juran, I. and Elias, V., "Soil Nailed Retaining Structures: Analysis of Case Histories," ASCE Geotechnical Special Publication No. 12, 1987, pp. 232 - 244.

Kakurai, M. and Hori, J., "Soil--Reinforcement with Steel Bars on a Cut Slope," Takenaka Technical Research Report No. 46, Takenaka Corporation, Tokyo, pp. 101-108.

Kosmatka, S. H. and Panerese, W. C., Design and Control of Concrete Mixtures, 13th ed., Portland Cement Association, 1990.

Leichner, C. H., "Case History of a Soil Nailed Wall, in Northhampton County, PA.," Transportation Research Board, 68th Annual Meeting, Meeting Preprint, 1989.

MacGregor, J., Reinforced Concrete, Mechanics and Design, Prentice Hall, 1988, pp. 259-260.

Mehta, P. K. and Monteiro, P. J., 2nd Edition, Concrete, Structure, Properties and Materials, 1993, pp. 66, 70, 89-111, 456.

Munfakh, G. A., "Soil Reinforcement: A Tale of Three Walls," Proceedings of the Twelfth International Conference on Soil Mechanics and Foundation Engineering, Rio de Janeiro, Brazil, Aug. 13-18, 1989, Vol. 2, pp. 1285-1288.

Neville, A. M., Creep of Concrete: Plain, Reinforced and Prestressed, North Holland Publishing Co., Amsterdam, (Elsevier), 1970, pp. 91-92, 220-225, 317, 387-392.

Pedley, M. J. and Jewell, R. A., "Analysis For Soil Reinforcement With Bending Stiffness," Journal of Geotechnical Engineering, ASCE, Oct., 1992, Vol. 118, pp. 1505-1528.

Pedley, M. J. and Jewell, R. A., "Soil Nailing Design: The Role of Bending Stiffness," Ground Engineering, Vol. 23, No. 2, March 1990, pp. 30-36.

Pedley, M. J. and Pugh, R.S., "Soil Nailing in the Hastings Beds," 28th Conference of the Engineering Group of the Geological Society, Manchester, England, Sept., 1992.

Pedley, M. J., Jewell, R. A. and Milligan, G. W. E., "A Large Scale Experimental Study of Soil Reinforcement Interaction. Part 1," Ground Engineering, Vol. 23, No. 6, July/August, 1990, pp. 44-50.

Pedley, M. J., Jewell, R. A. and Milligan, G. W. E., "A Large Scale Experimental Study of Soil Reinforcement Interaction. Part 2," Ground Engineering, Vol. 23, No. 7, Sept., 1990, pp. 45-49.

Pfister, P., "Permanent Ground Anchors - Soletanche Design Criteria," FHWA., Report No. RD-81/150.

Plumelle, C. and Schlosser, F., "Three full scale experiments of the french project on soil nailing: CLOUTERRE," Proceedings of the 70th Annual Meeting, Transportation Research Board, Washington, D.C., 1991.

Plumelle, C., Schlosser, F., Delage, P. and Knochenmus, G., "French National Research Project on Soil Nailing: CLOUTERRE," Design and Performance of Earth Retaining Structures, ASCE Special Publication No. 25, 1990, pp. 660-675.

Raphael, J. M., "Tensile Strength of Concrete," ACI Journal NO. 81-17, Mar-Apr, 1984.

Ross, A. D., "Creep of Concrete under Variable Stress," Journal of the American Concrete Institute, March 1958, Title No. 54-41, pp. 739-758.

Sakr, C., "Soil Nailing of a Bridge Fill Embankment," Construction Report, Federal Highway Administration Experimental Features, Oregon Dept. of Transportation, August, 1991.

Sakr, C. and Barrows, R., "Soil Nailing: Its Applicability to Bridge Embankment Retention," Western Bridge Engineer's Seminar, Seattle, WA, Sept. 23-25, 1991.

Salama, M. E., "Analysis of Soil Nail Retaining Walls," Ph. D. Thesis, University of Illinois at Urbana - Champaign, 1992.

Sawicki, A., Lesniewska, D. and Kulezykowski, M., "Measured and Predicted Stresses and Bearing Capacity of a Full Scale Slope Reinforced with Nails," Soils and Foundations, Vol. 28, No. 4, 1988, pp. 47-56.

Schlosser, F., "Behavior and Design of Soil Nailing," Proceedings of the International Symposium on Recent Developments in Ground Improvement, Bangkok, Nov. 29 - Dec. 3, 1982, pp. 399-413.

Schlosser, F. and Unterreiner, P., "French Design Practice," ASCE Specialty Conference on Grouting, Soil Improvement and Geosynthetics, New Orleans, Feb 25, 1992.

Schlosser, F., Unterreiner, P. and Plumelle, C., "French Research Program CLOUTERRE on Soil Nailing," Proceedings of the 1992 ASCE Specialty Conference on Grouting, Soil Improvement and Geosynthetics, Feb. 25-28, 1992, Geotechnical Special Publication No. 30, Vol. 2, pp. 739-751.

Schlosser, F. and Unterreiner, P., "Soil Nailing in France: Research and Practice," Transportation Research Board, 70th Annual Meeting, Washington, D.C., Jan., 1991.

Shen, C. K., Bang, S. and Herrman, L. R., "Ground Movement Analysis of Earth Support System," ASCE Journal of Geotechnical Engineering, Vol. 107, No. 12, Dec. 1981, pp. 1610-1624.

Shen, C. K., Bang, S., Herrman, L. R. and Romstad, K. M., "A Reinforced Lateral Earth Support System," Proceedings of a Symposium on Earth Reinforcement, ASCE, Pittsburg, PA, 1978.

Shen, C. K., Bang, S., Romstad, K. M., Kulchin, L. and DeNatale, J. S., "Field Measurements of an Earth Support System," ASCE Journal of Geotechnical Engineering, Vol. 107, No. 12, Dec., 1981, pp. 1625-1642.

Shen C. K., Herrman, L. R., Romstad, K. L., Bang, S., Kim, J., & DeNatale, J. S., "An In Situ Earth Reinforcement Lateral Support System," Department of Civil Engineering, University of California at Davis, Report No. 81-03, 1981.

Snail User's Manual, Version 2.05, Caltrans, Sept., 1992.

Steel Sheet Piling Design Manual, Pile Buck, Inc., 1987.

Stocker, M. F., Korber, G. W., Gässler, G. and Gudehus, G., "Soil Nailing," C.R. Coll. Int. Reinforcement des sols, Paris, 1979, pp. 469-474.

Stocker, M. and Riedinger, G., "The Bearing Behavior of Nailed Retaining Structures," Design and Performance of Earth Retaining Structures (G. S. P. 25), edited by Lambe, P. C. and Hansen, L. A., ASCE, New York, 1990, pp. 612-628.

Terzaghi, K. and Peck, Soil Mechanics in Engineering Practice, Wiley, 1967.

Thompson, S. R. and Miller, I. R., "Design, Construction, and Performance of a Soil Nailed Wall in Seattle, Washington," Design and Performance of Earth Retaining Structures, ASCE Special Publication No. 25, 1990, pp. 629-643.

U. S. Department of the Navy, Facilities Engineering Command (NAVFAC), Design Manual DM-7.01, U. S. Government Printing Office, Washington, D. C., 1986.

U. S. Department of the Navy, Facilities Engineering Command (NAVFAC), Design Manual DM-7.02, U. S. Government Printing Office, Washington, D. C., 1986.

Wood, S. L., "Evaluation of Long-term Properties of Concrete," ACI Materials Journal, Vol. 88, No. 6, 1991.

APPENDIX A

PROCEDURE FOR ESTIMATION OF SOIL NAIL LOADS

A step-by-step procedure which was used for estimating the soil nail loads is presented herein as a supporting document.

1) Assemble strain histories for all gauges.

Calculate strains from gauge readings (adjusted for temperature if possible).

2) Judge the quality of the data.

Make a plot of strain history for all gauges at one location and mark significant construction dates on the plot. Average strains for working gauges at each location to get axial strains. Throw out bad data and document what was discarded and why.

3) Choose an end of construction (EOC) date.

This will usually be when the strains in the bottom nail "level" off. Assume no significant load changes after this date unless otherwise noted.

4) Obtain steel material properties, E_S and A_S

5) Choose grout elastic material properties vs. time.

If none are provided with case history, assume a typical value of the 28 day compressive strength, $(f_c')_{28} = 20.7$ N/mm^2 (3000 psi). Use empirical relations recommended by ACI-209:

$$(f_c')_t = (f_c')_{28} \frac{t}{(4+0.85t)} \qquad \text{(A.1)}$$

$$(E_c^e)_t = 4800(f_c')_t^{\frac{1}{2}} \qquad \text{(A.2)}$$

$$(f_t')_t = 0.55(f_c')_t^{\frac{1}{2}} \qquad \text{(A.3)}$$

where t = age of grout in days, and $(f_c')_t$, $(f_t')_t$, and $(E_c^e)_t$ are in N/mm^2

6) Choose creep ratio equation, based on ACI - 209

$$v_d = 2.94 C_h C_w \left[\frac{d^{0.6}}{10+d^{0.6}}\right] t^{-0.118} \qquad \text{(A.4)}$$

d= duration of load in days, t = age of grout upon loading in days

C_h= humidity constant, C_W= thickness constant

7) Calculate time variables.

During construction: $t = d$ = (days since installed) / 2,

except for tensile strength of grout, $(f't)_t$ use t = days since installed

After construction: t = (EOC date – install date) / 2

d = (days since installed) – t ,

except for tensile strength of grout,$(f't)_t$, use t = EOC date - install date

8) Calculate effective grout modulus and grout tensile strength, versus time

$$\left(E_c^s\right)_d = \frac{\left(E_c\right)_t}{1+\nu_d} \text{ and } (f't)_t = 0.55(f'c)_t^{1/2} \qquad \text{(A.5)}$$

9) Calculate grout load, $P_c = \varepsilon A_c E_c^s$

10) Calculate steel load, $P_s = \varepsilon A_s E_s$

11) Calculate possible nail load for all dates

a) Calculate the limit grout load

b) Calculate limit nail load

$$\left(P_{sn}\right)_{\lim} = \left(P_c\right)_{\lim} + \varepsilon_{\lim} A_s E_s \quad \text{in which: } \varepsilon_{\lim} = \frac{f_t'}{E_c^s}$$

c) Calculate nail load, P_{sn}, for each date

If $P_c \le \left(P_c\right)_{\lim}$, $P_{sn} = P_s + P_c$

If $P_c > \left(P_c\right)_{\lim}$, $P_{sn} = \max\left|\left(P_{sn}\right)_{\lim}, P_s\right|$

12) Estimate Nail Load since EOC.

If, for all dates, $P_c \le \left(P_c\right)_{\lim}$, $P_{sn} = P_{sn(EOC)}$, with upper bound as $\max|P_{sn}|$

If, for any date, $P_c > \left(P_c\right)_{\lim}$, $P_{sn} = \max\left|\left(P_{sn}\right)_{\lim(EOC)}, P_s\right|$, with upper bound as $\max|P_s| + \left(P_c\right)_{\lim}$

13) Plot Nail Loads and upper bound estimates on each instrumented nail

APPENDIX B

INPUT PARAMETERS FOR EXAMPLE PROBLEMS

Example 1

C	ϕ	γ	Grout Diam.	Bar Diam.	Depth to 1st Nail	Ult. Nail Stress
psf.	Degrees	pcf.	in.	in.	ft.	ksi.
225	35	110	6	.875	2.5	60
Bond Stress	Wall Height	Nail Spac., S_h	Nail Spac., S_v	Length of Nail	E of Nail	Nail Inclination
psf.	ft.	ft.	ft.	ft.	ksi.	Degrees
2500	30	5	5	20	30000	15

SNAIL

Bond Stress	Punching Shear
psi.	kips.
17.36	Varies

STARS

$\beta 1$	$\beta 2$	$\beta 3$	Traction	Friction
Degrees	Degrees	Degrees	kN	kN/m
0	84.3	0	160	57

GOLDNAIL

Adhesion	Max. Nail Force	Face Pressure	Nail Length Factor
lbs/ft.	lbs.	psf.	
3927	36079	Varies	.67

NAIL-SOLVER

Ult. Nail Stress	H Max.	f_b	K_l
N/mm^2	m.		
414	9	1	2.26

NAILM

Nail X-Sect. Area	Unbonded Length	Average Pullout	A
in^2	ft.	psf.	
.6	0	2500	2

TALREN

QS	PL	KSB	LB	TR	ALB	IND	RCIS
kN/m	kPa		m	kN	Deg.		kN
57	0	0	1.5	160	0	1	0

CLOUDIM

QS	PL	KSB	LB	TR	ALB	IND	RCIS
kN/m	kPa		m	kN	Deg.		kN
57	0	0	1.5	160	0	1	0

Example 2

C	ϕ	γ	Grout Diam.	Bar Diam.	Depth to 1st Nail	Ult. Nail Stress
psf.	Degrees	pcf.	in.	in.	ft.	ksi.
225	35	110	6	.875	2.5	60
Bond Stress	Wall Height	Nail Spac., S_h	Nail Spac., S_v	Length of Nail	E of Nail	Nail Inclination
psf.	ft.	ft.	ft.	ft.	ksi.	Degrees
2500	60	5	5	20	30000	15

SNAIL

Bond Stress	Punching Shear
psi.	kips.
17.36	Varies

STARS

$\beta 1$	$\beta 2$	$\beta 3$	Traction	Friction
Degrees	Degrees	Degrees	kN	kN/m
0	84.3	0	160	57

GOLDNAIL

Adhesion	Max. Nail Force	Face Pressure	Nail Length Factor
lbs/ft.	lbs.	psf.	
3927	36079	Varies	.83

NAIL-SOLVER

Ult. Nail Stress	H Max.	f_b	K_l
N/mm^2	m.		
414	18	1	0.8

NAILM

Nail X-Sect. Area	Unbonded Length	Average Pullout	A
in^2	ft.	psf.	
.6	0	2500	2

TALREN

QS	PL	KSB	LB	TR	ALB	IND	RCIS
kN/m	kPa		m	kN	Deg.		kN
57	0	0	1.5	160	0	1	0

Example 3 (Upper Soil)

C	ϕ	γ	Grout Diam.	Bar Diam.	Depth to 1st Nail	Ult. Nail Stress
psf.	Degrees	pcf.	in.	in.	ft.	ksi.
225	35	110	6	.875	2.5	60
Bond Stress	Wall Height	Nail Spac., S_h	Nail Spac., S_v	Length of Nail	E of Nail	Nail Inclination
psf.	ft.	ft.	ft.	ft.	ksi.	Degrees
2500	30	5	5	20	30000	15

SNAIL

Bond Stress	Punching Shear
psi.	kips.
13.89	Varies

STARS

$\beta 1$	$\beta 2$	$\beta 3$	Traction	Friction
Degrees	Degrees	Degrees	kN	kN/m
	Not	Applicable		

GOLDNAIL

Adhesion	Max. Nail Force	Face Pressure	Nail Length Factor
lbs/ft.	lbs.	psf.	
3142	36079	Varies	.67

NAIL-SOLVER

Ult. Nail Stress	H Max.	f_b	K_l
N/mm^2	m.		
	Not	Applicable	

NAILM

Nail X-Sect. Area	Unbonded Length	Average Pullout	A
in^2	ft.	psf.	
	Not	Applicable	

TALREN

QS	PL	KSB	LB	TR	ALB	IND	RCIS
kN/m	kPa		m	kN	Deg.		kN
46	0	0	1.5	160	0	1	0

Example 3 (Lower Soil)

C	ϕ	γ	Grout Diam.	Bar Diam.	Depth to 1st Nail	Ult. Nail Stress
psf.	Degrees	pcf.	in.	in.	ft.	ksi.
500	35	110	6	.875	2.5	60
Bond Stress	Wall Height	Nail Spac., S_h	Nail Spac., S_v	Length of Nail	E of Nail	Nail Inclination
psf.	ft.	ft.	ft.	ft.	ksi.	Degrees
4000	30	5	5	20	30000	15

SNAIL

Bond Stress	Punching Shear
psi.	kips.
27.78	Varies

STARS

$\beta 1$	$\beta 2$	$\beta 3$	Traction	Friction
Degrees	Degrees	Degrees	kN	kN/m
	Not	Applicable		

GOLDNAIL

Adhesion	Max. Nail Force	Face Pressure	Nail Length Factor
lbs/ft.	lbs.	psf.	
6283	36079	Varies	.67

NAIL-SOLVER

Ult. Nail Stress	H Max.	f_b	K_l
N/mm^2	m.		
	Not	Applicable	

NAILM

Nail X-Sect. Area	Unbonded Length	Average Pullout	A
in^2	ft.	psf.	
	Not	Applicable	

TALREN

QS	PL	KSB	LB	TR	ALB	IND	RCIS
kN/m	kPa		m	kN	Deg.		kN
92	0	0	1.5	160	0	1	0

Example 4

C	ϕ	γ	Grout Diam.	Bar Diam.	Depth to 1st Nail	Ult. Nail Stress
psf.	Degrees	pcf.	in.	in.	ft.	ksi.
225	40	110	6	.875	2	60
Bond Stress	Wall Height	Nail Spac., S_h	Nail Spac., S_v	Length of Nail	E of Nail	Nail Inclination
psf.	ft.	ft.	ft.	ft.	ksi.	Degrees
3000	20	4	4	20	30000	15

SNAIL

Bond Stress	Punching Shear
psi.	kips.
20.83	Varies

STARS

$\beta 1$	$\beta 2$	$\beta 3$	Traction	Friction
Degrees	Degrees	Degrees	kN	kN/m
0	90	0	160	69

GOLDNAIL

Adhesion	Max. Nail Force	Face Pressure	Nail Length Factor
lbs/ft.	lbs.	psf.	
4712	36079	Varies	1

NAIL-SOLVER

Ult. Nail Stress	H Max.	f_b	K_l
N/mm^2	m.		
414	9	1	2.22

NAILM

Nail X-Sect. Area	Unbonded Length	Average Pullout	A
in^2	ft.	psf.	
	Not	Applicable	

TALREN

QS	PL	KSB	LB	TR	ALB	IND	RCIS
kN/m	kPa		m	kN	Deg.		kN
69	0	0	1.2	160	0	1	0

Example 5 (Top four nails)

C	ϕ	γ	Grout Diam.	Bar Diam.	Depth to 1st Nail	Ult. Nail Stress
psf.	Degrees	pcf.	in.	in.	ft.	ksi.
0	37	125	3.5	1	2.5	60
Bond Stress	Wall Height	Nail Spac., S_h	Nail Spac., S_v	Length of Nail	E of Nail	Nail Inclination
psf.	ft.	ft.	ft.	ft.	ksi.	Degrees
2456	40	4	5	19	30000	10

SNAIL

Bond Stress	Punching Shear
psi.	kips.
17.05	Varies

STARS

$\beta 1$	$\beta 2$	$\beta 3$	Traction	Friction
Degrees	Degrees	Degrees	kN	kN/m
27	76	0	210	33

GOLDNAIL

Adhesion	Max. Nail Force	Face Pressure	Nail Length Factor
lbs/ft.	lbs.	psf.	
2250	47124	Varies	0.6

NAIL-SOLVER

Ult. Nail Stress	H Max.	Nail Length	Bar Diam.	f_b	K_1
N/mm^2	m.	m.	mm.		
414	27	7.2	28.8	1	0.8

NAILM

Nail X-Sect. Area	Unbonded Length	Average Pullout	A
in^2	ft.	psf.	
	Not	Applicable	

TALREN

QS	PL	KSB	LB	TR	ALB	IND	RCIS
kN/m	kPa		m	kN	Deg.		kN
33	0	0	1.5	210	0	1	0

Example 5 (Bottom four nails)

C	ϕ	γ	Grout Diam.	Bar Diam.	Depth to 1st Nail	Ult. Nail Stress
psf.	Degrees	pcf.	in.	in.	ft.	ksi.
0	37	125	3.5	1.27		60
Bond Stress	Wall Height	Nail Spac., S_h	Nail Spac., S_v	Length of Nail	E of Nail	Nail Inclination
psf.	ft.	ft.	ft.	ft.	ksi.	Degrees
2456	40	4	5	29	30000	10

SNAIL

Bond Stress	Punching Shear
psi.	kips.
17.05	Varies

STARS

$\beta 1$	$\beta 2$	$\beta 3$	Traction	Friction
Degrees	Degrees	Degrees	kN	kN/m
27	76	0	338	33

GOLDNAIL

Adhesion	Max. Nail Force	Face Pressure	Nail Length Factor
lbs/ft.	lbs.	psf.	
2250	76006	Varies	0.6

NAIL-SOLVER

Ult. Nail Stress	H Max.	Nail Length	Bar Diam.	f_b	K_l
N/mm^2	m.	m.	mm.		
414	27	7.2	28.8	1	0.8

NAILM

Nail X-Sect. Area	Unbonded Length	Average Pullout	A
in^2	ft.	psf.	
	Not	Applicable	

TALREN

QS	PL	KSB	LB	TR	ALB	IND	RCIS
kN/m	kPa		m	kN	Deg.		kN
33	0	0	1.5	338	0	1	0

Example 6 (Upper Soil)

C	ϕ	γ	Grout Diam.	Bar Diam.	Depth to 1st Nail	Ult. Nail Stress
psf.	Degrees	pcf.	in.	in.	ft.	ksi.
0	35	125	6	0.875		60
Bond Stress	Wall Height	Nail Spac., S_h	Nail Spac., S_v	Length of Nail	E of Nail	Nail Inclination
psf.	ft.	ft.	ft.	ft.	ksi.	Degrees
5500	60	5	5	50	30000	15

SNAIL

Bond Stress	Punching Shear
psi.	kips.
38.2	Varies

STARS

$\beta 1$	$\beta 2$	$\beta 3$	Traction	Friction
Degrees	Degrees	Degrees	kN	kN/m
0	84.3	0	160	126

GOLDNAIL

Adhesion	Max. Nail Force	Face Pressure	Nail Length Factor
lbs/ft.	lbs.	psf.	
8639.3	36079	Varies	0.83

NAIL-SOLVER

Ult. Nail Stress	C	ϕ	γ	H Max.	f_b	K_l
N/mm^2	kN/m^2	degrees	kN/m^3	m.		
414	8.97	27	18.1	18	1	0.73

NAILM

Nail X-Sect. Area	Unbonded Length	Average Pullout	A
in^2	ft.	psf.	
0.6	0	3000	2

TALREN

QS	PL	KSB	LB	TR	ALB	IND	RCIS
kN/m	kPa		m	kN	Deg.		kN
126	0	0	1.5	160	0	1	0

Example 6 (Lower Soil)

C	ϕ	γ	Grout Diam.	Bar Diam.	Depth to 1st Nail	Ult. Nail Stress
psf.	Degrees	pcf.	in.	in.	ft.	ksi.
225	35	1110	6	0.875		60
Bond Stress	Wall Height	Nail Spac., S_h	Nail Spac., S_v	Length of Nail	E of Nail	Nail Inclination
psf.	ft.	ft.	ft.	ft.	ksi.	Degrees
2500	60	5	5	50	30000	15

SNAIL

Bond Stress	Punching Shear
psi.	kips.
17.36	Varies

STARS

$\beta 1$	$\beta 2$	$\beta 3$	Traction	Friction
Degrees	Degrees	Degrees	kN	kN/m
0	84.3	0	160	57

GOLDNAIL

Adhesion	Max. Nail Force	Face Pressure	Nail Length Factor
lbs/ft.	lbs.	psf.	
3927	36079	Varies	0.83

NAIL-SOLVER

Ult. Nail Stress	C	ϕ	γ	H Max.	f_b	K_l
N/mm^2	kN/m^2	degrees	kN/m^3	m.		
414	8.97	35	18.1	18	1	0.73

NAILM

Nail X-Sect. Area	Unbonded Length	Average Pullout	A
in^2	ft.	psf.	
0.6	0	3000	2

TALREN

QS	PL	KSB	LB	TR	ALB	IND	RCIS
kN/m	kPa		m	kN	Deg.		kN
57	0	0	1.5	160	0	1	0

Example 7

C	ϕ	γ	Grout Diam.	Bar Diam.	Depth to 1st Nail	Ult. Nail Stress
psf.	Degrees	pcf.	in.	in.	ft.	ksi.
225	35	115	8	1	2.5	60
Bond Stress	Wall Height	Nail Spac., S_h	Nail Spac., S_v	Length of Nail	E of Nail	Nail Inclination
psf.	ft.	ft.	ft.	ft.	ksi.	Degrees
2500	40	5	5	30	30000	15

SNAIL

Bond Stress	Punching Shear
psi.	kips.
17.36	Varies

STARS

β1	β2	β3	Traction	Friction
Degrees	Degrees	Degrees	kN	kN/m
0	90	0	210	76

GOLDNAIL

Adhesion	Max. Nail Force	Face Pressure	Nail Length Factor
lbs/ft.	lbs.	psf.	
5236	47124	Varies	0.75

NAIL-SOLVER

Ult. Nail Stress	H Max.	f_b	K_l
N/mm^2	m.		
414	12	1	3.32

NAILM

Nail X-Sect. Area	Unbonded Length	Average Pullout	A
in^2	ft.	psf.	
0.79	0	2500	2

TALREN

QS	PL	KSB	LB	TR	ALB	IND	RCIS
kN/m	kPa		m	kN	Deg.		kN
76	0	0	1.5	210	0	1	0

Example 8

C	ϕ	γ	Grout Diam.	Bar Diam.	Depth to 1st Nail	Ult. Nail Stress
psf.	Degrees	pcf.	in.	in.	ft.	ksi.
225	35	115	8	1	2.5	60
Bond Stress	Wall Height	Nail Spac., S_h	Nail Spac., S_v	Length of Nail	E of Nail	Nail Inclination
psf.	ft.	ft.	ft.	ft.	ksi.	Degrees
2500	40	5	5	30	30000	15

SNAIL

Bond Stress	Punching Shear
psi.	kips.
17.36	Varies

STARS

$\beta 1$	$\beta 2$	$\beta 3$	Traction	Friction
Degrees	Degrees	Degrees	kN	kN/m
20	90	0	210	76

GOLDNAIL

Adhesion	Max. Nail Force	Face Pressure	Nail Length Factor
lbs/ft.	lbs.	psf.	
5236	47124	Varies	0.75

NAIL-SOLVER

Ult. Nail Stress	H Max.	f_b	K_l
N/mm^2	m.		
414	22	1	0.8

NAILM

Nail X-Sect. Area	Unbonded Length	Average Pullout	A
in^2	ft.	psf.	
0.79	0	2500	2

TALREN

QS	PL	KSB	LB	TR	ALB	IND	RCIS
kN/m	kPa		m	kN	Deg.		kN
76	0	0	1.5	210	0	1	0

Example 9

C	ϕ	γ	Grout Diam.	Bar Diam.	Depth to 1st Nail	Ult. Nail Stress
psf.	Degrees	pcf.	in.	in.	ft.	ksi.
225	35	115	8	1	2.5	60
Bond Stress	Wall Height	Nail Spac., S_h	Nail Spac., S_v	Length of Nail	E of Nail	Nail Inclination
psf.	ft.	ft.	ft.	ft.	ksi.	Degrees
2500	40	5	5	30	30000	15

SNAIL

Bond Stress	Punching Shear
psi.	kips.
17.36	Varies

STARS

$\beta 1$	$\beta 2$	$\beta 3$	Traction	Friction
Degrees	Degrees	Degrees	kN	kN/m
20	80	0	210	76

GOLDNAIL

Adhesion	Max. Nail Force	Face Pressure	Nail Length Factor
lbs/ft.	lbs.	psf.	
5236	47124	Varies	0.75

NAIL-SOLVER

Ult. Nail Stress	H Max.	f_b	K_l
N/mm^2	m.		
414	22	1	1.11

NAILM

Nail X-Sect. Area	Unbonded Length	Average Pullout	A
in^2	ft.	psf.	
0.79	0	2500	2

TALREN

QS	PL	KSB	LB	TR	ALB	IND	RCIS
kN/m	kPa		m	kN	Deg.		kN
76	0	0	1.5	210	0	1	0

Example 10 (Top 4 Nails)

C	ϕ	γ	Grout Diam.	Bar Diam.	Depth to 1st Nail	Ult. Nail Stress
psf.	Degrees	pcf.	in.	in.	ft.	ksi.
500	35	125	8	1	2.5	60
Bond Stress	Wall Height	Nail Spac., S_h	Nail Spac., S_v	Length of Nail	E of Nail	Nail Inclination
psf.	ft.	ft.	ft.	ft.	ksi.	Degrees
1728	45	5	5	50	30000	15

SNAIL

Bond Stress	Punching Shear
psi.	kips.
12	Varies

STARS

β1	β2	β3	Traction	Friction
Degrees	Degrees	Degrees	kN	kN/m
27	90	20	210	53

GOLDNAIL

Adhesion	Max. Nail Force	Face Pressure	Nail Length Factor
lbs/ft.	lbs.	psf.	
3620	47124	Varies	1.3

NAIL-SOLVER

Ult. Nail Stress	H Max.	f_b	Nail Length	K_1
N/mm^2	m.		m.	
414	28.5	1	15.9	.53

NAILM

Nail X-Sect. Area	Unbonded Length	Average Pullout	A
in^2	ft.	psf.	
0.79	0	1950	2

TALREN

QS	PL	KSB	LB	TR	ALB	IND	RCIS
kN/m	kPa		m	kN	Deg.		kN
53	0	0	1.5	210	0	1	0

Example 10 (Lower Five Nails)

C	ϕ	γ	Grout Diam.	Bar Diam.	Depth to 1st Nail	Ult. Nail Stress
psf.	Degrees	pcf.	in.	in.	ft.	ksi.
500	35	125	8	1		60
Bond Stress	Wall Height	Nail Spac., S_h	Nail Spac., S_v	Length of Nail	E of Nail	Nail Inclination
psf.	ft.	ft.	ft.	ft.	ksi.	Degrees
2161	45	5	5	56	30000	15

SNAIL

Bond Stress	Punching Shear
psi.	kips.
15	Varies

STARS

$\beta 1$	$\beta 2$	$\beta 3$	Traction	Friction
Degrees	Degrees	Degrees	kN	kN/m
27	90	20	210	66

GOLDNAIL

Adhesion	Max. Nail Force	Face Pressure	Nail Length Factor
lbs/ft.	lbs.	psf.	
4525	47124	Varies	1.3

NAIL-SOLVER

Ult. Nail Stress	H Max.	f_b	Nail Length	K_l
N/mm^2	m.		m.	
414	28.5	1	15.9	.53

NAILM

Nail X-Sect. Area	Unbonded Length	Average Pullout	A
in^2	ft.	psf.	
0.79	0	1950	2

TALREN

QS	PL	KSB	LB	TR	ALB	IND	RCIS
kN/m	kPa		m	kN	Deg.		kN
66	0	0	1.5	210	0	1	0

San Bernadino Wall

C	ϕ	γ	Grout Diam.	Bar Diam.	Depth to 1st Nail	Ult. Nail Stress
psf.	Degrees	pcf.	in.	in.	ft.	ksi.
150	38	110	8	1	3	60
Bond Stress	Wall Height	Nail Spac., S_h	Nail Spac., S_v	Length of Nail	E of Nail	Nail Inclination
psf.	ft.	ft.	ft.	ft.	ksi.	Degrees
2387	25.5	5	5	22	30000	15

SNAIL

Bond Stress	Punching Shear
psi.	kips.
16.6	Varies

STARS

$\beta 1$	$\beta 2$	$\beta 3$	Traction	Friction
Degrees	Degrees	Degrees	kN	kN/m
10	84.3	0	210	73

GOLDNAIL

Adhesion	Max. Nail Force	Face Pressure	Nail Length Factor
lbs/ft.	lbs.	psf.	
5000	47124	Varies	0.86

NAIL-SOLVER

Ult. Nail Stress	H Max.	f_b	K_l
N/mm^2	m.		
414	12	1	3.2

NAILM

Nail X-Sect. Area	Unbonded Length	Average Pullout	A
in^2	ft.	psf.	
0.79	0	2387	2

TALREN

QS	PL	KSB	LB	TR	ALB	IND	RCIS
kN/m	kPa		m	kN	Deg.		kN
73	0	0	1.5	210	0	1	0

(after Juran & Elias, 1990a)

Swift Delta Wall (UV130+55.95)

C	ϕ	γ	Grout Diam.	Bar Diam.	Depth to 1st Nail	Ult. Nail Stress
psf.	Degrees	pcf.	in.	in.	ft.	ksi.
100	33	115	7	1	2.5	60
Bond Stress	Wall Height	Nail Spac., S_h	Nail Spac., S_v	Length of Nail	E of Nail	Nail Inclination
psf.	ft.	ft.	ft.	ft.	ksi.	Degrees
1000	27.5	4.5	3	21	30000	15

SNAIL

Bond Stress	Punching Shear
psi.	kips.
6.95	Varies

STARS

$\beta 1$	$\beta 2$	$\beta 3$	Traction	Friction
Degrees	Degrees	Degrees	kN	kN/m
0	85.2	0	210	27

GOLDNAIL

Adhesion	Max. Nail Force	Face Pressure	Nail Length Factor
lbs/ft.	lbs.	psf.	
1833	47124	Varies	0.8

NAIL-SOLVER

Ult. Nail Stress	H Max.	f_b	K_l
N/mm^2	m.		
	Not	Applicable	

NAILM

Nail X-Sect. Area	Unbonded Length	Average Pullout	A
in^2	ft.	psf.	
0.79	0	1000	2

TALREN

QS	PL	KSB	LB	TR	ALB	IND	RCIS
kN/m	kPa		m	kN	Deg.		kN
27	0	0	0.9	210	0	1	0

(after Sakr, 1991)

Polyclinic Wall (Upper Soil)

C	ϕ	γ	Grout Diam.	Bar Diam.	Depth to 1st Nail	Ult. Nail Stress
psf.	Degrees	pcf.	in.	in.	ft.	ksi.
0	30	120	8	1	5	60
Bond Stress	Wall Height	Nail Spac., S_h	Nail Spac., S_v	Length of Nail	E of Nail	Nail Inclination
psf.	ft.	ft.	ft.	ft.	ksi.	Degrees
1432	55	6	6	32	30000	20

SNAIL

Bond Stress	Punching Shear
psi.	kips.
9.95	varies

STARS

β1	β2	β3	Traction	Friction
Degrees	Degrees	Degrees	kN	kN/m
0	90	0	210	44

GOLDNAIL

Adhesion	Max. Nail Force	Face Pressure	Nail Length Factor
lbs/ft.	lbs.	psf.	
3000	47124	Varies	.6

NAIL-SOLVER

Ult. Nail Stress	C	f	g	H Max.	f_b	Nail Length	K_1
N/mm^2	kN/m^2	Degrees	kN/m^3	m.		m.	
414	9.6	38	20	16.5	1	10.5	1.01

NAILM

Nail X-Sect. Area	Unbonded Length	Average Pullout	A
in^2	ft.	psf.	
1.06	0	3820	2

TALREN

QS	PL	KSB	LB	TR	ALB	IND	RCIS
kN/m	kPa		m	kN	Deg.		kN
44	0	0	1.8	210	0	1	0

(after Thompson & Miller, 1990)

Polyclinic Wall (Lower Soil)

C	ϕ	γ	Grout Diam.	Bar Diam.	Depth to 1st Nail	Ult. Nail Stress
psf.	Degrees	pcf.	in.	in.	ft.	ksi.
200	38	130	8	1.27		60
Bond Stress	Wall Height	Nail Spac., S_h	Nail Spac., S_v	Length of Nail	E of Nail	Nail Inclination
psf.	ft.	ft.	ft.	ft.	ksi.	Degrees
3820	55	6	6	35	30000	15

SNAIL

Bond Stress	Punching Shear
psi.	kips.
26.53	varies

STARS

$\beta 1$	$\beta 2$	$\beta 3$	Traction	Friction
Degrees	Degrees	Degrees	kN	kN/m
0	90	0	338	117

GOLDNAIL

Adhesion	Max. Nail Force	Face Pressure	Nail Length Factor
lbs/ft.	lbs.	psf.	
8000	76006	Varies	.6

NAIL-SOLVER

Ult. Nail Stress	C	f	g	H Max.	f_b	Nail Length	K_l
N/mm^2	kN/m^2	Degrees	kN/m^3	m.		m.	
414	9.6	38	20	16.5	1	10.5	1.01

NAILM

Nail X-Sect. Area	Unbonded Length	Average Pullout	A
in^2	ft.	psf.	
1.06	0	3820	2

TALREN

QS	PL	KSB	LB	TR	ALB	IND	RCIS
kN/m	kPa		m	kN	Deg.		kN
15	0	0	1.4	131	0	1	0

(after Thompson & Miller, 1990)

Eparris Wall (Top and Bottom Nail)

C	ϕ	γ	Grout Diam.	Bar Diam.	Depth to 1st Nail	Ult. Nail Stress
psf.	Degrees	pcf.	in.	in.	ft.	ksi.
0	28	127	4	0.79	0	60
Bond Stress	Wall Height	Nail Spac., S_h	Nail Spac., S_v	Length of Nail	E of Nail	Nail Inclination
psf.	ft.	ft.	ft.	ft.	ksi.	Degrees
982	14	10	4.67	10/15	30000	20

SNAIL

Bond Stress	Punching Shear
psi.	kips.
6.82	40

STARS

$\beta 1$	$\beta 2$	$\beta 3$	Traction	Friction
Degrees	Degrees	Degrees	kN	kN/m
15	70	0	131	15

GOLDNAIL

Adhesion	Max. Nail Force	Face Pressure	Nail Length Factor
lbs/ft.	lbs.	psf.	
1028	29410	2000	0.83

NAIL-SOLVER

Ult. Nail Stress	H Max.	f_b	K_l
N/mm^2	m.		
	Not	Applicable	

NAILM

Nail X-Sect. Area	Unbonded Length	Average Pullout	A
in^2	ft.	psf.	
0.49	0	982	2

TALREN

QS	PL	KSB	LB	TR	ALB	IND	RCIS
kN/m	kPa		m	kN	Deg.		kN
15	0	0	1.4	131	0	1	0

(after Bruce & Jewell, 1987, also in Schlosser, 1985)

Eparris Wall (Middle 2 Nails)

C	ϕ	γ	Grout Diam.	Bar Diam.	Depth to 1st Nail	Ult. Nail Stress
psf.	Degrees	pcf.	in.	in.	ft.	ksi.
0	28	127	4	1.26		60
Bond Stress	Wall Height	Nail Spac., S_h	Nail Spac., S_v	Length of Nail	E of Nail	Nail Inclination
psf.	ft.	ft.	ft.	ft.	ksi.	Degrees
982	14	10	4.67	10/15	30000	20

SNAIL

Bond Stress	Punching Shear
psi.	kips.
6.82	40

STARS

$\beta 1$	$\beta 2$	$\beta 3$	Traction	Friction
Degrees	Degrees	Degrees	kN	kN/m
15	70	0	333	15

GOLDNAIL

Adhesion	Max. Nail Force	Face Pressure	Nail Length Factor
lbs/ft.	lbs.	psf.	
1028	74814	2000	0.83

NAIL-SOLVER

Ult. Nail Stress	H Max.	f_b	K_1
N/mm^2	m.		
	Not	Applicable	

NAILM

Nail X-Sect. Area	Unbonded Length	Average Pullout	A
in^2	ft.	psf.	
1.25	0	982	2

TALREN

QS	PL	KSB	LB	TR	ALB	IND	RCIS
kN/m	kPa		m	kN	Deg.		kN
15	0	0	1.4	333	0	1	0

(after Bruce & Jewell, 1987, also in Schlosser, 1985)

Bodenvernagelung (Top 3 Nails)

C	ϕ	γ	Grout Diam.	Bar Diam.	Depth to 1st Nail	Ult. Nail Stress
psf.	Degrees	pcf.	in.	in.	ft.	ksi.
104	35	99	4	0.875	3.33	60
Bond Stress	Wall Height	Nail Spac., S_h	Nail Spac., S_v	Length of Nail	E of Nail	Nail Inclination
psf.	ft.	ft.	ft.	ft.	ksi.	Degrees
1963	20	4	3.7	10	30000	10

SNAIL

Bond Stress	Punching Shear
psi.	kips.
13.63	50

STARS

$\beta 1$	$\beta 2$	$\beta 3$	Traction	Friction
Degrees	Degrees	Degrees	kN	kN/m
0	80.5	0	160	30

GOLDNAIL

Adhesion	Max. Nail Force	Face Pressure	Nail Length Factor
lbs/ft.	lbs.	psf.	
2056	36079	2000	0.5

NAIL-SOLVER

Ult. Nail Stress	H Max.	f_b	K_l
N/mm^2	m.		
	Not	Applicable	

NAILM

Nail X-Sect. Area	Unbonded Length	Average Pullout	A
in^2	ft.	psf.	
	Not	Applicable	

TALREN

QS	PL	KSB	LB	TR	ALB	IND	RCIS
kN/m	kPa		m	kN	Deg.		kN
30	0	0	1.11	160	0	1	0

(after Stocker et al., 1979)

Bodenvernagelung (Lower two Nails)

C	ϕ	γ	Grout Diam.	Bar Diam.	Depth to 1st Nail	Ult. Nail Stress
psf.	Degrees	pcf.	in.	in.	ft.	ksi.
104	35	99	4	0.875		60
Bond Stress	Wall Height	Nail Spac., S_h	Nail Spac., S_v	Length of Nail	E of Nail	Nail Inclination
psf.	ft.	ft.	ft.	ft.	ksi.	Degrees
1963	20	4	3.7	11.6	30000	10

SNAIL

Bond Stress	Punching Shear
psi.	kips.
13.63	50

STARS

$\beta 1$	$\beta 2$	$\beta 3$	Traction	Friction
Degrees	Degrees	Degrees	kN	kN/m
0	80.5	0	160	30

GOLDNAIL

Adhesion	Max. Nail Force	Face Pressure	Nail Length Factor
lbs/ft.	lbs.	psf.	
2056	36079	2000	0.5

NAIL-SOLVER

Ult. Nail Stress	H Max.	f_b	K_l
N/mm^2	m.		
	Not	Applicable	

TALREN

QS	PL	KSB	LB	TR	ALB	IND	RCIS
kN/m	kPa		m	kN	Deg.		kN
30	0	0	1.11	160	0	1	0

(after Stocker et al., 1979)

APPENDIX C

CLOUDIM PLOTS

Summary of Example Problems

Example No.	Brief description
Example 1	30' wall, horizontal backslope, 5.7° batter
Example 2	60' wall, horizontal backslope, 5.7° batter
Example 3	30' wall, sloped backslope, 14° batter
Example 4	20' wall, horizontal backslope, 0° batter, surcharge
Example 5	Benched 40' wall, sloped backslope, 0° batter
Example 6	60' wall, horizontal backslope, 5.7° batter, Layered soils
Example 7	40' wall, horizontal backslope, 0° batter
Example 8	40' wall, sloped backslope, 0°batter
Example 9	40' wall, sloped backslope, 10° batter
Example 10	45' wall, sloped backslope, toe slope, 0° batter
San Bernadino	25.5' wall, sloped backslope, 5.7° batter
Swift-Delta 1	27.5' wall, 4.8° batter, surcharge
Polyclinic	55' wall, horizontal backslope, 0° batter, Layered soils
Eparris	14' wall, sloped backslope, 20° batter
Bodenvernag-elung, Case B	20' wall, horizontal backslope, 9.5° batter, surcharge

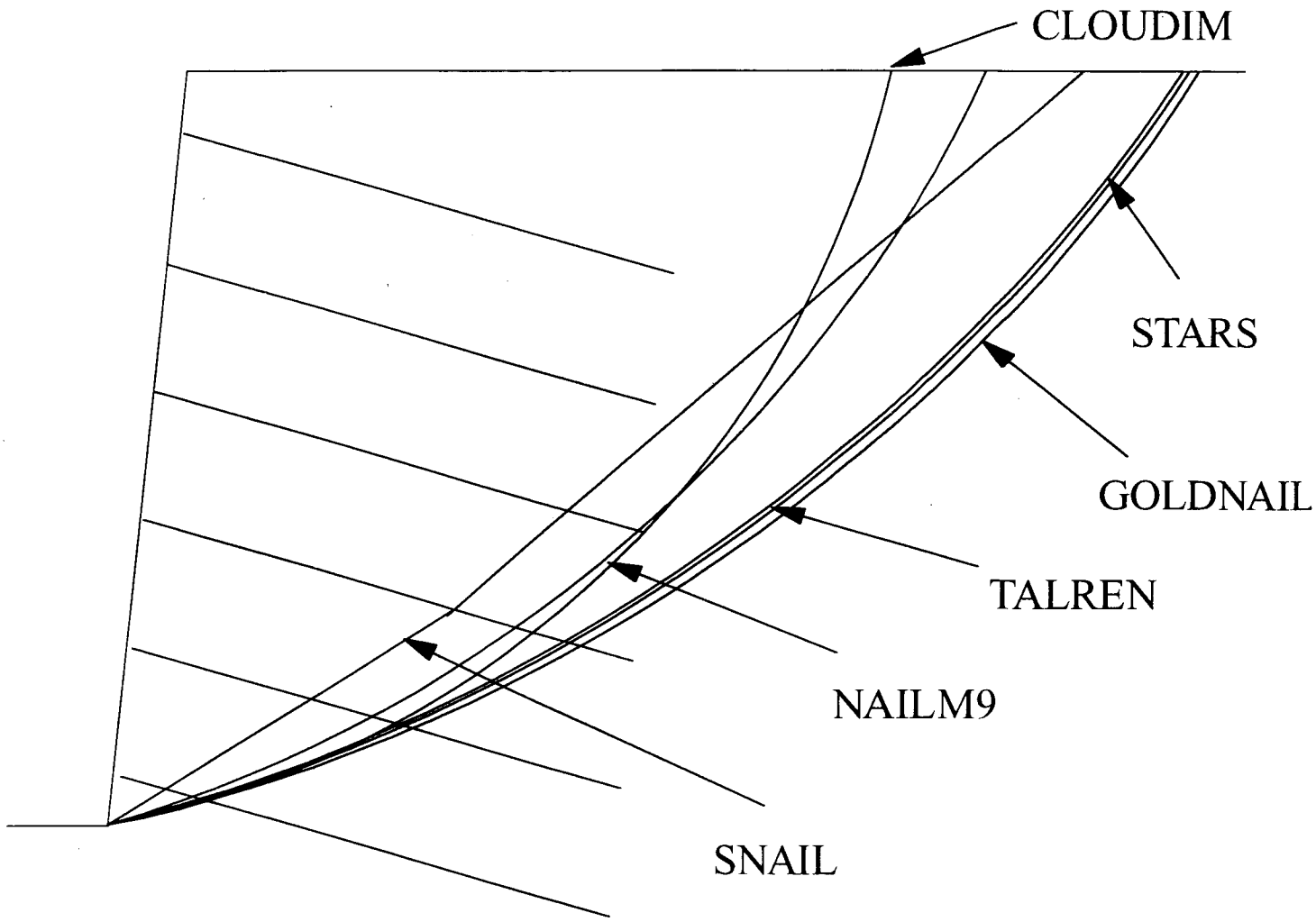

Comparison of computed results — Example 1

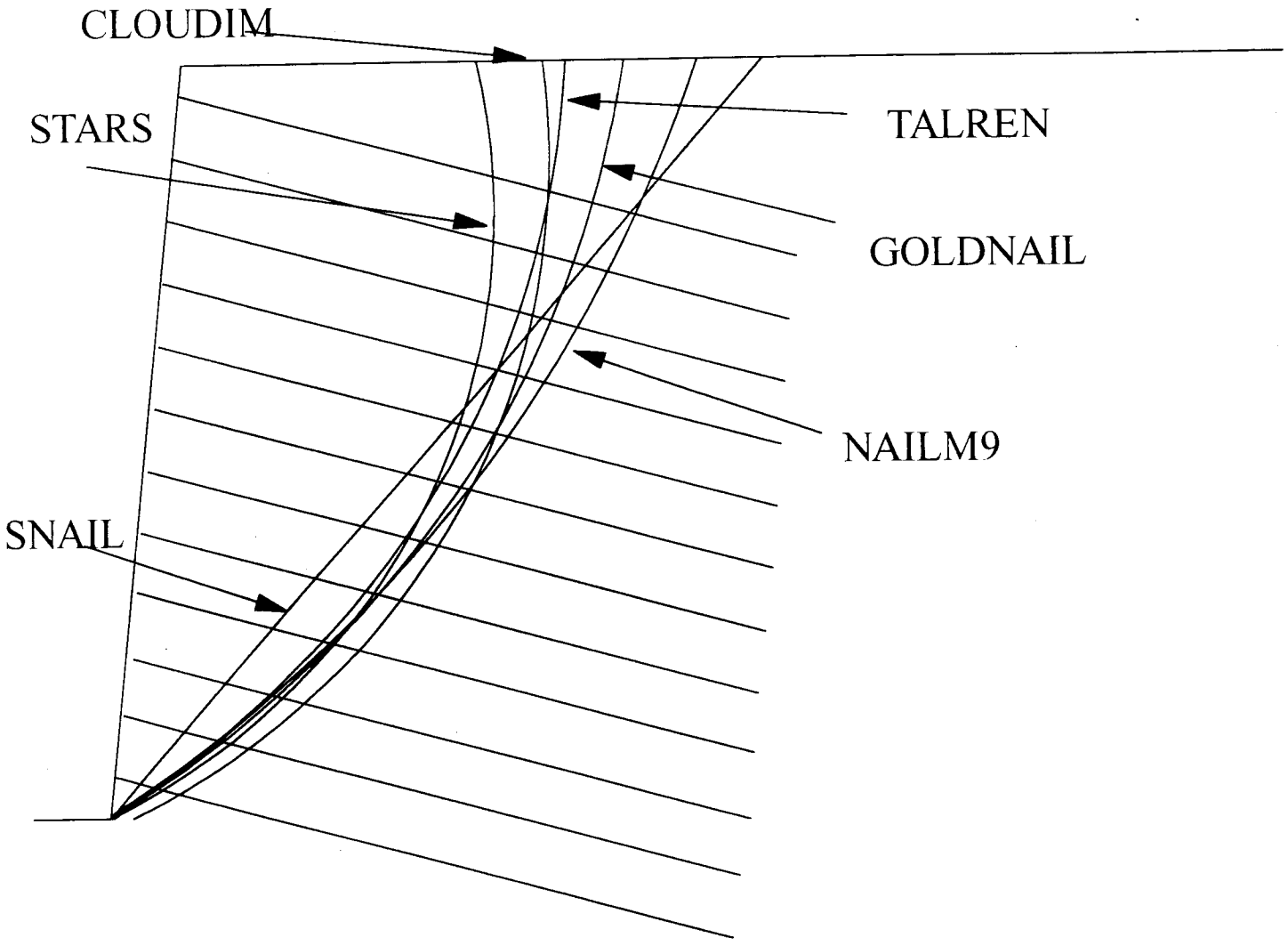

Comparison of computed results — Example 2

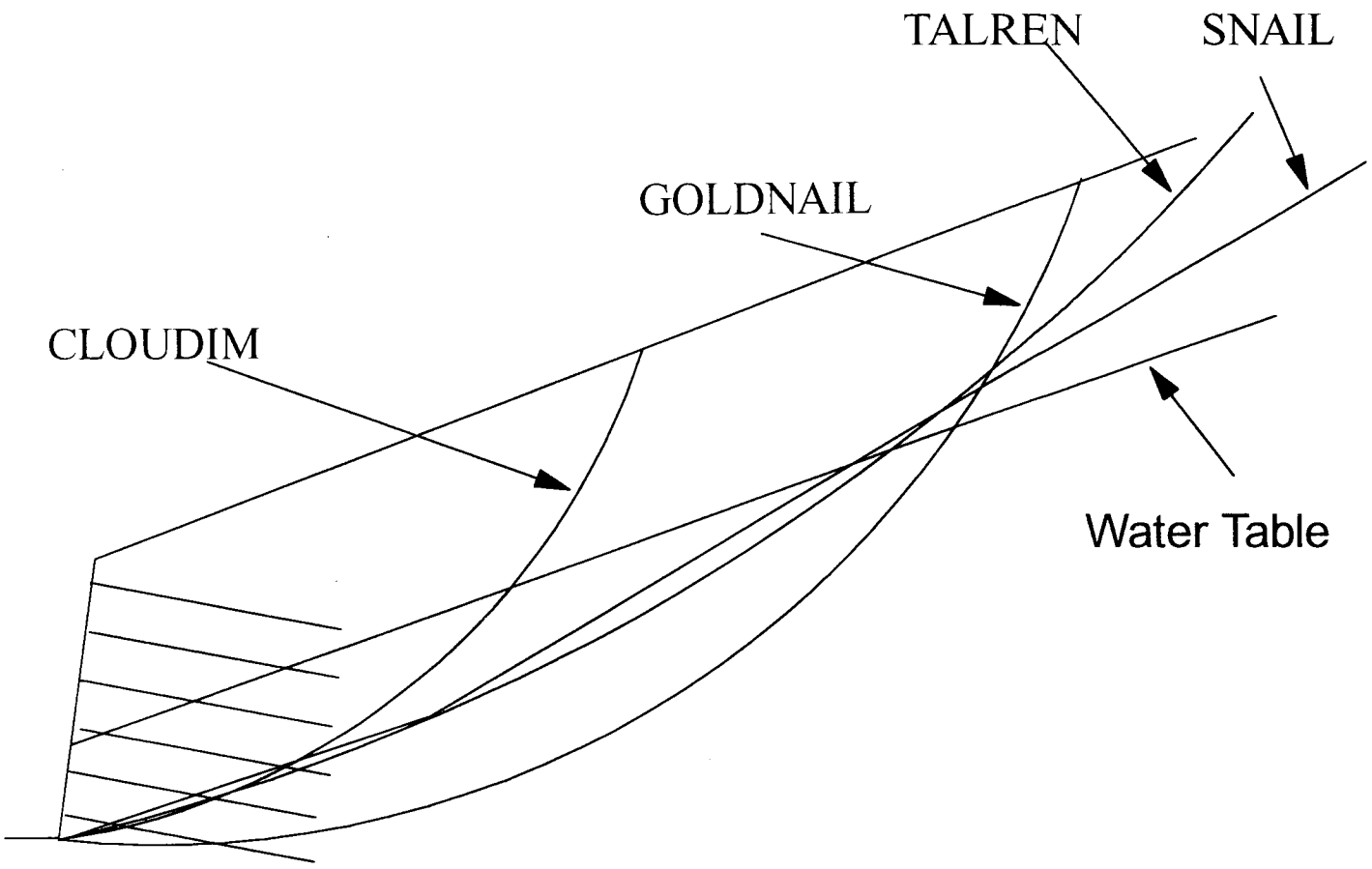

Comparison of computed results — Example 3

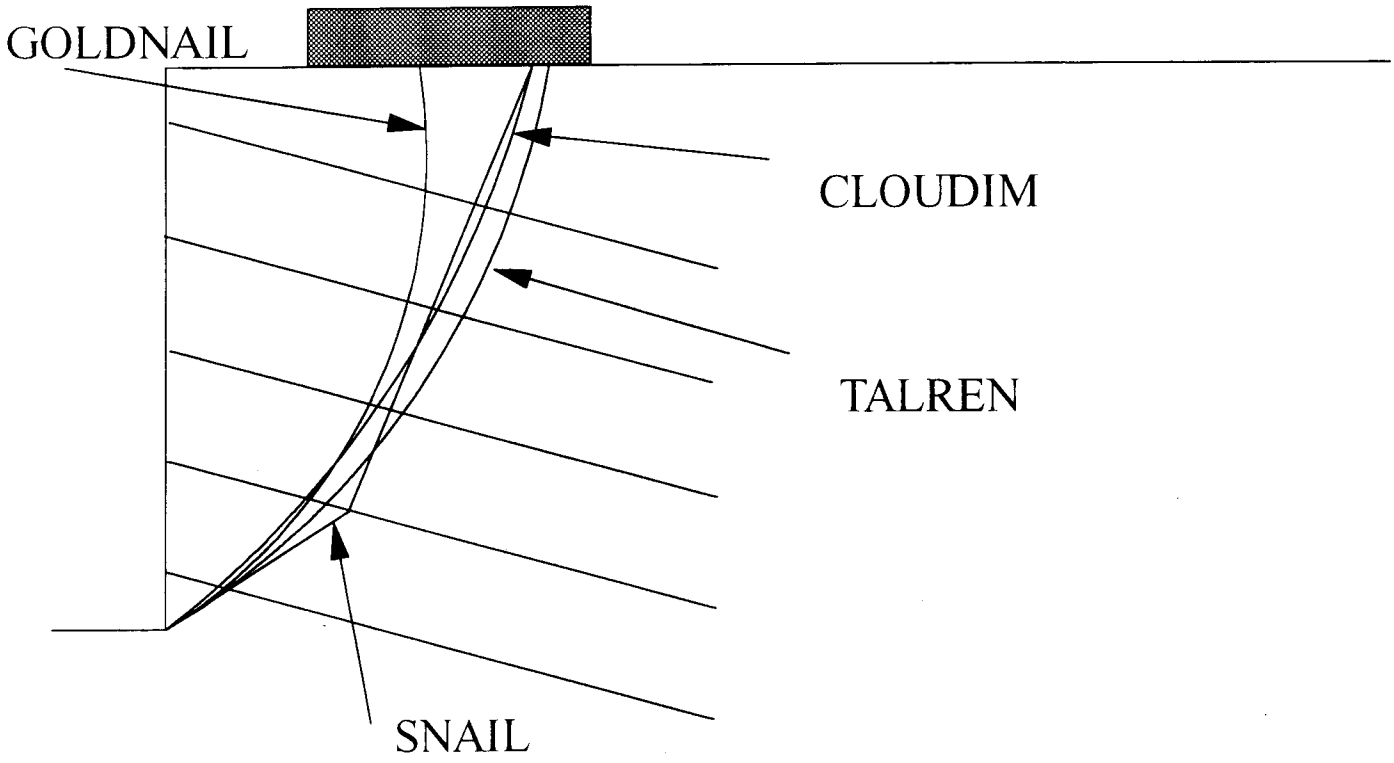

Comparison of computed results — Example 4

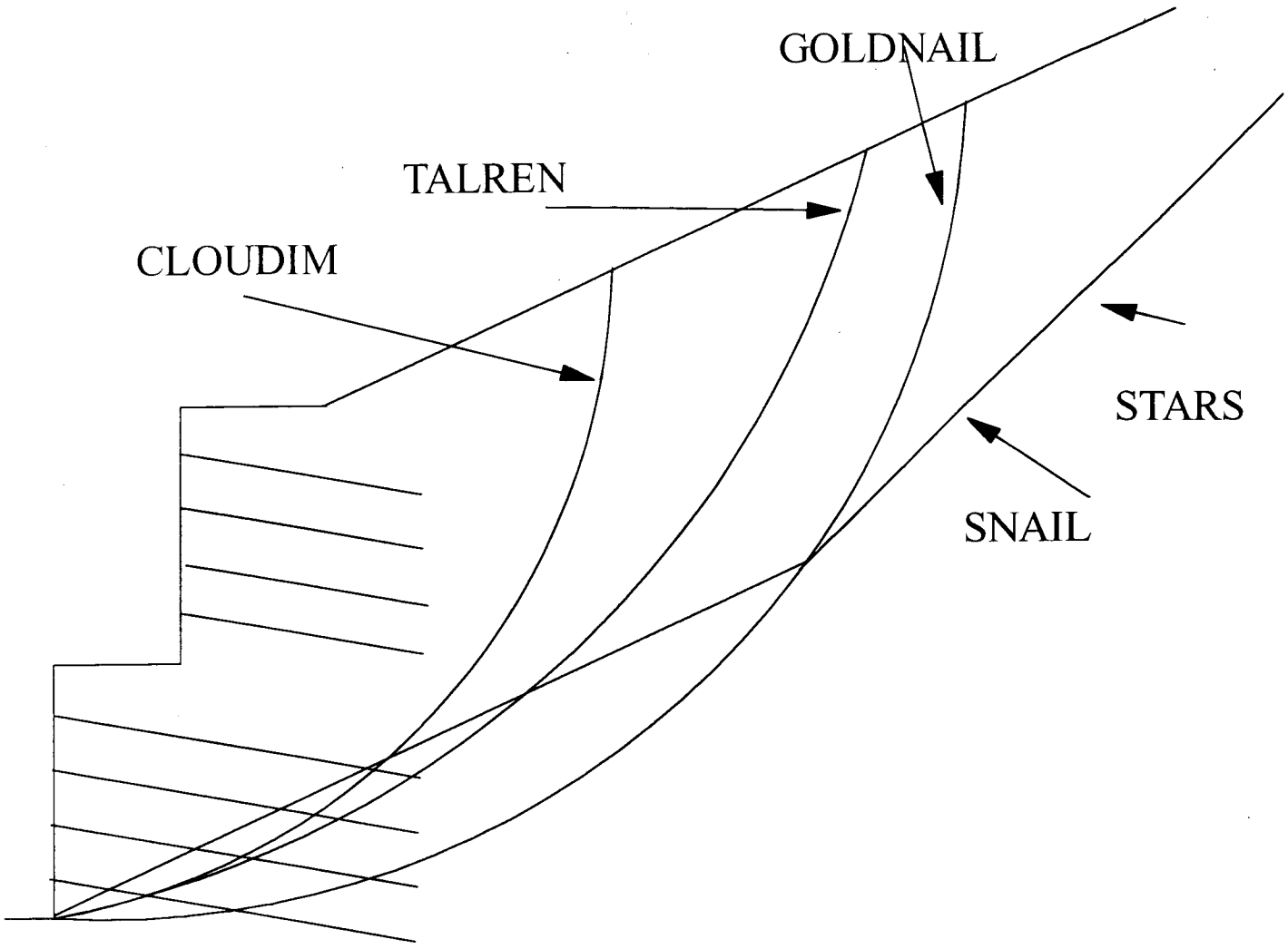

Comparison of computed results — Example 5

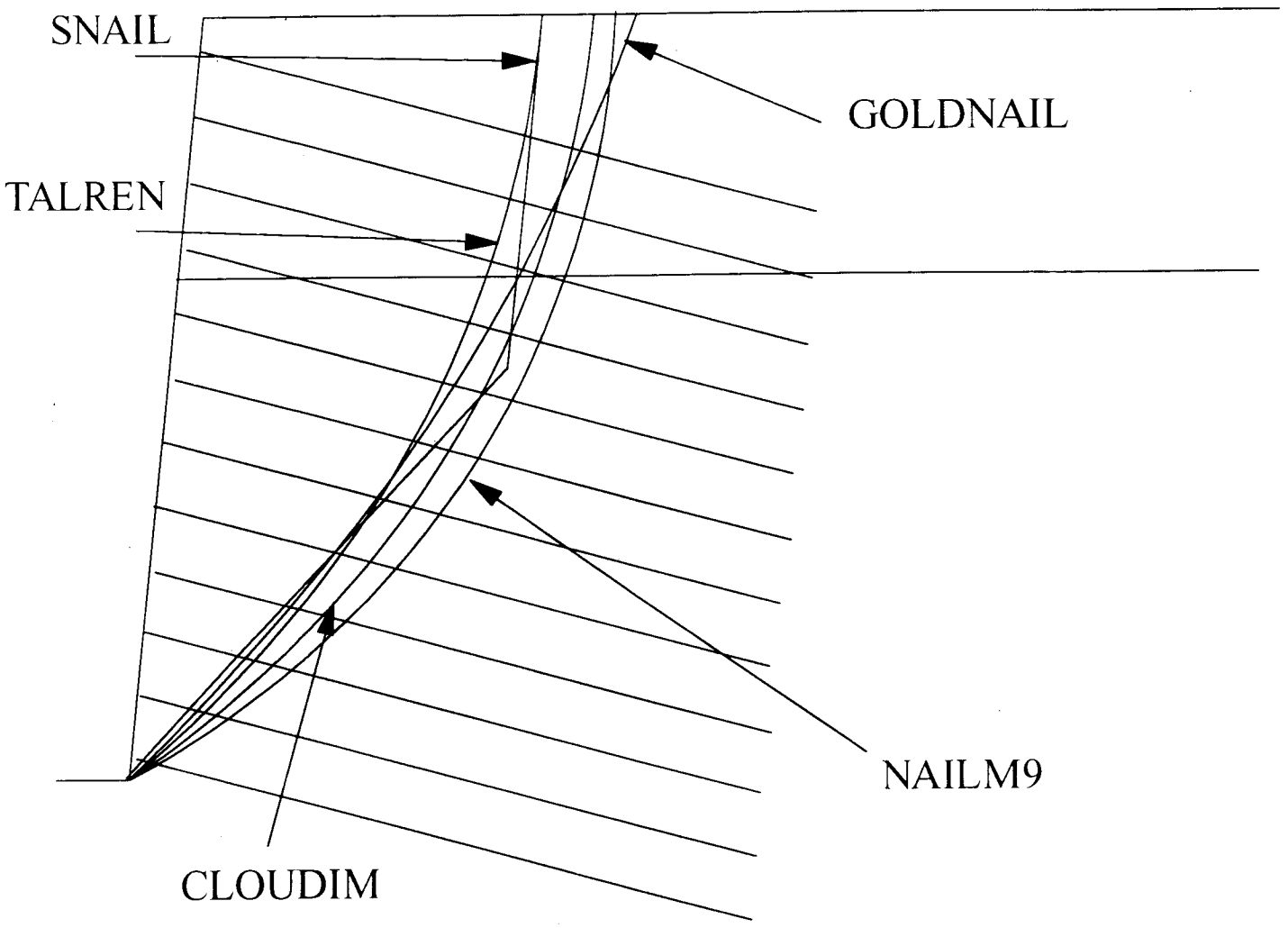

Comparison of computed results — Example 6

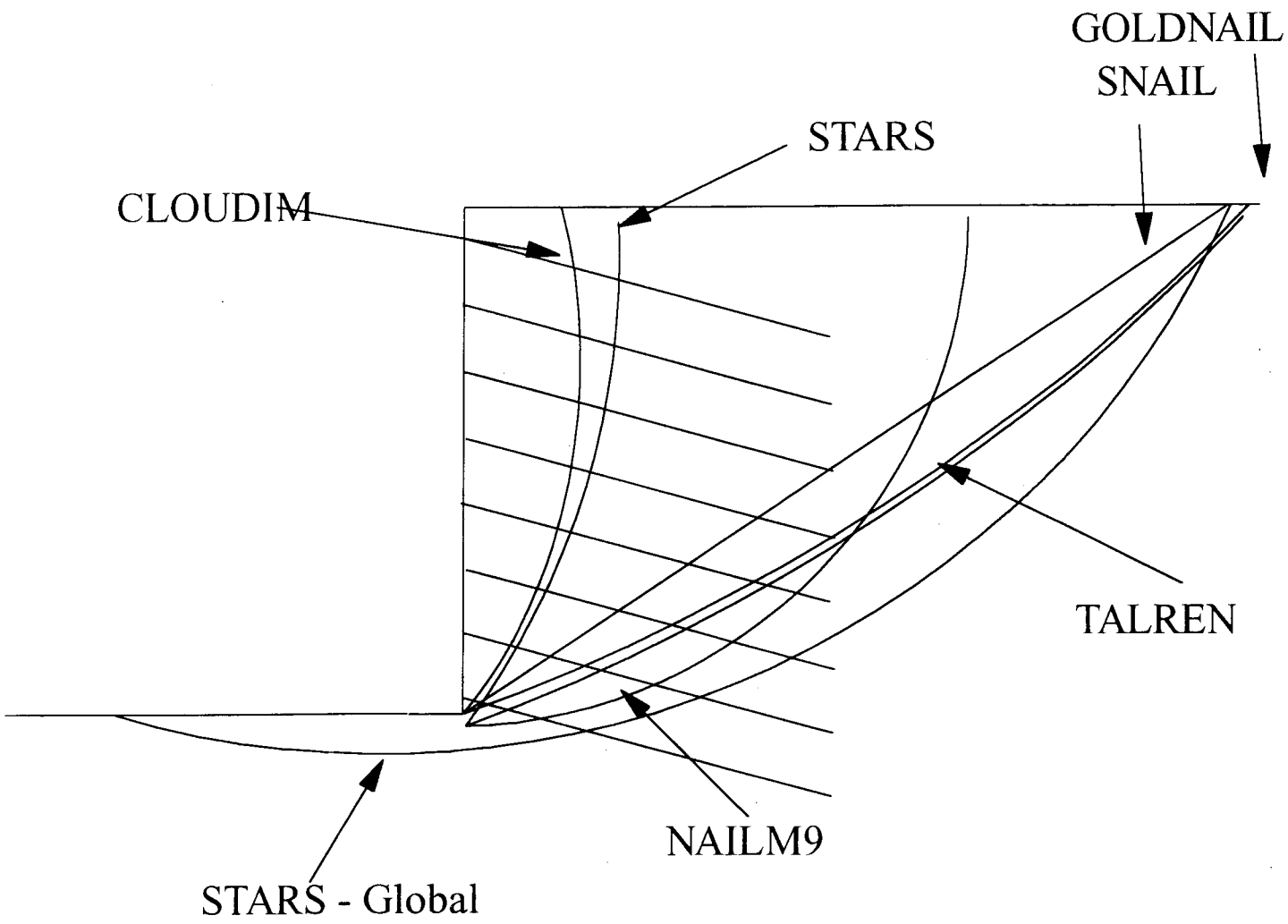

Comparison of computed results — Example 7

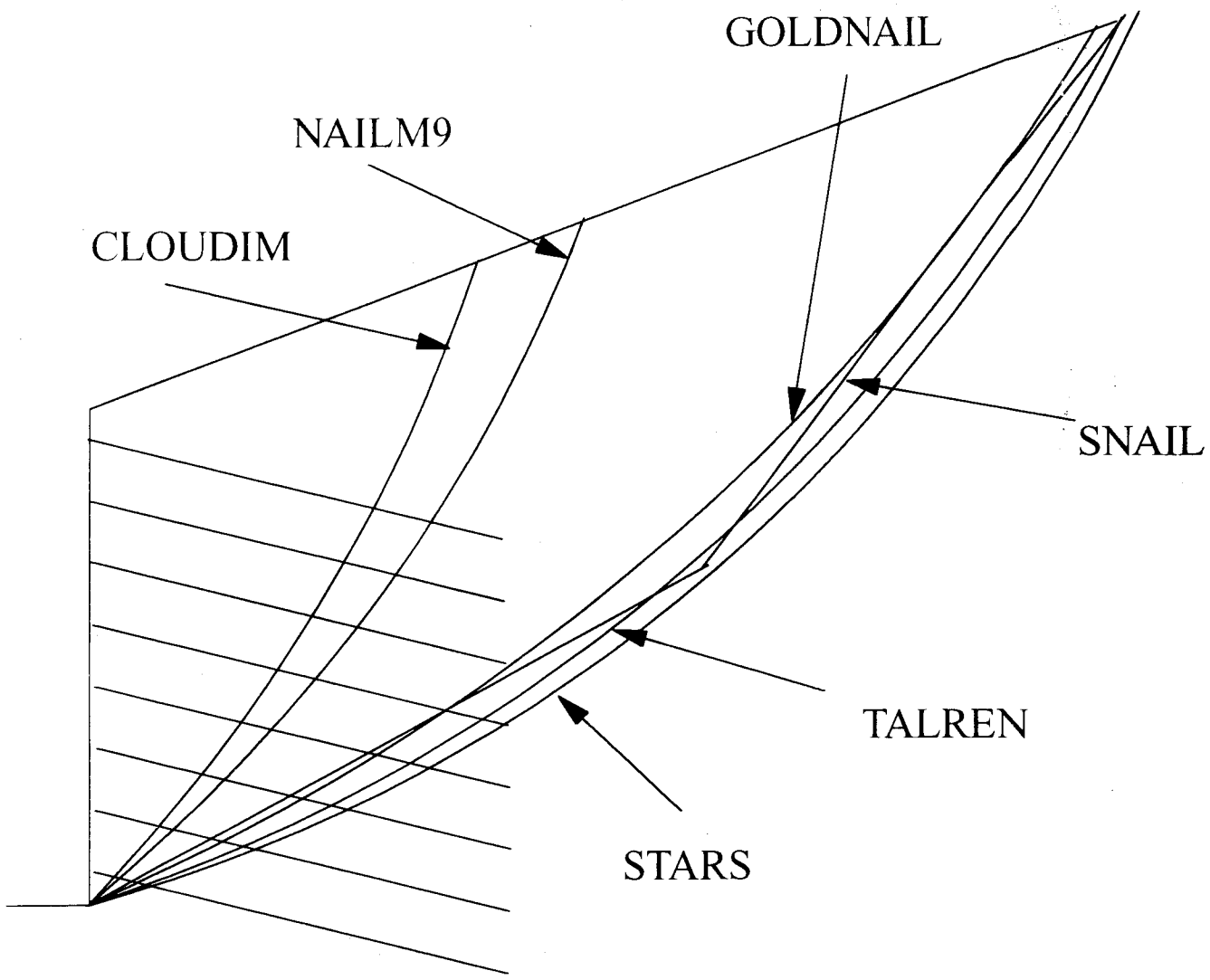

Comparison of computed results — Example 8

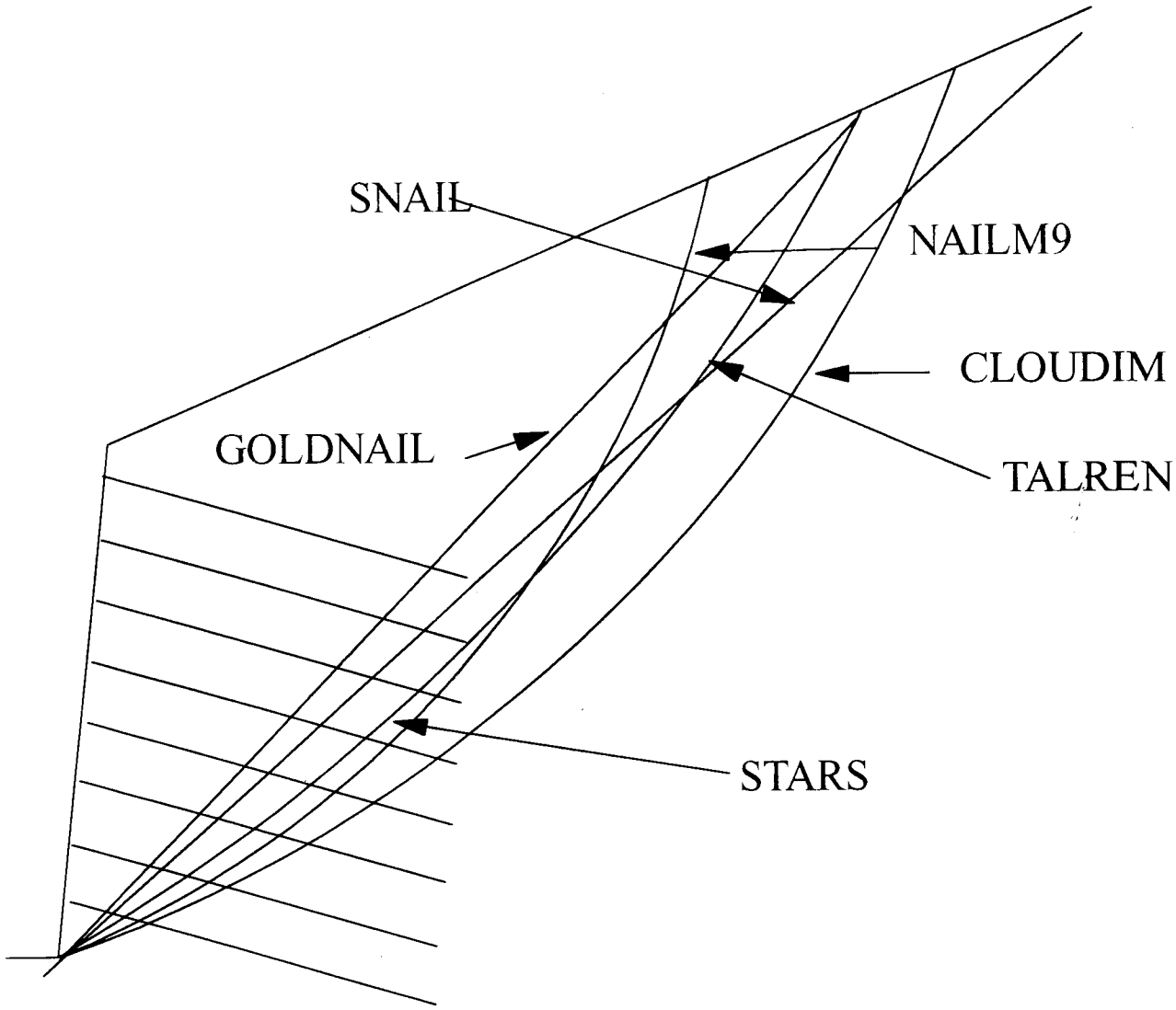

Comparison of computed results — Example 9

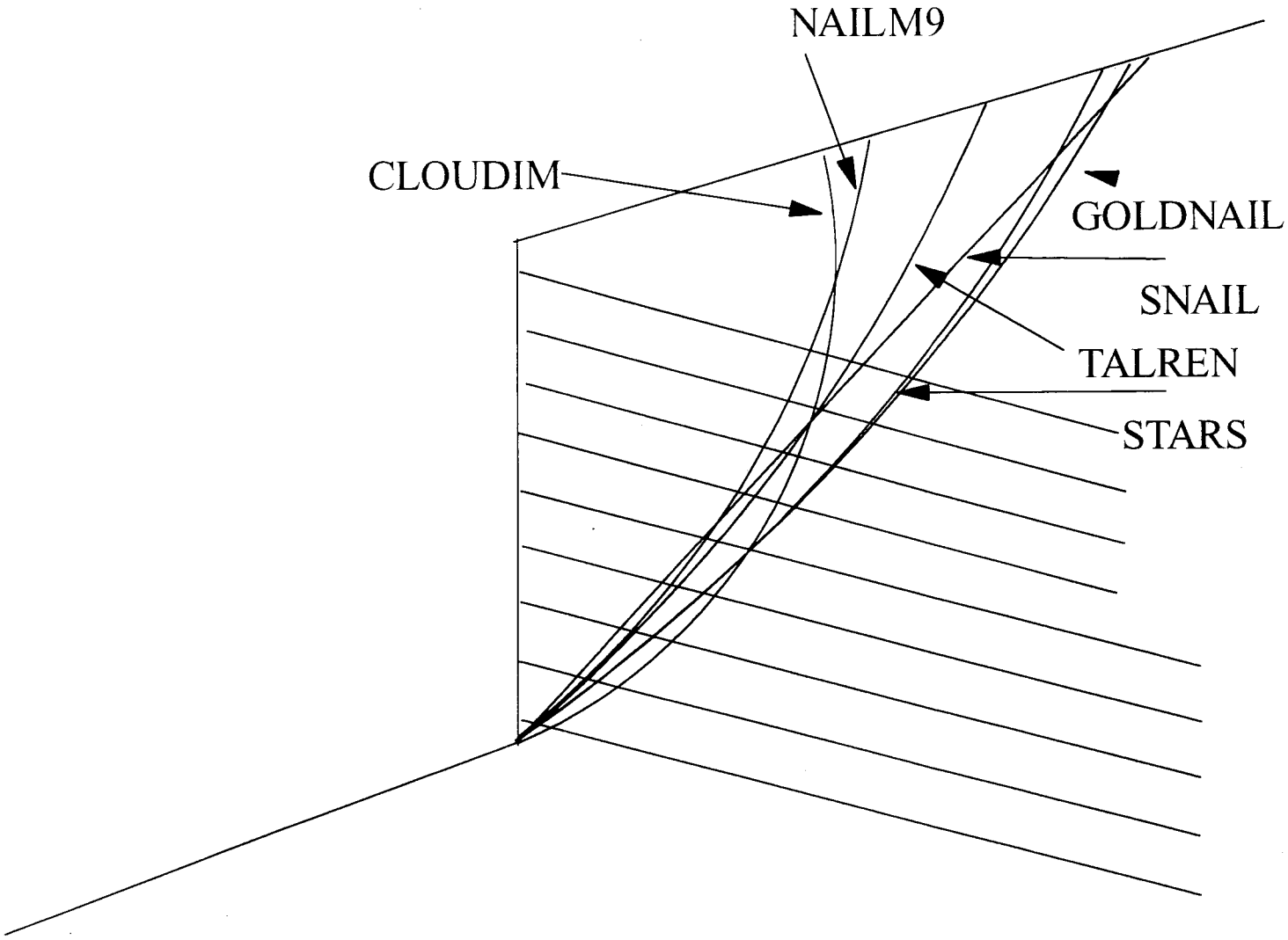

Comparison of computed results — Example 10

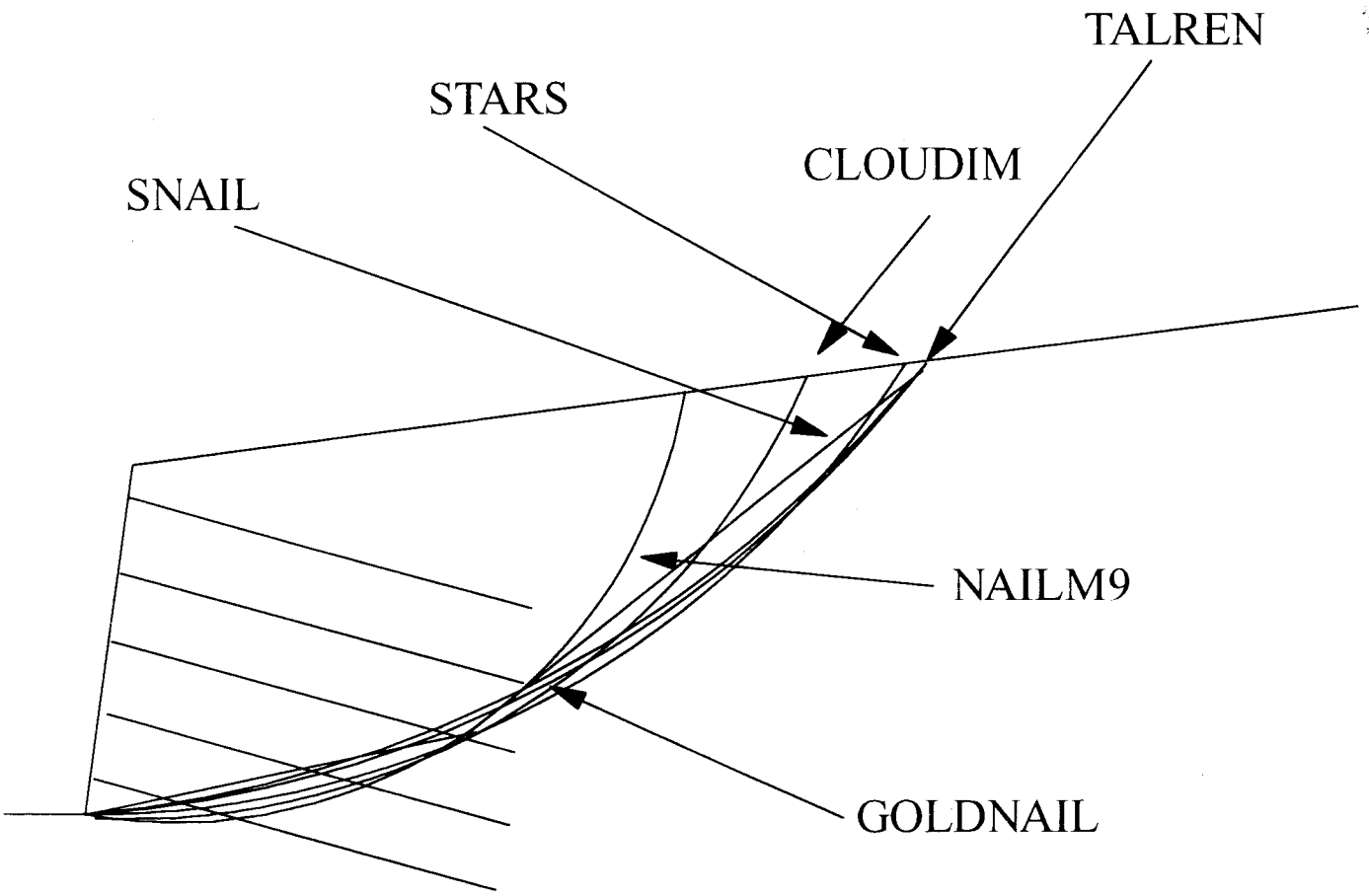

Comparison of computed results — San Bernadino Wall

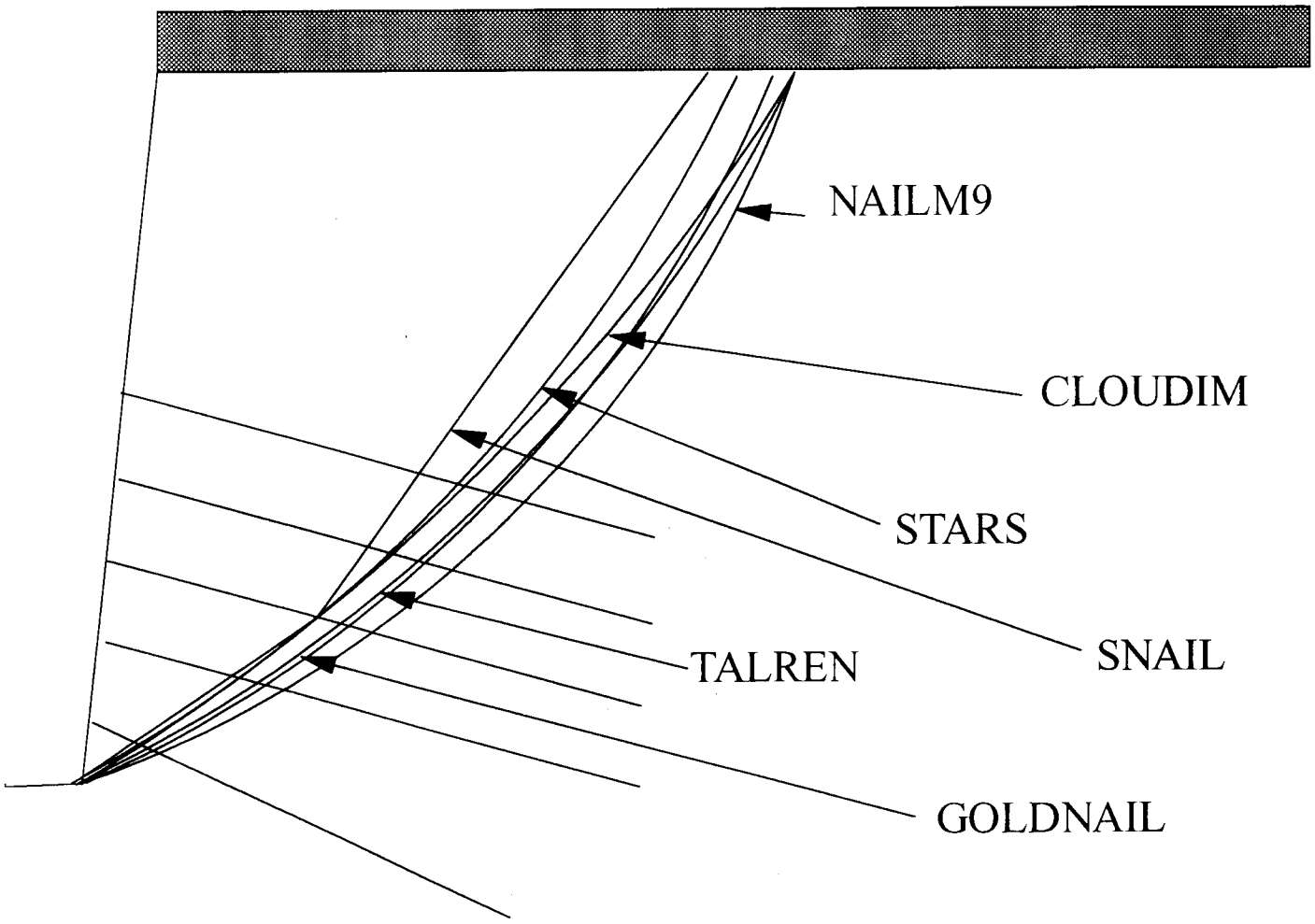

Comparison of computed results — Swift Delta 1 Wall

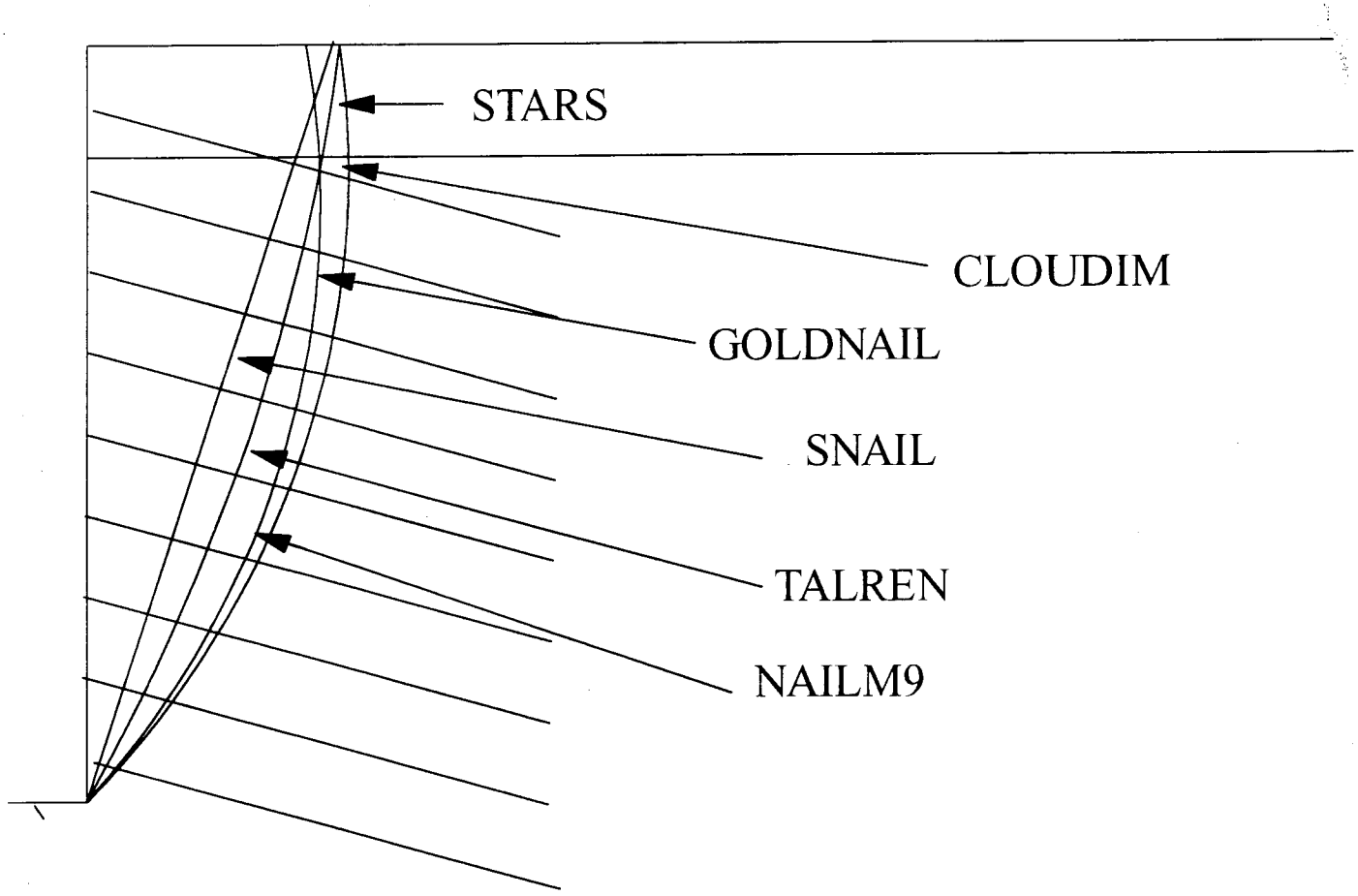

Comparison of computed results — Polyclinic Wall

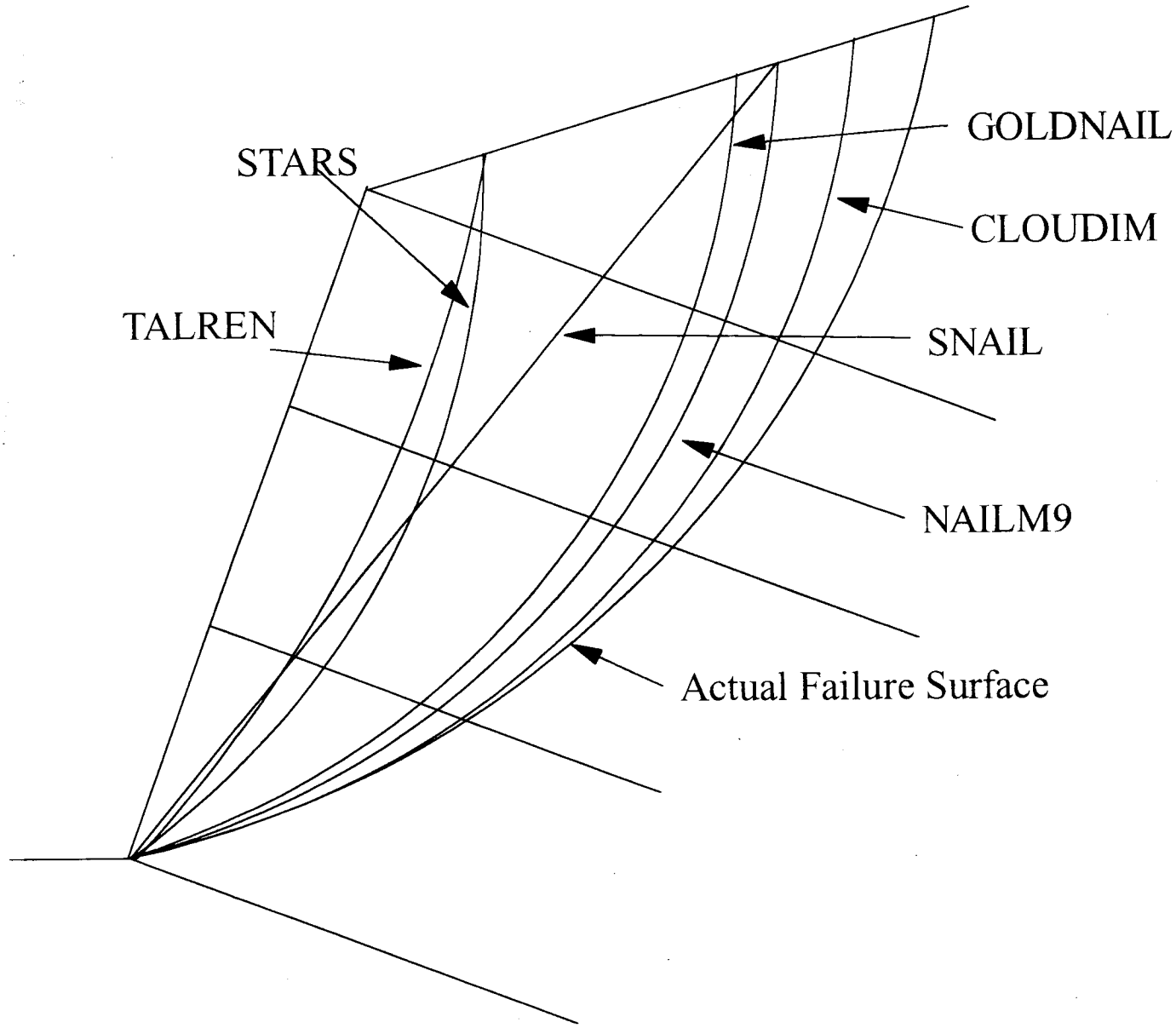

Comparison of computed results — Eparris Wall

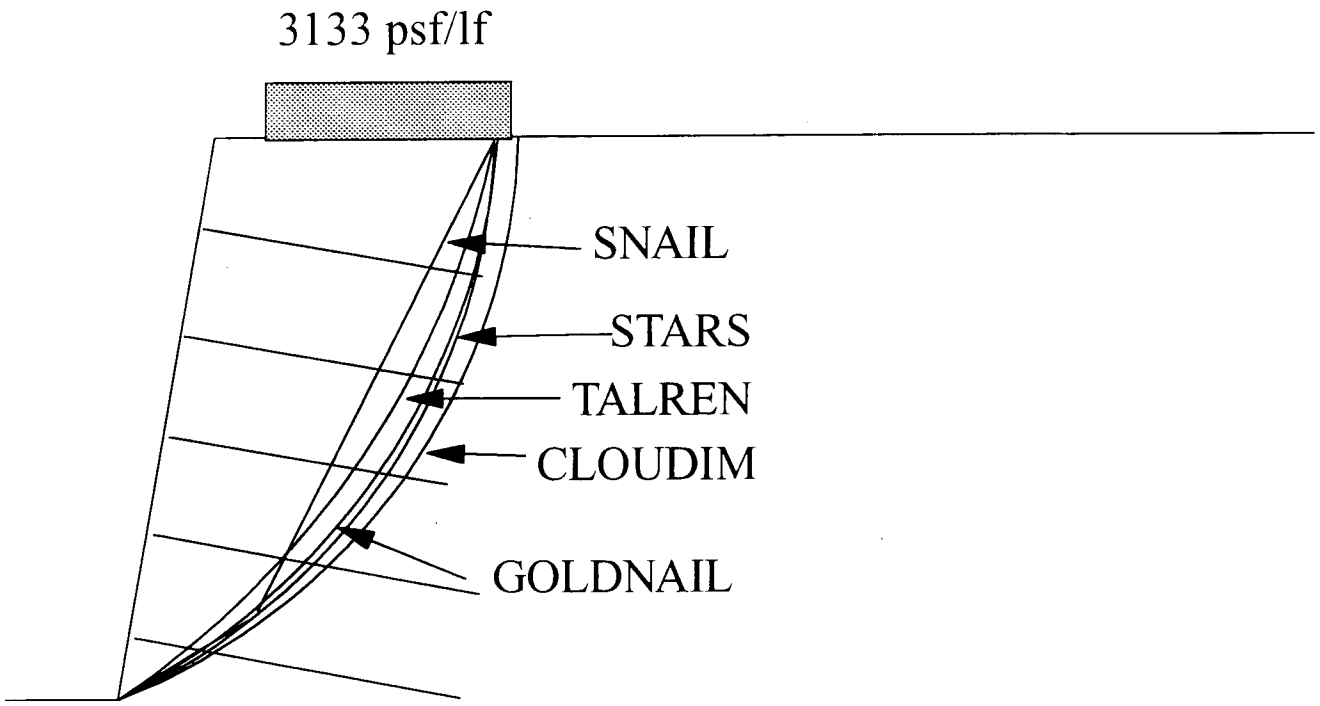

Comparison of computed results — Bodenvernag, B Wall